



University
of Glasgow

Techakriengkrai, Navapon (2016) *Investigating the role of target cell availability in the pathogenesis of feline immunodeficiency virus infection*. PhD thesis.

<http://theses.gla.ac.uk/7429/>

Copyright and moral rights for this work are retained by the author

A copy can be downloaded for personal non-commercial research or study, without prior permission or charge

This work cannot be reproduced or quoted extensively from without first obtaining permission in writing from the author

The content must not be changed in any way or sold commercially in any format or medium without the formal permission of the author

When referring to this work, full bibliographic details including the author, title, awarding institution and date of the thesis must be given

Enlighten:Theses
<http://theses.gla.ac.uk/>
theses@gla.ac.uk

Investigating the role of target cell availability in the pathogenesis of feline immunodeficiency virus infection

Navapon Techakriengkrai
DVM, MSc

Submitted in the fulfilment of the requirements for the
Degree of Doctor of Philosophy

Medical Research Council-Centre for Virus Research
College of Medical, Veterinary and Life Sciences
University of Glasgow

June 2016

Abstract

Feline immunodeficiency virus (FIV) is a naturally occurring lentivirus of domestic cats, which shares many similarities with its human counterpart, human immunodeficiency virus (HIV). FIV infects its main target cell, the CD4⁺ T lymphocyte, via interactions with its primary receptor CD134 (an activation marker expressed on activated CD4⁺ T lymphocytes), and, the chemokine receptor CXCR4. According to the different ways in which FIV isolates interact with CD134, FIV may be categorised into two groups. The first group contains strains that tend to dominate during the earlier phase of infection, such as GL8 and CPG41. These strains are characterized by their requirement for an additional interaction with the second cysteine rich domain (CRD2) of the CD134 molecule and are classified as “CRD2-dependent” strains. The second group, on the other hand, contains either laboratory-adapted isolates or isolates that emerge after several years of infection, such as PPR or the GL8 variants that emerged in cats 6 years post experimental infection and were studied in this thesis. These isolates are designated “CRD2-independent” as they can infect target cells without interacting with CRD2 of the CD134 molecule.

This study provides the first evidence that FIV compartmentalisation is related to FIV-CD134 usage and the tissue availability of CD134⁺ target cells. In tissue compartments containing high levels of CD134⁺ cells such as peripheral blood and lymph nodes, CRD2-dependent viruses predominated, whereas CRD2-independent viruses predominated in compartments with fewer CD134⁺ cells, such as the thymus. The dynamics of CD4⁺CD134⁺ T lymphocytes at different stages of FIV infection were also described. The levels of CD4⁺CD134⁺ T lymphocytes, which were very high in the early phase, gradually decreased in the later phase of infection. The dynamics of CD4⁺CD134⁺ T lymphocyte numbers appeared to correlate with FIV tropism switching, as more CRD2-independent viruses were isolated from cats in the late phase of infection. Moreover, it was observed that pseudotypes bearing Envs of CRD2-dependent variants infected CD134⁺ target cells more efficiently than pseudotypes bearing Envs of CRD2-independent variants, confirming the selective advantage of CRD2-dependent variants in environments with high levels of CD134⁺ target cells.

In conclusion, this study demonstrated that target cell types and numbers, as well as their dynamics, play important roles in the selection and expansion of FIV variants within the viral quasispecies. Improved understanding of the roles of target cells in FIV transmission and pathogenesis will provide important information required for the development of an improved, more successful protective FIV vaccine and will provide insight into the development of effective vaccines against other lentiviral infections such as HIV.

Table of Contents

Abstract	2
List of Table	10
List of Figure	12
Acknowledgements	16
Author's Declaration	17
List of Abbreviations	18
Chapter 1 Introduction	
1.1 Virology	23
1.1.1 Genomic organisation	23
1.1.2 Structure of FIV	25
1.1.3 The replication cycle of FIV	26
1.1.4 Virus entry and target cell tropism	27
1.2 Natural History of FIV infection	33
1.3 Epidemiology	35
1.4 FIV subtypes and global distribution	36
1.5 Immune responses to FIV infection	37
1.5.1 Cell-mediated immune responses	37
1.5.2 Humoral immune responses	38
1.6 Tissue compartmentalisation	38
1.6.1 Definition of tissue compartmentalisation	39
1.6.2 Compartmentalisation vs. tissue reservoirs	39
1.6.3 Mechanisms of tissue compartmentalisation	41
1.6.4 Evidence of tissue compartmentalisation in FIV infection	42
1.6.5 Target cell availability and tissue compartmentalisation?	43
1.7 Scope and objectives of this study	45
Chapter 2 Materials and Methods	
2.1 Molecular biology	46
2.1.1 Preparation of genomic DNA from buffy coat and tissue sample	46
2.1.2 Preparation of total RNA from cell pellet and tissue sample	47
2.1.3 Preparation of viral RNA from cell culture supernatant	47
2.1.4 Preparation of complementary DNA from RNA samples	47
2.1.5 Quantification of FIV proviral load by quantitative polymerase chain reaction (qPCR)	48

	5
2.1.6 Quantification of CD134 and CXCR4 messenger RNA (mRNA) by duplex qPCR	49
2.1.7 Polymerase chain reactions (PCR)	50
2.1.8 PCR product purification	51
2.1.9 Nucleic acid quantification	51
2.1.10 Restriction enzymes digestion and ligation	51
2.1.11 Transformation	52
2.1.12 Small scale DNA preparation	52
2.1.13 Medium scale DNA preparation	53
2.1.14 Large scale DNA preparation	53
2.1.15 Plasmid DNA sequencing	53
2.1.16 Sequences and phylogenetic analyses	53
2.2 Cell culture techniques	60
2.2.1 Cell lines	60
2.2.2 Peripheral Blood Mononuclear Cells (PBMC)	63
2.2.3 Cell counting	63
2.2.4 Cell cryopreservation	64
2.3 Study specific methods	64
2.3.1 HIV(FIV) pseudotype production	64
2.3.2 FIV-CD134 usage	65
2.3.3 Viral Neutralisation Assay	66
2.3.4 Protein immunoblotting	66
2.3.5 Flow Cytometry	67
2.4 Statistical analyses	69
2.5 Ethics statement	70
Chapter 3 Tissue compartmentalisation in cats experimentally infected with FIV	
3.1 Introduction	71
3.2 Study Background	73
3.3 Study Approach	74
3.4 Samples	74
3.5 Results	76
3.5.1 FIV proviral load (PVL) differed between tissue compartments	76
3.5.2 V5 variant PVL were highly diverse between tissue compartments	80

3.5.3 V5 variant PVL differed significantly between variants and tissue compartments	82
3.5.4 Lack of consensus pattern of compartmentalisation between cats	85
3.5.5 B28 was predominant in thymus but absent in bone marrow	86
3.5.6 Levels of CD134 and CXCR4 mRNA in tissue compartments	89
3.5.7 Relationships between the levels of CD134 and CXCR4 mRNA and FIV PVL	93
3.5.8 FIV infection associated with increased levels of CD134 and CXCR4 mRNA in bone marrow and spleen but not thymus	96
3.5.9 Thymus contained the lowest level of CD4 ⁺ CD134 ⁺ T lymphocytes as measured by flow cytometry	98
3.6 Discussion and Conclusion	99
Chapter 4 Investigating the role of CD4 ⁺ CD134 ⁺ T lymphocytes in the pathogenesis of natural FIV infection	
4.1 Introduction	107
4.2 Study Population	108
4.3 Study Approach	108
4.3.1 Determination of CD134 usage by HIV(FIV) pseudotypes	109
4.4 Results	110
4.4.1 FIV seropositive cats were mainly adult, mixed breed and male	110
4.4.2 Increased proportion of CD4 ⁺ CD134 ⁺ T lymphocytes in FIV positive cats	112
4.4.3 FIV serostatus and clinical status	117
4.4.4 Clinically ill FIV positive cats presumed to be in the terminal phase	117
4.4.5 Clinically healthy FIV infected cats presumed to be in the earlier phase of infection, compared to their sick counterparts	118
4.4.6 Similar percentages of CD4 ⁺ T lymphocytes between sick FIV negative and healthy FIV positive cats	118
4.4.7 Healthy FIV positive cats demonstrated the highest levels of CD4 ⁺ CD134 ⁺ T lymphocytes	119
4.4.8 Lower FIV PVL in healthy cats	120
4.4.9 Interrelationships between lymphocyte subpopulations in FIV negative cats	123

4.4.10 Interrelationships between lymphocyte subpopulations and PVL in FIV positive cats	124
4.4.11 A positive correlation between the percentage of CD4 ⁺ CD134 ⁺ T lymphocytes and FIV PVL in healthy FIV infected cats	125
4.4.12 Concurrent infections showed no effect on lymphocyte subpopulations in FIV negative cats with clinical signs	135
4.4.13 Higher PVL and CD4 ⁺ CD134 ⁺ T lymphocytes in FIV positive cats with co-infections	135
4.4.14 CD4 ⁺ CD134 ⁺ T lymphocyte percentages decline following infection	140
4.4.15 Decreasing CD4 ⁺ CD134 ⁺ T lymphocyte numbers might exert selective pressure on FIV population	141
4.4.16 High proportion of incomplete <i>env</i> genes detected in the cohort	141
4.4.17 Phylogenetic characterisation of FIV <i>env</i> gene	144
4.4.18 CD134 usage and FIV clinical status	149
4.4.19 Autologous neutralisation and FIV clinical status	152
4.5 Discussion and Conclusion	154
Chapter 5 Investigating the role of target cells as selective pressure for FIV	
5.1 Introduction	161
5.2 Development of red fluorescent protein (RFP) carrying lentiviral vector	161
5.2.1 Development of pCSRW vector	162
5.2.2 Lower infectivity and mean fluorescence intensity of TagRFP-pseudotype	163
5.2.3 Higher FP expression under the CMV promoter	164
5.3 Investigating the competition between infecting V5 FIV variants in the transmitted quasispecies for cell entry	167
5.3.1 Development of competitive entry assay	167
5.3.2 GL8 outcompeted V5 variants in CLL-FFF but not CLL-FFHH cells	169
5.4 Investigating the role of CD8 ⁺ T lymphocytes as target cells	171
5.4.1 <i>In vitro</i> expansion of T lymphocytes isolated from peripheral blood	171

5.4.2 FIV infects CD4 ⁺ CD134 ⁺ more efficiently than CD8 ⁺ CD134 ^{+/-} T lymphocytes	175
5.5 Discussion and Conclusion	179
Chapter 6 Final Conclusion	
6.1 Introduction	187
6.2 The role of CD134 ⁺ target cell availability in tissue compartmentalisation	187
6.3 The dominance of CRD2-dependent virus in the early phase	188
6.4 Emergence of CRD2-independent virus variants	189
6.5 The role of target cell availability in the emergence of CRD2- independent virus variants	190
6.6 CRD2-independent virus variants hiding place?	191
6.7 Concluding remarks	192
Appendices	
Appendix 3-1 Characteristics of V5 variants in terms of antagonistic sensitivities and CD134 usage	193
Appendix 3-2 Comparisons of FIV PVL between visceral and lymphoid organs	194
Appendix 3-3 Two-way ANOVA results of FIV PVL as determined by each set of primer and probe	194
Appendix 3-4 Comparisons of FIV PVL between 22 tissue compartments as determined by GL8 V5, B14, B19, B28 and B30 qPCRs	195
Appendix 3-5 Individual PCA plots of cats A825 - A828	195
Appendix 3-6 FIV PVL in thymus and bone marrow	200
Appendix 3-7 Level of CD134 and CXCR4 mRNA in nine tissues of four cats	200
Appendix 3-8 Level of CD134 and CXCR4 mRNA in each tissue compartments	201
Appendix 3-9 CD134 mRNA:CXCR4 mRNA ratio of each tissue	201
Appendix 3-10 Comparisons of the level of CD134 and CXCR4 mRNA in three tissue compartments of the FIV negative and positive cats	202
Appendix 4-1 Type and number of tests requested between groups	203
Appendix 4-2 Type and number of tests requested between groups	204
Appendix 4-3 Clinical History of FIV negative cats	205
Appendix 4-4 Lymphocyte subpopulations of FIV negative cats	208

Appendix 4-5 Clinical History of FIV positive cats	211
Appendix 4-6 Lymphocyte subpopulations of FIV positive cats	213
Appendix 4-7 Clinical History of FIV positive with FIV PVL below limit of detection	215
Appendix 4-8 Lymphocyte subpopulations of FIV positive with PVL below limit of detection	216
Appendix 4-9 Effect of FIV serostatus and clinical manifestation of gingivostomatitis	216
Appendix 4-10 Correlation between percentage of CD4 ⁺ CD134 ⁺ T lymphocytes and CD4 ⁺ T lymphocytes	217
Appendix 4-11 CD134-usage of pseudotypes bearing Envs from healthy and sick FIV positive cats	218
Appendix 4-13 Sample submission form for the diagnosis of feline infectious disease	219
Appendix 5-1 Representative gating strategy and contour plots to identify lymphocyte subpopulations of mitogen-stimulated PBMC	221
Appendix 5-2 Representative plots for the determination of viability, proliferation and lymphocyte subpopulations	222
Appendix 5-3 Map of Plasmid pLKO-fCD134-IP	222
Appendix 5-4 CD134 expression (as a percentage) of the inducible CD134 CLL cell line at different concentrations of doxycycline.	223
List of Reference	224

List of Tables

Table 2-1 Primers and probes used in this study	55
Table 2-1-1 FIV proviral load quantification	56
Table 2-1-2 Feline CD134 and CXCR4 mRNA quantification	56
Table 2-1-3 FIV envelope cloning and sequencing primers	57
Table 2-1-4 Colony PCR primers	57
Table 2-2 PCR recipes	58
Table 2-3 Thermocycling conditions for FIV full-length env and V5 PCR	59
Table 3-1 Tissue compartments investigated in this study	75
Table 3-2 FIV PVL in three tissue compartments	79
Table 3-3 Statistical comparisons of CD134 mRNA levels between compartments	90
Table 3-4 Statistical comparisons of CXCR4 mRNA levels between compartments	92
Table 3-5 Relationships between CD134 and CXCR4 mRNA and FIV PVL	94
Table 3-6 Relationship between CD134 mRNA: CXCR4 mRNA and FIV PVL	95
Table 4-1 Risk Factors for FIV infection in this study	111
Table 4-2 Demography, lymphocyte subpopulations and PVL data of study population according to FIV serology	113
Table 4-3 Demography, lymphocyte subpopulations and PVL data in FIV infected cats with detectable or undetectable PVL	114
Table 4-4 Demography, lymphocyte subpopulations and PVL data of the study population according to FIV serology and clinical status	121
Table 4-5 Interrelationships between age and lymphocyte subpopulations in FIV negative cats	127
Table 4-6 Interrelationships between age and lymphocyte subpopulations in healthy FIV negative cats	128
Table 4-7 Interrelationships between age and lymphocyte subpopulations in sick FIV negative cats	129
Table 4-8 Interrelationships between age, lymphocyte subpopulations and PVL in FIV positive cats	130
Table 4-9 Interrelationships between age, lymphocyte subpopulations and PVL in FIV positive cats with detectable proviral load	131
Table 4-10 Interrelationships between age and lymphocyte subpopulations in FIV positive cats with undetectable proviral load	132

Table 4-11 Interrelationships between age, lymphocyte subpopulations and PVL in healthy FIV positive cats with detectable proviral load	133
Table 4-12 Interrelationships between age, lymphocyte subpopulations and PVL in sick FIV positive cats with detectable proviral load	134
Table 4-13 Major findings recorded in sick FIV negative and positive cats	137
Table 4-14 Diagnosed co-infections of FIV negative and seropositive cats	137
Table 4-15 Demography, lymphocyte subpopulations and PVL of sick FIV negative and positive cats with and without co-infections	138
Table 4-16 Number of <i>env</i> successfully cloned, used to prepare pseudotypes and tested for CD134 usage from 20 healthy and sick FIV positive cats	143
Table 4-17 Demography, lymphocyte subpopulations and PVL of healthy and sick FIV positive cats from which functional pseudotypes were derived	150
Table 4-18 CD134 usage and autologous neutralisation of HIV(FIV) pseudotypes bearing Env variants from healthy and sick FIV positive cats	151
Table 5-1 Percentage and mean fluorescence intensity of VSVG-GFP or VSVG-TagRFP infection of MCC-fCD134 and CLL-fCD134 cells	164
Table 5-2 Percentage and mean fluorescence intensity of VSVG pseudotypes carrying pCSGW or pCCGW in MCC-fCD134 and CLL-fCD134 cells	165
Table 5-3 Effect of each mitogen on PBMC viability and proliferation at day seven	172
Table 5-4 Effect of concanavalin A and anti-feline CD3 antibody stimulation on lymphocyte subpopulations	174
Table 5-5 Lymphocyte subpopulations of PBMC cultures	176
Table 5-6 Proportions of CD134 ⁺ subpopulations and mean fluorescence intensity of CD134 expression in CD4 ⁺ and CD8 ⁺ T lymphocytes	176
Table 5-7 Percentage of GFP-positive cells in each lymphocyte subpopulation	177

List of Figures

Figure 1-1 Genomic organisation of FIV	24
Figure 1-2 Schematic representation of FIV virion	26
Figure 1-3 Schematic representation of FIV replication cycle	27
Figure 1-4 Schematic representation of FIV Env-receptor interactions and cell entry	28
Figure 1-5 Schematic representations of human, feline and chimaeric CD134 molecules	32
Figure 1-6 The course of FIV infection	34
Figure 1-7 Global distribution of FIV subtypes	37
Figure 1-8 Proposed models of tissue compartmentalisation	40
Figure 2-1 Representative standard curves for the determination of FIV <i>gag</i> and V5 quantity	49
Figure 2-2 Representative standard curves for the determination of fCD134 and fCXCR4 cDNA quantity	50
Figure 2-3 Surface markers staining of CLL-FFF and CLL-FFHH	61
Figure 2-4 Differentiation of CLL-FFF and CLL-FFHH by flow cytometry	62
Figure 2-5 Gating strategy for the identification of T lymphocyte subpopulations	69
Figure 3-1 Study background	73
Figure 3-2 Comparisons of FIV proviral load (PVL) as determined by <i>gag</i> quantitative PCR (qPCR) between 22 tissue compartments	78
Figure 3-3 Comparisons of FIV PVL as determined by GL8 V5 qPCR between 22 tissue compartments	78
Figure 3-4 Comparison of FIV PVL as determined by <i>gag</i> and GL8 V5 qPCRs in 22 compartments and their correlation	79
Figure 3-5 Comparisons of FIV PVL as determined by V5 variant qPCR between 22 tissue compartments	81
Figure 3-6 Comparisons of FIV PVL as determined by V5 variant qPCR between three tissue types	82
Figure 3-7 Absolute quantity of FIV PVL as determined by <i>gag</i> , GL8 V5, B14, B19, B28 and B30 qPCR in 22 compartments	84
Figure 3-8 Relationship between tissue compartments and PVL of V5 variants	85
Figure 3-9 Compartmentalisation of V5 variants	88

	13
Figure 3-10 Comparison of CD134 mRNA levels in nine compartments	90
Figure 3-11 Comparison of CXCR4 mRNA levels in nine compartments	91
Figure 3-12 Comparisons of CD134 and CXCR4 mRNA levels in each tissue compartment	92
Figure 3-13 Relationships between CD134 and CXCR4 mRNA and FIV PVL as determined by <i>gag</i> , GL8 V5, B14, B19, B28 and B30 qPCR in nine tissue compartments	94
Figure 3-14 Relationships between CD134:CXCR4 ratio and FIV PVL as determined by <i>gag</i> , GL8 V5, B14, B19, B28 and B30 qPCR in nine tissue compartments	96
Figure 3-15 Comparisons of CD134 mRNA and CXCR4 mRNA levels in three compartments of FIV negative cats	97
Figure 3-16 Comparisons of CD134 and CXCR4 mRNA levels in three lymphoid tissues between age-matched FIV negative and FIV positive cats	97
Figure 3-17 Comparison of percentage of CD4 ⁺ CD134 ⁺ T lymphocytes between four different compartments	98
Figure 4-1 Study approach	109
Figure 4-2 Effect of gender on FIV serostatus and comparisons of Age, CD4 ⁺ percentage, CD8 ⁺ percentage, CD4:CD8 ratio and CD4 ⁺ CD134 ⁺ percentage between between FIV negative or FIV positive cats	115
Figure 4-3 Effect of gender on FIV serostatus and comparisons of Age, CD4 ⁺ percentage, CD8 ⁺ percentage, CD4:CD8 ratio and CD4 ⁺ CD134 ⁺ percentage between cats testing FIV negative, FIV positive cats with detectable PVL and undetectable PVL	116
Figure 4-4 Effect of gender on FIV serostatus and clinical status and comparisons of Age, CD4 ⁺ percentage, CD8 ⁺ percentage, CD4:CD8 ratio and CD4 ⁺ CD134 ⁺ percentage between groups according to their FIV serostatus and clinical status	122
Figure 4-5 Correlations between percentage of CD4 ⁺ T lymphocytes and FIV PVL, CD4:CD8 ratio and FIV PVL in all FIV positive cats, relationship between CD4:CD8 ratio and percentage of CD4 ⁺ CD134 ⁺ T lymphocytes in FIV positive cats with detectable PVL, comparison of PVLs between healthy and sick FIV positive cats, relationship between percentages of CD4 ⁺ CD134 ⁺ T lymphocytes and FIV PVL in healthy FIV positive cats and sick FIV negative cats	126

Figure 4-6 Comparisons of Age, percentage of CD4 ⁺ lymphocytes, percentage of CD8 ⁺ lymphocytes, CD4:CD8 ratio and percentage of CD4 ⁺ CD134 ⁺ lymphocytes between groups according to their FIV serostatus and co-infections	139
Figure 4-7 The declining trend in the percentage of CD4 ⁺ CD134 ⁺ T lymphocytes	140
Figure 4-8 Unrooted maximum likelihood tree of 141 full SU amino acid sequences	146
Figure 4-9 Unrooted maximum likelihood tree of 141 amino acid sequences spanning V3-V6 loop	147
Figure 4-10 Unrooted maximum likelihood tree of 76 full-length Env amino acid sequences	148
Figure 4-11 Representative result of CD134-usage assay for HIV(FIV) pseudotypes bearing Env variants derived from healthy and sick FIV infected cats	152
Figure 4-12 Autologous viral neutralisation assay of HIV(FIV) pseudotypes bearing Envs derived from healthy and sick FIV positive cats	153
Figure 5-1 Agarose gel illustration and plasmid maps of pCSGW	163
Figure 5-2 Representative images of MCC-fCD134 and CLL-fCD134 infected with HIV(VSVG)-GFP or HIV(VSVG)-TagRFP pseudotypes	164
Figure 5-3 Representative images of MCC-fCD134 and CLL-fCD134 infected with VSVG pseudotypes carrying either pCSGW or pCCGW.	166
Figure 5-4 Plasmid maps of pCSRW and pCCRW	166
Figure 5-5 Outline of competitive entry assay	168
Figure 5-6 Representative image of HIV Capsid p24 immunoblot	169
Figure 5-7 Representative result of competitive entry assay in CLL-FFF and CLL-FFHH cells	170
Figure 5-8 Representative image of CLL-FFF and CLL-FFHH co-infected with GL8-TagRFP and B28-GFP pseudotypes	170
Figure 5-9 Representative images from inverted microscopy of mitogen-stimulated PBMC	173
Figure 5-10 PBMC viability and proliferation index after mitogens stimulation	173
Figure 5-11 Composition of lymphocyte subpopulations following ConA and anti-CD3 stimulation of PBMC	175

Figure 5-12 Representative contour plots of expanded lymphocyte cultures from three cats infected with B28-GFP pseudotype	177
Figure 5-13 Representative contour plots of expanded lymphocyte cultures from three cats stained for CD8 and CD134	178
Figure 5-14 Relationship between the percentage of CD134 ⁺ T lymphocytes in culture and infectivity of GFP-FIV pseudotypes	178
Figure 6-1 Proposed model for the role of resident CD134 ⁺ target cell availability in FIV tissue compartmentalisation	188
Figure 6-2 Proposed model for the role of CD134 ⁺ target cells in the emergence of CRD2-independent variants of FIV	190

Acknowledgements

First of all, I would like to express my deepest gratitude to my primary supervisor, Professor Margaret J. Hosie, for her kind support, encouragement and trust over the last three years.

I would also like to express my gratitude to my co-supervisor, Professor Brian J. Willett, for his opinions and support.

I would like to give thanks to the Petplan Charitable Trust for funding some part of this project.

I would like to give thanks to Dr. Sam Wilson for providing me plasmids, Dr. Idoia Busnadiego and Dr. Pawel Beczkowski for their opinions on some of the study approaches.

I also thank members of Veterinary Diagnostic Service, for their help with the samples and clinical history.

I thank my colleagues from the retrovirus research laboratory; Dr. Ayman Samman, Ms. Emily Goldstein, Mr. Matthew Harris, Ms. Nicola Logan, Ms. Linda McMonagle, Ms. Yasmin Parr, for their wonderful friendship.

I would like to express my gratitude to my scottish family, David and Lorraine Allan, my time in Scotland would be a lot harder without their friendship and hospitality.

I would like to express my sincere gratitude to Dr. Sureemas Nitikanchana for her belief and encouragement during the most critical time of the study.

Finally, I am forever indebted to my beloved family for their love, support and encouragement over the years. I dedicate this thesis to them.

Author's Declaration

I declare that this thesis is entirely the result of my own work, unless specifically stated and referenced. This thesis has not been previously submitted for any other degree at the University of Glasgow or any other institutions.

Navapon Techakriengkrai

June 2016

List of Abbreviations

Abbreviation	Definition
Ab	antibody
Ag	antigen
α 1-AGP	alpha-1-acid glycoprotein
ANOVA	analysis of variance
APC	antigen presenting cell
APOBEC	apolipoprotein B mRNA-editing catalytic polypeptide
A647	alexa fluor 647 fluorophore
BBB	blood-brain barrier
BHQ	black hole quencher dye
BM	bone marrow
bp	base pair
B14	B14 V5 variant of GL8 strain of FIV
B19	B19 V5 variant of GL8 strain of FIV
B28	B28 V5 variant of GL8 strain of FIV
B30	B30 V5 variant of GL8 strain of FIV
B2542	B2542 strain of FIV
°C	degree celsius
CA	capsid protein
cDNA	complementary deoxyribonucleic acid
CFSE	carboxyfluorescein succinimidyl ester
CI	confidence interval
CLL-FFF	canine chronic lymphocytic leukaemia cell line expressing feline CD134
CLL-FFHH	canine chronic lymphocytic leukaemia cell line expressing chimaeric feline/human CD134
CLL-HHH	canine chronic lymphocytic leukaemia cell line expressing human CD134
cm	centimetre
CM	central memory
CMI	cell-mediated immune responses
CMV	cytomegalovirus
CNS	central nervous system

Abbreviation	Definition
CPG41	CPG41 strain of FIV
CPM	count per minute
Con A	concanavalin A
CRD	cysteine rich domain
CrFK	Crandell Rees feline kidney cell line
Ct	cycle threshold
CTL	cytotoxic T lymphocyte
CV	coefficients of variation
DC	dendritic cell
DMEM	Dulbecco's modified Eagle's Medium
DMSO	dimethylsulfoxide
DNA	deoxyribonucleic acid
dNTPs	deoxynucleotide
DU	deoxyuridine triphosphatase
EDTA	ethylenediaminetetraacetic acid
ELISA	enzyme-linked immunosorbent assay
ELISpot	enzyme-linked immunospot assay
EM	effector memory
Env	envelope glycoprotein
FAM	6-carboxyfluorescein reporter dye
f β -actin	feline beta actin
FBS	fetal bovine serum
FCV	feline calicivirus
FCoV	feline coronavirus
FeLV	feline leukaemia virus
FeRV	feline retrovirus
FITC	fluorescein fluorophore
FIV	feline immunodeficiency virus
FHV	feline herpesvirus
FPs	fluorescent proteins
FPV	feline parvovirus
FSC-A	forward scatter area
x g	x times to gravity of earth
GALT	guts associated lymphoid tissue
gDNA	genomic deoxyribonucleic acid

Abbreviation	Definition
GFP	green fluorescent protein
GL8	Glasgow 8 strain of FIV
g/l	gram per litre
h	hour
HCV	hepatitis C virus
HEK293T	Human embryonic kidney cell line containing the simian vacuolating virus 40 (SV40) large T-antigen
HIV	human immunodeficiency virus
HMI	humoral immune responses
HRPO	horseradish peroxidase
IDU	intravenous drug user
IF	immunofluorescence
IL-2	interleukin 2
IN	integrase enzyme
KKS	KKS strain of FIV
LB broth	Luria-Bertani broth
LN	lymph node
LPS	lipopolysaccharide
LSSmOrange	large stokes shift mOrange fluorophore
LTR	long terminal repeat
M	month
MA	matrix protein
MDLN	mediastinal lymph node
MES	2-(N-morpholino)ethanesulfonic acid
MFI	mean fluorescent intensity
mg	milligram
min	minute
ml	millilitre
ML	maximum likelihood
mM	millimolar
mm	millimetre
mRNA	messenger ribonucleic acid
MSLN	mesenteric lymph node
NAb	neutralising antibody
NC	nucleocapsid protein

Abbreviation	Definition
NCSU1	NCSU1 strain of FIV
ng	nanogram
nm	nanometre
ORF	open reading frame
PBMC	peripheral blood mononuclear cell
PBS	phosphate buffer saline
PBST	PBS plus Tween® 20
PCA	principal component analysis
PCR	polymerase chain reaction
PCV	packed cell volume
PE	phycoerythrin fluorophore
PE-Cy7	phycoerythrin-Cy 7 fluorophore
PEI	Polyethylenimine
pg	picogram
PHA	phytohaemagglutinin
PLN	popliteal lymph node
pMHC	peptide-major histocompatibility complex
pMol	picomole
PPR	PPR strain of FIV
PR	protease enzyme
PSLN	prescapular lymph node
PVL	proviral load
qPCR	quantitative polymerase chain reaction
RER	rough endoplasmic reticulum
rev	regulator of expression of virion proteins
RNA	ribonucleic acid
RPLN	retropharyngeal lymph node
RPMI 1640	Roswell Park Memorial Institute medium 1640
RRE	rev-responsive element
RT	reverse transcriptase enzyme
R10	RPMI1640 supplemented with 10% FBS
SD	standard deviation
SDF-1	stromal cell-derived factor 1
sec	second
SFFV	spleen focus-forming virus

Abbreviation	Definition
SIV	simian immunodeficiency virus
SMLN	submandibular lymph node
SPF	specific pathogen free
SSC-A	side scatter area
SU	surface subunit of envelope glycoprotein
TagRFP	Tag red fluorescent protein
TagRFP 657	Tag red fluorescent protein 657
TAMRA	6-carboxytetramethylrhodamine quencher dye
TCID ₅₀	tissue culture infectious dose 50%
TCR	T cell receptor
TM	transmembrane subunit of envelope glycoprotein
TMB	3,3',5,5'-tetramethylbenzidine substrate
TM2	TM2 strain of FIV
TNF- α	tumour necrosis factor alpha
TNFR	tumour necrosis factor receptor
TRIM5	tripartite motif protein 5
Tween® 20	polyoxyethylene
UK	United Kingdom
μg	microgram
μl	microlitre
μM	micromolar
V loop	variable loop
vif	viral infectivity factor
VSVG	vesicular stomatitis virus
v/v	volume per volume
W	week
w/v	weight per volume
w/w	weight per weight
WHO	World Health Organization
Y	year
YFP	yellow fluorescent protein
YY	Yakuma Yellow reporter dye
7-AAD	7-aminoactinomycin D

Chapter 1 Introduction

Feline immunodeficiency virus (FIV) is an enveloped, RNA virus, which belongs to the genus *Lentivirus* within the *Retroviridae* family (Willett and Jarrett, 1995). Antibodies against FIV have been detected in more than 20 species within the Felidae family, including bobcats (*Lynx rufus*), lions (*Panthera leo*), pumas (*Puma concolor*), spotted hyenas (*Crocuta crocuta*) and members of the Hyaenidae family, as well as domestic cats (*Felis catus*) (Harrison et al., 2004, McEwan et al., 2008, Troyer et al., 2008, Lagana et al., 2013, Sykes, 2013). As well as being an important veterinary pathogen, FIV shares many analogies with its human counterpart, human immunodeficiency virus (HIV) (Bendinelli et al., 1995, Bienzle, 2014). Both viruses target similar cell types and demonstrate similar clinical manifestations, with the progressive decline in CD4⁺ T lymphocyte numbers and inversion of the CD4:CD8 ratio being hallmarks of both infections (Bendinelli et al., 1995, Yamamoto et al., 2007, Willett and Hosie, 2008, Willett and Hosie, 2013, Sykes, 2013). These similarities illustrate the comparative value of the study of FIV infection as an alternative model for HIV infection in people, in addition to its veterinary significance (Gardner, 1991, Yamamoto et al., 2010, Bienzle, 2014, Moench, 2014).

1.1 Virology

1.1.1 Genomic Organisation

The size of the FIV genome is approximately 9,500 base pairs. Similar to other retroviruses, long terminal repeats (LTR) border the 5' and 3' ends of the FIV genome (Figure 1-1). These LTR contain several elements important for transcriptional regulation (Miyazawa et al., 1994, Elder and Phillips, 1995). The FIV genome also contains the three major open reading frames (ORF), *gag*, *pol* and *env*, which are present in all retroviruses and encode the structural and non-structural proteins (Talbot et al., 1989, Miyazawa et al., 1994). The *gag* gene encodes the matrix (MA, p17), capsid (CA, p24) and nucleocapsid (NC, p7) proteins required for the formation of mature viral particles (Elder and Phillips, 1995, Affranchino and Gonzalez, 2010, Luttge and Freed, 2010). The *pol* gene of FIV encodes the enzyme deoxyuridine triphosphatase (DU, p14) in addition to the protease (PR, p13), reverse transcriptase (RT, p51) and integrase (IN, p31)

enzymes (Elder et al., 1992, Wagaman et al., 1993, Elder and Phillips, 1995). The DU enzyme is not present in any of the primate lentiviruses (Elder et al., 1992); it prevents misincorporation of uracil into DNA during reverse transcription and therefore increases the fidelity of FIV replication (Lerner et al., 1995). This function of DU is similar to that of the accessory protein encoded by the *vpr* gene, which is present in the HIV genome but not the FIV genome (Miyazawa et al., 1994, Elder and Phillips, 1995, Mansky et al., 2000, Malim and Emerman, 2008, Strebel, 2013). In addition to *vpr*, FIV also lacks the *vpu*, *nef* and *tat* genes that are found in HIV (Talbot et al., 1989, Miyazawa et al., 1994, Elder and Phillips, 1995); the accessory proteins Vpu, Nef and Tat play important roles in antagonising intra-cellular antiviral responses in HIV infected cells (Malim and Emerman, 2008, Strebel, 2013). However, similar to HIV, FIV contains an accessory gene (*vif*) that encodes viral infectivity factor (Vif); the FIV and HIV Vif proteins have similar functions, counteracting the cellular protein apolipoprotein B mRNA-editing catalytic polypeptide 3 (APOBEC3) (Elder et al., 2008, Malim and Emerman, 2008, Troyer et al., 2013, Strebel, 2013).

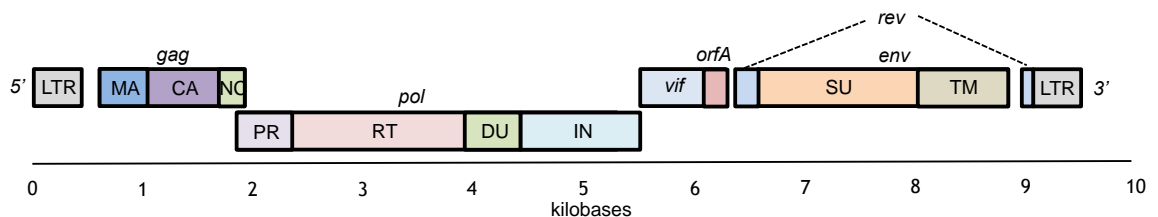


Figure 1-1 Genomic organisation of FIV; LTR: long terminal repeat, *gag*; MA: matrix, CA: capsid, NC: nucleocapsid, *pol*; PR: protease, RT: reverse transcriptase, DU: deoxyuridine triphosphatase, IN: integrase, *vif*: viral infectivity factor, *orfA*: open reading frame A, *rev*: regulator of expression of virion proteins, *env*; envelope glycoproteins, SU: surface, TM: transmembrane (adapted from (Elder and Phillips, 1995, Kenyon and Lever, 2011))

Another unique element in the FIV genome is the open reading frame A (*orfA*), originally known as *orf2* (Elder and Phillips, 1995). *OrfA* encodes a 77 amino acid non-structural protein that has been shown to play a role in viral particle formation, the induction of cell cycle arrest and transactivation of viral protein expression (de Parseval and Elder, 1999, Gemeniano et al., 2003, Gemeniano et al., 2004). This transactivating function of FIV *orfA* is similar to that of HIV *tat* (de Parseval and Elder, 1999). Moreover, *orfA* influences CD134 expression levels, host cell tropism and replicative capacity (Waters et al., 1996, Hong et al., 2010, Troyer et al., 2013). Immediately downstream of *orfA* is the

env gene, which encodes the surface (SU, gp120) and transmembrane (TM, gp41) subunits of the envelope (Env) protein (Talbot et al., 1989, Miyazawa et al., 1994, Elder and Phillips, 1995). Similar to HIV Env, the FIV Env is a heavily glycosylated protein in which the numbers of potential N-linked glycosylation sites on SU and TM differ between strains (Talbot et al., 1989, Stephens et al., 1991, Verschoor et al., 1993). The high-mannose glycans on Env play an important role in FIV and HIV immune evasion, by shielding neutralising epitopes from antibodies (Pejchal and Wilson, 2010, Yamamoto et al., 2010). Similar to the other lentiviruses, the *rev* (regulator of expression of virion proteins) gene sequence comprises two overlapping exons flanking *env* (Elder and Phillips, 1995). Rev is responsible for the regulation of viral protein transcription by binding to viral mRNA at the Rev-responsive element (RRE) located downstream of the *env* gene (Cochrane et al., 1990, Olsen et al., 1990a, Olsen et al., 1990b, Phillips et al., 1992).

1.1.2 Structure of FIV

Under the transmission electron microscope, the mature FIV virion appears ellipsoid in shape, approximately 100 to 125 nanometers in diameter, with a typical lentiviral cone-shaped nucleocapsid (Pedersen et al., 1987). Like all retroviruses, FIV is an enveloped virus with a three-layered structure (Figure 1-2). The genome-nucleocapsid complex comprises two identical, positive-sense, single strands of FIV genomic RNA, with helical symmetry, in association with the p7 nucleocapsid protein (NC). This complex is enclosed within an icosahedral capsid, formed by multimerisation of Gag p24 capsid proteins (CA, p24). The outermost envelope of FIV comprises a lipid membrane derived from the host cell membrane into which the trimeric glycoprotein spikes consisting of surface (SU, gp120) and transmembrane (TM, gp41) subunits of Env are inserted. The viral envelope is lined with the matrix protein (MA, p17), which provides the basic structure of the virion. In addition to the viral genome, the viral protease (PR, p13), reverse transcriptase (RT, p51) and integrase (IN, p31) enzymes also reside within the viral core.

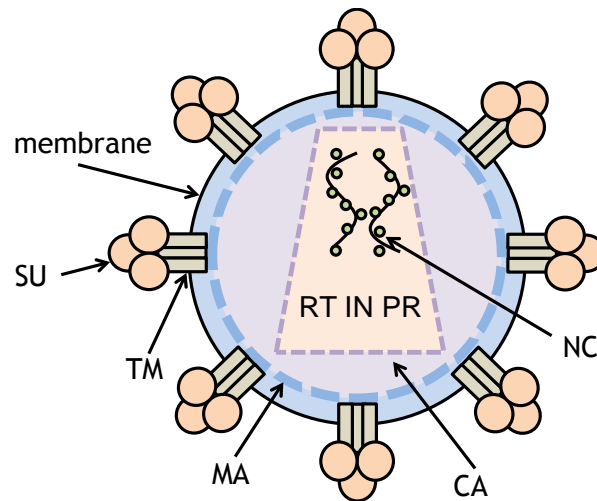


Figure 1-2 Schematic representation of the mature FIV virion. The outer layer of the mature FIV virion is composed of a cellular lipid bilayer membrane (envelope) containing multiple trimeric glycoprotein spikes (SU, gp120 and TM, gp41). This outer layer is lined with the matrix (MA, p17) protein. The icosahedral core is formed by p24 capsid (CA) multimers and contains 2 identical genome-nucleoprotein (NC) complexes, with helical symmetry, and the reverse transcriptase (RT), protease (PR) and integrase (IN) enzymes.

1.1.3 The replication cycle of FIV

FIV binds the target cell via interactions between the SU of Env and the primary receptor CD134 on the target cell surface (Figure 1-3, Step 1) (de Parseval et al., 2004a, Shimojima et al., 2004). This interaction leads to a conformational change which allows an interaction with the co-receptor CXCR4 to occur (Willett and Hosie, 2008). Target cell entry and FIV tropism are discussed in further detail below (Section 1.1.4). Co-receptor binding leads to membrane fusion and target cell entry (Figure 1-3, Step 2). After entering the target cell, the viral capsid core disintegrates and the nucleocapsid is released in the cytoplasm (Figure 1-3, Step 2). Next, the viral RNA is reverse transcribed into double-stranded DNA that interacts with cellular and viral proteins before being transported into the nucleus and integrated into the cellular genome as provirus (Figure 1-3, Step 3 and 4). Similar to the primate lentiviruses, the FIV provirus preferentially integrates into actively transcribed genes (Kang et al., 2006). Depending on the cellular activation state, proviral DNA may be transcriptionally active or inactive (McDonnell et al., 2013, Sykes, 2013). Upon receiving an activation signal, either from cytokines or by other mechanisms, the proviral DNA is transcribed by the host cellular RNA polymerase into full-length RNA transcripts (Kenyon and Lever, 2011, Flint et al., 2015). Some of these full-

length RNA transcripts are exported into the cytoplasm and serve as mRNA for viral protein production, whereas other transcripts become progeny viral genomes and are encapsidated into newly formed capsid cores (Figure 1-3, Step 5) (Kenyon and Lever, 2011, Flint et al., 2015). This core structure then migrates to the cell membrane where mature Env proteins are clustered, the virus receives its envelope derived from the host cell membrane and mature Env trimers, buds from the cell membrane and exits the cell (Figure 1-3, Step 6) (Kenyon and Lever, 2011).

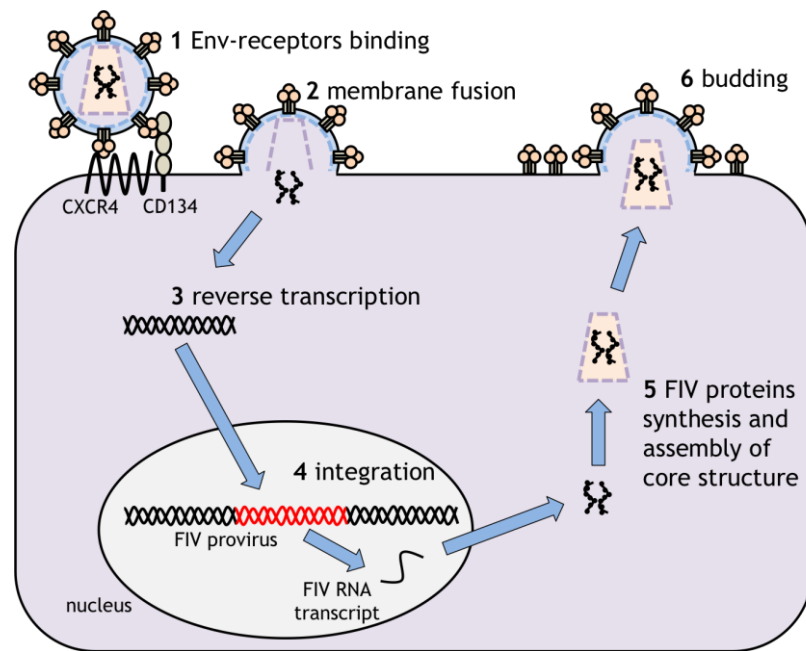


Figure 1-3 Schematic representation of FIV replication cycle (adapted from (Sykes, 2013))

1.1.4 Virus entry and target cell tropism

Virus entry is the first critical step of any viral infection, in which the interaction between the viral envelope and the receptor molecule on the surface of the host cell determines target cell tropism and pathogenesis. Similar to HIV, FIV utilises a two-receptor mechanism for infection (Elder et al., 2008, Willett and Hosie, 2008, Klasse, 2012), but unlike HIV, which utilises the CD4 molecule, the primary receptor for FIV infection is the T cell activation marker CD134 (de Parseval et al., 2004a, Shimojima et al., 2004). The interaction between FIV Env SU and CD134 (Figure 1-4, step 1) leads to a conformational modification of SU and a subsequent interaction between Env and CXCR4, the co-receptor for FIV infection (Figure 1-4, step 2). CXCR4 binding triggers the insertion of the fusion

peptide of TM into the cell membrane (Figure 1-4, step 3). To date, all FIV isolates utilise CXCR4 as the co-receptor and none interact with CCR5 (Kenyon and Lever, 2011, Willett and Hosie, 2008, Willett and Hosie, 2013).

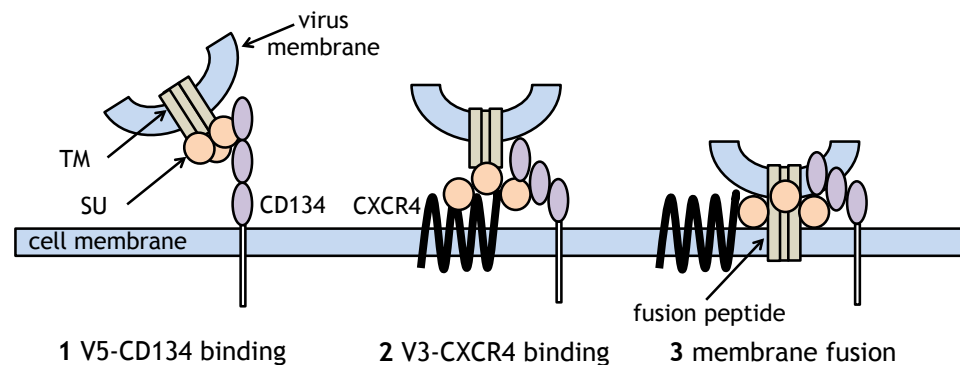


Figure 1-4 Schematic representation of FIV Env-receptor interactions and cell entry

1.1.4.1 Envelope glycoprotein

Similar to HIV, the mRNA transcribed from the FIV *env* gene is translated into a primary polyprotein on polyribosomes associated with the rough endoplasmic reticulum (RER), where the addition of N-linked carbohydrate occurs at the same time. The molecular weight of the Env precursor varies between FIV strains, depending on the number of potential N-linked glycosylation sites (Stephens et al., 1991, Verschoor et al., 1993). Approximately half of the Env mass is associated with the carbohydrate moieties. At the RER, Env monomers oligomerise and form trimers that are subsequently transported to the golgi complex and cleaved by cellular furin into mature SU (gp120) and TM (gp41) (McCune et al., 1988, Stephens et al., 1991, Verschoor et al., 1993). The mature SU and TM subunits are linked by a non-covalent association (Schulz et al., 1992) and the mature, trimeric gp160 glycoprotein is then transported to the cell surface, prior to incorporation into new virions (Affranchino and Gonzalez, 2014). There are eight variable regions (V) in Env distributed amongst the constant regions (C), six are located on SU (V1 - V5) and three on TM (V6 - V8) (Pancino et al., 1993). The V3 and V5 loops on SU are involved, respectively, in the interaction with CXCR4 and CD134 (de Parseval et al., 2005, Willett et al., 2006a, Willett et al., 2007, Sundstrom et al., 2008, Willett and Hosie, 2008, Hu et al., 2010, Willett et al., 2010, Hu et al., 2012).

Since Env is the only FIV protein exposed to the extracellular environment, it is under strong selective pressure from neutralising antibodies (NAb) and other restriction molecules. This leads to a high rate of mutation and the emergence of multiple Env variants during the course of infection (Hosie et al., 2002, Kraase et al., 2010, Willett et al., 2010, Beczkowski et al., 2014b). These variants often contain mutations in key amino acid residues responsible for the interactions between Env and cellular receptors which lead to altered cell tropism (see below in section 1.1.4.3) (Hosie et al., 2002, Kraase et al., 2010, Beczkowski et al., 2014b).

1.1.4.2 CD134

CD134 is a member of the tumour necrosis factor receptor (TNFR) superfamily (Croft, 2010). A high degree of similarity was observed between feline and human CD134, in both amino acid sequence and structure (Shimajima et al., 2004, de Parseval et al., 2005). However, despite these similarities, human CD134 does not mediate FIV infection (Shimajima et al., 2004, de Parseval et al., 2005), which is one of the mechanisms prohibiting cross-species transmission of FIV. FIV has been shown to bind and infect feline CD134-expressing target cell lines via a direct interaction between FIV Env SU and the CD134 molecule (de Parseval et al., 2004a, Shimajima et al., 2004). Also, pre-treatment with soluble CD134 allows FIV infection of CD134⁻CXCR4⁺ target cells, presumably by inducing a conformational change, consistent with the model shown in Figure 1.4 (de Parseval et al., 2005, de Parseval et al., 2006).

CD134 expression is highest on activated T lymphocytes, after antigen recognition, although lower levels of expression have been reported on human and murine B-lymphocytes and dendritic cells (DC) (Mallett et al., 1990, Gramaglia et al., 2000, Rogers et al., 2001, Croft, 2010). In the cat, CD134 expression is restricted to activated CD4⁺ T lymphocytes (de Parseval et al., 2004a, Shimajima et al., 2004, Willett et al., 2007). Activation of CD4⁺ T lymphocytes has 3 phases, namely the induction, proliferation and effector phases (Murphy and Janeway, 2012, Shipkova and Wieland, 2012). The induction phase requires 3 external signals; the first is a signal from T cell receptor (TCR) recognition of the major histocompatibility complex class II (MHC II)-peptide complex presented on professional antigen presenting cells (APC) (Murphy and

Janeway, 2012). Secondly, CD28, a costimulatory molecule constitutively expressed on T lymphocytes, signals engagement with its cognate ligand B7.1 (CD80) and B7.2 (CD86) expressed on the surface of the APC (Harding et al., 1992, Dubey et al., 1995). After this initial induction phase, activated T lymphocytes undergo massive clonal expansion and cytokines in the microenvironment, the third signal, play an important role in T lymphocyte polarisation (Murphy and Janeway, 2012). In this proliferation phase, prior CD28/B7 engagement results in CD134 expression on T lymphocytes, usually within 24-28 hours (Gramaglia et al., 1998, Walker et al., 1999). CD134 expression is important for T lymphocyte longevity and the generation of memory T lymphocytes (Gramaglia et al., 2000, Weinberg et al., 2004, Hori, 2005, Song et al., 2008, Murphy and Janeway, 2012). In the absence of a costimulatory signal from CD134/CD134L (CD252) engagement, activated CD4⁺ T lymphocytes undergo apoptosis (Weinberg et al., 1998, Rogers et al., 2001).

The high level of CD134 expression on CD4⁺ T lymphocytes is consistent with the selective infection of CD4⁺ T lymphocytes in the early phase of FIV infection and the decline in CD4⁺ T lymphocyte numbers observed during the course of infection (English et al., 1993, Willett and Hosie, 2013). However, as disease progresses, FIV tropism expands to include a broader range of target cells, such as B-lymphocytes, CD8⁺ T lymphocytes and cells of the monocyte/macrophage lineage (Brunner and Pedersen, 1989, English et al., 1993, Dean et al., 1996, de Parseval et al., 2004a, Shimojima et al., 2004). The susceptibility to FIV infection of CD8⁺ T lymphocytes and CD14⁺ monocytes during the chronic phase of infection is intriguing, as these cells do not express, or only express at low levels, CD134 (0.1% and 0.2%, respectively) (de Parseval et al., 2004a, Willett et al., 2007). Nonetheless, CD134 was shown to be upregulated when splenic macrophages were activated with lipopolysaccharide (LPS) (Willett et al., 2007). Increased levels of plasma LPS, as a result of microbial translocation, are frequently observed in HIV infected individuals in the later stage of infection (Sandler and Douek, 2012, Marchetti et al., 2013). Although this phenomenon has yet to be investigated in FIV-infected cats, it might explain the expanded tropism into cells of the monocyte/macrophage lineage displayed by FIV in the later phase of infection. Another explanation for the expanded tropism of FIV in late infection might be associated with the emergence of FIV variants that are less dependent on CD134 for infection (see 1.1.4.3 below).

1.1.4.3 Different CD134 usage amongst FIV strains

In common with other members of the TNFR superfamily, the feline CD134 molecule contains 3 cysteine rich domains (CRD 1-3) (Figure 1-4) (Bodmer et al., 2002, Willett et al., 2006b). The receptor-binding site of FIV Env was first mapped to the CRD1 region of the CD134 molecule, in studies using the PPR strain of FIV (de Parseval et al., 2005). However, subsequent studies reported that some strains of FIV require additional determinants on CRD2 for infection (Willett et al., 2006a, Willett et al., 2006b). According to the requirement for CRD2 as well as CRD1, FIV strains could be assigned to 2 groups, CRD2-dependent or CRD-2 independent (Figure 1-5). It has been postulated that the additional determinants on CRD2 might provide CRD2-dependent strains with more efficient interactions with CD134, as CRD2-dependent isolates have been shown to be more resistant to antagonism by a monoclonal antibody recognising feline CD134 as well as soluble CD134 ligand (Willett et al., 2009, Willett et al., 2007, Willett et al., 2010).

It was observed that CRD2-dependent strains of FIV were isolated from cats during the acute phase of infection (GL8, TM2, CPG41 and NCSU1) (Hosie and Jarrett, 1990, Miyazawa et al., 1991, Diehl et al., 1995, Yang et al., 1996), whereas CRD2-independent strains were either lab-adapted or were strains that emerged after several years of infection (PPR, B2542 and GL8 V5 variants) (Phillips et al., 1990, Sodora et al., 1995, Willett et al., 2010). The emergence of CRD2-independent Env variants was observed *in vivo*, in both experimentally and naturally infected cats (Kraase et al., 2010, Beczkowski et al., 2014b). Therefore there appeared to be a relationship between CRD2-dependence and the selection of dominant Env variants during the course of FIV infection. This hypothesis was supported by the findings from a study conducted in cats experimentally inoculated with a reconstituted quasispecies composed of GL8 and variants containing CRD2-dependent or -independent Envs (Willett et al., 2013). Throughout the 21 weeks period of study, the variants of GL8 containing CRD2-dependent Envs replicated faster and these variants selectively expanded in all cats. There was no evidence that the failure of the variants with CRD2-independent Envs variants to replicate was associated with either the presence of NAb or cellular immune responses (Willett et al., 2013).

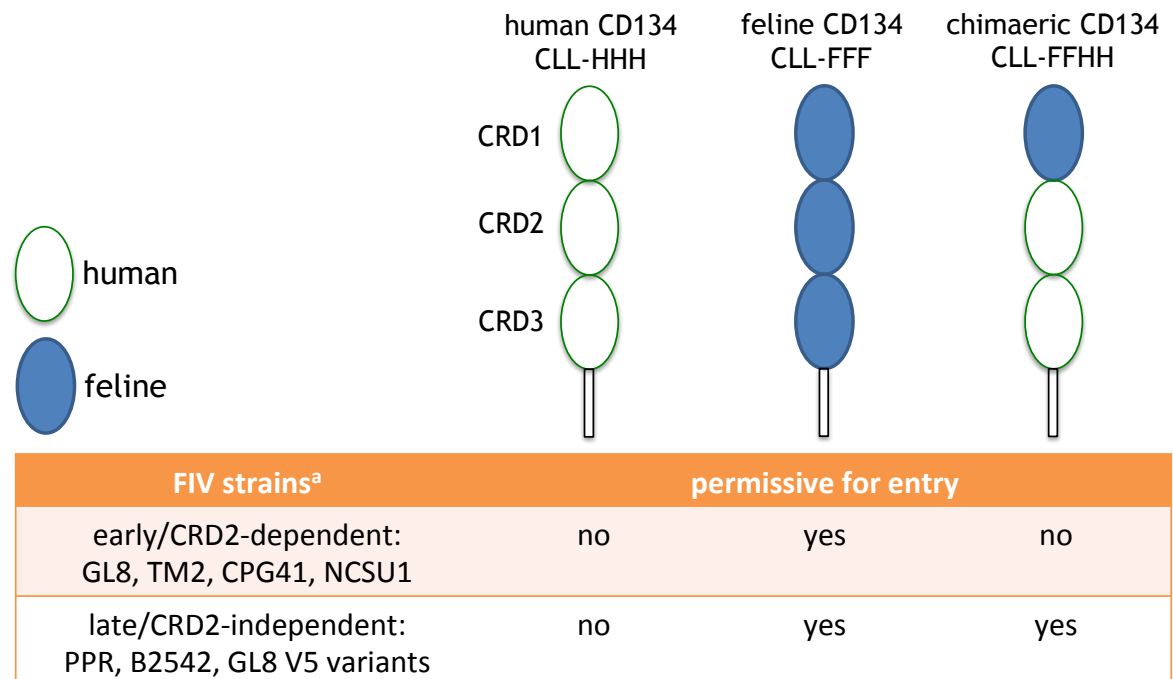


Figure 1-5 Schematic representations of human, feline and chimaeric CD134 molecules. Oval shapes represent cysteine rich domains (CRD) 1 to 3. Green and blue ovals represent domains of human and feline CD134, respectively. A panel of cell lines (CLL-HHH, CLL-FFF and CLL-FFHH, described in Section 2.2.1.2) expressing different chimaeric molecules of CD134 were used to determine the CRD2 dependence of FIV strains. ^asummarised from (Willett et al., 2006b, Willett et al., 2010)

1.1.4.4 Evolution of FIV CD134 usage

The results of these *in vivo* studies provided strong evidence that CRD2-dependent variants have a selective advantage over CRD2-independent variants in the early phase of FIV infection. As positive correlations between target cell numbers and viral replication have been reported in both HIV and SIV infections (Schwartz et al., 2002, Klatt et al., 2008), it is possible that CRD2-dependent FIV variants could infect and replicate more efficiently in the acute phase of infection due to the early expansion of activated CD4⁺CD134⁺ T lymphocytes. In contrast, later in infection, the decreasing numbers of CD4⁺ T lymphocytes removes this selective advantage and so CRD2-independent variants emerge. The expanded target cell tropism observed in the later phase of infection supports this hypothesis (Dean et al., 1996, English et al., 1993, Willett and Hosie, 2008, Willett and Hosie, 2013). The dynamics of the CD4⁺CD134⁺ T lymphocyte population and its role in FIV pathogenesis had not been addressed prior to this study, but were investigated and are reported in Chapter 4.

1.1.4.5 CXCR4

CXCR4 was identified as a co-receptor for FIV following the observation that mutations in the V3 loop of Env led to the induction of syncytium formation in CrFK cells (Siebelink et al., 1995, Verschoor et al., 1995), similar to an observation for HIV (Feng et al., 1996). The role of CXCR4 as an FIV receptor was confirmed when it was demonstrated that the addition of a CXCR4-specific antibody (12G5), the natural ligand for CXCR4 (stromal cell derived factor-1, SDF-1) or the anti-FIV Env monoclonal antibody vpg71.2 inhibited FIV-Env-mediated target cell fusion (Willett et al., 1997, Hosie et al., 1998). To date, all primary and lab-adapted isolates of FIV require CXCR4 for infection (Willett et al., 1997, Richardson et al., 1999, Willett and Hosie, 2008). The key residues involved in the Env-CXCR4 interaction were mapped to the V3 loop of SU and the second extracellular loop of CXCR4 (Willett et al., 1998, Hosie et al., 2002, Hu et al., 2010, Hu et al., 2012). Similar to HIV, binding of the FIV Env to the primary receptor results in conformational changes in Env and the exposure of residues which were previously hidden, which permits binding to the secondary receptor (Figure 1-4). It is notable that late FIV strains, such as PPR, were shown to have a more “open” conformation, which was associated with the ability to infect target cells without prior CD134 binding (Hu et al., 2012). However, exposure of the key determinants on the V3 region of Env involved in CXCR4 binding likely renders late strains of FIV more susceptible to antibody neutralisation (Hosie et al., 2002, Hu et al., 2012). This might explain why CRD2-independent variants emerge only in the later phase of infection, when host immune responses are already weakened.

1.2 Natural History of FIV infection

Similar to HIV, FIV infection can be divided into three phases; the primary (acute), latent and terminal (immunodeficiency) phases (Figure 1-6) (Sykes, 2013, Flint et al., 2015). The primary phase lasts 2-8 weeks, with mild fever, lethargy and peripheral lymphadenopathy being the most common clinical signs (Bendinelli et al., 1995, Hosie et al., 2009, Sykes, 2013). During this phase, FIV replicates exponentially and can be detected in plasma as early as 2 weeks post infection, with the peak viraemia being detected 8-12 weeks after infection, when virus is disseminated throughout the body (Bach et al., 1994, Beebe et al.,

1994, Hosie et al., 2009, Sykes, 2013). The level of viraemia was shown to be positively correlated with the inoculum dose (Roche et al., 2013). Concurrently with the increase in plasma viraemia, there is a decline in lymphocyte populations, especially the CD4⁺ T lymphocyte subset.

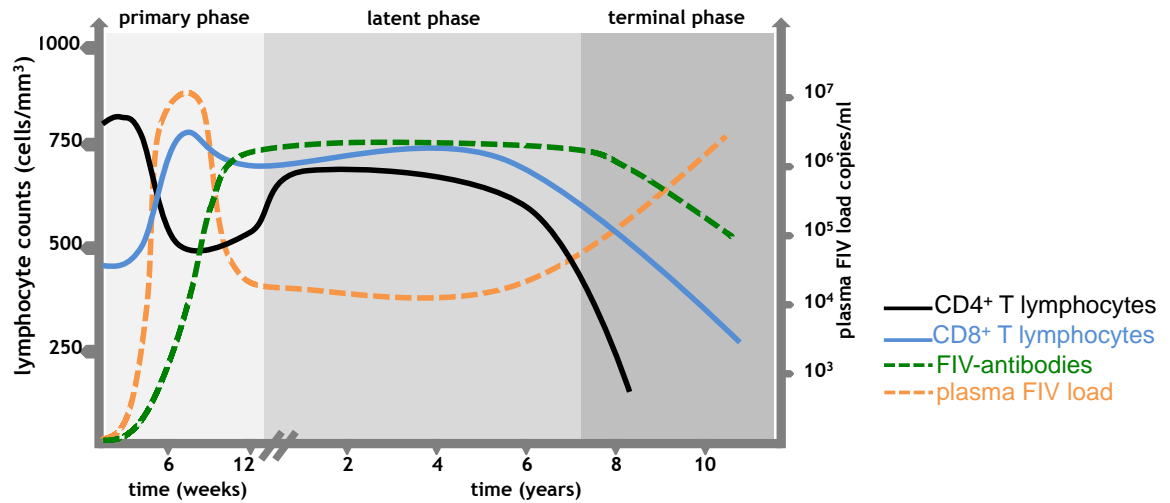


Figure 1-6 The course of FIV infection, showing the primary, latent and terminal phases. The X-axis shows the timescale in weeks for the primary phase and in years for the latent and terminal phases. The left Y-axis shows CD4⁺ and CD8⁺ T lymphocyte numbers (cells/mm³). The right Y-axis shows the plasma viral loads. (adapted from (Sykes, 2013))

After reaching its peak, the decline in FIV load coincides with the development of FIV-specific immune responses and the appearance of both CD8⁺ T lymphocytes and FIV specific antibodies (Egberink and Horzinek, 1992, Willett et al., 1993, English et al., 1994, Beatty et al., 1996, Yamamoto et al., 2007). Concurrently, CD4⁺ T lymphocytes numbers also increase, but never regain pre-infection levels. The progressive decline in CD4⁺ T lymphocytes, together with increasing numbers of CD8⁺ T lymphocytes, results in inversion of the CD4:CD8 ratio. The decrease in plasma FIV load and the replenishment of CD4⁺ T lymphocytes marks the beginning of the latent phase of FIV infection, in which infected cats remain free of clinical signs (Hartmann, 1998, Yamamoto et al., 2007, Hosie et al., 2009, Sykes, 2013). The duration of this phase is highly variable and can be life-long. In both HIV and FIV infections, the duration of the latent phase is strongly related to the level of viraemia and the numbers of immune-reconstituted CD4⁺ T lymphocytes at the start of this phase (Diehl et al., 1996, Mellors et al., 1996, Bajaria et al., 2002, Goto et al., 2002, Geskus et al., 2007). In FIV infected cats, changes in the CD4:CD8 ratio and CD8⁺ T

lymphocyte expansion are significantly correlated with viraemia (Roche et al., 2013). In a proportion of infected cats, the decrease in CD4⁺ T lymphocyte numbers, (WHO recommends that HIV infected patients should be treated when counts fall below 350 cells/mm³ (2013)), which usually accompanied by an uncontrolled increase in plasma viral load, marks the beginning of the terminal phase of infection. Consequently, infected cats in this stage are highly susceptible to opportunistic infections, have an increased risk of neoplasia and are less responsive to treatment for some common infections (Hartmann, 1998, Yamamoto et al., 2007, Hosie et al., 2009, Hartmann, 2012, Sykes, 2013, Beatty, 2014).

1.3 Epidemiology

In general, the seroprevalence of FIV in domestic pet cat populations is approximately 1-12% in healthy cats and can be as high as 44% in cats with clinical signs (Pedersen et al., 1987, Yamamoto et al., 1989, Courchamp and Pontier, 1994, Hartmann, 1998, Levy et al., 2006, Hayward and Rodrigo, 2010b). In the UK, the prevalence of FIV was estimated at 6% in healthy cats and 19% in sick cats (Hosie et al., 1989), although more recent estimates are required. Gender, age and outdoor access are considered to be important risk factors for FIV infection (Hartmann, 1998, Hosie et al., 2009, Hartmann, 2012, Sykes, 2013). A study in North America reported that male cats are approximately 4.7 times more likely to test FIV positive than female cats (Levy et al., 2006). Between 80-90% of infected cats are older than 2 years, with the average age at the time of diagnosis being 6 - 8 years (Sykes, 2013). Free-roaming cats are also more likely to be infected than cats kept indoors (Hosie et al., 1989, Addie et al., 2000). Territorial fighting is most likely linked to the higher risk of infection of free-roaming, adult male cats, as FIV transmission occurs mainly via biting (Pedersen et al., 1987, Yamamoto et al., 1989, Hartmann, 1998, Sykes, 2013). Vertical and sexual transmission of FIV do not occur commonly in nature but have been observed experimentally and infectious FIV can be recovered from the semen of FIV infected cats (Jordan et al., 1998b, Jordan et al., 1998a, Kolenda-Roberts et al., 2007). Vertical transmission from mother to kittens can also occur, with the risk of transmission being associated with the viral load of the pregnant queen (O'Neil et al., 1995, Burkhard and Dean, 2003).

1.4 FIV subtypes and global distribution

FIV has been classified into five different subtypes/clades, designated A-E, according to the nucleotide sequences of the *env* gene (Hosie et al., 2009, Stickney et al., 2013). Unlike HIV, there is no clear geographical origin of FIV subtypes. Subtypes A and B are the most widely distributed and are detected worldwide, followed by Subtype C, which has been detected in Canada, Japan and New Zealand (Hosie et al., 2009, Hayward and Rodrigo, 2010b, Stickney et al., 2013) (Figure 1-7). Subtype D occurs in Japan, Thailand and Vietnam, while subtype E has only been reported in Argentina (Kakinuma et al., 1995, Pecoraro et al., 1996, Nakamura et al., 2003, Keawcharoen et al., 2006). In addition, *env* sequences showing evidence of recombination between 2 or more subtypes (A/B, A/C, B/D and A/B/C recombinants) were isolated from infected cats in several countries (Bachmann et al., 1997, Reggeti and Bienzle, 2004, Hayward and Rodrigo, 2008, Hayward and Rodrigo, 2010b, Beczkowski et al., 2014a). In the UK, subtype A is the predominant subtype, with a single reported sequence showing a likely A/C recombination (Samman et al., 2011). A new subtype was proposed, which emerged as a subclade within subtype B, following the analysis of strains isolated in Texas, USA and Portugal (Weaver et al., 2004, Duarte and Tavares, 2006). Moreover, distinct *env* sequences were obtained from a group FIV infected cats in New Zealand (Hayward et al., 2007, Hayward and Rodrigo, 2008). These two putative subtypes were later designated as subtypes F and U-NZenv, respectively, in addition to subtypes A - E (Weaver et al., 2004, Duarte and Tavares, 2006, Hayward et al., 2007, Hayward and Rodrigo, 2008).

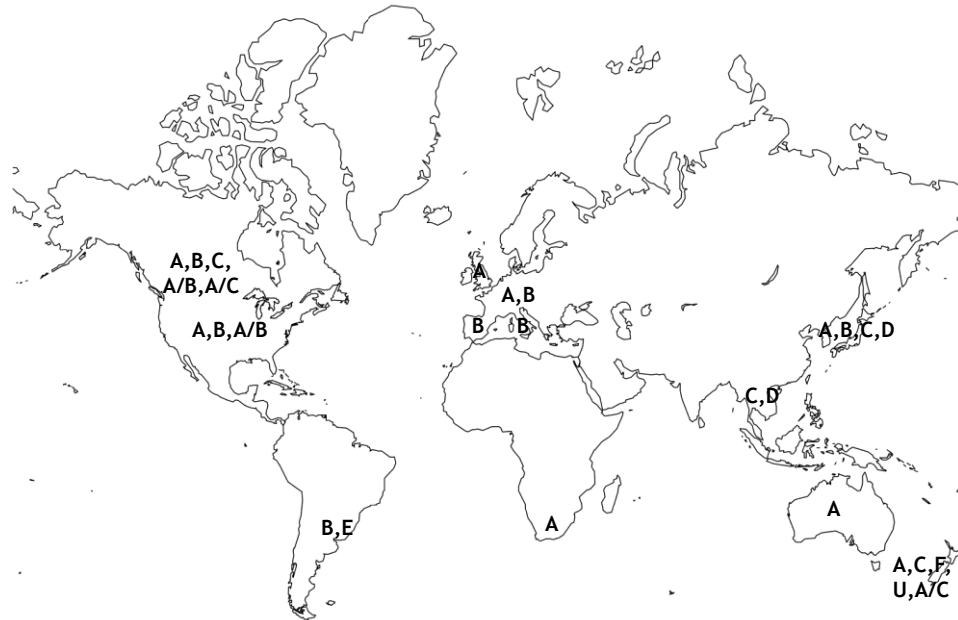


Figure 1-7 Global distribution of FIV subtypes (adapted from (Hosie et al., 2009))

1.5 Immune responses to FIV infection

Similar to other retroviral infections, the integration of FIV proviral DNA into the genome results in persistent infection. Although FIV-specific immune responses do not effectively clear an infection, nevertheless they play important roles in the containment of virus replication as well as in FIV pathogenesis. The concurrent appearance of FIV-specific immune responses and the reduction in plasma viraemia at the beginning of the latent phase provides evidence that the immune responses are involved in the control of FIV production.

1.5.1 Cell-mediated immune responses

FIV Gag-specific cytotoxic T lymphocytes (CTL) have been detected as early as 2 weeks after experimental infection (Callanan et al., 1992, Beatty et al., 1996). Responses against Env have also been reported, although with a slower onset (Flynn et al., 1995a, Flynn et al., 1995b, Beatty et al., 1996). Anti-FIV CD8⁺ T lymphocyte responses were detected in both the circulation and in lymphoid tissues and involved both cytolytic and non-cytolytic mechanisms (Flynn et al., 2002, Paillot et al., 2005). Anti-FIV-CTL persist for the duration of FIV infection, although their apoptosis-prone nature and limited clonality partly explain their apparent inability to clear persistent infection (Song et al., 1992,

Tompkins et al., 2002, Paillot et al., 2005, Miller et al., 2013). Similarly, extensive CD4⁺ T lymphocyte activation and expansion also occur during the acute phase of infection (Bienzle, 2014). However, these activated CD4⁺ T lymphocytes, expressing high levels of CD134, are highly susceptible to FIV infection and so the increased availability of target cells results in increased viral production, followed by cell death by virus-induced cytolysis, activation-induced cell death and CTL-mediated cytolysis, as occurs following HIV infection (Bendinelli et al., 1995, Hel et al., 2006, Tompkins and Tompkins, 2008, Swanstrom and Coffin, 2012).

1.5.2 Humoral immune responses

Antibodies recognising Gag and Env proteins have been detected later than CTL responses, at approximately 2 - 6 weeks after infection, and levels usually remain high (Yamamoto et al., 1988, Rimmelzwaan et al., 1994, Bendinelli et al., 1995, Willett et al., 2013). Whether antibodies recognising Env or Gag emerge first remains controversial and might depend on either the FIV strain used in the study or the sensitivity of antibody detection (Egberink et al., 1992, Rimmelzwaan et al., 1994, Willett et al., 2013). However, similar to HIV, these early antibodies are generally non-neutralising (Tomaras and Haynes, 2009, Bienzle, 2014). It has been shown in HIV infected individuals that the appearance of NAb is slower than the rapid evolution of Env, renders NAb ineffective in controlling disease progression (Moog et al., 1997, Richman et al., 2003, Mahalanabis et al., 2009, Overbaugh and Morris, 2012). It is likely that a similar scenario exists for FIV infection, since no association was observed between the magnitude of NAb responses and either clinical outcome or survival time (Beczowski et al., 2015b).

1.6 Tissue compartmentalisation

During the early stage of infection, FIV spreads into several lymphoid and non-lymphoid organs within the infected cat (Bach et al., 1994, Beebe et al., 1994, Hurtrel et al., 1994). However, virus migration within the body is not without limits. Indeed, it is relatively restricted between compartments by anatomical barriers such as the blood-brain barrier (BBB) and the blood-cerebrospinal-fluid barrier (Fletcher et al., 2011). And with its error-prone RT

enzyme and high replication rate, this could give rise to genetically distinct subpopulations between body compartments, the so-called “tissue compartmentalisation” that has been observed in HIV infection (Zhang et al., 2002, Zarate et al., 2007).

1.6.1 Definition of tissue compartmentalisation

Tissue compartmentalisation represents the detection of a distinct viral population in one tissue as compared to the other tissues. This definition relies on phylogenetic tree analysis in which tissue compartmentalisation can be visualized as a separate branch (Zarate et al., 2007). As has been observed in several evolutionary studies, FIV and HIV evolve and continue to diverge from their ancestors over a period of time (Shankarappa et al., 1999, Hosie et al., 2002). Assuming there is no restriction between compartments and virus spreads throughout the body, the viral sequences obtained from different tissues would be predicted to be interspersed randomly amongst each other (Figure 1-8A). In contrast, as shown in Figure 1-8B, in the presence of the blood-brain barrier that limits viral migration in and out of the central nervous system (CNS), virus becomes compartmentalised and starts to diverge from its ancestor, creating a subpopulation that evolves independently from virus within other tissues.

1.6.2 Compartmentalisation vs. tissue reservoirs

Tissue compartmentalisation is distinct from tissue reservoirs. In the case of compartmentalisation, viruses continue to undergo their normal replication cycle and evolve with time. However, due to the restriction of gene flow from other tissues, viral evolution in a secluded tissue is limited to a single gene pool, creating an independent viral population. In contrast, virus in a cellular reservoir, for example in resting memory CD4⁺ T cells, are kept in a latent state due to the limited transcription events in those cells (Alexaki et al., 2008). This results in a lower replication rate and less divergence from the founding ancestor (virus that disseminates throughout the body at the early stage of infection), compared to virus from non-reservoir but compartmentalised tissues (Nickle et al., 2003a). In order to distinguish between tissue compartmentalisation and tissue reservoirs, a phylogenetic tree containing viral sequences from different timepoints is required. Viral sequences from tissue

reservoirs would appear dispersed throughout the phylogenetic tree, since these sequences could infect reservoir cells and become latent at any time during infection (Figure 1-8C). In addition, it is important to consider that any tissue compartment might also act as a viral reservoir.

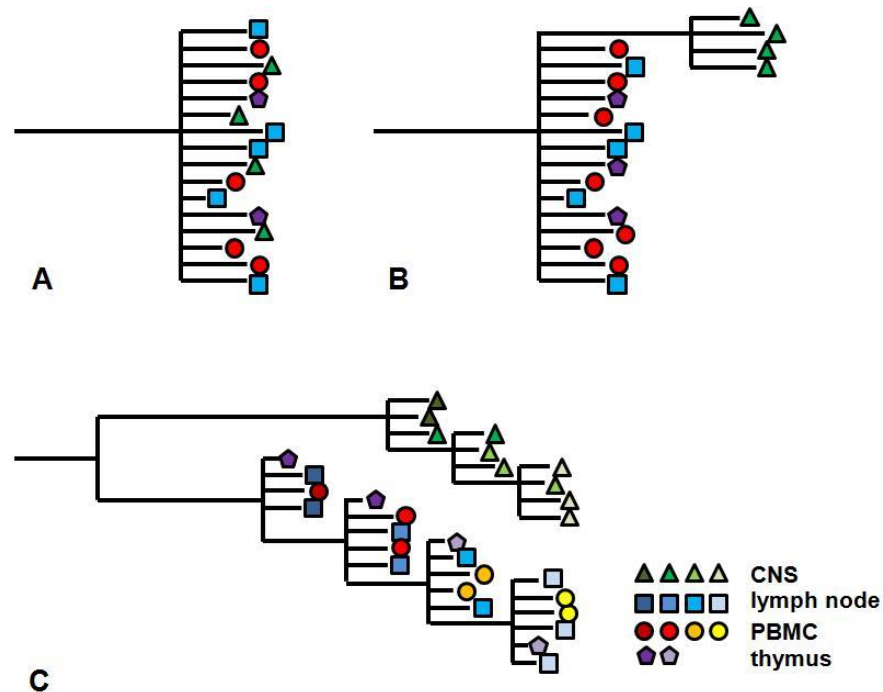


Figure 1-8 Proposed models of phylogenetic trees generated from FIV sequences from four different tissues: central nervous system, CNS (green triangles), lymph node (blue squares), peripheral blood mononuclear cells, PBMC (red circles) and thymus (purple pentagons) at a single timepoint (A and B) or at five time points (C). A) In the absence of any trafficking restrictions, viral evolution would occur at the same rate and be shared between each compartment throughout the body. Each tissue-derived sequence would randomly intersperse amongst the entire population. B) An example showing tissue restriction in the CNS. Virus within the CNS would evolve at a different rate compared to virus in other tissues. Sequences from three tissues would cluster together, while CNS sequences would segregate in a distinct branch. Note that all the sequences share the same ancestor and compartmentalised virus is more divergent than non-compartmentalised virus. C) Phylogenetic tree generated from four tissue-derived sequences at five time points. Color shading from darker to lighter represents sequences collected at earlier to later time points. FIV continues to evolve from the first ancestor as disease progresses, reflected by the clustering of viral variants from the same time point in a sub-branch that diverges further with time. As observed in a single time point, viral sequences in the compartment diverged from the same ancestor similar to virus from other tissues, but evolve and cluster together as a separate branch. Note that sequences from thymus (a reservoir in this example) are dispersed throughout the phylogenetic tree over time and show less divergence from the founding ancestor (adapted from (Nickle et al., 2003b)).

1.6.3 Mechanisms of tissue compartmentalisation

Several mechanisms have been proposed for tissue compartmentalisation. The first is “selective migration” of virus in which there is a tendency for some viral variants to preferentially migrate to particular tissues. This model is based on the fact that the cellular tropism of HIV and FIV is governed by amino acid variation in Env (Willett and Hosie, 2008). Therefore, it was suggested that different viral variants actively migrate to their preferred tissues according to their tropism. However, it was shown that the viral populations in PBMC, tonsil and rectum from acutely HIV infected patients are highly homogeneous, only becoming distinct and heterogeneous in the later, chronic phase (Zhang et al., 1993, Zhang et al., 2002). These findings ruled out the “selective migration” hypothesis and paved the way to the more likely explanation of “parallel evolution”. This model proposes that, during the initial phase of infection, the dominant homogeneous virus population spreads throughout the body and becomes the founding ancestor for the tissue-specific microevolution that occurs during the later stages of infection. The presence of a dominant homogeneous population after transmission might result from some selective process for that specific variants, such as the “mucosal gatekeeper” hypothesis proposed to explain the dominance of CCR5-tropic (R5) over CXCR4-tropic (X4) variants in HIV infection and/or to reflect the higher replicative capacity of some variants that dominate infection with a quasispecies, as has been speculated for FIV infection following infection via biting (Margolis and Shattock, 2006, Willett et al., 2013).

Evolutionary mechanisms that drive variants derived from the same ancestor to form distinct populations involve both host and viral factors and vary between tissue compartments. It appears that immune selection is the strongest pressure that shapes FIV and HIV evolution (Rambaut et al., 2004). Viral variants bearing CD8⁺ CTL escape epitope mutations are readily observed in chronically HIV-infected patients. FIV-specific CTL, capable of exerting similar selective forces, has also been demonstrated in infected cats, although the evidence for selection is not as strong as for HIV (Beatty et al., 1996, Willett et al., 2013). HIV and FIV-specific antibodies also play important roles in disease control and intra-host evolution (Rambaut et al., 2004). For example, it was shown that HIV compartmentalisation in blood and the female genital tract correlated significantly with the density of N-linked glycosylation sites on Env, reflecting

differences in HIV-specific antibody responses between the two compartments (Kemal et al., 2003). Also, differences in the permissiveness of tissues for antibody and immune cell infiltration could affect the level of immune-mediated selective pressures and therefore result in variation in viral evolution between compartments.

Another host factor, often disregarded, is the rate of cellular turnover. Due to their rapid replication rates, FIV and HIV virus progeny are produced at high rates in infected cells and rapidly infect other cells. This gives rise to a highly diverse viral population as a result of both reverse transcriptase-mediated mutations and immune-mediated selection, with the production of CTL that counteract actively infected cells and antibodies that bind free virions (Overbaugh and Bangham, 2001). However, FIV and HIV gene expression relies on cellular transcription factors and so the rate of virus replication and evolution depends on the rate of cell division (Alexaki et al., 2008). Therefore, FIV and HIV populations in tissues with higher cellular turnover rates might be predicted to be more diverse compared to tissues with lower cellular turnover rates.

Other host factors, such as different levels of intrinsic viral restriction proteins such as tripartite motif protein 5 (TRIM5), tetherin and APOBEC3, could influence FIV and HIV evolution between tissue compartments (Dietrich et al., 2011a, Dietrich et al., 2011b, Zielonka and Munk, 2011, Dietrich, 2012, Telenti and Johnson, 2012, Fourati et al., 2014). In addition, the levels of FIV and HIV accessory proteins, such as Vif, which counteracts APOBEC3, could also affect tissue-specific evolution (Shacklett and Luciw, 1994, Sheehy et al., 2003). However, there have been few studies investigating the roles of these host anti-viral factors in tissue-specific viral evolution and more detailed investigations are required.

1.6.4 Evidence of tissue compartmentalisation in FIV infection

Tissue compartmentalisation has long been recognised in HIV infection, since different HIV variants have been detected in blood, lung, male-female genitourinary tract and the CNS (Wong et al., 1997, Zhang et al., 1993, Singh et al., 1999, Zhang et al., 2002, Kemal et al., 2003). However, little is known about this phenomenon in FIV infected cats. The most compelling evidence of tissue

compartmentalisation in FIV infection has been found in the CNS. Early reports documented behavioural changes in cats naturally infected with FIV, suggesting a neurological effect of FIV infection (Pedersen et al., 1987). This finding was confirmed by subsequent studies conducted in experimental cats demonstrating that FIV-specific antibody could be detected and FIV could be isolated from the CSF of infected cats and that astrocytes and microglia, but not endothelial cells, were infected with FIV (Dow et al., 1990, Dow et al., 1992). It was shown that, following inoculation with FIV intra-cerebroventricularly or intraperitoneally, compartmentalisation of FIV Env variants was rapidly established (Liu et al., 2006). Moreover, considerable variation in the viral variants dwelling in different regions of the CNS, such as the frontal cortex, basal ganglia and choroid plexus, was also reported in this study, as well as in studies of HIV-1 and HIV-2 infection (Sankale et al., 1996, Shapshak et al., 1999). The intracranial compartmentalisation could have been the result of different evolutionary rates between tissues, since the FIV dynamics had been shown to differ between PBMC and CNS and also between different regions of the CNS (Ryan et al., 2003). Such findings of genetically different viral variants in different regions of the CNS suggested that tissue compartmentalisation of FIV might occur not only in different body tissues but also in subcompartments within individual organs.

Although both FIV RNA and DNA have been detected in several organs, there is little evidence for FIV compartmentalisation in tissues other than the CNS (Bach et al., 1994, Beebe et al., 1994). Hayward *et al* used the “Maddison-Slatkin” test to calculate the level of gene flow between seven tissues (lymph node, tongue, liver, lung, kidney, testis and brain stem) (Hayward and Rodrigo, 2010a). This method determines whether sequences grouped in any given tissue type arose by a stochastic process or as a true gene flow restriction (Slatkin and Maddison, 1990). In this study, one of eight cats showed a significant result, however a monophyletic branch indicative of tissue-specific evolution was not observed (Hayward and Rodrigo, 2010a).

1.6.5 Target cell availability and tissue compartmentalisation?

Another host factor, rarely considered as a key player in the virus-host interaction is target cell availability. It was shown in SIV-infected macaques that the number of activated CD4⁺ T lymphocytes was directly correlated with the

level of viraemia (Klatt et al., 2008) and the observed relationship reflected their role as target cells rather than their roles in immune control of infection. Also, in an HIV *in vitro* model, higher numbers of CD4⁺ T lymphocytes were associated with increased viral production (Schwartz et al., 2002). In addition, the observation that R5 tropic SIV preferentially infected CCR5⁺ memory cells while X4 tropic viruses selectively infected resting, CXCR4⁺ naïve CD4⁺ T lymphocytes suggested roles for the type and quantity of resident cells in tissue compartmentalisation (Mattapallil et al., 2005, Nishimura et al., 2005).

FIV infects its major target cell, the CD4⁺ T-helper cell, via an interaction between Env and the CD134 and CXCR4 molecules on the cell surface (Shimojima et al., 2004, Willett et al., 2006b, Willett and Hosie, 2008, Willett et al., 2013, Willett and Hosie, 2013). It has been shown that FIV tropism is dependent on residues in the V5 region of Env, which affect CD134 binding (Willett and Hosie, 2008, Kraase et al., 2010, Willett et al., 2010, Willett et al., 2013). Therefore, we speculated that differences in receptor expression and/or target cell numbers in different tissue compartments could exert selective pressure on the FIV population within each compartment.

Following transmission, FIV disseminates throughout the body into different tissue compartments. Once inside a tissue, the fittest variant, that which replicates most rapidly and outcompetes the others, is preferentially selected by the number of appropriate target cells, namely the number of CD4⁺ CD134⁺ T lymphocytes inside the tissue. This speculative process mirrors the selection of R5-tropic over X4-tropic HIV variants and the selective depletion of CCR5⁺CD4⁺ memory T lymphocytes in the gut associated lymphoid tissue (GALT) observed during the first 2 weeks of HIV infection (Mehandru et al., 2004, Mattapallil et al., 2005). In addition, the finding that R5 tropic SIV preferentially infected CCR5⁺ memory cells while X4 tropic virus selectively infected resting, CXCR4⁺ naïve CD4⁺ T lymphocytes, was consistent with the type and quantity of resident cells having a significant impact on tissue compartmentalisation (Mattapallil et al., 2005, Nishimura et al., 2005). In Chapter 3 of this thesis, studies are described in which the role of target cell availability in FIV tissue compartmentalisation was investigated in 21 tissue compartments and PBMC in a cohort of experimentally infected cats.

1.7 Scope and objectives of this study

The aim of this study was to investigate the role of the CD134⁺ target cell in the pathogenesis of FIV infection. It was hypothesised that target cell availability in different tissues, and at different time points, could exert pressure on the FIV variant population, leading to selection of the most fit variants.

The objectives of this study were:

- 1 To investigate tissue compartmentalisation in cats experimentally infected with FIV.
- 2 To investigate the role of target cell availability in tissue compartmentalisation.
- 3 To compare the numbers of CD4⁺CD134⁺ T lymphocytes between cats naturally infected with FIV and uninfected control cats.
- 4 To examine the relationship between CD4⁺CD134⁺ T lymphocyte numbers and FIV tropism switching in cats naturally infected with FIV.
- 5 To investigate the mechanism of target cell selection by FIV variants within a quasispecies.

Chapter 2 Materials and Methods

2.1 Molecular biology

2.1.1 Preparation of genomic DNA from buffy coat and tissue sample

Genomic DNA (gDNA) was extracted from the buffy coats of blood samples or from tissue samples using QIAamp[®] DNA Blood mini kit (Qiagen Ltd., UK), according to the manufacturer's protocol.

Briefly, whole blood samples collected into ethylenediaminetetraacetic (EDTA) anti-coagulant were centrifuged at 200 x g for 10 min with the brake-off to separate the buffy coat suspension. Plasma was collected, aliquoted and stored at -80 degrees Celsius (°C) until required. The buffy coat layer was carefully aspirated and the cells were washed with phosphate buffer saline (PBS) (Invitrogen, Paisley, UK), pelleted and then resuspended in 200 µl PBS. Next, the cells were transferred into 1.5 ml microcentrifuge tubes with 20 µl of Proteinase K before 200 µl of buffer AL were added. After briefly mixing, the mixture was heated to 56°C for 10 min.

For tissue samples, 25 mg of tissue were disrupted using scalpel blades, transferred into 1.5 ml microcentrifuge tubes with 180 µl of buffer ATL and 20 µl of Proteinase K, mixed and incubated at 56°C for 3 h. The lysate was homogenized using a QIAshredder[®] column (Qiagen Ltd., UK) and incubated with 200 µl of buffer AL and 4 µl of RNase at 70°C for 10 min.

The resulting lysate, from either buffy coat or tissue sample, was then mixed with 200 µl of absolute ethanol and transferred to a QIAamp[®] Minispin column for washing with 500 µl of buffer AW1 and AW2, respectively. Finally, gDNA was eluted with 50 µl of buffer AE after incubating at room temperature for 5 min. Eluted gDNA was quantified (Section 2.1.9), adjusted, aliquoted into 4 aliquots at a concentration of 200 ng/µl and stored at -80°C until use.

2.1.2 Preparation of total RNA from cell pellet and tissue sample

Total RNA was extracted from blood cell pellets and cat tissue using the Qiagen RNeasy® mini kit (Qiagen Ltd., UK), as per manufacturer's protocol. Briefly, 5×10^6 cells were harvested and pelleted by centrifugation at $300 \times g$ for 5 min. For tissue samples, 20 mg of tissue were disrupted with a scalpel blade. Six hundred μl of buffer RLT were then added to the cell pellet or disrupted tissue. The suspension was next homogenized using a QIAshredder® column (Qiagen Ltd., UK). The resulting lysate was then mixed with 600 μl of absolute ethanol and transferred to a QIAamp® Minispin column for washing with 700 μl of buffer RW1 and 500 μl of buffer RPE, respectively. Finally, RNA was eluted with 30 μl of RNase-free water after incubating at room temperature for 5 min. Eluted RNA was quantified (Section 2.1.9) and used to make cDNA immediately (Section 2.1.4).

2.1.3 Preparation of viral RNA from cell culture supernatant

Viral RNA was prepared from cell culture fluids using the QIAGEN® Viral RNA minikit (Qiagen Ltd., UK) as per the manufacturer's protocol. In brief, 140 μl of culture supernatant were added to 560 μl of buffer AVL containing carrier RNA, mixed well and incubated at room temperature for 10 min. Five hundred and sixty μl of absolute ethanol were then added to the mixture, mixed well and transferred into a QIAamp spin column (provided by the manufacturer). The column was washed twice with 500 μl of buffer AW1 and buffer AW2, respectively. Viral RNA was eluted by adding 30 μl of buffer AVE after incubating at room temperature for 5 min. Eluted viral RNA was quantified (Section 2.1.9) and used to make cDNA immediately (Section 2.1.4).

2.1.4 Preparation of complementary DNA from RNA samples

Complementary DNA (cDNA) was prepared using the Transcriptor High Fidelity cDNA Synthesis Kit (Roche Diagnostic, Mannheim, Germany) according to the manufacturer's protocol. Briefly, 10.4 μl of RNA were mixed with 1 μl of Anchored-oligo(dT)18 primer (50 pmol/ μl) and heated at 65°C for 10 min. The

tube contents were immediately cooled on ice and then used as a template in the reverse transcription reaction as follows;

	volume (μ l)
5x Transcriptor High Fidelity Reverse Transcriptase	4
Reaction buffer	
Protector RNase inhibitor (40 units/ μ l)	0.5
Deoxynucleotide mix (dNTPs) (10mM)	2
DTT	1
Transcriptor High Fidelity Reverse Transcriptase	1.1

The reaction was incubated at 50°C for 30 min, followed by 85°C for 5 min and held at 4°C. The resulting cDNA was quantified (Section 2.1.9) and stored in 3.5 μ l aliquots at -80°C until required.

2.1.5 Quantification of FIV proviral load by quantitative polymerase chain reaction (qPCR)

Two hundred ng of each gDNA sample were used as a template in a 20 μ l real-time PCR reaction containing 20 pmol of primer, 10 pmol of probe and TaqMan® Universal PCR Master Mix (Applied Biosystems, Paisley, UK). Sequences of primers and probes are shown in Table 2.1.1. Tenfold-dilutions of plasmid DNA standard for each V5 variant (VR1012, (Hartikka et al., 1996, Willett et al., 2013)) and FIV *gag* (pBR328-GL8-MYA), covering 10 to 10⁸ copy numbers, were used to construct a standard curve (Figure 2.1). All FIV proviral load quantifications were normalized against 18S ribosomal DNA (rDNA) quantity. A standard curve of 18S rDNA was prepared using five-fold dilutions of gDNA extracted from the feline primary T lymphoblastoid cell line MYA-1 (Section 2.2.1.1), extending from 5.12 pg to 400 ng (Miyazawa et al., 1989). All reactions were performed in triplicate using an ABI Prism® 7500 real time PCR system (Applied Biosystems, UK). Coefficients of variation (CV) were calculated and CV <25% was used to control for intra-test variation (Leutenegger et al., 1999). Absolute quantities were estimated by adjusting with 18S rDNA quantity and calculated using the following equation (adapted from (Klein et al., 1999)):

$$\text{absolute quantity (copies}/10^6\text{ cells)} = \left(\frac{\text{FIV quantity (copies number)}}{\text{18S rDNA quantity (nanogram)}} \right) * 5000$$

2.1.6 Quantification of CD134 and CXCR4 messenger RNA (mRNA) by duplex qPCR

One hundred ng of cDNA were used as a template in a 20 μ l duplex qPCR reaction containing 20 pmol of primer, 10 pmol of probe and TaqMan® Universal PCR Master Mix (Applied Biosystems, UK). Sequences of primers and probes were as shown in Table 2.1.2. Tenfold-dilutions of plasmid DNA standard for feline CD134 (pDON-AI-fCD134) (Willett et al., 2006b) and feline CXCR4 (pBABEpuro-fCXCR4) (Willett et al., 2002), from 10 to 10⁸ copy numbers, were used to construct a standard curve (Figure 2.2). All reactions were performed in triplicate using an ABI Prism® 7500 real time PCR system (Applied Biosystems, UK). Coefficients of variation (CV) were calculated and CV <25% was used to control for intra-test variation (Leutenegger et al., 1999). Absolute quantities were estimated by adjusting with β -actin Ct (cycle threshold) value and calculated using the following equation (adapted from (Scott et al., 2008)):

$$\text{normalized quantity (plasmid copies number)} = \left(\frac{f_{\text{CD134 or fCXCR4 Ct value}}}{f_{\beta\text{actin Ct value}}} \right) * \text{quantity}$$

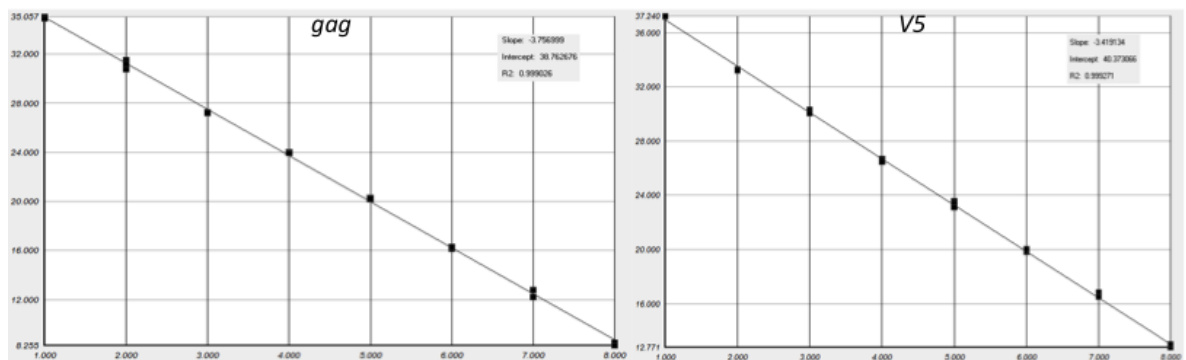


Figure 2-1 Representative standard curves for the determination of FIV *gag* (left) and V5 (right) quantity, with a series of ten-fold dilutions of plasmid DNA standards, ranging from 10 - 10⁸ copy numbers.

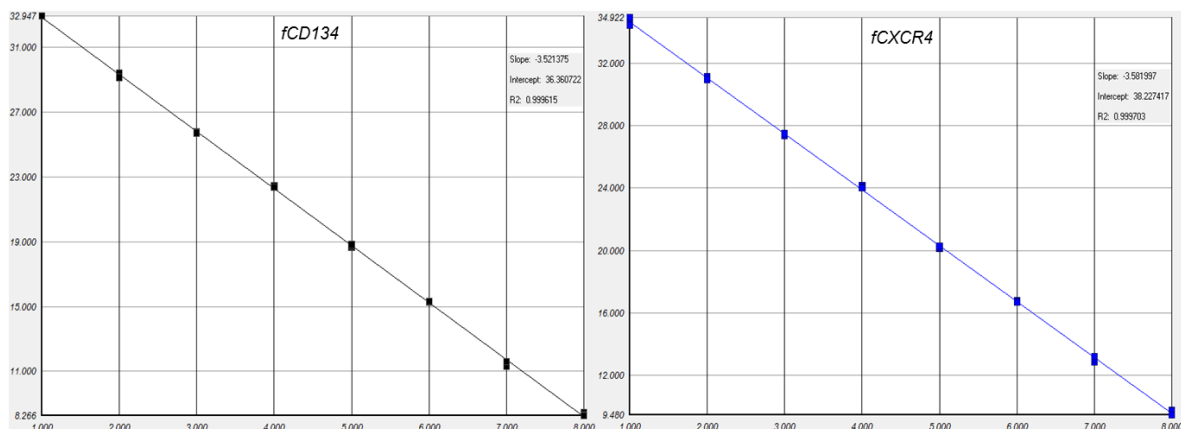


Figure 2-2 Representative standard curves for the determination of fCD134 (left) and fCXCR4 (right) cDNA quantity, with a series of ten-fold dilutions of plasmid DNA standards, ranging from 10^1 - 10^8 copy numbers.

2.1.7 Polymerase chain reactions

Full-length FIV *env* or *V5* segments were amplified from gDNA using the set of primers shown in Table 2-1-3. Phusion® high-fidelity DNA polymerase (New England Biolabs, UK), which has 50 times greater fidelity than regular *Taq* polymerase, was used for amplification to minimise the introduction of errors introduced during the PCR. All PCR reactions were performed using a GeneAmp PCR system 9700 thermocycler (Applied Biosystems, UK).

The *V5* loop region of FIV *env* was amplified using the primer pair Sal7799F and G8Not8030R in a 50 μ l reaction. The reaction mix and thermocycling conditions are shown in Tables 2-2 and 2-3 below, respectively.

To amplify full-length *env*, 200 ng of gDNA were used as a template in a two-steps nested PCR. The first round PCR was performed using either 2F2/1R4 or 1F4/XR2 primer pairs. The reaction mix and thermocycling conditions are shown in Tables 2-2 and 2-3 below, respectively. The purified PCR product from the first round PCR was used as the template for the second round PCR. The second round primers were designed with Sal 1 and Not 1 restriction sites to permit further cloning into the VR1012 expression vector. The second round amplification was performed using a different combination of primer pairs, shown in Table 2-1-3.

To confirm that the correct insert (~2,500 bp) was cloned into the VR1012 expression vector, a colony PCR was performed using GoTaq® Flexi DNA polymerase (Promega, Southampton, UK) as per the manufacturer's protocol. Individual colonies were picked and resuspended in 20 µl DNase free water. Two microliters of this suspension were used as the template. The reaction mix and thermocycling conditions are shown in Tables 2-2 and 2-3 below, respectively.

All PCR products were mixed with 6x loading dye (New England Biolabs, UK), examined by electrophoresis on a 1% agarose gel (Thermo Fisher Scientific, UK) containing 1 mg/ml ethidium bromide (Sigma Aldrich, Gillingham, UK) and visualised using an UV trans illuminator (Syngene Bio Imaging, Cambridge, UK).

2.1.8 PCR product purification

The correct PCR product bands were visualized over an UV trans illuminator (Syngene Bio Imaging, UK) and excised using sterile scalpel blades. DNA was purified from agarose gel fragments using the QIAquick® gel extraction kit (Qiagen Ltd., UK) as per the manufacturer's protocol. In brief, each gel fragment was dissolved in three gel volumes of buffer QG at 56 °C for 10 min. One gel volume of isopropanol was then added to the suspension. The suspension was mixed and transferred into a Qiaquick® column and spun down at 17,900 x g for 1 min and washed once with 750 µl of buffer PE. DNA was eluted with 30 µl of buffer EB after incubating at room temperature for 5 min.

2.1.9 Nucleic acid quantification

Plasmid DNA, genomic DNA, total RNA, viral RNA and cDNA, were quantified using a NANOdrop 2000 spectrophotometer (Thermo Fisher Scientific, UK).

2.1.10 Restriction enzymes digestion and ligation

PCR products, either full-length *env* genes or V5 segments were double-digested with Sal 1-HF® and Not 1-HF® restriction enzymes (New England Biolabs, UK). The expression vector VR1012 was also double-digested with the same enzymes in a larger quantity, checked for linearity by agarose-gel

electrophoresis, purified, aliquoted and frozen at -20°C until required. All digestion reactions were performed according to the manufacturer's protocol. In brief, one unit of each enzyme was added to an appropriate amount of DNA, assuming that $1\ \mu\text{g}$ of DNA will be completely digested by one unit of enzyme within 1 h at 37°C , with Cutsmart® buffer (provided by the manufacturer).

Each digested DNA fragment was then purified using the QIAquick® gel extraction kit (Qiagen Ltd., UK) as per the manufacturer's protocol and ligated into the VR1012 vector using T4 DNA Ligase (Promega, UK) at 14°C overnight. A vector:insert molar ratio of 5:1 was used in each $20\ \mu\text{l}$ ligation reaction. For each ligation performed, a "vector only" control was included to determine ligation efficiency.

2.1.11 Transformation

The ligated construct was then transformed into *Escherichia coli* MAX Efficiency® DH5 α^{TM} Competent cells (Invitrogen, UK) using the heat shock method, as per the manufacturer's protocol. In brief, $3\ \mu\text{l}$ of ligated construct were added to $30\ \mu\text{l}$ of bacteria, incubated on ice for 30 min, heat-shocked at 42°C for 40 sec and then immediately returned on ice for a further 2 min. Transformed competent cells were cultured in $400\ \mu\text{l}$ of super optimal culture (SOC) medium (provided by manufacturer) at 37°C for an hour on an orbital shaker. Next, each culture was spread on a freshly prepared Luria-Bertani (LB) agar plate (Thermo Fisher Scientific, UK) containing $50\ \mu\text{g}/\text{ml}$ of kanamycin (Sigma Aldrich, UK) and incubated at 30°C for 20-24 h. Single colonies were picked and either screened using the colony PCR method (Section 2.1.7) or further expanded for small scale DNA preparation (Section 2.1.10). A minimum of 50 colonies was picked for each sample.

2.1.12 Small scale DNA preparation

For the preparation of plasmid DNA, each individual colony was picked and cultured in 3 ml of LB broth (Thermo Fisher Scientific, UK) containing $50\ \mu\text{g}/\text{ml}$ of kanamycin (Sigma Aldrich, UK) at 30°C for 20-24 h in an orbital shaker. Plasmid DNA was then prepared from the culture using the QIAGEN® spin miniprep kit (Qiagen Ltd., UK) as per the manufacturer's protocol. In brief,

bacteria were pelleted by centrifugation at 17,900 x g for 4 min using a refrigerated microcentrifuge. Next, 250 μ l of buffer P1, with RNase A, were added to resuspend the pellet. The suspension was then lysed with 250 μ l of buffer P2 for 5 min and neutralized by adding 350 μ l of buffer N3. A supernatant was prepared from the suspension by centrifugation at 17,900 x g for 10 min and was transferred into a QIAprep spin column. Each column was washed once with 750 μ l of buffer PE. Plasmid DNA was eluted with 50 μ l buffer EB after incubating at room temperature for 5 min. To check for the presence of the correct insert (2,500 bp), plasmid DNA was double-digested with NotI/Sall (Section 2.1.10), examined on a 1% agarose electrophoresis gel containing 1 mg/ml ethidium bromide (Sigma Aldrich, UK) and viewed using an UV trans illuminator (Syngene Bio Imaging, UK).

2.1.13 Medium scale DNA preparation

For the medium scale preparation of plasmid DNA (up to 1 μ g of DNA), 100 μ l of the small scale culture were expanded in 100 ml LB broth (Thermo Fisher Scientific, UK) containing 50 μ g/ml of kanamycin (Sigma Aldrich, UK) at 30°C for 20-24 h in an orbital shaker. Plasmid DNA was then prepared from the culture using the QIAGEN® Plasmid midiprep kit (Qiagen Ltd., UK) as per the manufacturer's protocol. In brief, bacteria were pelleted by centrifugation at 6,000 x g for 10 min at 4°C using swing bucket. Next, 4 ml of buffer P1, with RNase A, was added to resuspend the pellet. The suspension was then lysed with 4 ml of buffer P2 for 5 min at room temperature and neutralized by adding 4 ml of buffer P3. The suspension was incubated on ice for 15 min and centrifuged at 20,000 x g for 30 min at 4°C using swing bucket. Culture supernatant was transferred to a QIAGEN-tip, recently equilibrated with 4 ml of buffer QBT, and allowed to flow through by gravity. Next, the QIAGEN-tip was washed twice with 10 ml of buffer QC. Plasmid DNA was eluted with 5 ml of buffer QF into a clean 15 ml tube. Plasmid DNA was precipitated by the addition of 3.5 ml of isopropanol and centrifuged at 15,000 x g for 30 min at 4°C. The plasmid DNA pellet was washed with 1 ml of 70% ethanol and allowed to dry at room temperature for 10-15 min. Plasmid DNA was quantified (Section 2.1.9) and stored at -20°C until required.

2.1.14 Large scale DNA preparation

For the large scale preparation of plasmid DNA (more than 2 µg of DNA), 100 µl of the small scale culture was expanded in 200 ml LB broth (Thermo Fisher Scientific, UK) containing 50 µg/ml of kanamycin (Sigma Aldrich, UK) at 30°C for 20-24 h in an orbital shaker. Plasmid DNA was then prepared from the culture using the PureLink® Hi Pure Plasmid Filter DNA Purification Kit (Invitrogen, UK) as per the manufacturer's protocol. In brief, bacteria were pelleted by centrifugation at 6,000 x g for 10 min at 4°C using a swing bucket rotor. Next, 10 ml of buffer R3, with RNase A, were added to resuspend the pellet. The suspension was then lysed with 10 ml of buffer L7 for 5 min and neutralized by adding 10 ml of buffer N3. A supernatant was prepared from the suspension by centrifugation at 20,000 x g for 10 min using a swing bucket rotor and was transferred to a High Pure filter column, recently equilibrated with 15 ml of buffer EQ1, and allowed to flow through by gravity. The column was washed once with 50 ml of buffer W8. Plasmid DNA was then eluted with 15 ml of buffer E4 into a clean 50 ml tube. Plasmid DNA was precipitated by the addition of 10.5 ml of isopropanol and centrifuged at 20,000 x g for 30 min at 4°C using swing bucket. Plasmid DNA pellet was washed with 5 ml of 70% ethanol and allowed to dry at room temperature for 10-15 min. Plasmid DNA was quantified (Section 2.1.9) and stored at -20°C until required.

2.1.15 Plasmid DNA sequencing

Plasmid DNA was sequenced commercially using Sanger's chain terminator method, either in a 96 well plate format by Beckman Coulter Genomics, Essex, UK, or in a single sample format by GATC biotech, London, UK.

2.1.16 Sequences and phylogenetic analysis

All sequences were analysed using DNADynamo version 1.423 (Blue Tractor Software, UK) and BioEdit Sequence Alignment Editor version 7.0.9.0 (Hall, 1999). The full-length *env* was assembled using seven sequencing reads that overlapped by approximately 250 bp. (Table 2-1-3). Phylogenetic analysis was performed using MEGA software version 5.1 (Tamura et al., 2011). First, multiple sequences were aligned using ClustalX alignment package in BioEdit software

and exported as a FASTA file. Initial nucleotide sequences translations were performed on ExPasy Bioinformatics Resources Portal, www.expasy.org (Swiss Institute of Bioinformatics). Phylogenetic trees were generated using the Maximum Likelihood method. Re-sampling tree evaluations were performed by Bootstrapping with 1,000 replicates. The Tajima-Nei and Jones-Taylor-Thornton substitutional models were used to estimate the evolutionary distances of nucleotide and amino acids sequences, respectively.

Table 2-1 Primers and probes used in this study

All primers and TaqMan® probes used in this study were obtained commercially from Eurofins-MWG (Ebersberg, Germany) and/or Integrated DNA Technologies (Leuven, Belgium) and are listed below.

2-1-1 FIV proviral load quantification*

V5 variants		
B14	sense:	5'-GTACAAATAGTAGTAGTACAAACAGTAGT-3'
B19	sense:	5'-ATATGAATTGTAATTGTACAAATAGCAGTACA-3'
B28	sense:	5'-CAAATAGTAGTAGTACAAATCGGCAAA-3'
B30	sense:	5'-GTACAAATAGTAGTAGTACAAATAGTACA-3'
GL8	sense:	5'-GCATTTCAATATGACAAAAGCT-3'
reverse	antisense:	5'-GCTACGGGGTTATACCAATTC-3'
V5 probe**	FAM-5'-ATAGTGTTAAAATGGCATGTCCTAAAAATCAAGGCATCT-3'-BHQ1	
FIV gag		
	sense:	5'-CCATTCGAACGTCTGCCCTA-3'
	antisense:	5'-TCACCCGTGGTCACCATG-3'
gag probe**	FAM-5'-ATAGTGTTAAAATGGCATGTCCTAAAAATCAAGGCATCT-3'-BHQ1	
18s rDNA		
	sense:	5'-CCATTCGAACGTCTGCCCTA-3'
	antisense:	5'-TCACCCGTGGTCACCATG-3'
18s probe**	FAM-5'-CGATGGTAGTCGCCGTGCCTA-3'-BHQ1	

*adapted from (Willett et al., 2013)

**FAM: 6-carboxyfluorescein reporter dye, BHQ1: Black Hole Quencher 1 dye

2-1-2 Feline CD134 and CXCR4 mRNA quantification*

feline CD134		
	sense:	5'-CAGGTTATGGGATGGAGAGTCG-3'
	antisense:	5'-TGCAAGGCTCGTAGTTCACG-3'
fCD134 probe	FAM-TGACCAGGACACCAAGTGCCTCCAGTG-BHQ1	
feline CXCR4		
	sense:	5'-AAGGCAGTCCATGTCATCTACAC-3'
	antisense:	5'-AGACCACCTTTTCAGCCAACAG-3'
fCXCR4 probe	FAM-ACCTCTACAGCAGTGCCTCATCTGC-BHQ1	
feline β -actin		
	sense:	5'-GACTACCTCATGAAGATCCTCACG-3'
	antisense:	5'-CCTTGATGTCACGCACAATTTCC-3'
fβ-actin probe	YY-ACAGTTTCACCACCACCGCCGAGC-BHQ1	

*adapted from (Scott et al., 2008)

**FAM: 6-carboxyfluorescein reporter dye, YY: Yakuma Yellow reporter dye, BHQ1: Black Hole Quencher 1 dye

2-1-3 FIV envelope cloning and sequencing primers

V5 cloning*	
Sal7799F	sense: 5'-GTTTACTATGAAG GTCGAC GACCTTAT-3'
G8Not8030R	antisense: 5'-GG GCGGCCGC TACCACTAAGTAATCTGGTT-3'
full-length env cloning	
first round primers**	
1F4	sense: 5'-TATTATTGGCARTTGCAATCTACMTTATC-3'
2F2	sense: 5'-CCAATAMCWTCCTCCAGTCCACCCTT-3'
1R4	antisense: 5'-CCAATAMTCWTCCTCCAGTCCACCCTT-3'
XR2	antisense: 5'-CCTCAAAGGGAACAAATCAGCTCA-3'
second round primers*	
GL8_Sal1F	sense: 5'-GG GTCGAC ACCATGGCAGAAGGGTTTGCAGCA-3'
M11_Sal1F	sense: 5'-ACCTG GTCGAC ACCATGGCAGAGGGAGGATTTAATCAA-3'
M31_Sal1F	sense: 5'-ACTG GTCGAC ACCATGGCAGAGGGAGGATTTACTCAA-3'
M46_Sal1F	sense: 5'-ACTG GTCGAC ACCATGGCAGAGGGAGGATTTACTCAG-3'
M_Not1R	antisense: 5'-ACAG GCGGCCGC CATCATTCTCCTCTTTTTTCAG-3'
M31_Not1R	antisense: 5'-ACAG GCGGCCGC GATCATTCTCCTCTTTTTTCAGAC-3'
M46_Not1R	antisense: 5'-ACAG GCGGCCGC CATCATTCTCCTCTTTTTTCAGAC-3'
sequencing Primers	
VR1012F	sense: 5'-CTTTTCTGCAGTCACCGTCG-3'
M780F	sense: 5'-TGGAAATGAGACTATAACAGG-3'
7822F	sense: 5'-ACAAAAGCTGTAGAAATGTA-3'
VR1012R	antisense: 5'-CTGGATCCAGGCGCCTGGTCTA-3'
M2090R	antisense: 5'-GATTACATCCTAATTCTTGCATAG-3'
GL8_211	antisense: 5'-CCTCTTCCAGTTTTACCTCTTG-3'
M_Not1R	antisense: 5'-ACAGCGGCCGCCATCATTCTCCTCTTTTTTCAG-3'

*contains Sal 1 and Not 1 restriction site, as highlighted in red, respectively

**R is either A or G, M is either A or C and W is either A or T.

2-1-4 Colony PCR primers

VR1012F	sense: 5'-CTTTTCTGCAGTCACCGTCG-3'
VR1012R	antisense: 5'-CTGGATCCAGGCGCCTGGTCTA-3'

Table 2-2 PCR recipes**V5 PCR**

	volume (μ l)
5x Phusion® buffer	10
dNTP (10 mM)	1
Sal7799F primer (10 mM)	2.5
G8Not8030R primer (10 mM)	2.5
DMSO*	1.5
Phusion® enzyme	0.5
template	2.5
DNase free water	29.5

Full-length *env* PCR, first round and second round

	volume (μ l)
5x Phusion® buffer	10
dNTP (10 mM)	1
forward primer (10 mM)	2.5
reverse primer (10 mM)	2.5
DMSO	1.5
Phusion® enzyme	0.5
template	2.5
DNase free water	29.5

Colony PCR

	volume (μ l)
5x GoTaq® buffer	4
dNTP (10 mM)	0.4
VR1012F primer (10 mM)	1
VR1012R primer (10 mM)	1
Mg ₂ Cl	1.2
goTaq® enzyme	0.1
template	2
DNase free water	10.3

Table 2-3 Thermocycling conditions for FIV full-length *env* and V5 PCR**V5 PCR**

	number of cycles	temperature (°C)	time
initital denaturation	1	98	30 sec
denaturation		98	10 sec
annealing	35	51	30 sec
elongation		72	60 sec
final extension	1	72	10 min
hold	1	4	

Full-length *env* PCR, first round

	number of cycles	temperature (°C)	time
initital denaturation	1	98	30 sec
denaturation		98	10 sec
annealing	35	64.5	30 sec
elongation		72	90 sec
final extension	1	72	10 min
hold	1	4	

Full-length *env* PCR, second round

	number of cycles	temperature (°C)	time
initital denaturation	1	98	30 sec
denaturation		98	10 sec
annealing	35	70.2	30 sec
elongation		72	90 sec
final extension	1	72	10 min
hold	1	4	

Colony PCR for checking the insert

	number of cycles	temperature (°C)	time
initital denaturation	1	95	30 sec
denaturation		95	10 sec
annealing	35	60.5	30 sec
elongation		72	90 sec
final extension	1	72	5 min
hold	1	4	

2.2 Cell culture techniques

2.2.1 Cell lines

All cell lines used in this study came from stocks stored long-term in liquid nitrogen. Frozen cells were thawed immediately, washed once with 10 ml of the appropriate culture medium and resuspended in 10 ml of the same medium in T75 culture flasks (Corning, Corning, USA). Cell lines were incubated at 37°C with 5% CO₂. Cell lines were monitored daily and passaged or scaled up as required.

All suspension cell lines were grown in R10; Roswell Park Memorial Institute 1640 medium (RPMI 1640, Invitrogen, UK) supplemented with 10% v/v heat-inactivated foetal bovine serum (FBS) (Perbio Science, Cramlington, UK), 2 mM L-glutamine (Invitrogen, UK), 50 µM 2-mercaptoethanol (Invitrogen), 100 IU/ml Penicillin and 100 µg/ml streptomycin (Invitrogen).

Adherent cell lines were grown in complete Dulbecco's modified Eagle's Medium (DMEM, Invitrogen, UK) supplemented with 10% v/v heat-inactivated foetal bovine serum, 2 mM L-glutamine (Invitrogen, UK), 100 IU/ml penicillin and 100 µg/ml streptomycin (Invitrogen, UK).

2.2.1.1 Feline primary T lymphoblastoid cell line

The interleukin-2 (IL-2)-dependent feline primary T lymphoblastoid cell line MYA-1 was used in this study to produce replicative competent virus and as a target cell for FIV infection experiments. This cell line had been established following the prolonged culture of a specific pathogen free cat's peripheral blood mononuclear cells (PBMC), which had been inoculated with blood from an FIV seropositive cat (Miyazawa et al., 1989). MYA-1 cells express CD4, CXCR4 and CD134 at levels similar to those on mitogen-activated T lymphocytes (Willett et al., 2013). MYA-1 cells were maintained in R10 culture medium supplemented with 100 IU/ml of recombinant IL-2 (kindly provided by Prof. Hattori, University of Tokyo, Japan).

2.2.1.2 Canine Chronic Lymphocytic Leukaemia cell line

The canine chronic lymphocytic leukaemia cell line, “CLL”, was established in our laboratory following the prolonged culture of PBMC isolated from a leukaemic dog. This cell line expresses CD4, CD8 and CXCR4 on its surface (Figure 2-3). CLL cells were used as target cells for FIV infection/competition studies following the stable transduction of different forms of recombinant feline CD134 described previously (Willett et al., 2006b). CLL-FFF is a CLL cell line stably expressing feline CD134 while CLL-FFHH stably expresses a chimaeric feline/human unshared CD134 molecule containing the cysteine rich domain 2 (CRD2) of human CD134. CLL-FFF and CLL-FFHH could be differentiated from each other by surface staining with anti feline CD134 (7D6) and anti human CD134 (Ber-ACT35) (Figure 2-4). Since CLL-FFHH expresses a chimaeric feline/human form of CD134, it is detectable by both antibodies while CLL-FFF only stains positive for anti feline CD134 (7D6). Both CLL variants were maintained in R10 medium, selected with Geneticin® (G-418, Thermo Fisher Scientific, UK) at 400 µg/ml and passaged every 3-4 days.

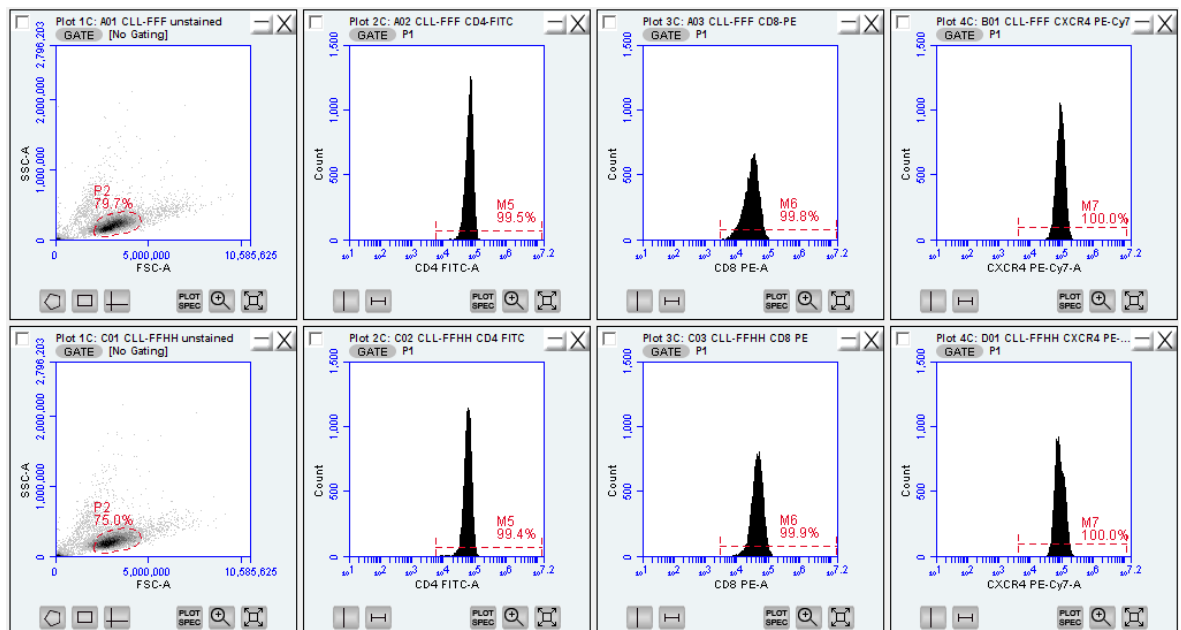


Figure 2-3 Surface markers staining of CLL-FFF (upper) and CLL-FFHH (lower); both cell lines are positive for CD4 (middle left), CD8 (middle right) and CXCR4 (right) expression.

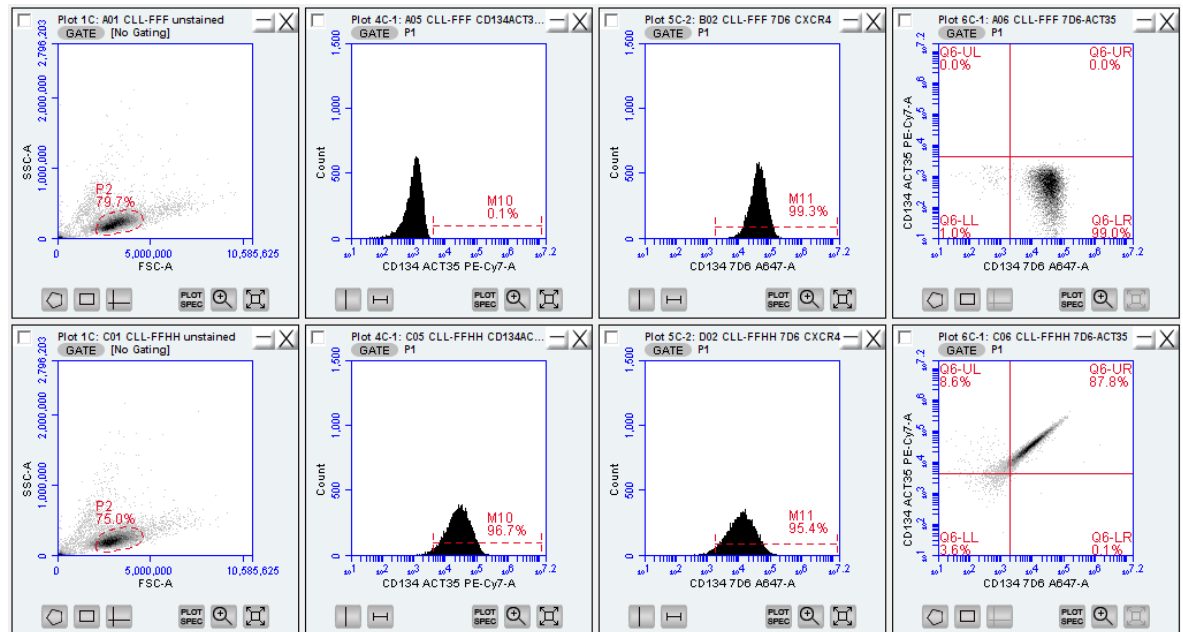


Figure 2-4 CLL-FFF (upper) and CLL-FFHH (lower) could be differentiated by staining with the anti-human CD134 monoclonal antibody Ber-ACT35. CLL-FFHH expresses a chimaeric feline/human CD134 molecule containing the cysteine rich domain 2 (CRD2) of human CD134 and is stained by both anti human CD134 (Ber-ACT35, middle left) and anti feline CD134 monoclonal antibodies (7D6, middle right). In contrast, CLL-FFF expresses the natural form of feline CD134 and stains positive for only feline CD134 (7D6, middle right).

2.2.1.3 Feline Large Granular Lymphoma cell line

The feline large granular lymphoma cell line, “MCC”, was derived from an abdominal mass from a 13 year old castrated male cat (Cheney et al., 1990). The MCC cell line has large membrane bound granules, similar to natural killer precursor cells. MCC cells express high levels of CXCR4 on their surface and, following stable transduction with feline CD134, have been used as target cells in the study of FIV-receptor interactions (Willett et al., 2006a, Willett et al., 2006b, Willett et al., 2007, Willett et al., 2009). MCC-fCD134 cells were maintained in R10 medium, selected with Geneticin® (G-418, Thermo Fisher Scientific, UK) at 400 µg/ml and passaged every 3-4 days.

2.2.1.4 Human Embryonic Kidney 293 T cell line

Human embryonic kidney cells containing the simian vacuolating virus 40 (SV40) large T-antigen (HEK293T) were used as producer cells for pseudotype production. This line originated from the HEK293 cell line, human embryonic

kidney cells transformed with sheared adenovirus 5 DNA (Graham et al., 1977). The SV40 large T-antigen in HEK293T cell permits episomal replication of transfected vector carrying the SV40 origin of replication and has been widely used for retroviral production as it yields high titers (Pear et al., 1993). HEK293T cells were cultured in 10 cm cell culture plates (Corning, USA) with complete DMEM. To harvest the cells, culture medium was removed, the cells were washed with sterile PBS and treated with 3 ml of 0.05% w/v trypsin (Invitrogen, UK) for 5 min at 37°C. Seven ml of fresh complete DMEM were added to stop the reaction. Cells were then centrifuged at 200 x g for 5 min and resuspended in fresh medium, counted (Section 2.2.3) and cultured for further use.

2.2.2 Peripheral Blood Mononuclear Cells (PBMC)

Peripheral blood mononuclear cells (PBMC) were isolated from whole cat blood collected in EDTA by standard density-gradient centrifugation using Ficoll-Paque PLUS (GE Healthcare Life Sciences, UK). One ml of blood in EDTA was centrifuged at 200 x g for 5 min. Plasma was collected and stored at -80°C for further use. The cellular fraction was then diluted with 5 ml of sterile PBS and layered over 3 ml of Ficoll-Hypaque PLUS (density gradient 1.077 g/l) in 15 ml sterile tubes and centrifuged at 400 x g for 30 min at 25°C using a swing bucket rotor with the brake off. The PBMC were aspirated from the interface, transferred to a fresh 15 ml tube and washed twice with 10 ml of sterile PBS. The PBMC were then resuspended in R10 medium.

2.2.3 Cell counting

Cell numbers and viability were determined by standard trypan blue staining (Invitrogen, UK), using a Neubauer haemocytometer (Weber Scientific International, Lancing, UK). Cell suspensions were mixed with trypan blue (Invitrogen, UK) at a ratio of 1:10 ratio (10 µl cell suspension and 90 µl trypan blue). Only viable cells, which remained unstained with trypan blue, were counted in all four quadrants of the haemocytometer. The total number of viable cells was calculated using the standard formula:

$$\text{total cell number (x } 10^5 \text{ cells/ml)} = [(\text{total cell count} / 4) \times 10 \text{ (dilution factor)}]$$

2.2.4 Cell cryopreservation

For the long-term storage of cell lines and PBMC, cells were cryopreserved in liquid nitrogen. Firstly, cell suspensions were centrifuged at $200 \times g$ for 5 min at 25°C and resuspended in 1 ml of pre-cooled freezing medium per 1×10^7 PBMC; freezing medium consisted of 10% dimethyl sulfoxide (DMSO) (Sigma Aldrich, UK) and 80% FBS. Cell suspensions were then transferred to 2 ml sterile cryo-tubes (Sarstedt, Beaumont Leys, UK) and placed in a freezing container (Nalgene, USA) at -80°C for 24 h before being transferred to a liquid nitrogen storage tank (-196°C).

2.3 Study specific methods

2.3.1 HIV(FIV) pseudotype production

HIV(FIV) pseudotypes carrying the firefly luciferase reporter gene (HIV(FIV)-luc) were prepared following the transient co-transfection of the VR1012 vector containing full-length FIV *env* or *V5* and the HIV pNL4-3 backbone containing the firefly luciferase gene in place of the *nef* deletion (pNL4-3.Luc.R⁻.E⁻, (He et al., 1995, He and Landau, 1995, Connor et al., 1995)).

HIV(FIV) pseudotypes carrying different fluorescent proteins (HIV(FIV)-FP), carrying either green (GFP), red (TagRFP) fluorescent tags, were prepared by the transient co-transfection of HEK 293T cells with three different expression vectors: the VR1012 vector containing a full-length FIV *env* or *V5*, the HIV *gag* backbone under the CMV promoter (pCMV-dR8.2 dvpr, (Stewart et al., 2003)) and a vector containing one of the fluorescent protein genes under the CMV promoter (pCCGW or pCCRW).

HEK 293 T cells were cultured, 2×10^6 cells in 10 ml of complete DMEM per 10 cm plate (Corning, USA) overnight. The following day, at approximately 70-80% confluence, HEK 293T cells were co-transfected with 5 μg of VR1012-*env* and pNL4-3.Luc.R⁻.E⁻, or a mixture of VR1012-*env* (1.25 μg), pCMV-dR8.2 dvpr (2.5 μg) and pCCFPW (5 μg) in 1 ml of serum free DMEM, for the luciferase and fluorescent protein carrying pseudotypes, respectively. Polyethylenimine (PEI) was used as the transfection agent at a ratio of 3:1 (weight/weight) of PEI:total

DNA. Cultures were maintained at 37°C, in an atmosphere of 5% CO₂ for 72 h. On day 3, culture medium containing the pseudotypes was harvested, centrifuged at 300 x g for 5 min, filtered through a 0.45 µm filter (Sarstedt, UK), aliquoted and stored at -80°C until required.

The infectivity of each luciferase pseudotype was determined by adding 50 µl of pseudotype to 50 µl containing 10⁶ cells/ml of CLL-FFF cells in the wells of a CulturPlate™-96 assay plate (Perkin Elmer, Beaconsfield, UK). After an incubation period of 72 h at 37°C, 5% CO₂, the luciferase activity was measured by adding 100 µl of HTS steadylite substrate (Perkin Elmer, UK) per well of the HIV(FIV)-luc infection plate which was then read using a 1450 MicroBeta Luminometer (Perkin Elmer, UK). All tests were performed in triplicate.

The infectivity of pseudotypes containing fluorescent proteins was determined by adding 500 µl of each pseudotype into 500 µl of culture medium containing 1 x 10⁶ cells/ml of CLL-FFF cells in 48 well plates (Corning, USA), followed by spinoculation at 300 x g for 60 min. Plates were cultured for 48 h at 37°C, 5% CO₂. On day 2, cells were harvested, washed with sterile PBS and read on a BD Accuri™ C6 flow cytometer using CFlow® Sampler software (BD Bioscience, Oxford, UK). All tests were performed in triplicate.

2.3.2 FIV-CD134 usage

The HIV(FIV)-luc pseudotypes were tested for the ability to infect CLL cells expressing either the natural form of feline CD134 (FFF) or the chimaeric feline/human CD134 molecule (FFHH). Since the chimaeric CD134 receptor (FFHH) contained human CRD2 rather than feline CRD2, pseudotypes that could infect both CLL-FFF and CLL-FFHH were defined as CRD2-independent. Fifty µl of either CLL-FFF or CLL-FFHH cells (Section 2.2.1.2) at 1 x 10⁶ cells/ml were cultured with 50 µl of each HIV(FIV)-luc pseudotype and incubated for 72 h at 37°C, in a humid incubator with an atmosphere containing 5% CO₂. Luciferase activity was measured by adding 100 µl of HTS steadylite substrate (Perkin Elmer, UK) into each well and plates were read using a 1450 MicroBeta Luminometer (Perkin Elmer, UK). All tests were performed in triplicate. Pseudotypes bearing the Envs of FIV clade A, Glasgow 8 (Genbank accession number X69496.1) and clade B B2542 (Genbank accession number U11820) were

used as reference pseudotypes for CRD2 dependent and CRD2 independent FIV entry, respectively (Beczowski et al., 2014b). A pseudotype was considered to be “CRD2 dependent” if the FFF/FFHH ratio was similar to that of GL8 (high ratio) and “CRD2 independent” if it was similar to B2542 (ratio below 30). Pseudotypes with intermediate FFF/FFHH ratios such as the FIV/A strain KKS (Genbank accession number NC_001482.1) were designated as “intermediate” and were presumed to be evolving towards CRD-2 independent usage.

2.3.3 Viral Neutralisation Assay

Plasma samples were heat-inactivated at 56 °C for 30 min before being diluted in R10 medium (dilution factors of 1:10, 1:100, 1:1,000 and 1:10,000). Twenty five µl of each plasma dilution were incubated with 25 µl of HIV(FIV)-luc pseudotype (Section 2.3) in CulturPlate™-96 assay plates (Perkin Elmer, UK) for 1 h at 37 °C, in an atmosphere of 5% CO₂. Fifty µl of CLL-FFF cells at 1 x 10⁶ cells/ml were added to each well and incubated for a further 72 h. Luciferase activity was measured following the addition of 100 µl of HTS steadylite substrate (Perkin Elmer, UK) to each well and reading the plates on a 1450 MicroBeta Luminometer (Perkin Elmer, UK). All tests were performed in triplicate.

2.3.4 Protein immunoblotting

Pseudotype concentrations were compared by measuring HIV CA p24 capsid protein by immunoblotting. In brief, 1 ml of each pseudotype was centrifuged at 20,800 x g, 4 °C for 2 h. After discarding the supernatant, the pellet was resuspended in 10 µl of protein loading dye (Invitrogen, UK), incubated at 95 °C for 5 min and then run on a 4-12% NuPAGE® Bis-Tris Mini Gel in 2-(N-morpholino)ethanesulfonic acid (MES) containing running buffer (Life Technologies, USA) at 120 V for 1 h. Protein bands were then transferred onto a nitrocellulose membrane using the iBlot® Gel Transfer Device (Thermo Fisher Scientific, UK). The membrane was blocked with blocking buffer (1:4 v/v FBS:PBS containing 0.1% sodium azide (Sigma Aldrich, UK)) at 4 °C overnight. P24 bands were developed by incubating the nitrocellulose membrane with mouse anti-HIV p24 antibody (diluted 1:1000 v/v with blocking buffer, clone 183-H12-5C, NIH AIDS Reagent Program, USA) at 37 °C for 1 h followed by goat anti-

mouse IgG DyLight™ 800 (diluted 1:1000 v/v with blocking buffer, Thermo Fisher Scientific, UK) at 37°C for 1 h. The fluorescence intensity of the p24 bands of each pseudotype was determined using the ODYSSEY™ system (LI-COR® Bioscience, Cambridge, UK).

2.3.5 Flow Cytometry

To measure the cell surface expression level of feline CD134 (FFF), chimaeric feline/human CD134 (FFHH) and feline CXCR4 on CLL cells, 1×10^6 cells were stained with 5 µl of the following antibodies on ice for 30 min: anti-feline CD134-alexa fluor 647 (clone 7D6, AbD Serotec, Kidlington, UK), anti-human CD134-PE-Cy7 (clone Ber-ACT35, BioLegend, London, UK) and anti-feline CXCR4 (clone 374606, R&D systems, Abingdon, UK). Cells were washed once with staining buffer (PBS + 1% w/v bovine serum albumin (Sigma Aldrich, UK) + 0.1% sodium azide (Sigma Aldrich, UK)), resuspended in 100 µl of staining buffer and then 2.5 µl of polyclonal goat anti-mouse IgG2A PE-Cy7 (AbCam, Cambridge, UK) were added to detect feline CXCR4 expression. Samples were resuspended in 1 ml of staining buffer.

To measure the proportions of CD4⁺, CD8⁺ and CD4⁺CD134⁺ T lymphocyte subpopulations, 200 µl of whole blood in 5 ml polystyrene round-bottom tubes (BD Bioscience, UK) were lysed with 3 ml of 1X BD Pharm Lyse™ Lysing Buffer (BD Bioscience, UK) and stained with 5 µl of anti-feline CD4-FITC, anti-feline CD8-PE and anti-feline CD134-alexa fluor 647 for 30 min at room temperature. All antibodies were obtained from AbD Serotec, UK. Cells were then washed once with staining buffer and then the pelleted cells were resuspended in 1 ml of staining buffer.

To identify each T lymphocyte subpopulation, lymphocytes were first selected from PBMC by plotting side scatter area (SSC-A) on the y-axis versus forward scatter area (FSC-A) on the x-axis. Next, CD4⁺ and CD8⁺ lymphocyte subpopulations were selected by plotting the CD4-FITC area (CD4-FITC-A) and the CD8-PE area (CD8-PE-A) on the y-axis versus the event number on the x-axis (Figure 2-5). The CD4-FITC-area on the y-axis was plotted against the CD8-PE-area on the x-axis to identify the single positive CD4⁺CD8⁻ and CD4⁻CD8⁺ lymphocyte subpopulations (Figure 2-5). The CD4⁺CD134⁺ subpopulation was

sequentially gated from the CD4⁺ T lymphocyte population (Figure 2-5). Each positive subpopulation cut-off value was set according to the background level observed in the negative control for each individual sample. At least 10,000 events were recorded and analysed for each sample.

When required, PBMC were stained with carboxyfluorescein succinimidyl ester (CFSE) at a final concentration of 5 μ M (Invitrogen, UK) in order to measure proliferation. Briefly, CFSE was added to the cell suspension and incubated at 37°C for 15 min. Cells were then washed once with sterile PBS, resuspended in warm R10 at 37°C for 30 min, washed again with sterile PBS and then cultured in 12 well plates at 1 x 10⁶ cells/well in R10. PBMC viability was then determined by staining with 7-aminoactinomycin D (7-AAD) (Thermo Fisher Scientific, UK). One μ l of 7-AAD was added to 10⁶ PBMC in 1 ml of R10 medium, the cells were incubated on ice for 30 min and analysed immediately.

All flow cytometry-based analyses were performed on a BD AccuriTM C6 flow cytometer, using CFlow® Sampler software (BD Bioscience, UK).

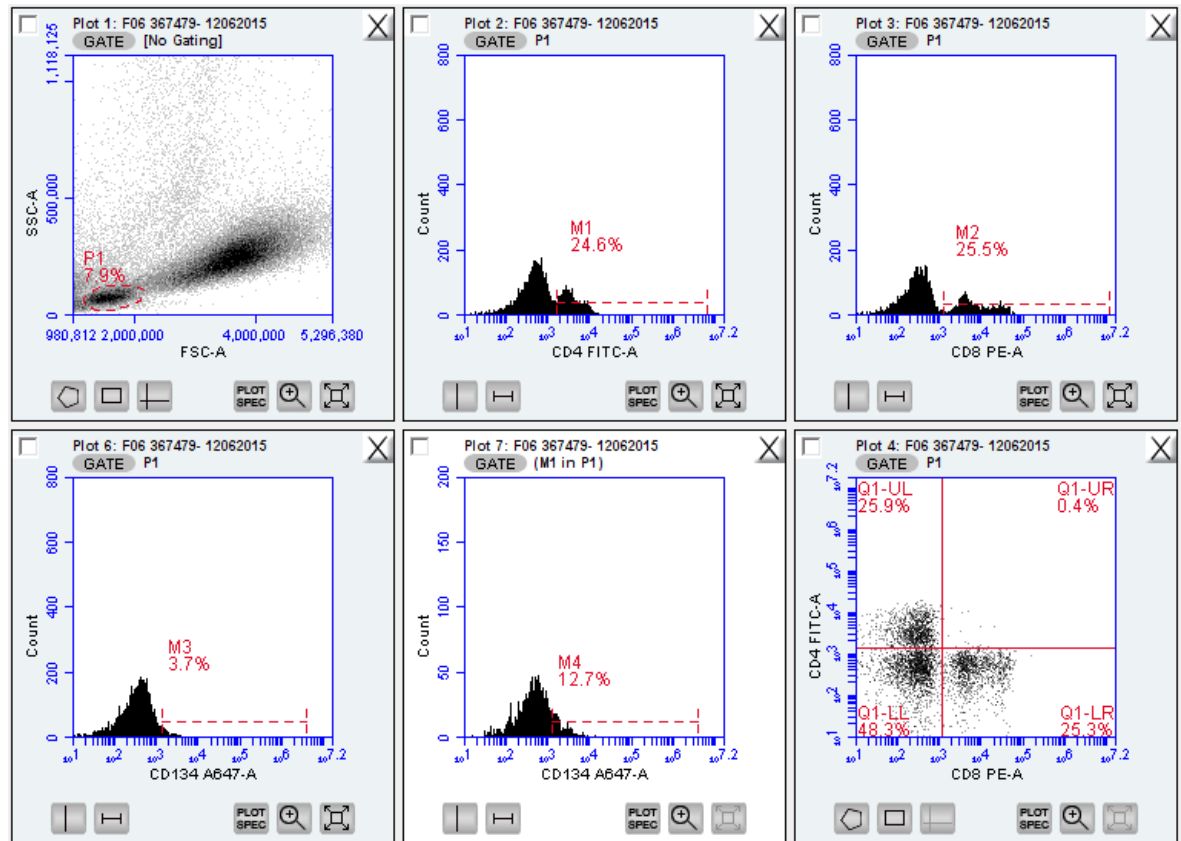


Figure 2-5 Gating strategy for the identification of T lymphocyte subpopulations. Lymphocytes (P1) were identified by size (forward scatter area, FSC-A, X-axis) and granularity (size scatter area, SSC-A, y-axis) (upper left). The percentages of the CD4⁺ (M1), CD8⁺ (M2) and CD134⁺ subpopulations (M3) within the total lymphocyte population were measured using the CD4-FITC-A (upper middle), CD8-PE-A (upper right) and CD134-A647-A (lower left) histograms, respectively. The percentage of the CD134⁺ population within the CD4⁺ population (M4) was measured using CD134-A647-A (lower middle) in the M1 population. A scatter plot displaying CD4-FITC-A against CD8-PE-A (lower right) was used to measure the single CD4⁺ (Q1-UL) and CD8⁺ (Q1-LR) populations.

2.4 Statistical analyses

All statistical analyses were performed using Prism software version 6.0 (Graphpad Software, La Jolla, USA). Two-tailed, Mann-Whitney and Kruskal-Wallis tests with Dunns' post tests were used to compare group medians. Fischer's exact and Spearman tests were used to analyse the effects of risk factors and to determine correlations between two variables, respectively. Two way ANOVA with Tukey's multiple comparisons were used to assess correlations between quantity of V5 variants and tissue compartments (Chapter 3). To analyse inter-relationships between multiple variables, principal component analysis (PCA) was performed using Unscrambler software version 9.7 (CAMO

Software, Oslo, Norway). P values less than 0.05 were considered to be statistically significant.

2.5 Ethics statement

The *in vivo* pathogenesis study, from which stored tissues were analysed for this project, was approved by the University of Glasgow Institutional Animal Care and Use Committee (OLAW Assurance A5181-01) “The control of feline retroviral infection in domestic cats” and was conducted under license from the UK Government Home Office under the Animals (Scientific Procedures) Act 1986. The use of recombinant viruses was approved by the Health and Safety Executive under The Genetically Modified Organisms (Contained Use) Regulations 2000.

The use of blood samples obtained from the University of Glasgow Veterinary Diagnostic Service was approved by the Ethics & Welfare Committee of the School of Veterinary Medicine, University of Glasgow under the application “Developing an algorithm to predict the outcome for cats infected with feline immunodeficiency virus” (reference no. 22a/13).

Chapter 3 Tissue compartmentalisation in cats experimentally infected with FIV

3.1 Introduction

Following experimental infection of cats with single strains of FIV, it has been shown that the dominant homogeneous FIV population spreads into several lymphoid and non-lymphoid organs during the early stage of infection (Bach et al., 1994, Beebe et al., 1994, Kenyon and Lever, 2011). Together with anatomical barriers, the error-prone reverse transcriptase enzyme and high rate of viral replication could potentially give rise to genetically distinct subpopulations, evolved from a single founding ancestor, in different body compartments, so called “tissue compartmentalisation” (Zhang et al., 2002, Zarate et al., 2007, Fletcher et al., 2011). Tissue compartmentalisation has long been observed in HIV infection. Different HIV variants have been detected in blood, lung, male-female genitourinary tract and central nervous system (CNS) (Wong et al., 1997, Singh et al., 1999, Zhang et al., 2002, Kemal et al., 2003, Karris and Smith, 2011). However, little is known about this phenomenon in FIV infected cats other than in the CNS (Pedersen et al., 1987, Dow et al., 1990, Dow et al., 1992, Ryan et al., 2003, Liu et al., 2006, Fletcher et al., 2011).

FIV transmission naturally occurs via biting (Hartmann, 1998, Yamamoto et al., 2007, Sykes, 2013). This route promotes transfer of the quasispecies rather than single virus variants, similar to HIV-1 transmission in intravenous drug users (IDU) (Bar et al., 2010). Analogous to the model of infection using single strains of virus, it is postulated that the variants within the FIV quasispecies also disseminate throughout the body into different tissue compartments following transmission to a new host (Bach et al., 1994, Beebe et al., 1994). Following infection, specific tissue microenvironments would select for the fittest variant, which is most able to replicate and so outcompetes the other variants, establishing its lineage within that tissue. Host and viral factors, such as target cell availability and tropism might play important roles in the selection of a distinct FIV population that evolved from the ancestral virus. FIV infects its major target cells, CD4⁺ T lymphocytes, via an interaction between its envelope glycoprotein (Env) and the CD134 and CXCR4 molecules on the cell surface (Shimojima et al., 2004, Willett et al., 2006b, Willett and Hosie, 2008,

Willett and Hosie, 2013, Willett et al., 2013). Moreover, FIV tropism is governed by sequence variation in the fifth variable loop (V5) of Env, which is involved in the interaction between Env and CD134 (Willett and Hosie, 2008, Kraase et al., 2010, Willett et al., 2010, Willett et al., 2013).

The number of appropriate target cells, namely CD4⁺CD134⁺ T lymphocytes, could also exert pressure on the quasispecies and preferentially select for the fittest variant within a particular tissue. This speculation is in line with the selection of CCR5 (R5) tropic over CXCR4 (X4) tropic HIV-1 variants and the selective depletion of CD4⁺CCR5⁺ memory T lymphocytes in GALT in the first 2 weeks following HIV infection (Mehandru et al., 2004, Mattapallil et al., 2005, Flint et al., 2015). In addition, the finding that R5 tropic SIV preferentially infected CCR5⁺ memory cells while X4 tropic viruses selectively infected resting, CXCR4⁺ naïve CD4⁺ T lymphocytes also reflects the impact of the type and quantity of the resident cell populations on tissue compartmentalisation (Mattapallil et al., 2005, Nishimura et al., 2005).

Therefore, we speculated that differences in the expression of receptors and/or numbers of target cells in different tissue compartments could exert selective pressure on the FIV population migrating to that compartment. In this chapter, tissue compartmentalisation in FIV infection was investigated in peripheral blood mononuclear cells (PBMC) and 21 tissues collected post mortem from 4 cats that had been experimentally inoculated with a reconstituted quasispecies comprising 6 closely-related FIV variants with different Env V5 sequences (Willett et al., 2013). The expression levels of CD134 and CXCR4 mRNA in the tissues were quantified and compared, together with the loads of each FIV V5 variant, in order to examine the effects of target cell availability and tissue specific selection.

3.2 Study Background

This study was designed to examine in more detail the pathogenesis of FIV infection, by studying samples stored from experimental infections conducted previously (Figure 3-1). The emergence of CRD2-independent variants was observed in a cat experimentally infected with FIV clade A strain GL8 for 322 weeks (Kraase et al., 2010). These late variants contained different amino acid sequences in the variable loops of Env, which were related to resistance to neutralising antibodies and CRD2-independent infection. The selective expansion of CRD2-dependent, GL8-like variants was observed in PBMC when a reconstituted quasispecies was inoculated into a cohort of four naïve cats that were then monitored for 21 weeks (Willett et al., 2013). Since the decreased replication of the CRD2-independent variants was not associated with either neutralising antibodies (NAb) or cytotoxic T lymphocyte (CTL) responses, it was most likely that CRD2-dependent variants replicated more efficiently in PBMC (Willett et al., 2013). These findings suggested a link between replicative capacity and receptor usage. Therefore we hypothesized that selective pressure from the number of target cells expressing the appropriate receptor molecules played a role in the selective expansion of the CRD2-dependent variants in early infection.

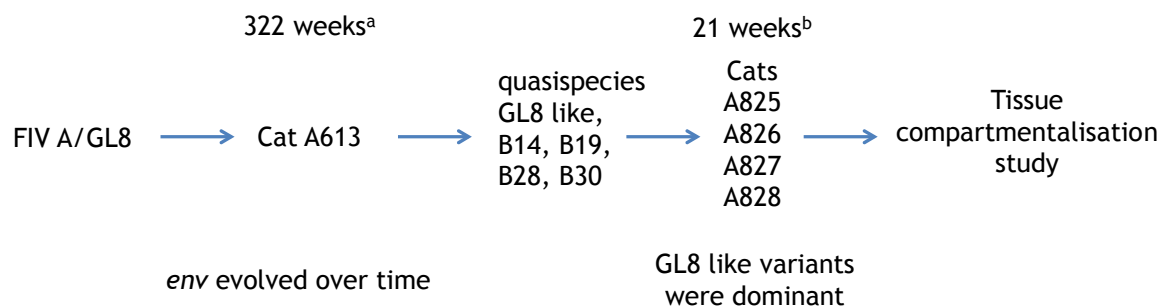


Figure 3-1 The present study was an extension of two previous studies conducted by our group; a) 322 weeks post infection with FIV clade A strain GL8 (UK8, accession no: X69496.1), a group of FIV variants with different V5 loop sequences (B14, B19, B28 and B30) emerged in cat A613 (Kraase et al., 2010), and b) GL8-like variants were dominant after infection of a reconstituted quasispecies into a cohort of four cats for 21 weeks (Willett et al., 2013). In the present study, tissues collected post mortem from these four cats were analysed for evidence of compartmentalisation.

3.3 Study Approach

Firstly, tissue compartmentalisation was investigated by performing variant-specific quantitative polymerase chain reaction (qPCR) using genomic DNA (gDNA) extracted from peripheral blood mononuclear cells (PBMC) and 21 frozen tissues (Table 3-1). Six sets of primers and probe were designed in order to determine the absolute proviral DNA load, based on the levels of *gag* and *env* of the GL8, B14, B19, B28 and B30 V5 variants. Next, the FIV V5 genes were amplified from the same gDNA template, cloned into an expression vector and analysed to confirm the qPCR results and the presence of tissue compartmentalisation. Finally, in an attempt to determine the roles of target cell availability, CD134 and CXCR4 transcripts were quantified in total RNA extracted from the same tissue samples.

3.4 Samples

Four cats (A825-828) had been inoculated intra-peritoneally with a mixture containing equivalent TCID₅₀ of six distinct Env V5 variants (B14, B19, B28, B30, B31 and B32) (Figure 3-1) (Willett et al., 2013). These V5 variants had evolved in one cat infected with the FIV GL8 molecular clone over the six year period of infection (Kraase et al., 2010). The variants displayed distinct biological properties, including receptor-usage and sensitivity to FIV-neutralizing antibodies (Appendix 3-1) (Willett et al., 2010, Willett et al., 2013). PBMC and 21 tissues (Table 3-1) were collected post-mortem, 21 weeks post infection, frozen immediately in liquid nitrogen and then stored frozen at -80°C.

Table 3-1 Tissue compartments investigated in this study

Visceral organs	Lymphoid organs
Salivary gland	Tonsil
Thyroid gland	Submandibular lymph node (SMLN)
Lung	Retropharyngeal lymph node (RPLN)
Liver	Prescapular lymph node (PRLN)
Stomach	Mediastinal lymph node (MDLN)
Pancreas	Spleen
Small intestine	Mesenteric lymph node (MSLN)
Large intestine	Popliteal lymph node (PLN)
Kidney	Bone marrow (BM)
Urinary bladder	Thymus
Reproductive organs	Peripheral blood mononuclear cells (PBMC)

3.5 Results

3.5.1 FIV proviral load differed between tissue compartments

The six V5 variants (B14, B19, B28, B30, B31 and B32) contained within the reconstituted quasispecies inoculum differed only in *env*, as each contained the same *gag-pol* backbone (Willett et al., 2013). Therefore, a *gag*-specific quantitative PCR was performed first to determine the total FIV proviral load (PVL) in each of the 22 tissue compartments. The *gag* qPCR amplified the region most conserved among different FIV strains, to reduce the effects of potential mutations in the primer binding regions during the course of the study (Klein et al., 1999). As shown in Figure 3-2A, FIV provirus (determined by *gag* qPCR) was detected in all 22 compartments. The FIV PVLs were significantly different amongst the 22 compartments ($p < 0.0001^{****}$, Kruskal-Wallis test). Thymus contained the highest PVL (49,907 copies/ 10^6 cells), followed by bone marrow and PBMC (26,491 and 17,083 copies/ 10^6 cells, respectively, Figure 3-2A). It was notable that a relatively high FIV PVL was detected in the thyroid gland (6,615 copies/ 10^6 cells). Next, tissue compartments were categorized into three types, namely the visceral organs (11 tissues), the lymphoid organs (10) and PBMC (Table 3-2). Lymphoid organs and PBMC harboured significantly higher FIV PVLs compared to the visceral organs (medians of 1,856 and 17,083 vs. 229 copies/ 10^6 cells, respectively) (Table 3-2, Figure 3-2B and Appendix 3-2).

Next, PVLs were determined using GL8 V5 primers and probes targeting the conserved region of GL8 V5 to quantify all V5 variants (Willett et al., 2013). From the 22 compartments examined in this study, FIV was undetectable using the GL8 V5 qPCR in five tissues, namely the salivary gland, pancreas, bladder, kidney and reproductive organs of all four cats (the lower limit of detection was 10 copies/ 10^6 cells) (Figure 3-3 and 3-4). These five tissues also demonstrated the lowest PVLs by *gag* qPCR, confirming their low viral burdens (Figure 3-3A). As observed with the *gag* qPCR, the FIV PVL varied markedly between tissue compartments (Figure 3-3A). These differences were statistically significant, although slightly weaker for the GL8 V5 qPCR compared to the *gag* qPCR (Kruskal-Wallis test, p value = 0.0004^{***}).

Although the highest PVL determined by GL8 *gag* qPCR was observed in the thymus of cat A825 (865,399 copies/ 10^6 cells), the median FIV load was highest in bone marrow when measured by GL8 V5 qPCR (142,050 copies/ 10^6 cells) followed by thymus and mesenteric lymph node (71,216 and 22,409 copies/ 10^6 cells, respectively) (Figure 3-3A). The thyroid gland also contained large amounts of FIV provirus (7,575 copies/ 10^6 cells) (Figure 3-3A). Similar to the *gag* qPCR, the GL8 V5 qPCR demonstrated that the PVLs in lymphoid organs were significantly greater compared to the PVLs of the visceral organs (median of 9,559 vs. 2,577 copies/ 10^6 cells, $p = 0.0011^{**}$) (Table 3-2, Figure 3-3B and Appendix 3-2). The lymphoid organs also contained higher PVLs than PBMC, although this difference was not statistically significant (9,559 vs. 6,199 copies/ 10^6 cells, $p = 0.2172$) (Table 3-2 and Figure 3-3B).

Although a similar lower limit of detection (10 copies/ 10^6 cells) was observed between the *gag* and GL8 V5 qPCR methods, the *gag* qPCR appeared to be more sensitive as it detected FIV provirus in 5 tissues in which virus was undetectable using the GL8 V5 qPCR (Figures 3-2A, 3-3B and 3-4A). However, greater PVLs (determined by GL8 V5 qPCR) were observed in most tissues, with the exception of submandibular lymph node (800 vs. 1,774 copies/ 10^6 cells), thymus (38,472 vs. 49,907 copies/ 10^6 cells) and PBMC (6,199 vs. 17,083 copies/ 10^6 cells) (Figure 3-4A). Nevertheless, these differences were small and were not statistically significant in any of the 22 compartments investigated ($p = 0.1896$, two-way ANOVA with Tukey's multiple comparisons) (Figure 3-4A). Moreover, a strong positive correlation was observed between the FIV PVLs determined by the two methods (Spearman $r = 0.9035$, $p < 0.0001^{****}$, Figure 3-4B).

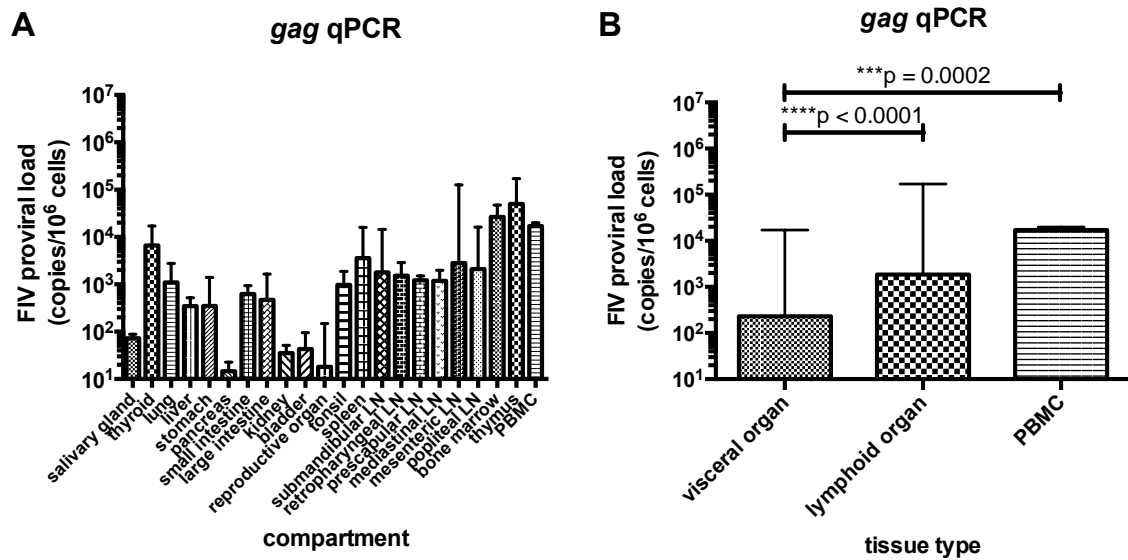


Figure 3-2 Comparisons of FIV PVL (copies/10⁶ cells) as determined by *gag* quantitative PCR (qPCR) between 22 tissue compartments (A) and between three tissue types; visceral organs, lymphoid organs and peripheral blood mononuclear cells (PBMC) (B). Each bar represents the median with the range for four cats. The Y-axis is shown from the lower limit of detection (≤ 10 copies/10⁶ cells). Quantification of PVL was performed in triplicate. Kruskal-Wallis test (A) and Mann-Whitney test (B)

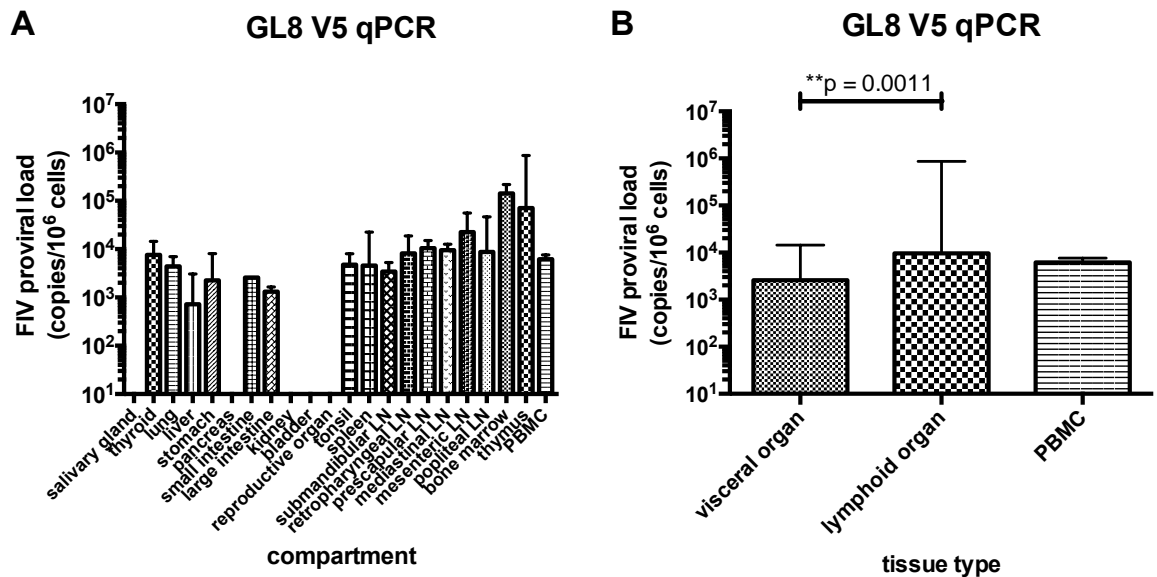


Figure 3-3 Comparisons of FIV PVL (copies/10⁶ cells) as determined by GL8 V5 qPCR between 22 tissue compartments (A) and between three tissue types; visceral organs, lymphoid organs and peripheral blood mononuclear cells (PBMC) (B). Each bar represents the median with the range for four cats. The Y-axis is shown from the lower limit of detection (≤ 10 copies/10⁶ cells). Quantification of PVL was performed in triplicate. Kruskal-Wallis test (A) and Mann-Whitney test (B)

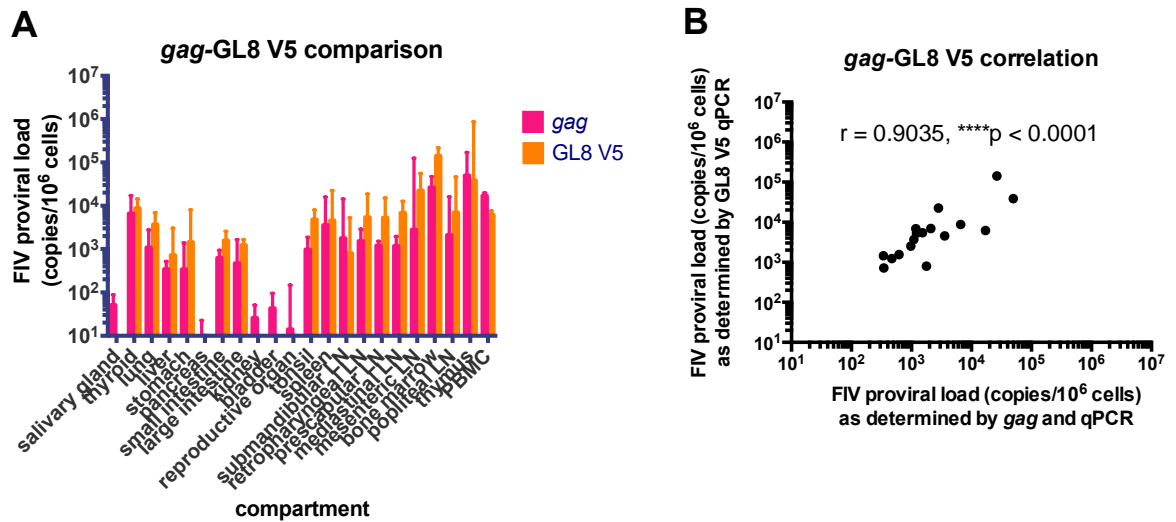


Figure 3-4 Comparison of FIV PVL as determined by *gag* and GL8 V5 qPCRs in 22 compartments, each bar representing the median with the range for four cats. The Y-axis is shown from the lower limit of detection (≤ 10 copies/ 10^6 cells), two-way ANOVA with Tukey's multiple comparisons (A). Spearman correlation between FIV PVL as determined by *gag* and GL8 V5 qPCRs (B). Quantification of PVL was performed in triplicate.

Table 3-2 FIV PVL in three tissue compartments

	visceral organs ^a	lymphoid organs ^b	PBMC
gag	229 (10 - 17,102)	1,856 (85 - 170,874)	17,083 (2,526 - 19,926)
GL8 V5	2,577 (132 - 14,309)	9,559 (110 - 865,399)	6,199 (1,771 - 7,633)
B14**	681	583 (495 - 6,953)	2,175 (2,074 - 5,231)
B19	888 (301 - 5,453)	3,934 (555 - 27,273)	7,695 (3,359 - 12,674)
B28	3,586 (1,005 - 31,101)	4,278 (691 - 1,397,646)	1,686 (154 - 8,747)
B30	1,407 (106 - 216,531)	2,301 (89 - 61,688)	10,171 (2,403 - 13,359)

^avisceral organs: salivary gland, thyroid, lung, liver, stomach, pancreas, small intestine, large intestine, kidney, urinary bladder, reproductive organs, ^blymphoid organs: tonsil, spleen, submandibular LN, retropharyngeal LN, prescapular LN, mediastinal LN, mesenteric LN, popliteal LN, bone marrow and thymus, *median (copies/ 10^6 cells with the range in brackets) was calculated from PVL of all tissues in the same category for four cats, **B14 was only detectable in prescapular lymph node, mediastinal lymph node and thymus of cat A825, liver of cat A826 and PBMC of cats A825, A827 and A828

3.5.2 V5 variant PVL were highly diverse between tissue compartments

The PVLs of each of the FIV V5 variants were measured using variant-specific primers and probes, targeting the individual V5 loop sequence of each variant (Willett et al., 2013). B14 was rarely observed in tissues, only being detectable in the prescapular lymph node, mediastinal lymph node and thymus of cat A825, liver of cat A826 and PBMC of cats A825, A827 and A828 (Figure 3-5A). This finding was not unexpected, since impaired replication of B14 had been observed throughout the study period of 21 weeks (Willett et al., 2013). Overall, V5 variants were detected in all but five compartments; salivary gland, pancreas, bladder, kidney and reproductive organs of all 4 cats tested negative (Figure 3-5B to 3-5D). In addition to these five compartments, B28 was also undetectable in bone marrow of all four cats (Figure 3-5C). Similar to the results of the *gag* and GL8 V5 qPCR analyses, the quantities of V5 variants were statistically different between the tissue compartments (Kruskal-Wallis test, $p = 0.0002^{***}$, $p = 0.0003^{***}$ and $p = 0.002^{***}$ for B19, B28 and B30, respectively) (Figure 3-5B to 3-5D). The sample size of B14 was too small to permit statistical analysis (Figure 3-5A).

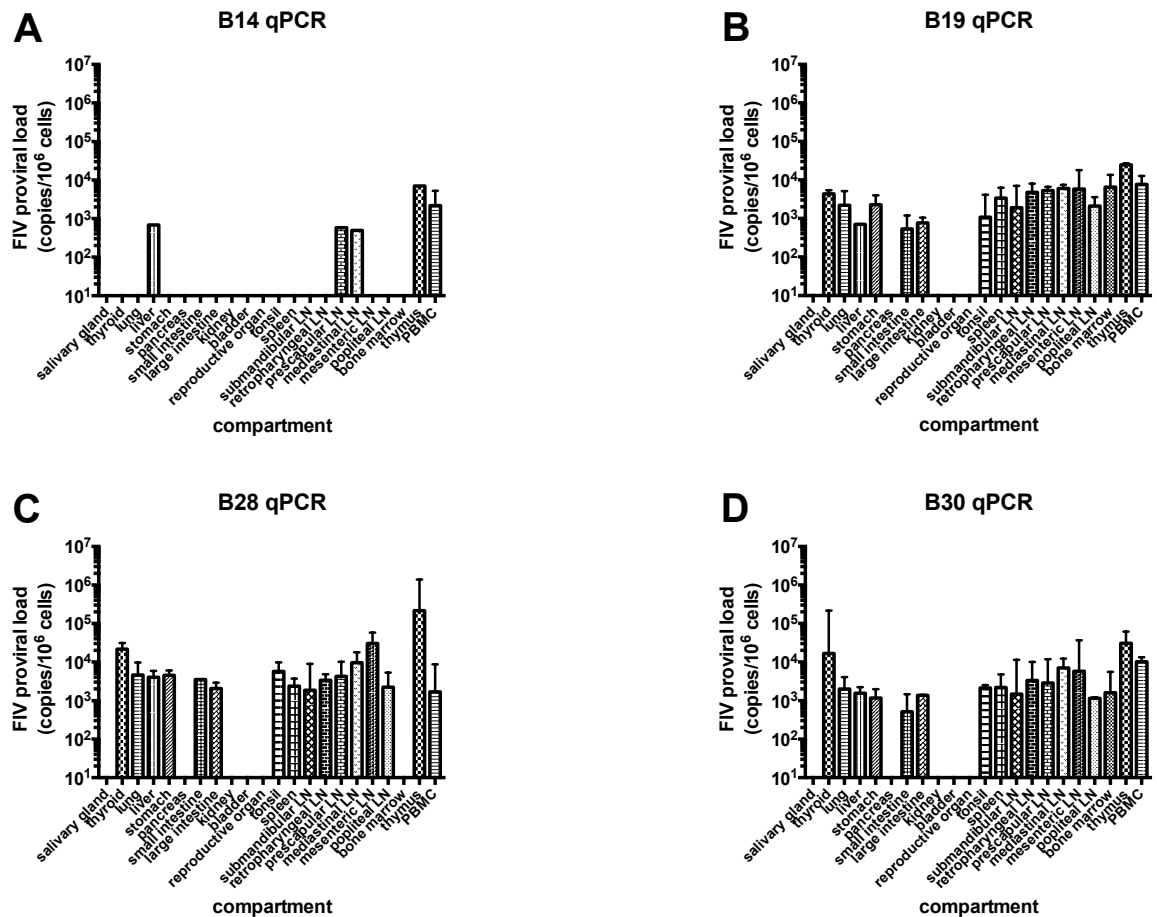


Figure 3-5 Comparisons of FIV PVL (copies/10⁶ cells) between 22 tissue compartments as determined by B14 (A), B19 (B), B28 (C) and B30 (D) qPCR. Each bar represents the median with the range for four cats. The Y-axis is shown from the lower limit of detection (≤ 10 copies/10⁶). Quantification of PVL was performed in triplicate. Kruskal-Wallis test

Similar to the qPCR analyses for *gag* and GL8 V5, the PVL of B19 in PBMC and lymphoid organs was significantly higher than in the visceral organs (3,934 and 7,695 vs. 888 copies/10⁶ cells, $p = 0.0009^{***}$ and $p = 0.0118^*$, respectively) (Table 3-2 and Figure 3-6B). For B30, only the PVL in PBMC was significantly higher than in the visceral organs (10,171 vs. 1,407 copies/10⁶ cells, $p = 0.0404^*$) (Table 3-2 and Figure 3-6D). It was notable that the PVLs of B14 and B28 were relatively similar between tissue types (Figure 3.6A and 3.6C). For B14, this might be related to the small number of tissues in which virus was detected (one visceral organ, three lymphoid organs), which hindered statistical analysis. For B28, despite the high PVL in the thymus (median of four cats was 217,040 copies/10⁶ cells), the median loads in the visceral and lymphoid organs did not differ significantly (3,586 and 4,278, respectively) (Table 3-2 and Figure 3-6C).

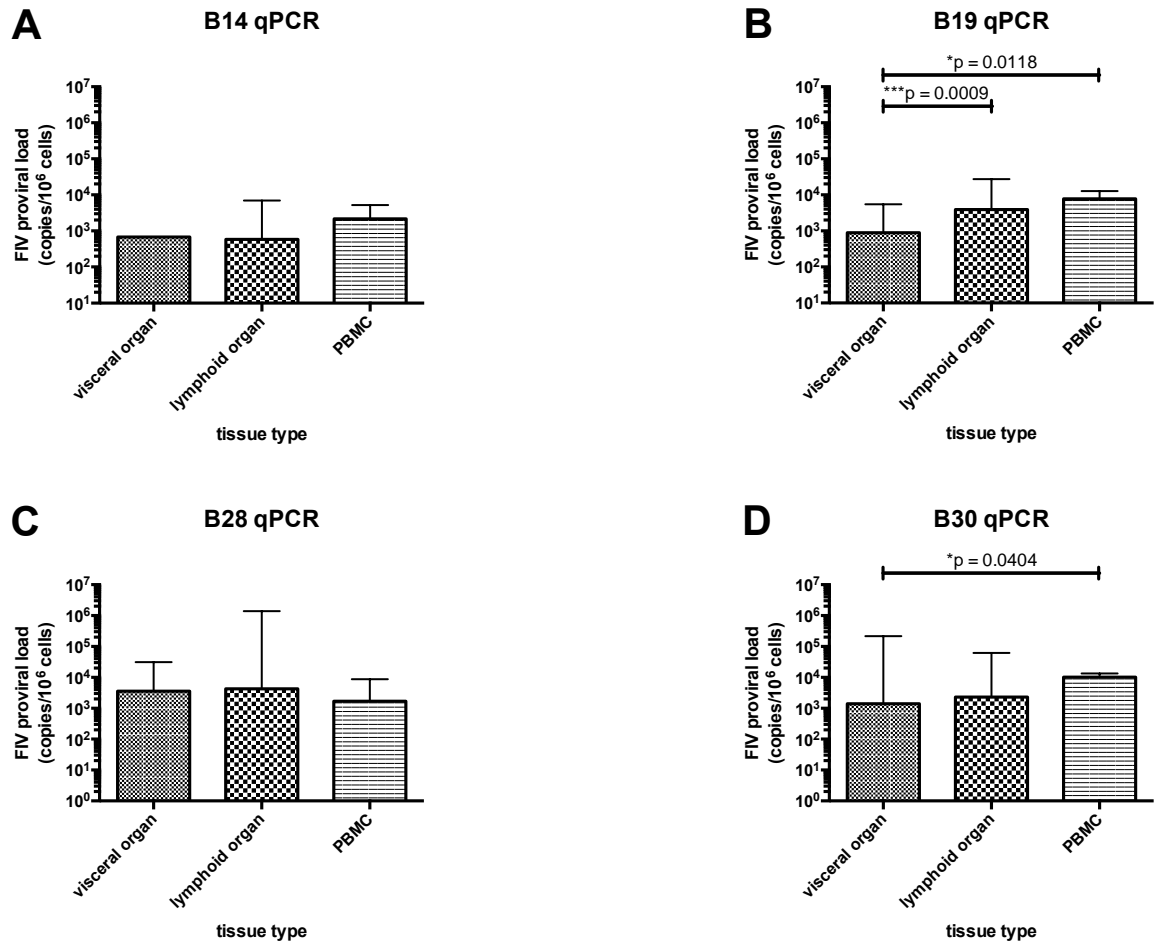


Figure 3-6 Comparisons of FIV PVL (copies/10⁶ cells) between three tissue types; visceral organs, lymphoid organs and peripheral blood mononuclear cells (PBMC) as determined by B14 (A), B19 (B), B28 (C) and B30 (D) qPCR. Each bar represents the median with the range for four cats. Quantification of PVLs was performed in triplicate. The Y-axis is shown from the lower limit of detection (≤ 10 copies/10⁶). Mann-Whitney test

3.5.3 V5 variant PVL differed significantly between variants and tissue compartments

As shown above, the total FIV PVL as determined by both the *gag* and GL8 V5 qPCR methods, and also the quantity of each of the V5 variants, varied significantly between tissue compartments, and lymphoid tissues were observed to be the main viral reservoir. We next investigated whether the PVL of each of the V5 variants (B14, B19, B28 and B30) varied within and between compartments. To address this question, a two-factor analysis of variance (two-way ANOVA) was performed with the V5 variants and tissue compartments as column and row factors, respectively. Since none of the four V5 variants were detectable in salivary gland, pancreas, kidney, urinary bladder or reproductive

organs, these five compartments were excluded from the analysis. Figure 3-7 summarises the FIV PVL determined using each qPCR method in 22 tissue compartments of four cats.

The two-way ANOVA showed a significant interaction between tissue compartments and variants (accounting for 31.07% of total variance, $p < 0.0006^{***}$) (Appendix 3-3). This interaction indicated that the variations between each of the four V5 variant PVLs were statistically significantly different, as were the differences between the 22 tissue compartments examined. Moreover, statistically significant differences were not observed when total FIV PVLs (determined by *gag* and GL8 V5 qPCR) were analysed ($p = 0.3114$), confirming that the variability between each V5 variant, rather than the variations in PVL determined by different qPCR methods, accounted for the interaction observed between tissue compartments and variants (Appendix 3-3).

The differences between the PVL of each V5 variant were statistically significant (accounting for 2.56% of total variance, $p = 0.0494^*$). Significant variability was also observed amongst the 22 tissue compartments (accounting for 10.04% of total variance, $p = 0.0186^*$) (Appendix 3-3). Using Tukey's multiple comparisons, the PVL of B28 in thymus was the highest. It was significantly higher than the level in the other 17 tissue compartments examined ($p < 0.0001^{****}$) and it was also significantly higher than the PVL of B14, B19 and B30 in all 17 compartments ($p < 0.0001^{****}$). No differences between variants were observed when total FIV PVLs (determined by *gag* and GL8 V5 qPCRs) were included in the analysis.

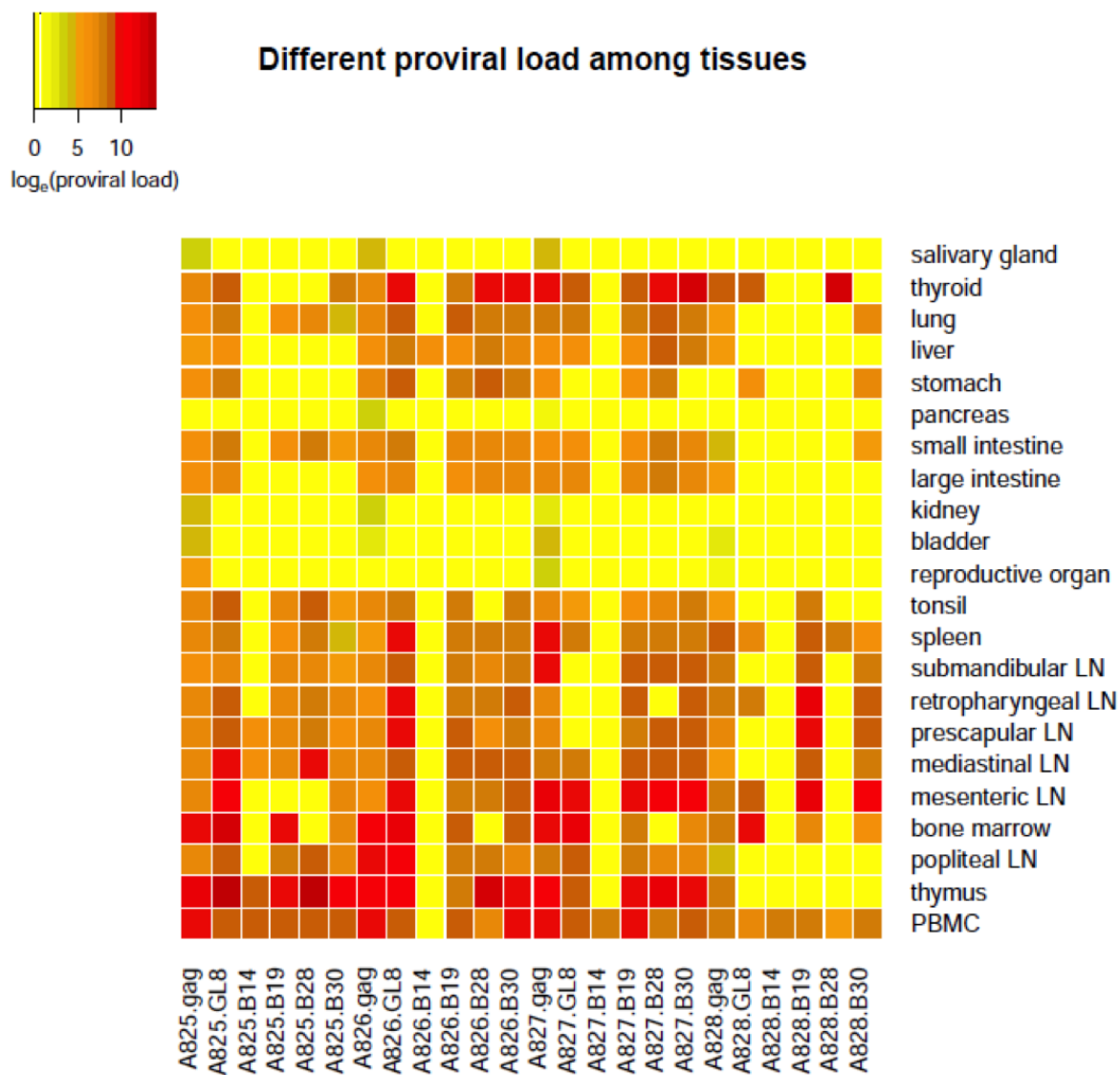


Figure 3-7 Absolute quantity (copies/10⁶ cells) of FIV PVL as determined by *gag*, GL8 V5, B14, B19, B28 and B30 qPCR in 22 tissue compartments. Log scale of PVL is indicated by the colour spectrum located at the top left. Yellow indicates PVL below the lower limit of detection (≤ 10 copies/10⁶). Quantifications of PVL were performed in triplicate. Median V5 variant (B14, B19, B28 and B30) or median *gag* and GL8 V5 PVLs of four cats (A825 - A828) were analysed by two-way ANOVA with Tukey's multiple comparisons

3.5.4 Lack of consensus pattern of compartmentalisation between cats

In order to investigate whether there was a shared pattern of V5 variant selection within the 22 tissue compartments, a principal component analysis (PCA) was performed. PCA is a powerful statistical technique used to observe inter-relationships between large numbers of variables. Since our aim was to determine whether there was tissue specific-selection of V5 variants, the 22 tissues were defined as “loading”, the determinants of the relationship while the PVL of each V5 variant in these tissues was defined as “score”, the hypothetical values that drive the relationship. In PCA, the original variables are plotted in a multidimensional space and then linearly transformed into “principal components (PC)”, each of which retains the maximal amount of information about the variables. If a V5 variant had been consistently selected in any given tissues in all four cats, the tissues (loading) should group together and lie in the same direction as the V5 variant (score) that drives the relationship on the PC plot.

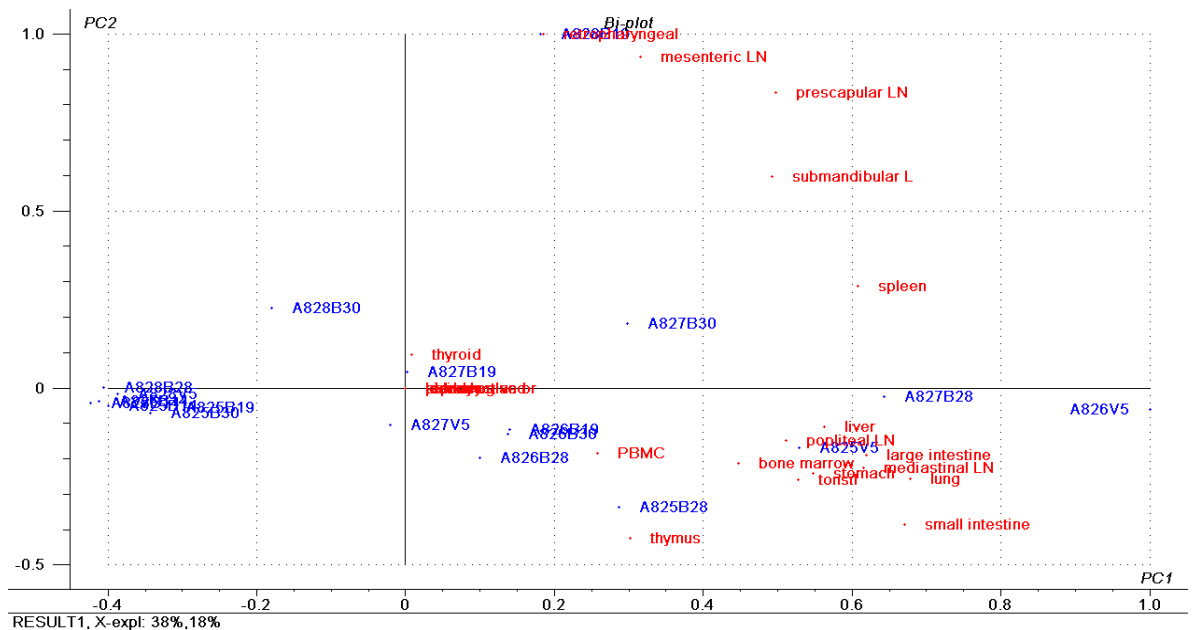


Figure 3-8 Relationship between tissue compartments and PVL of Env V5 variants. The figure shows a principal component analysis (PCA) bi-plot (loading and score) of the first two principal components (PC); PC1 on X-axis and PC2 on Y-axis. As shown in the lower left region of the figure, these 2 PC accounted for 56% (38% + 18%) of total variables. This PC value indicates the percentage of the original variable that could be explained by that PC. Tissue compartments (loading) and V5 variant PVL (score) are shown in red and blue, respectively.

As shown in Figure 3-8, when the quantities of each V5 variant in each compartment of all four cats were analysed altogether, no consistent relationships were observed. From the combined PC1 and PC2 value of 56%, the pattern observed here only accounted for approximately half of the variables, indicating that there was no dominant component when all four cats were analysed together. This was mainly due to the high variations between cats, reflected by the different tissue-dominant variants in each cat (Appendix 3-4 and 3-5). Nevertheless, evidence of compartmentalisation of B28 in thymus was detected in three of the four cats. In cats A825, 826 and 827, the position of thymus on the loading plots was consistently driven by the quantity of B28 PVL (Appendix 3-5A to 3-5F). For cat A828, FIV PVL was undetectable in the thymus, explaining the lack of B28 compartmentalisation in the thymus for this cat (Appendix 3-5G and 3-5H).

3.5.5 B28 was predominant in thymus but absent in bone marrow

Although the pattern of tissue-specific selection of V5 variants remained inconclusive, some findings were consistently observed in the bone marrow and thymus with variant B28. In all cats, B28 was uniformly absent from the bone marrow but demonstrated the highest PVL in the thymus (Figures 3-5C and 3-7). In addition, the association of B28 PVL and thymus was observed in PCA analyses of three of the four cats examined (Appendix 3-5A to 3-5F). To confirm these findings, a region of *env* spanning the entire V5 loop was amplified from proviral DNA prepared from bone marrow and thymus from all four cats. PCR amplicons were then cloned and the nucleotide sequences obtained. As shown in Figure 3-9A, with the exception of cat A828 in which FIV provirus could not be detected in thymus using any of the qPCR methods, B28 was indeed the major variant within the thymus (76.0%, 116/150 clones). The second most dominant variant was B30 (12.66%, 19/150), followed by B19 (4.67%, 7/150), the GL8-like variants (B31+B32) (4.0%, 6/150) and B14 (2.67%, 4/150) (Figure 3-9A, bottom panel). This finding agreed with the qPCR result, confirming that B28 PVL was predominant in thymus (median of four cats = 192,167 copies/10⁶ cells), followed by B30 (25,317 copies/10⁶ cells) and B19 (16,600 copies/10⁶ cells) (Figure 3-9A, top panel). B14 was only detected in cat A825 and the PVL was similar to that of B19.

The absence of variants B14 and B28 in the bone marrow, as demonstrated by qPCR, was confirmed by the colony sequencing results. As shown in Figure 3-9B, the GL8-like variants (B31+B32) were dominant in bone marrow (86.06%, 173/201), followed by B19 (8.95%, 18/201) and B30 (3.98%, 8/201) (Figure 3-9B, bottom panel). B14 and B28 were not detected, even when 50 colonies from each cat were screened. This observation was consistent with the quantities of the variants determined by qPCR: the PVL of B19 was higher than B30 (median PVL of four cats were 9,675 and 1,606 copies/ 10^6 cells, respectively) (Figure 3-9B, top panel). However, the absolute quantities of the GL8-like variants (B31+B32) could not be determined, since the GL8 V5 qPCR method detected all V5 variants. Nonetheless, the median FIV PVL as determined by GL8 qPCR was 108,883 copies/ 10^6 cells, which far exceeded the PVL of B19 (9,675 copies/ 10^6 cells) and B30 (1,606 copies/ 10^6 cells) combined, confirming that GL8-like variants predominated in the bone marrow, as had been observed by colony sequencing (Appendix 3-6).

Taken together, the significantly different PVLs of each V5 variant observed, both within and between the tissue compartments examined, and the predominance of B28 in the thymus and its absence from the bone marrow, demonstrate that tissue specific selection had arisen following the experimental infection of FIV quasispecies and resulted in the expansion of particular variants over others in the tissues, i.e. “tissue compartmentalisation”.

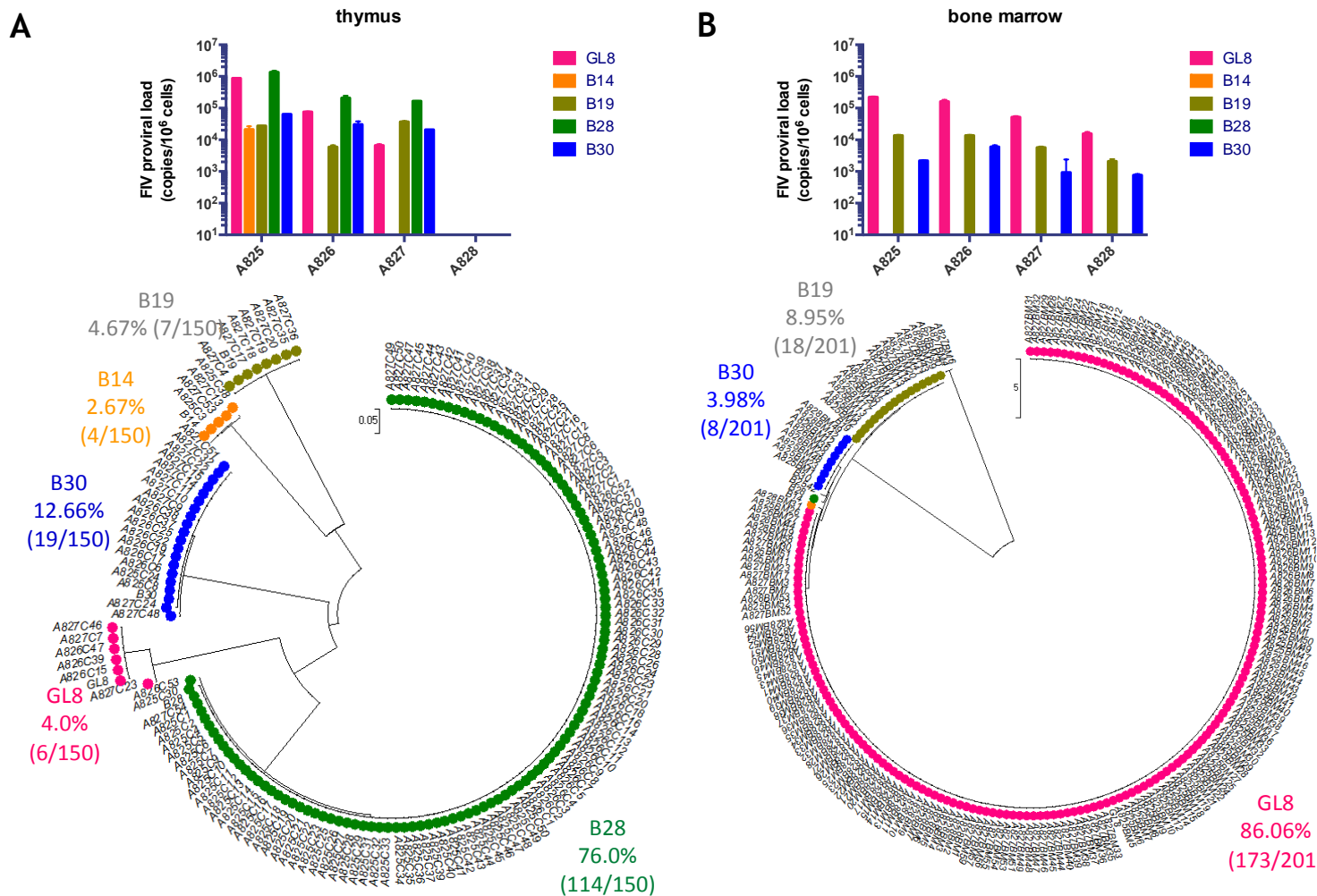


Figure 3-9 Compartmentalisation of V5 variants, Top: FIV PVL in thymus (A) and bone marrow (B) as determined by each V5 variant specific qPCR for each cat. Bottom: Unrooted maximum likelihood phylogenetic trees, comparing *env* V5 sequences derived from thymus (A) and bone marrow (B) of cats A825-828. Each tree contains 150 - 200 *env* V5 sequences, 50 from each cat (no PCR products were amplified from the thymus of cat A828), and five reference sequences. Coloured circles indicate sequence similarity to the reference sequences: GL8-like variants (B31 + B32) (pink), B14 (orange), B19 (drab), B28 (green) and B30 (blue). The percentages and frequencies of each V5 variant are shown next to the relevant cluster.

3.5.6 Levels of CD134 and CXCR4 mRNA in tissue compartments

Since the FIV V5 variant B28 was absent from the bone marrow but predominated in the thymus of all four cats, we speculated that the PVL of each V5 variant might be related to the number of CD134⁺ target cells in each tissue compartment. This speculation was based on the finding that the FIV V5 variants in this study showed distinct CD134 usage characteristics, reflected by different sensitivities to inhibition with neutralising antibodies, anti-CD134 antibody, soluble CD134 and CD134 ligand (Appendix 3-1) (Willett et al., 2010). Since these variants did not require CRD2 for infection, they might possess a selective advantage in low CD134⁺ cell compartments over CRD2-dependent variants such as their parental GL8.

As all tissue samples had been stored frozen, it was not possible to test this hypothesis by direct enumeration of CD134⁺ T lymphocytes by flow cytometry. Therefore, a duplex quantitative PCR specific for feline CD134 or CXCR4 mRNA together with feline β -actin was used (Scott et al., 2008). From the 22 compartments examined in this study, nine tissues with significant differences in FIV V5 variant PVL were selected for further investigation; thyroid gland, spleen, submandibular lymph node (SMLN), retropharyngeal lymph node (RPLN), prescapular lymph node (PSLN), mesenteric lymph node (MSLN), popliteal lymph node (PLN), bone marrow (BM) and thymus.

As shown in Figure 3-10, the levels of CD134 mRNA in nine compartments differed significantly, both between and within cats ($p < 0.0001^{****}$, two-way ANOVA with Tukey's multiple comparisons). Cat A826 contained the highest level of CD134 mRNA, followed by cats A828, A827 and A825 (medians = 2,494, 1,897, 1,715 and 1,190 plasmid copies, respectively) (Appendix 3-7). CD134 mRNA levels were highest in MSLN followed by PSLN, PLN and thymus (median = 3,484, 2,505, 2,306 and 2,268 plasmid copies, respectively) (Appendix 3-8). The levels of CD134 mRNA of both MSLN and PSLN were significantly higher compared to the other tissue compartments (Table 3-3). Surprisingly, similar levels of CD134 mRNA were observed in primary (bone marrow and thymus) and secondary lymphoid tissues (spleen, MSLN, PLN, PSLN, RPLN and SMLN) (median values of 1,922 vs. 2,086 plasmid copies, $p = 0.6038$, Mann-Whitney test). This finding was unexpected, since CD134 is expressed on the surface of CD4⁺ T lymphocytes

following antigen stimulation, which generally occurs in the secondary lymphoid tissues (Reggeti et al., 2008).

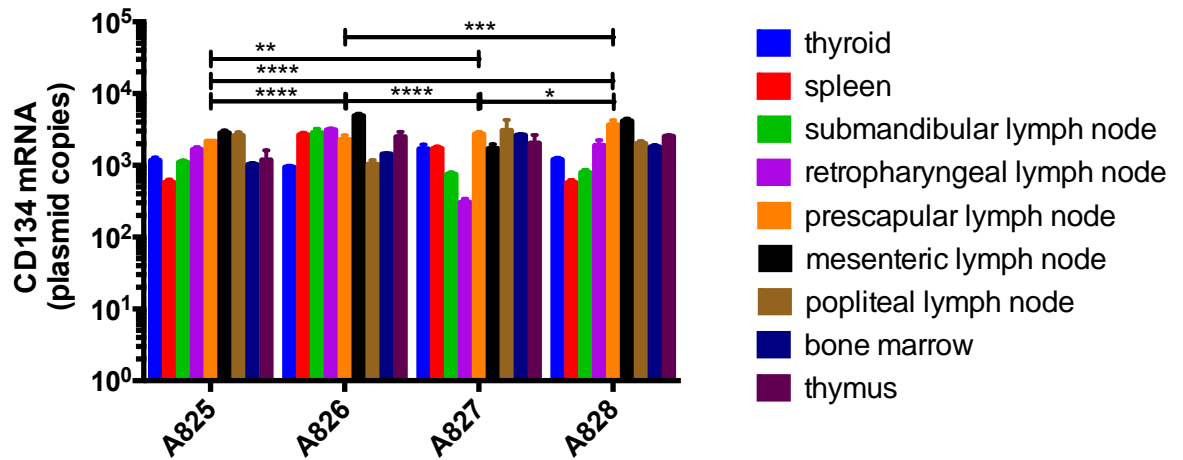


Figure 3-10 Comparison of CD134 mRNA levels in nine compartments of four cats, each bar shows the mean value with standard deviation (SD) of three replicates. Two-way ANOVA with Tukey's multiple comparisons, *, **, *** and **** indicated p values of < 0.05, < 0.01, < 0.05 and < 0.0001, respectively.

Table 3-3 Statistical comparisons of CD134 mRNA levels between compartments*

	thyroid	spleen	SMLN	RPLN	PSLN	MSLN	PLN	BM
spleen	ns							
SMLN	ns	ns						
RPLN	**	ns	ns					
PSLN	****	****	****	****				
MSLN	****	****	****	****	****			
PLN	****	****	****	*	**	****		
BM	*	ns	ns	ns	****	****	*	
thymus	****	****	****	ns	***	****	ns	ns

* Comparison of mean levels in four cats using Tukey's multiple comparisons, the median value with the range of individual tissues are shown in Appendix 3-8, *, **, *** and **** indicate p values of < 0.05, < 0.01, < 0.05 and < 0.0001, respectively, ns = not significant

Similar to CD134 mRNA, the levels of CXCR4 mRNA differed significantly between tissues and between cats ($p < 0.0001^{****}$, two way ANOVA with Tukey's multiple comparisons) (Figure 3-11). The level of CXCR4 mRNA was highest in cat A826 (13,787 plasmid copies), followed by cats A828, A827 and A825 (median values 6,838, 3,544 and 3,306 plasmid copies, respectively) (Appendix 3-8). MSLN contained the highest level of CXCR4 mRNA followed by PSLN, thymus gland, RPLN and SMLN (median values 36,428, 32,224, 17,281, 11,845 and 7,366 plasmid copies, respectively) (Appendix 3-9). The levels observed in these five tissues were statistically significantly greater than those in the other tissues examined (Table 3-4). When the tissues were categorized into primary and secondary lymphoid organs, the levels of CXCR4 mRNA were similar, as had been observed with CD134 mRNA (4,985 vs. 6,540 plasmid copies number, $p = 0.6337$, Mann-Whitney test).

In all tissues except popliteal lymph node, the levels of CXCR4 mRNA were significantly higher than the levels of CD134 mRNA (median of 8,256 vs. 1,746, $p = 0.0012^{**}$, Mann-Whitney test) (Figure 3-12). When individual tissues were examined, the CXCR4 mRNA quantity was significantly higher in MSLN (36,428 vs. 3,484 plasmid copies number, $p < 0.0001^{****}$), PSLN (32,224 vs. 2,505 plasmid copies number, $p < 0.0001^{****}$) and thymus (17,281 vs. 2,268 plasmid copies number, $p < 0.01^{**}$) compared to the other tissues (Appendix 3-8).

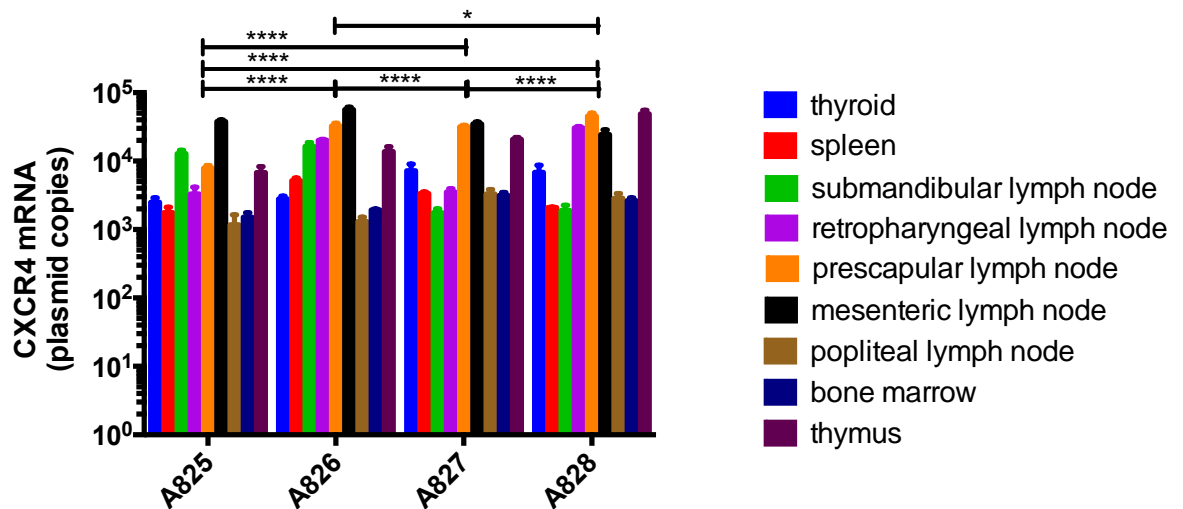


Figure 3-11 Comparison of CXCR4 mRNA levels in nine compartments between four cats, each bar shows the mean value with standard deviation (SD) of three replicates. Two way ANOVA with Tukey's multiple comparisons, * and **** indicates p values of < 0.05 and < 0.0001 , respectively.

Table 3-4 Statistical comparisons of CXCR4 mRNA levels between compartments*

	thyroid	spleen	SMLN	RPLN	PSLN	MSLN	PLN	BM
spleen	ns							
SMLN	***	****						
RPLN	****	****	****					
PSLN	****	****	****	****				
MSLN	****	****	****	****	****			
PLN	*	ns	****	****	****	****		
BM	*	ns	****	****	****	****	ns	
thymus	****	****	****	****	****	****	****	****

*Comparison of mean level of four cats using Tukey's multiple comparisons, median value with the range of individual tissue were shown in Appendix 3-8, *, ** and **** indicate p values of < 0.05, < 0.005 and < 0.0001, respectively, ns = not significant

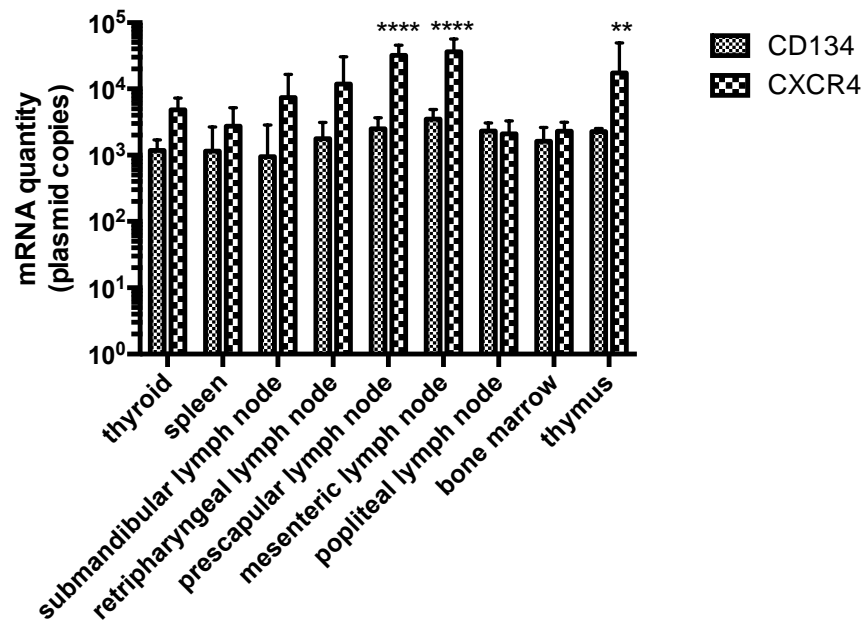


Figure 3-12 Comparison of CD134 and CXCR4 mRNA levels in each tissue compartment, each bar representing the median with the range for four cats, Two-way ANOVA with Sidak's multiple comparisons, ** and **** indicate p values of < 0.01 and < 0.0001, respectively.

3.5.7 Relationships between the levels of CD134 and CXCR4 mRNA and FIV PVL

Since the quantity of each V5 variant differed significantly and different levels of CD134 and CXCR4 mRNA were also observed between tissues, we next investigated whether there was any correlation between the level of CD134 or CXCR4 mRNA and the quantity of each of the V5 variants in each tissue (Table 3-5 and Figure 3-13). Overall, the relationship between CD134 mRNA and total PVL as determined by *gag* and GL8 V5 qPCR was inconclusive, with very broad 95% confidence intervals (0.5887 to 0.02683 for *gag* and -0.2429 to 0.4957 for GL8 V5) (Table 3-5 and Figure 3-13A). This ambiguity was also observed for CXCR4 mRNA (Table 3-5 and Figure 3-13B). The lack of correlation might be related to the different characteristics of each variant in the quasispecies (Appendix 3-1), as reflected by the high variations and different correlations observed between variants B19, B28 and B30 (Table 3-5). B14 was undetectable in most of the tissues examined and so could not be included in this analysis. While the PVL of B19 showed no statistically significant correlation with CD134 mRNA levels, the positive correlation with CXCR4 mRNA levels almost reached statistical significance ($r = 0.3306$, $p = 0.0692$) (Table 3-5). In addition, although not statistically significant, a negative correlation was observed between B28 PVL and CD134 mRNA ($r = -0.3587$, $p = 0.0928$). Positive correlations were observed between B30 PVL and both the levels of CD134 and CXCR4 mRNA (Table 3-5), although only the correlation with CXCR4 mRNA ($r = 0.4552$, Spearman test) was statistically significant ($p = 0.0078^{**}$).

Table 3-5 Relationships between CD134 and CXCR4 mRNA and FIV PVL*

CD134 mRNA against

	r	95% CI	P value
<i>gag</i>	-0.3135	-0.5887 to 0.02683	0.0626
GL8 V5	0.1468	-0.2429 to 0.4957	0.4473
B14	na	na	na
B19	0.008065	-0.3568 to 0.3709	0.9657
B28	-0.3587	-0.6786 to 0.07568	0.0928
B30	0.1748	-0.1895 to 0.4968	0.3306

CXCR4 mRNA against

	r	95% CI	P value
<i>gag</i>	-0.2221	-0.5206 to 0.1247	0.1929
GL8 V5	0.03448	-0.3463 to 0.4055	0.8591
B14	na	na	na
B19	0.3306	-0.03778 to 0.6199	0.0692
B28	0.0009881	-0.4221 to 0.4237	0.9964
B30	0.4552	0.1222 to 0.6961	**0.0078

*Spearman correlation, B14 PVL in tissues was too low for inclusion in the analysis (na = not analysed), ** indicates p values of < 0.01

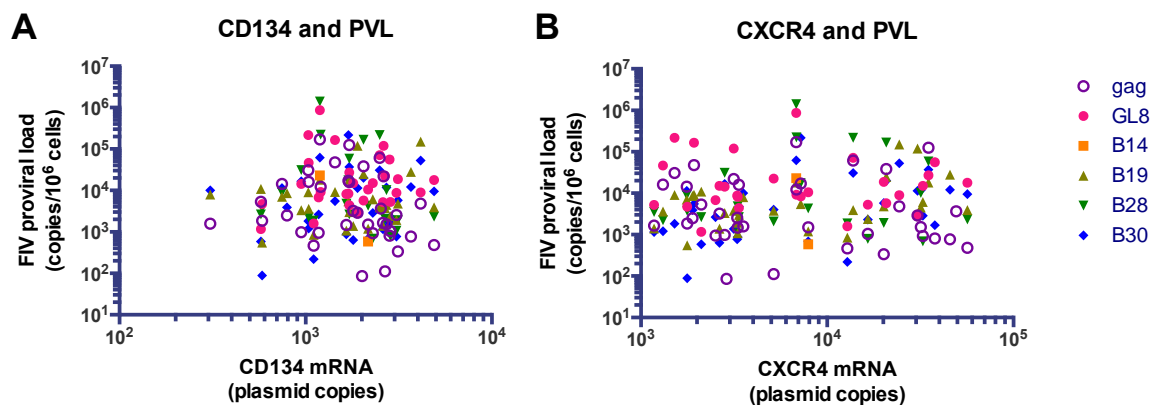


Figure 3-13 Relationship between CD134 (A) and CXCR4 (B) mRNA and FIV PVL as determined by *gag* (opened purple circle), GL8 V5 (pink circle), B14 (yellow square), B19 (drab upward triangle), B28 (green downward triangle) and B30 (blue diamond) qPCR in nine tissue compartments; thyroid, spleen, SMLN, RPLN, PSLN, MSLN, PLN, bone marrow and thymus. Each symbol represents the mean value for individual tissues from each of the four cats. Quantifications of PVL and mRNA were performed in triplicate. Spearman test

It was reported previously in both humans (Soulie et al., 2012) and cats (Reggeti et al., 2008) that lymphocyte activation resulted in increased expression of CD134 and decreased CXCR4 expression. In addition, at least in human T lymphocytes, while CXCR4 is constitutively expressed, CD134 is only expressed on the cell surface after stimulation via the T cell receptor-peptide major histocompatibility complex (TCR-pMHC) complex and CD28 signaling pathway (Gerard and Rollins, 2001, Croft, 2014). Therefore, we proposed that the CD134 mRNA:CXCR4 mRNA ratio might reflect the level of activated T lymphocytes in the tissues, while the CXCR4 mRNA:CD134 mRNA ratio might reflect the level of naïve cells. It was observed that the CD134:CXCR4 mRNA ratio was highest in PLN (0.86), followed by bone marrow (0.71) and spleen (0.42) (Appendix 3-9).

We next examined relationships between the CD134:CXCR4 mRNA ratio and PVL, as determined using each primer and probe set. No significant correlation was observed between the total FIV PVL as determined by *gag* or GL8 V5 qPCR and the CD134:CXCR4 mRNA ratio, most likely reflecting the high degree of variation, given the broad 95% confidence interval (Table 3-6). With the exception of the B14 variant, which was precluded from the statistical analysis because of the small sample size, a negative correlation was observed between the CD134:CXCR4 mRNA ratio and the PVL of the other V5 variants, namely B19 ($r = -0.4391$), B28 ($r = -0.1123$) and B30 ($r = -0.4403$); this correlation was statistically significant for variants B19 and B30 (p values = 0.0135* and 0.0103*, respectively) (Table 3-6 and Figure 3-14).

Table 3-6 Relationship between CD134 mRNA:CXCR4 mRNA ratio and FIV PVL*

	r	95% CI	P value
<i>gag</i>	0.1482	-0.1993 to 0.4626	0.3884
GL8 V5	0.09543	-0.2913 to 0.4554	0.6224
B14	na	na	na
B19	-0.4391	-0.6923 to -0.08948	*0.0135
B28	-0.1123	-0.5110 to 0.3260	0.6098
B30	-0.4403	-0.6864 to -0.1039	*0.0103

*Spearman correlation, number of copies of variant B14 in tissues was too small for analysis (na = not analysed), * indicates p values of < 0.05

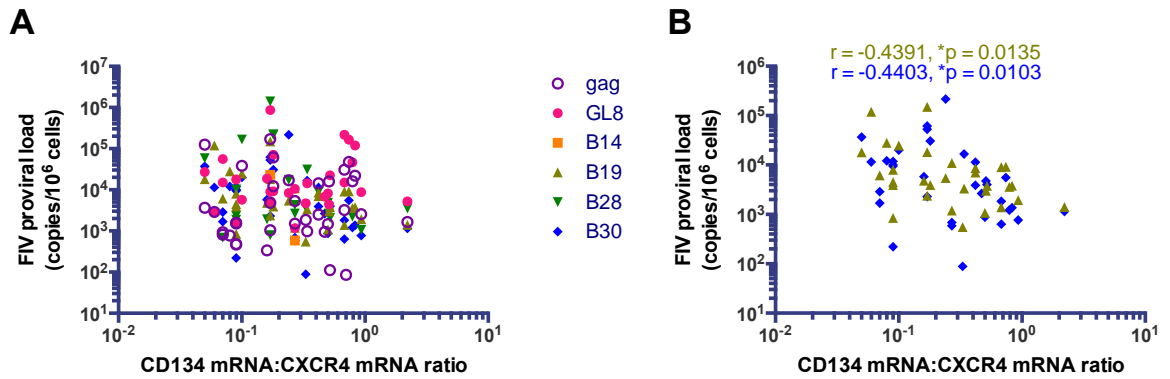


Figure 3-14 Relationship between CD134 mRNA:CXCR4 mRNA ratio and FIV PVL as determined by *gag* (opened purple circle), GL8 V5 (pink circle), B14 (yellow square), B19 (drab upward triangle), B28 (green downward triangle) and B30 (blue diamond) qPCR in nine tissue compartments (A). Relationship between CD134:CXCR4 mRNA ratios and PVL of variants B19 and B30 (B). Each symbol represents the mean value for individual tissues from each of the four cats. Quantifications of PVL and mRNA were performed in triplicate. Spearman test

3.5.8 FIV infection associated with increased levels of CD134 and CXCR4 mRNA in bone marrow and spleen but not thymus

Hyper-activation of the immune system is one of the key events in the pathogenesis of FIV infection (Silvotti et al., 1997, Tompkins and Tompkins, 2008, Taniwaki et al., 2013). As CD134 and CXCR4 mRNA expression levels vary according to the activation status of the cell, changes in expression could reflect the level of immune activation of the tissue compartments. To investigate this issue, the expression levels of CD134 and CXCR4 mRNA in bone marrow, spleen and thymus were compared with those of age-matched, uninfected, specific pathogen free (SPF) cats.

Similar to the FIV infected cats, the expression levels of CD134 and CXCR4 mRNA differed significantly between compartments and between individuals amongst three uninfected SPF cats ($p < 0.0001^{****}$, two-way ANOVA with Tukey's multiple comparisons) (Figure 3-15 and Appendix 3-10). Of the three tissues examined, the thymus contained the highest amount of both CD134 and CXCR4 mRNA (363 and 2,238 plasmid copies, respectively), followed by bone marrow (98 and 114 plasmid copies, respectively) and spleen (37 and 13 plasmid copies, respectively). As shown in Figure 3-16, FIV infection was associated with significantly increased expression of CD134 and CXCR4 mRNA in bone marrow and spleen, whereas the expression levels of both CD134 and CXCR4 mRNA in

thymus were similar in FIV positive and negative cats (Figure 3-16). The CD134:CXCR4 mRNA ratio was slightly higher in the bone marrow and thymus of FIV infected cats, but this difference was not statistically significant (1.20 vs. 0.83 and 0.33 vs. 0.21, respectively).

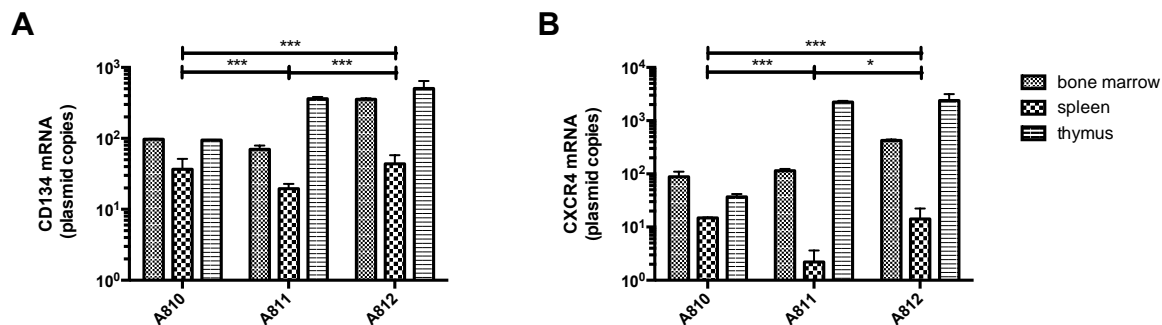


Figure 3-15 Comparisons of CD134 mRNA (A) and CXCR4 mRNA (B) levels in three compartments; bone marrow, spleen and thymus of three FIV negative SPF cats; each bar represents the mean with standard deviation (SD) of results measured in triplicate. Two-way ANOVA with Tukey's multiple comparisons, * and *** indicate p values of < 0.05 and < 0.001, respectively.

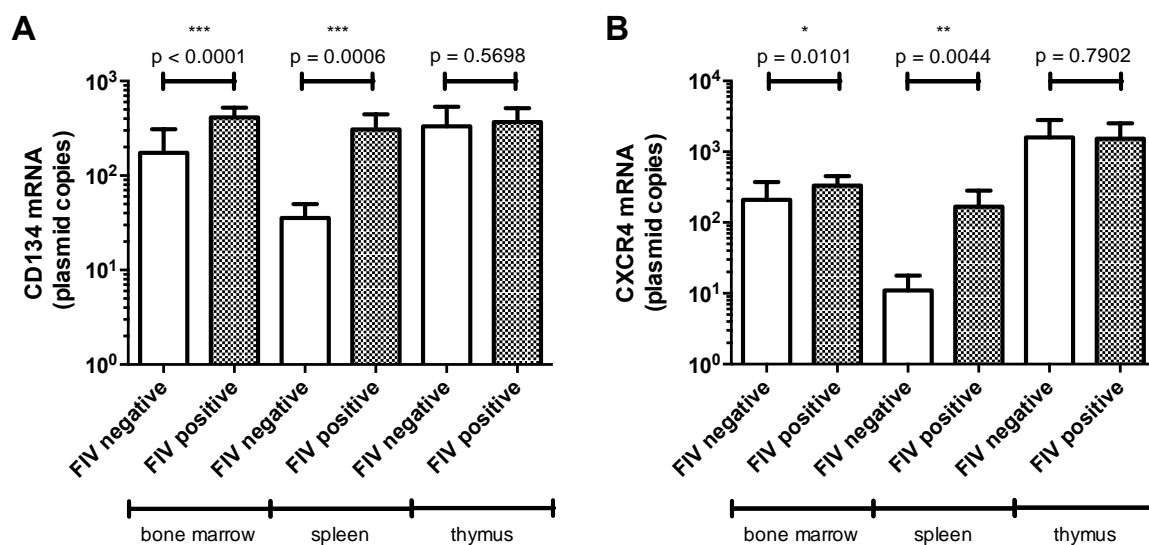


Figure 3-16 Comparisons of CD134 (A) and CXCR4 (B) mRNA levels in bone marrow, spleen and thymus in age-matched FIV negative (open bars) and FIV positive (shaded bars) cats. Each bar represents the median with the range for three cats (FIV negative) and for four cats (FIV positive). Mann-Whitney test

3.5.9 Thymus contained the lowest level of CD4⁺CD134⁺ T lymphocytes as measured by flow cytometry

As significantly different levels of CD134 mRNA expression were observed in the nine tissue compartments investigated here (Figure 3-10), in order to confirm this findings, the percentages of CD4⁺CD134⁺ T lymphocytes were assessed in cells freshly isolated from samples of mesenteric lymph node (MSLN), spleen, thymus and PBMC from another group of four cats, experimentally infected with FIV for 44 weeks (ongoing study, unpublished data). As shown in Figure 3-17, compared to other tissue compartments, thymus contained the fewest CD4⁺CD134⁺ T lymphocytes (median of 1.35%, range 0.9% - 2.9%). This result was consistent with a previous study in FIV infected cats, using the same anti-feline CD134 antibodies, which demonstrated that thymus contained fewer CD4⁺CD134⁺ T lymphocytes than MSLN and spleen (Willett et al., 2007).

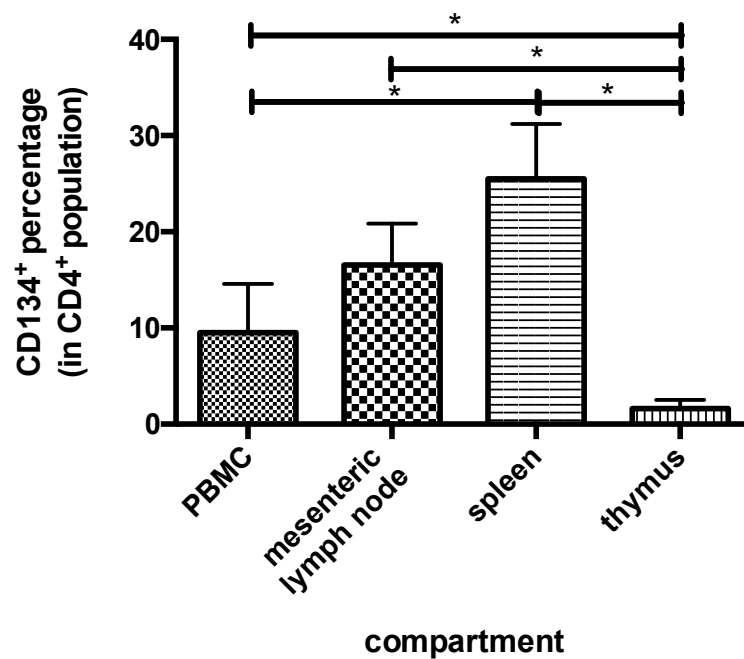


Figure 3-17 Comparison of percentage of CD4⁺CD134⁺ T lymphocytes in PBMC, mesenteric lymph node, spleen and thymus. Each bar represents the median with the range for four cats. The Y-axis shows the percentage of CD134⁺ cells in the CD4⁺ T lymphocyte population. Mann-Whitney test, * indicates p value < 0.05

3.6 Discussion and Conclusion

Tissue compartmentalisation is a phenomenon that has been well described for HIV and that likely exists also in FIV infection (Wong et al., 1997, Singh et al., 1999, Zhang et al., 2002, Kemal et al., 2003, Kenyon and Lever, 2011). In this chapter, evidence of FIV compartmentalisation was reported, since we observed quantitative differences in the PVLs of the FIV Env V5 variants amongst 22 tissue compartments. The dominance of variant B28 in the thymus and its absence from the bone marrow, a result that was confirmed using conventional phylogenetic tree analysis, provided strong support for the existence of tissue compartmentalisation of FIV variants that differed only in sequence changes in the V5 loop of Env. Different levels of CD134 and CXCR4 mRNA, transcripts of the primary receptor and co-receptor for FIV infection, were also observed between tissues, although it remained inconclusive whether these differences were associated with tissue-specific selection of FIV V5 variants. To date, this is the most comprehensive study of tissue compartmentalisation in FIV infection.

Several mechanisms have been proposed for tissue compartmentalisation. One of the strongest selective pressures that shapes both FIV and HIV evolution results from specific immune responses (Rambaut et al., 2004). Virus variants containing both neutralising antibody and CD8⁺ cytotoxic-T lymphocyte (CTL) escape mutations have been reported in patients chronically infected with HIV (Goulder and Watkins, 2004, Rambaut et al., 2004) and cats infected with FIV (Beatty et al., 1996, Hosie et al., 2002, Kraase et al., 2010, Samman et al., 2010, Willett et al., 2013). The level of immune selection in tissue compartments is related to the permissiveness for the entry or infiltration of antibodies or immune cells, which could lead to differences in the viral variants selected between compartments. Therefore, the tissue compartmentalisation observed in this study might be associated with differences in antibody permeation between tissues, since Env V5 variants showed different sensitivities to neutralisation by homologous plasma (Willett et al., 2010). However, the absence of neutralising antibodies against any of the six inoculated variants in the plasma of these four cats argued against the roles of neutralising antibody-associated selections (Willett et al., 2013). In these four cats, strong cell-mediated immune responses, determined by interferon- γ ELISpot (Enzyme-

Linked ImmunoSpot) assays using inactivated whole GL8 virus, were observed. Furthermore, different responses were observed among cells derived from spleen, PLN, MSLN and PBMC, suggesting that there might have been different cell-mediated immune responses (CMI) exerting selective pressure in different tissue compartments. However, when CMI epitopes were mapped against whole Env- and V5-derived peptides, the relationships between T cell responses against epitopes unique to each V5 variant and their strength remained elusive (Willett et al., 2013). Nevertheless, since cell-mediated immune responses against FIV variants were observed in this cohort, further investigations would be necessary in order to explore the role of cellular immune responses in FIV tissue compartmentalisation.

The tropism of FIV (Willett and Hosie, 2008, Willett and Hosie, 2013), HIV (McKnight et al., 1995, Mehandru et al., 2004, Obermeier et al., 2012) and SIV (Mattapallil et al., 2005, Nishimura et al., 2005) is governed by amino acid variation within Env, such that some viral variants preferentially dominate in particular tissues according to their tropisms. This appeared to be a likely explanation for the findings of this study, since different tropisms of the V5 variants within the experimental inoculum had been observed previously (Appendix 3-1) (Willett et al., 2010). However, FIV tropism study appears to be more complex compared to HIV where, according to the ability of HIV to utilise CCR5 (R5), CXCR4 (X4) or both co-receptors (R5X4), two or three distinct target cell populations could be defined (Berger et al., 1998, Berger et al., 1999, Willett and Hosie, 2008). CCR5 is expressed mainly on memory T lymphocytes and cells from the monocyte/macrophage lineage such as macrophages and dendritic cells, whereas CXCR4 is expressed mainly on naïve T lymphocytes (Bleul et al., 1997, Lee et al., 1999). As a result, HIV compartmentalisation is, in part if not directly, under the influence of target cell availability within tissues. For example, CCR5-tropic viruses predominate in the CNS and GALT where CCR5⁺ macrophage/microglial cells and memory CD4⁺ T lymphocytes, respectively are present at high frequency (Albright et al., 1999, Mehandru et al., 2004, Peters et al., 2007, Douek et al., 2009).

In contrast, FIV tropism cannot be defined by co-receptor usage, since all FIV isolates tested to date utilise CXCR4 for infection (Willett and Hosie, 2008). Rather, FIV tropism appears to be defined by the interaction of Env with the

primary receptor CD134 (Willett et al., 2006b, Willett et al., 2010, Willett and Hosie, 2013, Beczkowski et al., 2014b). FIV isolates recovered during the early phase of infection, such as GL8 and CPG41, require both CRD1 and CRD2 of CD134 (Willett et al., 2006b, Willett and Hosie, 2013). In contrast, strains recovered during the later stages of infection, such as PRR, B2542 and the V5 variants in this study, only require CRD1 and CXCR4, or utilise CXCR4 alone for infection (de Parseval et al., 2004b, de Parseval et al., 2005, Willett et al., 2006b, Beczkowski et al., 2014b). The requirement for the additional amino acid motif 78NYE80 on CRD2 might reflect a stronger affinity and/or a more efficient interaction between the Env of early FIV strains and CD134 (Willett et al., 2006a, Willett et al., 2006b, Willett and Hosie, 2013). In addition, since CRD2-dependent viruses can bind CD134, even when bound by its ligand CD134L, this might give CRD2-dependent variants a replicative advantage over CRD2-independent variants, as the ability to infect cells where CD134 is engaged by CD134L results in an increased number of target cells being available for infection (Takahashi et al., 2001, Soroosh et al., 2006, Song et al., 2008, Willett and Hosie, 2013). Moreover, it was reported that CD134-CD134L interaction lead to an enhanced HIV production (Takahashi et al., 2001). Thus, the expression levels of CD134, in terms of both the number of target cells expressing CD134⁺ and the level of cell surface expression, might be critical in the selection of the fittest variant(s) in the transmitted quasispecies, as well as in tissue compartmentalisation. This speculation was in part supported in this study by the observation that GL8 like variants were the most abundant variant in bone marrow (Figure 3-8B), as well as the negative correlations observed between B19 and B30 PVLs and CD134:CXCR4 mRNA ratios, the surrogate marker for activated CD134⁺ T lymphocytes (Figure 3-14B). As the Envs of these late, CRD2-independent variants bound CD134 with a lower affinity than the Envs of CRD2-dependent variants, it is likely that the CRD2-independent variants were outcompeted by the fitter, CRD2-dependent GL8 in tissue compartments containing more CD134⁺ target cells, such as the bone marrow.

Although the statistical significance varied, the PVLs of total FIV as well as each of the V5 variants were higher in lymphoid tissues than visceral organs (Table 3-2, Figure 3-2B, 3-3B and 3-6). This finding is consistent with studies of HIV-1 pathogenesis, in which HIV-1 was found to replicate extensively in secondary lymphoid organs where the main target cell, the CD4⁺ T lymphocyte,

is activated following an interaction with an APC (Fauci, 1993, Haase, 1999, Yukl et al., 2010). Differences in the FIV PVL between lymphoid organs and PBMC, on the other hand, were not statistically significant (Table 3-2, Figure 3-2B, 3-3B and 3-6). This might be explained by the continuous migration of activated CD4⁺CD134⁺ T lymphocytes from secondary lymphoid organs into the circulation (Evans et al., 2001, Murphy and Janeway, 2012). Nevertheless, it is important to consider the variation in PVL observed between tissues, since statistically significant differences were observed in all qPCR results (Figure 3-2A, 3-3A and 3-5). It is possible that the high variability in the PVL between tissues decreased the statistical power when the median values of tissues were compared with the median in PBMCs.

The detection of variant B14 in the thymus of cat A827 by single colony sequencing was intriguing, since B14 was undetectable in thymus by qPCR (Figure 3-9A). This finding might reflect the poor replicative capacity of B14 *per se*, regardless of the tissue compartment, as B14 was not detected in most of the tissues examined (Figure 3-5A and 3-7) and replicated poorly in PBMC throughout the 21 weeks study period (Willett et al., 2013). In contrast, variant B28 was dominant in the thymus, but had a low PVL in PBMC and was undetectable in bone marrow, providing evidence of tissue compartmentalisation (Figure 3-5C and 3-7). Given the consistency of this finding in all cats, this study provides evidence that strongly supports the preferential selection of variant B28 in thymus.

The similar levels of CD134 and CXCR4 mRNA observed here between primary and secondary lymphoid tissues might reflect the heterogeneity of these tissues. It is generally accepted that the main function of the thymus is to educate precursor cells to develop into self-tolerant, mature T lymphocytes (Blom and Spits, 2006, Murphy and Janeway, 2012). Immature progenitor cells expressing CXCR4⁺ migrate to the thymus according to the high level of CXCL12 expression on thymic epithelial cells (TEC) in the thymic stroma and subsequently develop into thymocytes (Ishii et al., 1999). It has been shown that CXCR4 is expressed at all stages of human thymocyte development, although studies have shown that expression levels vary at different stages (Kitchen and Zack, 1997, Zaitseva et al., 1998). This explains the high levels of CXCR4 mRNA observed in thymus of all four cats examined in this study. However, at least in

humans, the thymic medulla contains a venule, similar to the high endothelial venule (HEV) of lymph nodes, through which cells, including antigen-activated lymphoid cells, can enter the thymus from the circulation (Pabst, 2007). This route might allow CD4⁺CD134⁺ T lymphocytes to re-enter thymus. Nevertheless, we presume that the level of CD4⁺CD134⁺ T lymphocyte migration through the thymus is relatively low as thymus contains few CD134⁺ T lymphocytes as shown by flow cytometry (Figure 3-17). Moreover, FIV infection did not appear to impact upon the level of CD4⁺CD134⁺ T lymphocytes in thymus as the levels of CD134 mRNA were similar between FIV negative and FIV positive cats (Figure 3-16). This unique environment in the thymus, where it was shown by flow cytometry that CD134 cell numbers and expression levels are low, but CXCR4 expression is high, might allow CRD2-independent variants to outcompete CRD2-dependent variants, consistent with the observed dominance of B28 in thymus. To prove this hypothesis, we attempted to directly compete GL8 and B28 infectivity for thymocytes. However, this was unsuccessful because the feline cytokines required for maintaining thymocytes in culture are not available and so this important research question remains.

The spleen is composed of three anatomically distinct zones; red pulp, marginal zone and white pulp, which share many similarities with lymph nodes (Mebius and Kraal, 2005, Murphy and Janeway, 2012). However, since the spleen lacks both HEV and afferent lymphatic vessels, lymphocytes migrate into the white pulp using different mechanisms compared to lymph nodes (Nolte et al., 2002, Crivellato et al., 2004). It was reported in humans that lymphocyte migration to and through the spleen is several fold greater compared to the recirculation via lymph nodes (Pabst, 1988). This unrestricted migration of target cells between the blood circulation and spleen likely explains the dominance of GL8 observed in the PBMC and spleen. It might also explain the discrepancy between CD134 mRNA levels and the percentage of CD4⁺CD134⁺ T lymphocytes determined by flow cytometry (Table 3-6, Figure 3-10 and 3-17). Spleen contained the highest levels of CD4⁺CD134⁺ T lymphocytes by flow cytometry but low levels of CD134 mRNA. Since the absolute mRNA level in this study was calculated by dividing the ct value of the CD134 mRNA with ct value of Bactin, the presence of large numbers of non-activated cells led to an apparent decrease in the levels of CD134 mRNA. Similarly, bone marrow is a primary lymphoid organ for B lymphocytes (Murphy and Janeway, 2012), but also

contains dendritic cells, memory CD4⁺ and CD8⁺ T lymphocytes (Cavanagh et al., 2005, Di Rosa and Pabst, 2005, Mazo et al., 2005). Therefore, although it is conventionally designated as a primary lymphoid organ, the bone marrow contains both progenitor and mature cells from the circulation, which might explain the dominance of GL8 over other V5 variants that was observed in the bone marrow, similar to the observations in the lymph nodes, spleen and PBMC.

Further supporting evidence for the positive correlation between target cell availability and tissue compartmentalisation was provided by the detection of HIV in the CNS, even in patients with undetectable plasma viral loads (Canestri et al., 2010, Valcour et al., 2011). Although this finding might have been associated with the inability of anti-retroviral drugs to cross the blood-brain-barrier, it did not rule out an effect of different target cell populations between the two compartments (Wynn et al., 2002, Potschka, 2010). HIV infiltration into the CNS led to downregulation of MHC class I and II and upregulation of Fas ligand in neurons, microglia and astrocytes that, in turn, limited the activation, proliferation and induced apoptosis of both CD8⁺ and CD4⁺ T lymphocytes (Massa, 1993, Massa et al., 1993, Bai et al., 2009, Choi and Benveniste, 2004). As a result, the decreased number of activated CD4⁺ T lymphocytes directly affected the composition of the virus population, as minor variants were more able to infect other target cells.

Different viral burdens between tissue compartments were also evident in other tissues from an HIV infected patient with significantly higher levels of HIV DNA and RNA in GALT compared to PBMC (Yukl et al., 2010, Yukl et al., 2013). Moreover, it was reported that while HIV DNA predominated in CD4⁺CCR7⁺ central memory (CM) T lymphocytes in the circulation, CD4⁺CCR7⁻ effector memory (EM) T lymphocytes harboured greater PVL in GALT (Yukl et al., 2013). This finding suggested that the cell types and their relative quantities in different compartments played important roles in tissue compartmentalisation, together with anatomical barriers.

It is also important to consider the short duration (21 weeks) of this study when interpreting the data. It has been shown that the viral populations within tissues of patients acutely infected with HIV were homogeneous and only became distinct during the later, chronic phase of infection (Zhang et al., 1993,

Zhang et al., 2002). Therefore, it is possible that had the cats been infected for a longer period, a more diverse population might have been observed, as a result of the accumulation of mutations/deletions, which, in turn, could have affected the magnitude of compartmentalisation.

Another limitation of this study was the inability to enumerate target cell numbers in tissues by flow cytometry, because tissue samples had been stored frozen. With this limitation, the target cell numbers in each compartment were measured indirectly, according to the levels of CD134 and CXCR4 mRNA. Discrepancies between mRNA and actual protein expression levels have been observed in previous studies and their correlations showed only 40% explanatory power (de Sousa Abreu et al., 2009, Maier et al., 2009, Vogel and Marcotte, 2012). This is mainly related to the other regulatory mechanisms between transcripts and proteins (Maier et al., 2009). Similar discrepancies were also observed in this study, for example spleen contained low levels of CD134 mRNA (Appendix 3-9 and Figure 3-15) and yet showed the highest percentage of CD4⁺CD134⁺ T lymphocytes by flow cytometry (Figure 3-17). Likewise, the level of CD134 mRNA in thymus was relatively high (Appendix 3-8) but the percentage of CD4⁺CD134⁺ T lymphocytes was very low (Figure 3-17). Although the percentage of CD4⁺CD134⁺ T lymphocytes was analysed from a different cohort of cats, the consistency of the levels in each tissue type between cats confirmed the validity of the measurement (Figure 3-17). However, this limitation confounded observations of a relationship between target cell numbers and FIV variants selection in tissue compartments. Further studies, combining the use of a cell sorter to separate different cell types from each tissue and variant specific qPCR to quantify the PVL of each FIV variant in the population, would provide a better understanding in the role of target cell specific selection and FIV tissue compartmentalisation.

There are additional potential explanations for the lack of a clear demonstration of tissue compartmentalisation in FIV infection in this study. Firstly, the FIV viral load and PVL tend to be lower for FIV than for HIV or SIV infection, so that the PVL may be below the level of detection in some tissues. Secondly, FIV pathogenesis studies are normally conducted in small groups of cats (typically less than ten individuals) and so it is possible that a larger study, examining more infected cats and tissue samples, might be required in order to

detect a clear relationship between target cell numbers and tissue compartmentalisation. Finally, it has been suggested that a more sophisticated approach, combining both phylogenetic and statistical analyses, should be considered where a conventional tree-based analysis fails to demonstrate tissue compartmentalisation in FIV-infected cats (Zarate et al., 2007, Hayward and Rodrigo, 2010a).

In conclusion, a correlation between sequence variation in the V5 region of FIV Env variants and tissue compartmentalisation was observed in this study. The impact of differences in cell tropism and/or target cell availability in FIV compartmentalisation was investigated but it is evident that this phenomenon results from complex host-pathogen interrelationships. Further studies examining the mechanism underlying compartmentalisation will not only pave the way towards a better understanding of intra-host FIV dynamics and evolution, but will also shed light on the immunological mechanisms underlying this phenomenon. Ultimately, this information will assist the development of a successful and broadly protective FIV vaccine.

Chapter 4 Investigating the role of CD4⁺CD134⁺ T lymphocytes in the pathogenesis of natural FIV infection

4.1 Introduction

Feline immunodeficiency virus, FIV, infects its main target cell, the CD4⁺ T lymphocyte, via an interaction between the viral envelope glycoprotein (Env) and CD134, a secondary co-stimulatory molecule expressed exclusively on antigen-activated CD4⁺ T lymphocytes (Shimojima et al., 2004, Willett et al., 2007, Willett and Hosie, 2013). It was shown previously that the Env-CD134 interaction plays an important role in the selection of the dominant viral variants, cell tropism and the clinical outcome of FIV infection (Willett et al., 2013, Willett and Hosie, 2013, Beczkowski et al., 2014b, Beczkowski et al., 2015a). However, few data are available to describe the numbers and dynamics of CD4⁺CD134⁺ T lymphocytes in cats naturally infected with FIV. Therefore, the first aim of the studies described in this chapter was to measure CD4⁺CD134⁺ T lymphocytes and investigate potential relationships with FIV proviral load (PVL) and clinical status in a cohort of more than 200 FIV positive and negative cats exhibiting different clinical signs.

It has been well documented that different FIV variants interact differently with CD134 (Willett et al., 2006b, Willett et al., 2009, Willett and Hosie, 2013). While FIV variants isolated from cats in the early phase of infection required both cysteine rich domain (CRD) 1 and CRD2 of CD134 for infection, variants isolated from cats in the later stage of infection were CRD2-independent, either utilising CRD1 and the co-receptor CXCR4 or, rarely, utilising CXCR4 alone for infection (de Parseval et al., 2004b, de Parseval et al., 2005, Willett et al., 2006b). Moreover, the emergence of CRD2-independent variants in the late phase of infection has been reported in both experimentally and naturally infected cats (Kraase et al., 2010, Willett et al., 2013, Beczkowski et al., 2014b), suggesting that this switch in receptor usage has functional significance.

It was shown in Chapter 3 that the tissue availability of CD4⁺CD134⁺ T lymphocytes could exert pressure on the composition of the FIV quasispecies, selecting for particular variants and leading to tissue compartmentalisation. We

speculated that CD4⁺CD134⁺ T lymphocyte availability at different stages of infection might also exert selective pressure, similar to that already observed in tissues, and could play a role in switching the tropism from a CRD2-dependent to a CRD2-independent interaction. Therefore, the second aim of this chapter was to investigate the relationship between the number of CD4⁺CD134⁺ T lymphocytes and the CRD2-dependence of FIV variants in this cohort of cats naturally infected with FIV.

4.2 Study Population

Two hundred and eight whole blood samples collected in ethylenediaminetetraacetic acid (EDTA) anticoagulant were included in this study. All samples had been submitted to Veterinary Diagnostic Services, School of Veterinary Medicine, College of Medical, Veterinary and Life Sciences, University of Glasgow, between September 2014 and August 2015 and had tested negative for FeLV infection. Complete clinical histories and signalments were recorded from the accompanying sample submission forms (Appendix 4-13). The samples examined comprised 114 that tested FIV negative and 94 that tested FIV positive. Details of the types and number of tests requested by the submitting veterinarian are shown in Appendix 4-1.

4.3 Study Approach

Whole blood samples were analysed using flow cytometry to determine the percentages of CD4⁺ and CD8⁺ T lymphocytes, CD4:CD8 T lymphocyte ratios and percentages of CD4⁺CD134⁺ T lymphocytes (Section 2.3.5). FIV proviral loads (PVL) were determined in FIV seropositive cats using a quantitative PCR (Section 2.1.5). Genomic DNA was extracted from the remainders of blood samples from cats diagnosed with FIV infection and was used as a template to amplify full-length FIV *env* sequences by PCR (Section 2.1.7). Full-length FIV *env* genes were cloned into an expression vector to prepare HIV(FIV) pseudotypes (Section 2.3.1). Each HIV(FIV) pseudotype was assessed for CRD2-dependence, as well as for susceptibility to autologous neutralisation (Section 2.3.2 and 2.3.3). These data, as well as PVL, lymphocyte subpopulation data, cats' clinical histories and signalments, were then analysed for evidence of associations between the various parameters (Figure 4-1). PVL, lymphocyte subpopulation data, clinical

histories and signalments of individual cats are tabulated in Appendices 4-2 to 4-7.

4.3.1 Determination of CD134 usage by HIV(FIV) pseudotypes

CD134 usage of the HIV(FIV) pseudotypes was determined using the method described in section 2.3.2. The luciferase activity detected following infection of CLL-FFF and CLL-FFHH cells with each pseudotype was expressed as the FFF/FFHH ratio; these values were compared against the prototypic CRD2-dependent and CRD2-independent pseudotypes (GL8 and B2542 respectively), in order to classify the CD134 usage of each pseudotype. A pseudotype was considered to be “CRD2 dependent” if the FFF/FFHH ratio was similar to that of GL8 (high ratio) or “CRD2 independent” if it was similar to that of B2542 (ratio below 30). Pseudotypes with ratios that fell in between these two extremes, such as FIV/A strain KKS, were designated “intermediate”; it was presumed that such Envs were evolving towards CRD-2 independent usage.

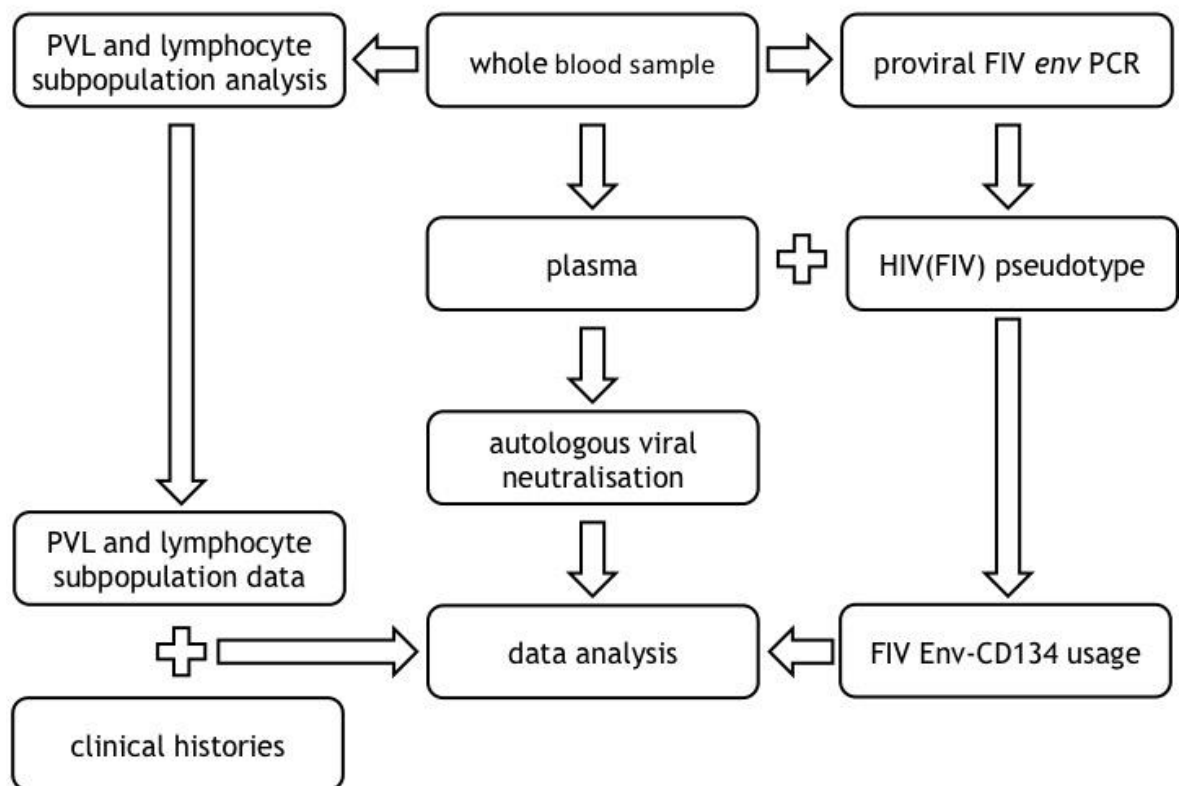


Figure 4-1 Study approach

4.4 Results

4.4.1 FIV seropositive cats were mainly adult, mixed breed and male

The FIV infected cats in this study were predominantly male (83 male vs. 10 female, 1 unknown) with a relative risk of 4.761 (95% confidence interval (CI) 2.637 to 8.595) and an odds ratio of 11.55 (95% CI 5.412 to 24.64), Fisher's exact test, $p < 0.0001^{****}$ (Table 4-1, 4-2 and Figure 4-2A). The finding that male cats were 4.8 times more likely to be infected with FIV than female cats was consistent with the findings of a study conducted in North America in 2006 (Levy et al., 2006). Mixed breed was also considered to be a risk factor for FIV infection, with a relative risk of 9.560 (95% CI 1.406 to 65.01) and an odds ratio of 17.40 (95% CI 2.280 to 132.8), Fisher's exact test, $p = 0.0002^{***}$ (Table 4-1). FIV infected cats were also significantly older than uninfected cats (5 years 9 months vs. 3 years, $p = 0.0081$, Table 4-2 and Figure 4-2B). These findings were consistent with several previous studies showing that adult, mixed breed and male cats have the highest risk of FIV infection (Levy et al., 2006, Hartmann, 2012, Chhetri et al., 2015).

Table 4-1 Risk Factors for FIV infection in this study

Risk	Number of FIV positive	Number of FIV negative	Odds Ratio (95%CI)	P value ^a
Gender^b				
Male	83	46	-	<0.0001****
Female	10	64	11.55 (5.412 - 24.64)	
Neutering^b				
Neutered male	35	25	-	0.4519
Intact male	16	7	0.4518 (0.2195 - 1.709)	
Neutered female	3	33	-	0.2838
Intact female	1	2	0.1818 (0.01251 - 2.642)	
Breed^{b,c}				
Mixed	87	95	-	0.0002***
Purebred	1	19	17.40 (2.280 - 132.8)	
Number of cats in household^b				
Single cat	4	1	-	0.6236
Multiple cats	15	11	2.933 (0.2866 - 30.03)	

^aFisher's exact test, ^bOnly cats with the relevant information recorded on the submission form were included in this analysis, ^cCat breeds shown in Appendices 4-2 and 4-4.

4.4.2 Increased proportion of CD4⁺CD134⁺ T lymphocytes in FIV positive cats

Similar to HIV infection, the percentage of CD4⁺ T lymphocytes was significantly lower in FIV infected cats compared to uninfected cats (18.12% vs. 23.75%, $p = 0.0013^{**}$) (Table 4-2 and Figure 4-2C) (Weiss, 1993). FIV infected cats also demonstrated significantly higher percentages of CD8⁺ T lymphocytes compared to uninfected cats (14.90% vs. 11.48%, $p = 0.0154^*$) (Table 4-2 and Figure 4-2D). Decreased percentages of CD4⁺ T lymphocytes, together with the increased percentages of CD8⁺ T lymphocytes accounted for the observed decreased CD4:CD8 ratio in FIV positive cats compared to uninfected cats (1.330 vs. 1.925, $p < 0.0001^{****}$) (Table 4-2 and Figure 4-2E). FIV infected cats were also found to have significantly higher levels of immune activation, as demonstrated by an increased (greater than two fold) proportion of activated CD134⁺ T lymphocytes within the CD4⁺ T lymphocyte population (27.80% vs. 11.20%, $p < 0.0001^{****}$) (Table 4-2 and Figure 4-2F).

Fourteen of the 94 FIV seropositive cats enrolled in this study displayed PVL below the limit of detection (< 10 copies/ 10^6 cells) (Table 4-3). The undetectable PVL in these cats could not be attributed to the sample preparation, since good quality genomic DNA was obtained and the housekeeping gene 18s rDNA was detected by qPCR (Section 2.1.5) (data not shown). Gender had no effect on PVL detectability, since both groups were predominantly male (Figure 4-3A). Most of the parameters (namely age, percentages of CD4⁺ and CD8⁺ T lymphocytes and CD4:CD8 ratios) of FIV infected cats with undetectable PVL appeared to be similar to those of their counterparts with detectable PVL (Table 4-3 and Figure 4-3B to 4-3E). Moreover, these parameters were not significantly different between FIV positive with undetectable PVL and FIV negative cats. This lack of statistical significance was most likely due to the small sample size of only 14 FIV positive with undetectable PVL cats. Thus, it was demonstrated that the percentage of CD4⁺CD134⁺ T lymphocytes was significantly higher in FIV infected cats compared to FIV negative cats, whether or not proviral DNA was detectable (11.20% vs. 26.98% and 33.70%, respectively, both $p < 0.0001^{****}$) (Table 4-3 and Figure 4-3F). To our knowledge, the dramatic elevation of CD4⁺CD134⁺ T lymphocytes observed in the FIV infected cats in this study has not been reported previously.

Table 4-2 Demography, lymphocyte subpopulations and PVL data of study population according to FIV serology

	FIV negative	FIV positive
Number	114	94
Age	2Y 11M (1M - 17Y)	5Y 9M ^{**} (7 M - 16Y)
Gender (male:female)	46:64 (4 unknown)	83:10 ^{***} (1 unknown)
CD4⁺ lymphocytes (%)	23.75 (0.51-58.30)	18.12 ^{**} (0.03 - 42.94)
CD8⁺ lymphocytes (%)	11.48 (0.32-45.35)	14.90 [†] (0.34 - 53.16)
CD4:CD8 ratio	1.92 (0.27-17.15)	1.33 ^{****} (0.04 - 7.16)
CD4⁺CD134⁺ lymphocytes (%)	11.20 (1.15-71.31)	27.80 ^{****} (5.10 - 96.96)
FIV proviral load (copies/10⁶ cells)	n.a.	2,764 (11 - 1,758,848)

Age: Y = years, M= months and W = weeks, values are shown as group medians with range, CD4⁺ and CD8⁺ lymphocytes expressed as percentages of total lymphocytes, CD4⁺CD134⁺ lymphocytes shown as percentage of the CD4⁺ lymphocyte population, *, **, *** and **** indicate significantly different values at p values < 0.05, < 0.01, < 0.005 and < 0.0001 respectively, Fisher's exact test and Mann-Whitney test. n.a. = not analysed

Table 4-3 Demography, lymphocyte subpopulations and PVL data in FIV infected cats with detectable or undetectable PVL

	Detectable FIV proviral load	Undetectable FIV proviral load
Number	80	14
Age	5Y 6M (7M - 14Y)	5Y 9M (1Y - 16Y)
Gender (male:female)	71:9	12:1 (1 unknown)
CD4⁺ lymphocytes (%)	18.57 (0.03 - 42.94)	17 (7.03 - 38.16)
CD8⁺ lymphocytes (%)	15.21 (0.34 - 53.16)	10.90 (3.71 - 24.96)
CD4:CD8 ratio	1.25 (0.04 - 7.16)	1.54 (0.96 - 3.61)
CD4⁺CD134⁺ lymphocytes (%)	26.98 (5.10 - 96.96)	33.70 (13.28 - 93.17)
FIV proviral load (copies/10⁶ cells)	2,764 (11 - 1,758,848)	undetectable

Age: Y = years, M= months and W = weeks, values are shown as group median with range, CD4⁺ and CD8⁺ lymphocytes expressed as percentages of total lymphocytes, CD4⁺CD134⁺ lymphocytes shown as percentage of the CD4⁺ lymphocyte population, Fisher's exact test and Mann-Whitney test.

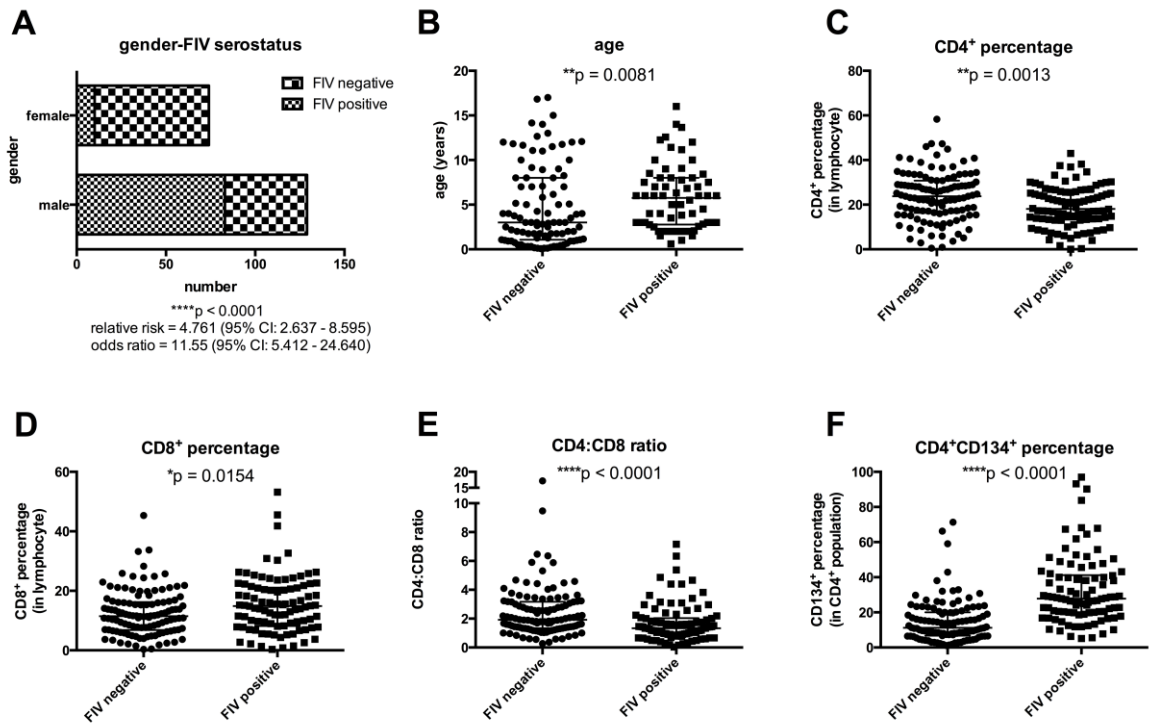


Figure 4-2 Effect of gender on FIV serostatus (A) and comparisons of Age (B), CD4⁺ percentage (C), CD8⁺ percentage (D), CD4:CD8 ratio (E) and CD4⁺CD134⁺ percentage (F) between FIV negative and positive cats. Horizontal lines depict group median values with interquartile ranges. Statistical significance was determined by Mann-Whitney test. The effect of gender and FIV serostatus (A) was determined by Fisher's exact test and presented as relative risk and odds ratio. 95% CI: 95% confidence interval

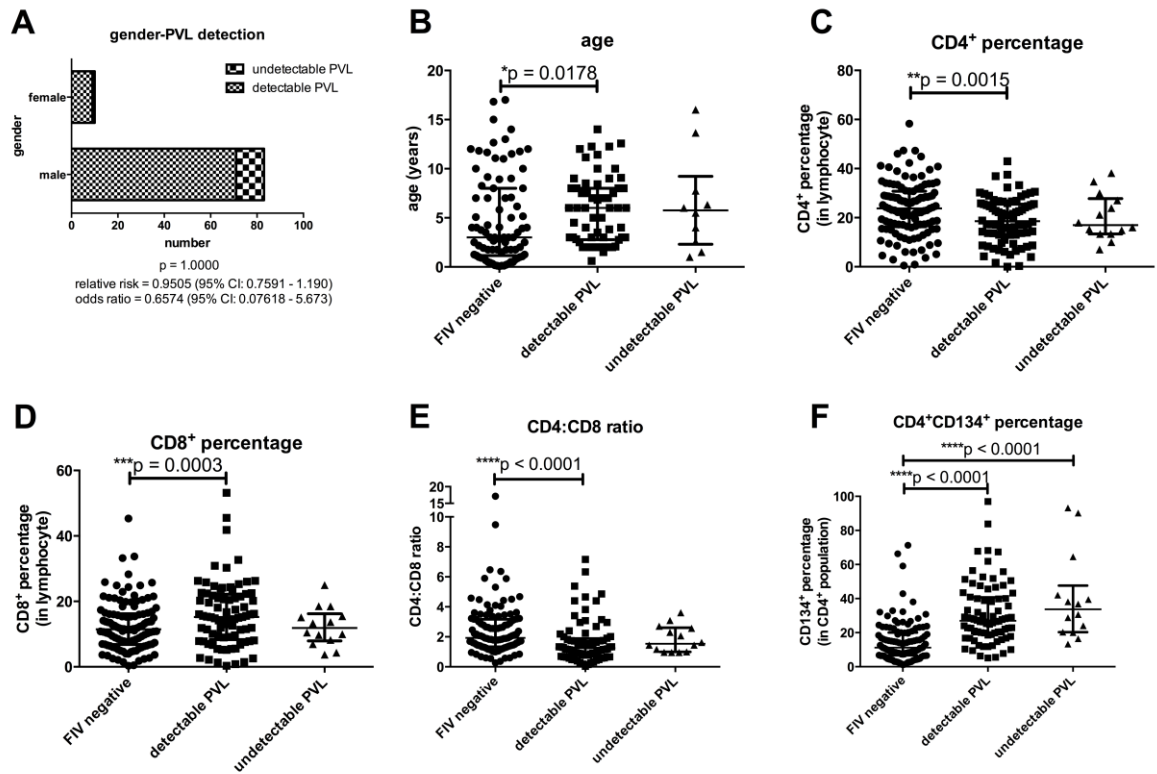


Figure 4-3 Effect of gender on FIV proviral load (PVL) detection (A) and comparisons of Age (B), CD4⁺ percentage (C), CD8⁺ percentage (D), CD4:CD8 ratio (E) and CD4⁺CD134⁺ percentage (F) between FIV negative (left), FIV positive cats with detectable PVL (centre) and undetectable PVL (right). Horizontal lines depict group medians and interquartile range values. Statistical significance was determined using the Mann-Whitney test. The effect of gender and FIV PVL detection (A) was determined by Fisher's exact test and presented as relative risk and odds ratio. 95% CI: 95% confidence interval

4.4.3 FIV serostatus and clinical status

Sample submission forms (Appendix 4-13), submitted by the veterinary practitioner with each blood sample to be tested, contained tick boxes to indicate whether the patient was healthy or sick according to the veterinarian's clinical examination. Although this information was not available for all of the cats, a sufficient sample size was collected to further categorise the cats into 4 groups according to their clinical status; healthy FIV negative, sick FIV negative, healthy FIV positive and sick FIV positive cats (Table 4-4). This categorisation of cats was strictly restricted to the information provided, without any interpretation from the researcher.

It was shown that FIV serostatus showed no correlation with clinical status, as determined by Fisher's exact test (Figure 4-4A). This was mainly due to the similar proportions of sick cats in the FIV negative and positive groups (Table 4-4). The high proportion of sick animals in this study likely reflected that the blood samples had been submitted to Veterinary Diagnostic Services, either for virological screening or because the cats displayed clinical signs. Most of the healthy cats, both FIV seronegative and seropositive, were stray cats being screened for viral infections at the time of entering a sanctuary. Some healthy FIV negative cats were pedigree cats being screened prior to exportation. While the majority of FIV negative samples were submitted for feline retrovirus screening (FeLV antigen and FIV antibody) (45.61% (52/114)), the majority of the FIV positive samples were submitted for confirmation of FIV infection (FIV antibody) (80% (64/80)), following positive results in point-of-care tests (Appendix 4-1).

4.4.4 Clinically ill FIV positive cats presumed to be in the terminal phase

Clinically sick FIV infected cats tended to be older than the other cats within the study group (Table 4-4 and Figure 4-4B). This was not unexpected, since it takes some time after seroconversion for the clinical manifestations of immunodeficiency to become evident (Hartmann, 2012, Sykes, 2013). These cats also displayed the lowest percentages of CD4⁺ T lymphocytes (Table 4-4 and Figure 4-4C). This decline in CD4⁺ T lymphocytes was associated with low (almost inverted) CD4:CD8 ratios, a hallmark of immunodeficiency, being observed in the

sick FIV positive cats (1.10, $p < 0.0001^{****}$) (Table 4-4 and Figure 4-4E) (Egberink and Horzinek, 1992, Yamamoto et al., 2007). The decreased percentages of CD4⁺ T lymphocytes and low CD4:CD8 ratios observed in these cats, together with their older ages, suggested that the clinically ill FIV positive cats were likely to be in the terminal, immunodeficiency phase of FIV infection.

4.4.5 Clinically healthy FIV infected cats presumed to be in the earlier phase of infection, compared to their sick counterparts

Since the healthy FIV infected cats were significantly younger than their sick counterparts (median age of 2 years and 6 months vs. 7 years and 9 months, $p = 0.0018^{**}$) (Table 4-4 and Figure 4-4B), showed higher percentages of CD4⁺ T lymphocytes (24.60% vs. 15.87%, $p = 0.0073^{**}$) and appeared clinically healthy, it is likely that these cats had been infected for a shorter period of time and/or might still be at an earlier stage of infection (Egberink and Horzinek, 1992, Yamamoto et al., 2007, Hartmann, 2012, Sykes, 2013). In addition, these cats also displayed three fold lower FIV PVLs, although this difference was not statistically significant (1,010 vs. 3,142 copies/ 10^6 cells, $p = 0.0710$) (Table 4-4 and Figure 4-5D). However, with no dates of seroconversion being known, which is common for naturally infected cats, staging of FIV infection could only be estimated.

4.4.6 Similar percentages of CD4⁺ T lymphocytes between sick FIV negative and healthy FIV positive cats

The percentages of CD4⁺ T lymphocytes in healthy FIV negative, sick FIV negative and healthy FIV positive cats were similar (28.12%, 24.77% and 24.60%, respectively) (Table 4-4 and Figure 4-4C). Although a progressive CD4⁺ T lymphocyte depletion is a hallmark of FIV infection, in this study it was not possible to distinguish clinically healthy FIV infected cats from FIV negative cats on the basis of the percentage of CD4⁺ T lymphocytes alone. However, the higher percentage of CD4⁺ T lymphocytes in healthy FIV positive cats might be related to their better clinical status compared to their sick counterparts (24.60% vs. 15.87%, $p = 0.0073^{**}$) (Table 4-4 and Figure 4-4C).

Although the healthy FIV negative cats demonstrated lower percentages of CD8⁺ T lymphocytes compared to the other three groups, this difference was not statistically significant (8.95% compared to 13.16%, 14.19% and 14.57%, respectively) (Table 4-4 and Figure 4-4D). The similar percentages observed between sick FIV negative and both healthy and sick FIV positive cats suggested that elevation of CD8⁺ T lymphocytes was a common finding associated with illness or infection. However, when the percentages of CD4⁺ and CD8⁺ T lymphocytes were analysed together as CD4:CD8 ratios, healthy FIV negative cats were found to display significantly higher ratios compared to sick FIV negative cats (3.16 vs. 1.79, $p = 0.0079^{**}$), healthy FIV positive cats (3.16 vs. 1.46, $p = 0.0395^*$) and sick FIV positive cats (3.16 vs. 1.10, $p < 0.0001^{****}$). It was notable that the CD4:CD8 ratios of sick FIV infected cats were lower than those of senior cats almost twice their age, reported previously (1.10 in this study vs. 1.35 in the study of (Campbell et al., 2004), age ranged from 10 to 14 years old). This apparent acceleration of immunosenescence observed in sick FIV infected cats might be the direct result of persistent immune activation and immune dysregulation following FIV infection (Tompkins and Tompkins, 2008).

From these findings, the CD4:CD8 ratio appears to be a more sensitive index for monitoring the progression of infection in FIV-infected cats, since it is influenced by both decreases in CD4⁺ T lymphocyte numbers and increases in CD8⁺ T lymphocyte numbers (Table 4-4 and Figure 4-4C to Figure 4-4E). However, the CD4:CD8 ratio could not be used to differentiate FIV infection from any other illness because values were similar between sick FIV negative cats and healthy FIV infected cats (1.79 vs. 1.46, $p = 0.4772$) (Table 4-4 and Figure 4-4E).

4.4.7 Healthy FIV positive cats demonstrated the highest levels of CD4⁺CD134⁺ T lymphocytes

In general, FIV infected cats, regardless of their clinical status, demonstrated significantly higher levels of CD4⁺CD134⁺ T lymphocytes compared to both healthy and sick FIV negative cats (Table 4-4 and Figure 4-4F). This elevation appeared to be specific to FIV infection rather than related to another infection or illness, since the percentages of CD4⁺CD134⁺ T lymphocytes in sick FIV negative cats and healthy FIV negative cats were similar (10.02% vs. 9.96%, p

= 0.4520) (Table 4-4 and Figure 4-4F). Although the difference was not statistically significant, most likely as a result of the small sample size ($n = 17$), the mean percentage of $CD4^+CD134^+$ T lymphocytes was higher in clinically healthy FIV positive cats compared to sick FIV positive cats (39.75% vs. 26.68%, $p = 0.2210$) (Table 4-4 and Figure 4-4F).

4.4.8 Lower FIV proviral loads in healthy cats

FIV PVL were three fold lower in clinically healthy cats compared to sick cats (1,010 vs. 3,142 copies/ 10^6 cells, $p = 0.0710$) (Table 4-4, Figure 4-5D) and the healthy cats harboured higher percentages of $CD4^+CD134^+$ T lymphocytes (39.75% vs. 26.68%, $p = 0.2210$) (Table 4-4 and Figure 4-4F). This finding might appear counterintuitive, if one assumes that FIV production is a dependent variable of infected cells in an active state, i.e. antigen activated $CD4^+CD134^+$ T lymphocytes (Weinberg et al., 2004, Hori, 2005). However, the higher percentage of $CD4^+CD134^+$ T lymphocytes observed in the healthy cats might reflect a more intact immune system (as the healthy cats were younger), or it might reflect clonal expansion of primary T cells following antigen recognition, since it is likely that the healthy cats had been infected for a shorter period of time (Gramaglia et al., 2000, Zaunders et al., 2009). These high levels of CD134-expressing, anti-viral T lymphocytes could in turn have facilitated control of FIV production since a CD134 signalling pathway has been shown to play an important role in the control of persistent viral infection (Boettler et al., 2012).

On the other hand, a high FIV PVL in the presence of high percentages of $CD4^+CD134^+$ T lymphocytes in sick FIV positive cats (26.68% compared to 10.02% in healthy negative cats, $p = 0.0006^{***}$) might reflect their collapsing immune systems. As a result of chronic immune activation in response to persistent antigen presentation, similar to older cats, activated T lymphocytes in the later phase of FIV infection were shown to have reduced antigenic responses (Day, 2010, Sykes, 2013). However, it was not possible to determine causality in this cross sectional study. In order to test these hypotheses, it would be necessary to examine qualitatively the FIV-specific T lymphocyte responses, using functional quality and/or viral suppression assays (Techakriengkrai et al., 2013, Tansiri et al., 2015). Nevertheless, such assays were beyond the scope of this study.

Table 4-4 Demography, lymphocyte subpopulations and PVL data of the study population according to FIV serology and clinical status

	FIV negative (78, 36 unknown)		FIV positive (46, 34 unknown) ^a	
	Healthy	Sick	Healthy	Sick
Number	21	57	17	29
Age	2Y 11M (2M - 11Y 8M)	3Y (1M - 16Y 10M)	2Y 6M (2Y - 6Y 10M)	7Y 9M ^{****§§□□} (7M - 14Y)
Gender (male:female)	5:15 (1 unknown)	22:34 (1 unknown)	16:1	24:5
CD4⁺ lymphocytes (%)	28.12 (11.76 - 46.01)	24.77 (2.88 - 58.30)	24.60 (4.21 - 37.50)	15.87 ^{****§§§□□} (0.03 - 29.70)
CD8⁺ lymphocytes (%)	8.95 (3.69 - 21.83)	13.16 (2.40 - 45.35)	14.19 (5.17 - 30.29)	14.57 (0.34 - 53.16)
CD4:CD8 ratio	3.16 (1.01 - 6.47)	1.79 ^{**} (0.27 - 17.15)	1.46 [*] (0.48 - 7.16)	1.10 ^{****§§§§} (0.04 - 4.40)
CD4⁺CD134⁺ lymphocytes (%)	10.02 (1.4 - 71.31)	9.96 (1.15 - 66.27)	39.75 ^{****§§§§} (7.75 - 96.96)	26.68 ^{****§§§§} (5.10 - 67.83)
FIV proviral load (copies/10⁶ cells)	n.a.	n.a.	1,010 (21 - 117,882)	3,142 (11 - 1,758,848)

^aFIV seropositive cats with undetectable PVL were not included in this analysis. Unknown = unknown health status, Age: Y = years, M= months and W = weeks, values are shown as group medians with range, CD4⁺ and CD8⁺ lymphocytes expressed as percentage of total lymphocytes, CD4⁺CD134⁺ lymphocytes shown as percentage of the CD4⁺ lymphocyte population, *, **, *** and **** indicate significantly different values compared to healthy FIV negative groups, with p values < 0.05, < 0.01, < 0.005 and < 0.0001 respectively, §§, §§§ and §§§§ indicate significantly different values compared to sick FIV negative groups, with p values < 0.01, < 0.005 and < 0.0001, respectively, □□ indicates significantly different values compared to healthy FIV positive groups with p value < 0.01, Statistical significance was determined using the Mann-Whitney test.

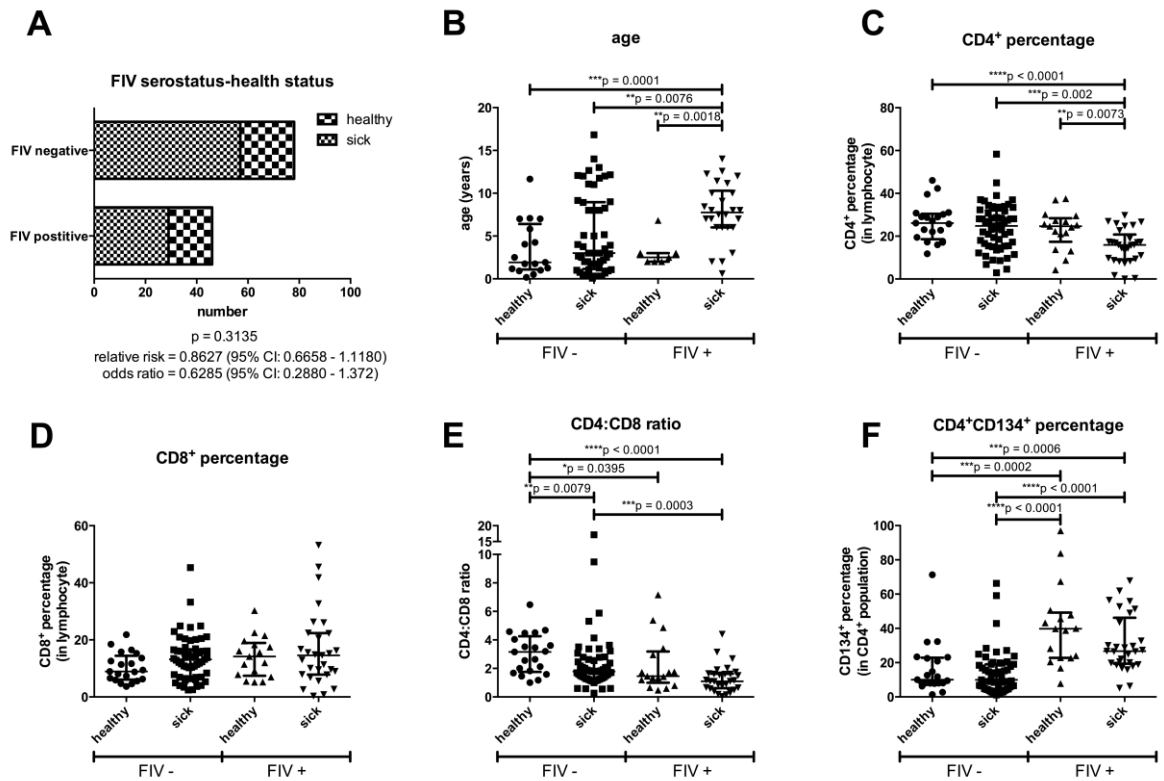


Figure 4-4 Effect of FIV serostatus and clinical status (A) and comparisons of Age (B), CD4⁺ percentage (C), CD8⁺ percentage (D), CD4:CD8 ratio (E) and CD4⁺CD134⁺ percentage (F) between groups according to their FIV serostatus and clinical status. Horizontal lines depict group median values with interquartile ranges. Statistical significance was determined by Mann-Whitney tests. The effect of FIV serostatus and clinical status (A) was determined by Fisher's exact test and presented as relative risk and odds ratio. 95% CI: 95% confidence interval

4.4.9 Interrelationships between lymphocyte subpopulations in FIV negative cats

In FIV negative cats, a positive correlation was observed between age and the percentage of CD8⁺ T lymphocytes ($r = 0.2256$, $p = 0.0271^*$) (Table 4-5). As well as the weak negative correlation between age and percentage of CD4⁺ T lymphocytes ($r = -0.1372$, $p = 0.1824$), age showed a strong negative correlation with CD4:CD8 ratio ($r = -0.3470$, $p = 0.0005^{***}$) (Table 4-5). This finding was in accordance with previous studies in which aged cats displayed decreased CD4⁺ T lymphocyte numbers, increased CD8⁺ T lymphocyte numbers and reduced CD4:CD8 ratios (Heaton et al., 2002, Day, 2010). Age also showed a significant positive correlation with the percentage of CD4⁺CD134⁺ T lymphocytes ($r = 0.3185$, $p = 0.0016^{**}$) (Table 4-5). Taken together, these findings led to the assumption that older cats had encountered a higher degree of immune activation compared to younger cats. This assumption is supported by the observation that CD134 is upregulated on activated CD4⁺ T lymphocytes after antigen recognition (Paterson et al., 1987, Weinberg et al., 2004, Sadler et al., 2014). Moreover, it is most likely that antigen exposure increases with age. Here, the significant positive correlation between the percentage of CD4⁺CD134⁺ T lymphocytes and age observed in sick cats also supported this assumption ($r = 0.4994$, $p = 0.0001^{***}$) (Table 4-7).

A significant positive correlation was observed between the percentages of CD4⁺ and CD8⁺ T lymphocytes in a group of FIV negative cats ($r = 0.3615$, $p < 0.0001^{****}$) (Table 4-5). When cats were categorised according to their clinical signs as either healthy or sick, the observed positive correlation between CD4⁺ and CD8⁺ T lymphocytes was only observed in sick cats ($r = 0.3138$, $p = 0.0175^*$) and was not observed in healthy cats ($r = 0.2922$, $p = 0.1987$) (Table 4-6 and Table 4-7). This might reflect an expansion of total lymphocytes in the presence of infectious agents in sick cats, since lymphocytosis is a normal feature of infection. However, this positive correlation might be absent in particular conditions that lead to a biased elimination, or elevation, of specific lymphocyte subpopulations, such as the marked CD4⁺ T lymphocyte depletion that occurs following FIV infection and in some malignancies such as CD4⁺ large granular lymphocytosis (Lima et al., 2003, Roelke et al., 2006).

As would be predicted, the CD4:CD8 ratio showed significant positive and negative correlations with the percentages of CD4⁺ and CD8⁺ T lymphocytes respectively in most categories (Tables 4-5 to 4-12). However, there was one exception; in FIV positive cats with undetectable FIV PVL, the positive correlation between the percentage of CD4⁺ T lymphocytes and CD4:CD8 ratios was not statistically significant ($r = 0.4374$, $p = 0.1198$) (Table 4-10), perhaps reflecting the limited number of cats in this group ($n = 14$). These significant correlations could simply be explained from the fact that CD4:CD8 ratio is their dependent variable.

4.4.10 Interrelationships between lymphocyte subpopulations and PVL in FIV positive cats

In contrast to FIV negative cats, no correlations were observed between age and the variables analysed in any of the categories of FIV positive cats (Table 4-8 to Table 4-12). However, although not statistically significant, both CD4⁺ and CD8⁺ T lymphocyte numbers were negatively correlated with age (Table 4-8). This might reflect a decline in total lymphocytes with disease progression. Also, the positive correlation observed between CD4⁺ and CD8⁺ T lymphocyte numbers in FIV negative cats was absent in the FIV positive cats (Table 4-8 to Table 4-11), with the exception of the sick FIV positive cats (Table 4-12). This significant positive correlation ($r = 0.4015$, $p = 0.0309^*$) confirmed an overall decrease in all lymphocyte compartments and was a typical finding in FIV infected cats in the late stages of infection (Table 4-12) (Sykes, 2013). Similar to FIV negative cats, significant correlations were observed between CD4:CD8 ratio and the percentages of CD4⁺ and CD8⁺ T lymphocytes according to their direct influences (Table 4-8 to Table 4-12).

A significant negative correlation was observed between the percentage of CD4⁺ T lymphocytes and FIV PVL ($r = -0.2281$, $p = 0.419^*$) (Table 4-8 to Table 4-9 and Figure 4-5A), consistent with CD4⁺ T lymphocytes being the main cellular targets for FIV infection. Similarly, a negative correlation was observed between the CD4:CD8 ratio and FIV PVL (Table 4-8 to Table 4-9 and Figure 4-5B), although this relationship was not statistically significant ($r = -0.2127$, $p = 0.0582$). Intriguingly, when FIV infected cats were categorised according to their clinical status as sick or healthy, a higher degree of negative correlation was observed

between age and PVL in healthy cats ($r = -0.7111$, $p = 0.0524$) (Table 4-11). However, this was not statistically significant, perhaps reflecting the small sample size (information about age was only available for 7 of 17 healthy FIV infected cats). This correlation might reflect the dynamics of FIV replication over time, in which the high PVL observed very early after infection, continuously decreases, approaching the viral set point as disease progress and remaining at that point until the terminal stage of infection (Yamamoto et al., 2007, Sykes, 2013).

4.4.11 A positive correlation between the percentage of CD4⁺CD134⁺ T lymphocytes and FIV PVL in healthy FIV infected cats

A positive correlation was observed between the percentage of CD4⁺CD134⁺ T lymphocytes and FIV PVL in clinically healthy cats, but not in sick cats (Table 4-11 to Table 4-12 and Figure 4-5E to Figure 4-5F), despite the FIV PVL being lower in clinically healthy cats compared to sick cats (1,010 vs. 3,142 copies/10⁶ cells) (Table 4-4 and Figure 4-5D). In contrast, the percentage of CD4⁺CD134⁺ T lymphocytes appeared to be negatively correlated with FIV PVL in sick cats ($r = -0.1399$, $p = 0.4692$) (Table 4-12 and Figure 4-5F), although this was not statistically significant. CD4⁺CD134⁺ T lymphocytes might decline in number as the FIV PVL increases in sick cats during the terminal phase of FIV infection; it is possible that the collapsing immune system is no longer able to reconstitute the lost T lymphocytes and so the FIV PVL increases unabated (Egberink and Horzinek, 1992, Yamamoto et al., 2007, Sykes, 2013).

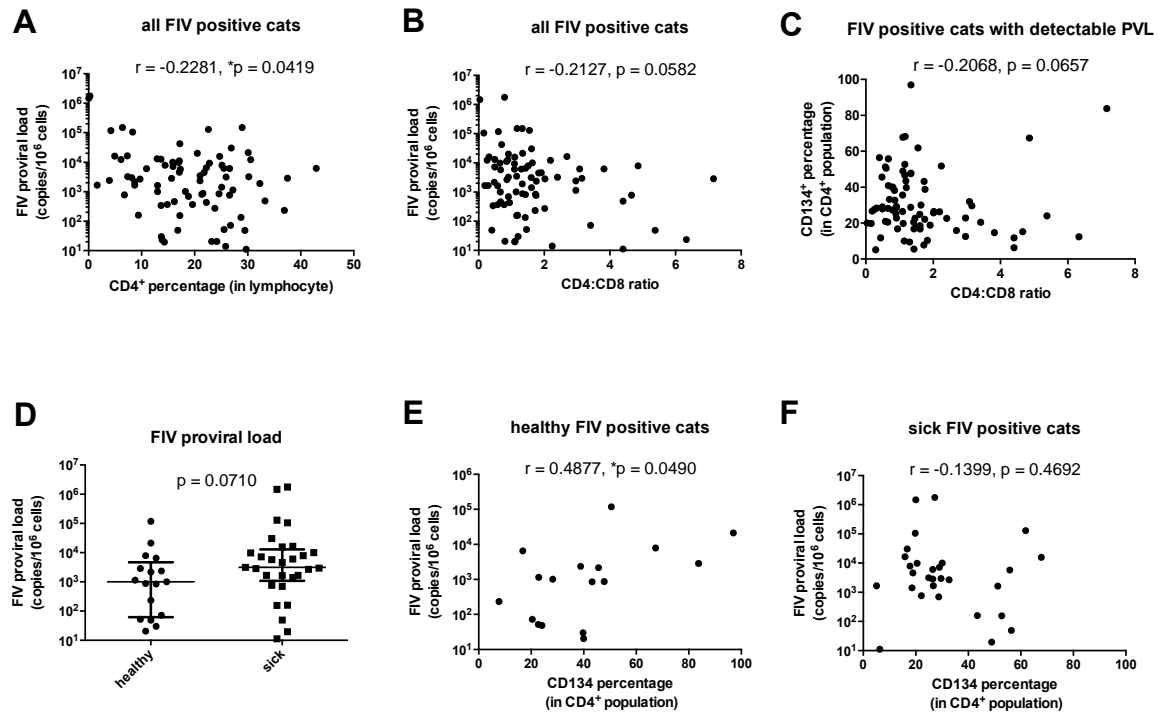


Figure 4-5 Correlations between percentage of CD4⁺ T lymphocytes and FIV PVL (A), CD4:CD8 ratio and FIV PVL in all FIV positive cats (B), relationship between CD4:CD8 ratio and percentage of CD4⁺CD134⁺ T lymphocytes in FIV positive cats with detectable PVL (C), comparison of PVLs between healthy and sick FIV positive cats (D), relationship between percentages of CD4⁺CD134⁺ T lymphocytes and FIV PVL in healthy FIV positive cats (E) and sick FIV negative cats (F). Spearman correlation and Mann-Whitney tests, horizontal lines depict group medians with interquartile ranges (D).

Table 4-5 Interrelationships between age and lymphocyte subpopulations in FIV negative cats

age against (n = 96)

	r	95%CI	p value
%CD4	-0.1372	-0.3340 to 0.07101	0.1824
%CD8	0.2256	-0.02025 to 0.4126	0.0271*
%CD4CD134	0.3185	0.1201 to 0.4924	0.0016**
CD4:CD8	-0.3470	-0.5163 to -0.1516	0.0005***

%CD4 against (n = 114)

	r	95%CI	p value
%CD8	0.3615	0.1849 to 0.5154	<0.0001****
%CD4CD134	-0.2387	-0.4094 to -0.05180	0.0105*
CD4:CD8	0.3787	0.2041 to 0.5300	<0.0001****

%CD8 against (n = 114)

	r	95%CI	p value
%CD4CD134	0.07616	-0.1147 to 0.2616	0.4206
CD4:CD8	-0.6422	-0.7413 to 0.5156	<0.0001****

%CD4CD134 against (n = 114)

	r	95%CI	p value
CD4:CD8	-0.2512	-0.4204 to -0.06506	0.0070**

Relationships between each pair of study parameters were determined using the Spearman correlation. *, **, *** and **** indicate significantly different values at p values < 0.05, < 0.01, < 0.005 and < 0.0001 respectively.

Table 4-6 Interrelationships between age and lymphocyte subpopulations in healthy FIV negative cats

age against (n = 17)

	r	95%CI	p value
%CD4	-0.4454	-0.7692 to 0.06029	0.0736
%CD8	0.2528	-0.2738 to 0.6627	0.3252
%CD4CD134	0.1006	-0.4123 to 0.5651	0.6992
CD4:CD8	-0.4810	-0.7870 to 0.01505	0.0516

%CD4 against (n = 21)

	r	95%CI	p value
%CD8	0.2922	-0.1729 to 0.6508	0.1987
%CD4CD134	-0.5013	-0.7726 to -0.07527	0.0206*
CD4:CD8	0.3610	-0.09724 to 0.6930	0.1078

%CD8 against (n = 21)

	r	95%CI	p value
%CD4CD134	-0.1156	-0.5311 to 0.3448	0.6178
CD4:CD8	-0.7429	-0.8922 to -0.4472	0.0001***

%CD4CD134 against (n = 21)

	r	95%CI	p value
CD4:CD8	-0.2221	-0.6053 to 0.2447	0.3333

Relationships between each pair of study parameters were determined using the Spearman correlation. *, **, *** and **** indicate significantly different values at p values < 0.05, < 0.01, < 0.005 and < 0.0001 respectively.

Table 4-7 Interrelationships between age and lymphocyte subpopulations in sick FIV negative cats

age against (n = 53)

	r	95%CI	p value
%CD4	-0.2295	-0.4769 to 0.05171	0.0984
%CD8	0.05354	-0.2277 to 0.3266	0.7034
%CD4CD134	0.4994	0.2573 to 0.6826	0.0001***
CD4:CD8	-0.3217	-0.5504 to -0.04818	0.0188*

%CD4 against (n = 57)

	r	95%CI	p value
%CD8	0.3138	0.05006 to 0.5366	0.0175*
%CD4CD134	-0.1808	-0.4280 to 0.09156	0.1784
CD4:CD8	0.4610	0.2203 to 0.6488	0.0003***

%CD8 against (n = 57)

	r	95%CI	p value
%CD4CD134	0.03912	-0.2312 to 0.3038	0.7727
CD4:CD8	-0.5817	-0.7351 to -0.3718	<0.0001****

%CD4CD134 against (n = 57)

	r	95%CI	p value
CD4:CD8	-0.2414	-0.4784 to 0.02830	0.0704

Relationships between each pair of study parameters were determined using the Spearman correlation. *, **, *** and **** indicate significantly different values at p values < 0.05, < 0.01, < 0.005 and < 0.0001 respectively.

Table 4-8 Interrelationships between age, lymphocyte subpopulations and PVL in FIV positive cats

age against (n = 64)

	r	95%CI	p value
%CD4	-0.1448	-0.3836 to 0.1120	0.2535
%CD8	-0.1158	-0.3581 to 0.1411	0.3623
%CD4CD134	0.04375	-0.2114 to 0.2933	0.7314
CD4:CD8	-0.009982	-0.2621 to 0.2434	0.9376
FIV PVL	-0.1288	-0.3902 to 0.1519	0.3534

%CD4 against (n = 94)

	r	95%CI	p value
%CD8	0.1860	-0.02338 to 0.3797	0.0727
%CD4CD134	0.05221	-0.1579 to 0.2578	0.6173
CD4:CD8	0.5251	0.3555 to 0.6611	<0.0001****
FIV PVL	-0.2281	-0.4318 to -0.002193	0.0419*

%CD8 against (n = 94)

	r	95%CI	p value
%CD4CD134	0.1790	-0.03058 to 0.3735	0.0843
CD4:CD8	-0.6229	-0.7358 to -0.4763	<0.0001****
FIV PVL	-0.007572	-0.2332 to 0.2188	0.9469

%CD4CD134 against (n = 94)

	r	95%CI	p value
CD4:CD8	-0.1613	-0.3577 to 0.04874	0.1203
FIV PVL	0.1517	-0.07689 to 0.3652	0.1791

CD4:CD8 against (n = 94)

	r	95%CI	p value
FIV PVL	-0.2127	-0.4185 to 0.01400	0.0582

Relationships between each pair of study parameters were determined using the Spearman correlation. *, **, *** and **** indicate significantly different values at p values < 0.05, < 0.01, < 0.005 and < 0.0001 respectively.

Table 4-9 Interrelationships between age, lymphocyte subpopulations and PVL in FIV positive cats with detectable PVL

age against (n = 54)

	r	95%CI	p value
%CD4	-0.1805	-0.4342 to 0.09971	0.1915
%CD8	-0.08810	-0.3548 to 0.1918	0.5264
%CD4CD134	0.01797	-0.2586 to 0.2918	0.8974
CD4:CD8	-0.03987	-0.3117 to 0.2380	0.7447
FIV PVL	-0.1288	-0.3902 to 0.1519	0.3534

%CD4 against (n = 80)

	r	95%CI	p value
%CD8	0.1330	-0.09590 to 0.3485	0.2397
%CD4CD134	-0.02616	-0.2511 to 0.2005	0.8144
CD4:CD8	0.5607	0.3833 to 0.6982	<0.0001****
FIV PVL	-0.2281	-0.4318 to -0.002193	0.0419*

%CD8 against (n = 80)

	r	95%CI	p value
%CD4CD134	0.1783	-0.04974 to 0.3886	0.1136
CD4:CD8	-0.6165	-0.7395 to -0.4538	<0.0001****
FIV PVL	-0.007572	-0.2332 to 0.2188	0.9469

%CD4CD134 against (n = 80)

	r	95%CI	p value
CD4:CD8	-0.2068	-0.4135 to 0.02014	0.0657
FIV PVL	0.1517	-0.07689 to 0.3652	0.1791

CD4:CD8 against (n = 80)

	r	95%CI	p value
FIV PVL	-0.2127	-0.4185 to 0.01400	0.0582

Relationships between each pair of study parameters were determined using the Spearman correlation. *, **, *** and **** indicate significantly different values at p values < 0.05, < 0.01, < 0.005 and < 0.0001 respectively.

Table 4-10 Interrelationships between age and lymphocyte subpopulations in FIV positive cats with undetectable PVL

age against (n = 10)

	r	95%CI	p value
%CD4	-0.05455	-	0.8916
%CD8	-0.2485	-	0.4918
%CD4CD134	-0.01818	-	0.9730
CD4:CD8	0.1277	-	0.7247

%CD4 against (n = 14)

	r	95%CI	p value
%CD8	0.4945	-0.06632 to 0.8179	0.0750
%CD4CD134	0.4374	-0.1386 to 0.7922	0.1198
CD4:CD8	0.2863	-0.3039 to 0.7178	0.3183

%CD8 against (n = 14)

	r	95%CI	p value
%CD4CD134	0.3582	-0.2294 to 0.7545	0.2090
CD4:CD8	-0.6608	-0.8859 to -0.1837	0.0117*

%CD4CD134 against (n = 14)

	r	95%CI	p value
CD4:CD8	-0.08811	-0.6023 to 0.4778	0.7582

Relationships between each pair of study parameters were determined using the Spearman correlation. *, **, *** and **** indicate significantly different values at p values < 0.05, < 0.01, < 0.005 and < 0.0001 respectively.

Table 4-11 Interrelationships between age, lymphocyte subpopulations and PVL in healthy FIV positive cats with detectable PVL

age against (n = 7)

	r	95%CI^a	p value
%CD4	-0.03742	-	0.8524
%CD8	-0.4865	-	0.2190
%CD4CD134	-0.01871	-	0.8810
CD4:CD8	0.3742	-	0.3857
FIV PVL	-0.7111	-	0.0524

%CD4 against (n = 17)

	r	95%CI	p value
%CD8	-0.1176	-0.5767 to 0.3979	0.6526
%CD4CD134	-0.1201	-0.5784 to 0.3958	0.6458
CD4:CD8	0.7321	0.3747 to 0.9000	0.0012**
FIV PVL	-0.1054	-0.5684 to 0.4083	0.6873

%CD8 against (n = 17)

	r	95%CI	p value
%CD4CD134	-0.1544	-0.6012 to 0.3659	0.5530
CD4:CD8	-0.6315	-0.8573 to 0.2018	0.0076**
FIV PVL	-0.2279	-0.6477 to 0.2980	0.3474

%CD4CD134 against (n = 17)

	r	95%CI	p value
CD4:CD8	-0.1398	-0.5915 to 0.3787	0.5869
FIV PVL	0.4877	-0.006211 to 0.7904	0.0490*

CD4:CD8 against (n = 17)

	r	95%CI	p value
FIV PVL	-0.02943	-0.5144 to 0.4698	0.9079

Relationships between each pair of study parameters were determined using the Spearman correlation. *, **, *** and **** indicate significantly different values at p values < 0.05, < 0.01, < 0.005 and < 0.0001 respectively.

^asample size was too small for the calculation of 95% confidence intervals.

Table 4-12 Interrelationships between age, lymphocyte subpopulations and PVL in sick FIV positive cats with detectable PVL

age against (n = 26)

	r	95%CI	p value
%CD4	0.2072	-0.2074 to 0.5588	0.3097
%CD8	0.006519	-0.3921 to 0.4030	0.9748
%CD4CD134	0.04255	-0.3611 to 0.4328	0.8365
CD4:CD8	0.1194	-0.2920 to 0.4936	0.5612
FIV PVL	-0.1764	-0.5363 to 0.2379	0.3888

%CD4 against (n = 29)

	r	95%CI	p value
%CD8	0.4015	0.02966 to 0.6757	0.0309*
%CD4CD134	0.05911	-0.3244 to 0.4259	0.7607
CD4:CD8	0.4210	0.05316 to 0.6883	0.0229*
FIV PVL	-0.2463	-0.5698 to 0.1433	0.1977

%CD8 against (n = 29)

	r	95%CI	p value
%CD4CD134	0.3232	-0.06051 to 0.6236	0.0873
CD4:CD8	-0.4506	-0.7070 to -0.08947	0.0142*
FIV PVL	-0.09310	-0.4535 to 0.2935	0.6310

%CD4CD134 against (n = 29)

	r	95%CI	p value
CD4:CD8	-0.2148	-0.5469 to 0.1757	0.2631
FIV PVL	-0.1399	-0.4904 to 0.2495	0.4692

CD4:CD8 against (n = 29)

	r	95%CI	p value
FIV PVL	-0.1261	-0.4797 to 0.2626	0.5144

Relationships between each pair of study parameters were determined using the Spearman correlation. *, **, *** and **** indicate significantly different values at p values < 0.05, < 0.01, < 0.005 and < 0.0001 respectively.

4.4.12 Concurrent infections showed no effect on lymphocyte subpopulations in FIV negative cats with clinical signs

As shown above, with the exception of the percentages of CD4⁺CD134⁺ T lymphocytes, similar lymphocyte subpopulations were observed between sick FIV negative cats and healthy FIV positive cats (Table 4-4 and Figure 4-4). Of note, decreased CD4:CD8 ratios, the hallmark of FIV infection, were also observed in sick FIV negative cats. In order to examine the underlying causes of these findings, lymphocyte subpopulations of sick FIV negative cats with and without diagnosed concurrent infections were compared.

The most frequent major clinical sign in sick FIV negative cats in this study was gingivitis (23/57), in which nine of the cats tested positive for feline calicivirus (FCV) (Table 4-13 and Table 4-14). In addition, nine cats tested positive for feline coronavirus (FCoV), six tested *Toxoplasma gondii* positive and one was infected with *Mycoplasma* (Table 4-14). Unexpectedly, no differences in any of the parameters measured in this study were observed amongst sick FIV negative cats with and without these viral, protozoan and bacterial infections (Table 4-15 and Figure 4-6). Nevertheless, it was not possible to exclude the possibility that other, unidentified, pathogens might have led to the decreased CD4:CD8 ratio observed in these sick FIV negative cats.

4.4.13 Higher PVL and CD4⁺CD134⁺ T lymphocytes in FIV positive cats with co-infections

Gingivostomatitis and lethargy/vomiting were the two most frequent signs reported in the sick FIV positive cats in this study, consistent with previous studies (Hartmann, 2012, Sykes, 2013). However, in contrast to previous studies, no association was observed between FIV infection and gingivostomatitis in sick cats (8/35 vs. 23/57, Fisher's exact test, $p = 0.1126$, Table 4-13 and Appendix 4-9). Moreover, when these cases were analysed as proportions of the total study population, FIV seropositive cats appeared to have a lower risk of gingivostomatitis compared to FIV seronegative cats (8/94 vs. 23/114, Fisher's exact test, $*p = 0.0198$, Appendix 4-9).

In HIV infection, co-infection with other viruses such as hepatitis C virus (HCV) was associated with inverted CD4:CD8 ratios, even in clinically healthy patients with CD4⁺ lymphocyte numbers > 500 cells/mm³ and complete antiretroviral drug suppression of viral load (Brites-Alves et al., 2015). However, in this study, co-infections were detected only in sick FIV positive cats, thereby preventing an analysis of the effect of co-infections in healthy cats (Table 4-14 and Figure 4-6). Sick FIV positive cats with co-infections displayed slightly higher percentages of CD4⁺ T lymphocytes (17.20% vs. 15.98%) and lower percentages of CD8⁺ T lymphocytes (9.98% vs. 13.31%) than those without co-infections (Table 4-15 and Figure 4-6). However, their median CD4:CD8 ratios were lower than those of cats without co-infections (1.16 vs. 1.32, Table 4-15 and Figure 4-6). This result appeared counterintuitive, as the CD4:CD8 ratio is dependent on the CD4⁺ and CD8⁺ T lymphocyte percentages and therefore higher CD4⁺ and lower CD8⁺ T lymphocyte percentages would give rise to higher CD4:CD8 ratios. The wide range of ratios observed in these cats, together with their small number (n = 7) might attribute to this apparently contradicting finding (Table 4-15).

As shown in Table 4-15 and Figure 4-6E, the percentage of CD4⁺CD134⁺ T lymphocytes in sick FIV positive cats with co-infections was almost two-fold greater compared to cats without co-infections (51.25% vs. 26.58%). This increase was not associated with higher CD4⁺ T lymphocyte percentages as CD134⁺ T lymphocytes were sequentially measured as a proportion of the total CD4⁺ T lymphocyte population (Section 2.3.7). The FIV PVLs of the co-infected cats were also higher (8,695 vs. 3,143 copies/10⁶ cells, Table 4-15 and Figure 4-6F); however, no correlation was observed between CD4⁺CD134⁺ T lymphocyte numbers and PVL in either group (Appendix 4-10A). Interestingly, although not statistically significant, a strong negative correlation was observed between CD4⁺ T lymphocyte numbers and FIV PVL in sick FIV positive cats with co-infections ($r = -0.8286$, Spearman test, $p = 0.0583$, Appendix 4-10B). Hence co-infected cats might have shown more marked immune activation, with greater numbers of lymphocytes expressing CD134⁺ in FIV infected cats. Consequently the observed two-fold higher PVL might reflect the increased number of target cells and/or activation of latently infected CD4⁺ T lymphocytes.

Table 4-13 Major findings recorded in sick FIV negative and positive cats

Findings	FIV negative (n = 57)*	FIV positive (n= 35)**
decreased PCV	3	1
gingivostomatitis	23	8
lethargy and vomiting	7	8
malignancies	0	1
pyrexia	8	5
respiratory signs	7	1
positive rapid test kit result	0	6
uveitis	3	3
wound	1	2

*No information provided for five cats from which samples were submitted for feline gingivitis profile (FHV & FCV isolation, FeLV Ag, FIV Ab). ** Both sick FIV positive cats with detectable and undetectable FIV PVL were included in this analysis.

Table 4-14 Diagnosed co-infections of FIV negative and positive cats^a

	FIV negative (n = 114)			FIV positive (n = 94)*		
	healthy (n = 21)	sick (n = 57)	unknown (n = 36)	healthy (n = 19)	sick (n = 35)	unknown (n = 40)
<i>Chlamydia felis</i>			1			
feline calicivirus	1	9			4	
feline coronavirus	2	9	1			
feline herpesvirus			1			
feline parvovirus					1	
<i>Mycoplasma</i>		1				
<i>Toxoplasma gondii</i>		6	2		2	

^aDiagnostic technique for each infection as follows; *C. felis* PCR, FCV by virus isolation, FCoV by antibody detection, FHV by PCR and/or virus isolation, FPV by PCR *Mycoplasma* by cell culture and *T. gondii* by antibody detection. FIV positive cats with both detectable and undetectable FIV PVL were included in this analysis.

Table 4-15 Demography, lymphocyte subpopulations and PVL of sick FIV negative and positive cats with and without co-infections^a

co-infections	sick FIV negative cats		sick FIV positive cats ^b	
	without	with	without	with
Number	33	24	28	7
Age	2Y 5M (1M - 12Y 8M)	5Y (4M - 16Y 10M)	7Y 9M ^{***} (2Y - 14Y)	7Y 6M (7M - 16Y)
Gender (male:female)	10:23	12:11 (1 unknown)	24:4	6:1
CD4 ⁺ percentage	24.77 (4.58 - 44.87)	24.19 (2.88 - 58.30)	15.98 ^{**s} (0.03 - 38.16)	17.20 (0.27 - 29.7)
CD8 ⁺ percentage	12.33 (2.4 - 24.86)	13.67 (2.52 - 45.35)	13.31 (0.80 - 53.16)	9.98 (0.34 - 22.43)
CD4:CD8 ratio	1.79 (0.58 - 5.88)	1.82 (0.27 - 17.15)	1.32 ^{**s} (0.04 - 3.15)	1.16 (0.58 - 4.40)
CD4 ⁺ CD134 ⁺ percentage	9.41 (1.15 - 66.27)	10.54 (2.74 - 24.96)	26.58 ^{****s} (5.1 - 90.2)	51.25 ^{**} (6.30 - 67.83)
FIV PVL (copies/10 ⁶ cells)	n.a.	n.a.	3,143 (20 - 1,467,822)	8,695 (11 - 1,758,848)

^a Values are shown as group medians with range in brackets. ^bBoth sick FIV positive cats with detectable and undetectable FIV PVL were included in this analysis. Age: Y = years, M= months and W = weeks, CD4⁺ and CD8⁺ lymphocytes are shown as the percentage of total lymphocytes, CD4⁺CD134⁺ expressed as the percentage of CD4⁺ lymphocyte population, **, *** and **** indicate significantly different values when compared to sick FIV negative cats without co-infections, at p values < 0.01, < 0.005 and < 0.0001 respectively, ^s and ^{ssss} indicate significantly different values compared to sick FIV negative cats with co-infections, p values < 0.05 and < 0.0001, respectively, Statistical significance was determined using the Mann-Whitney test.

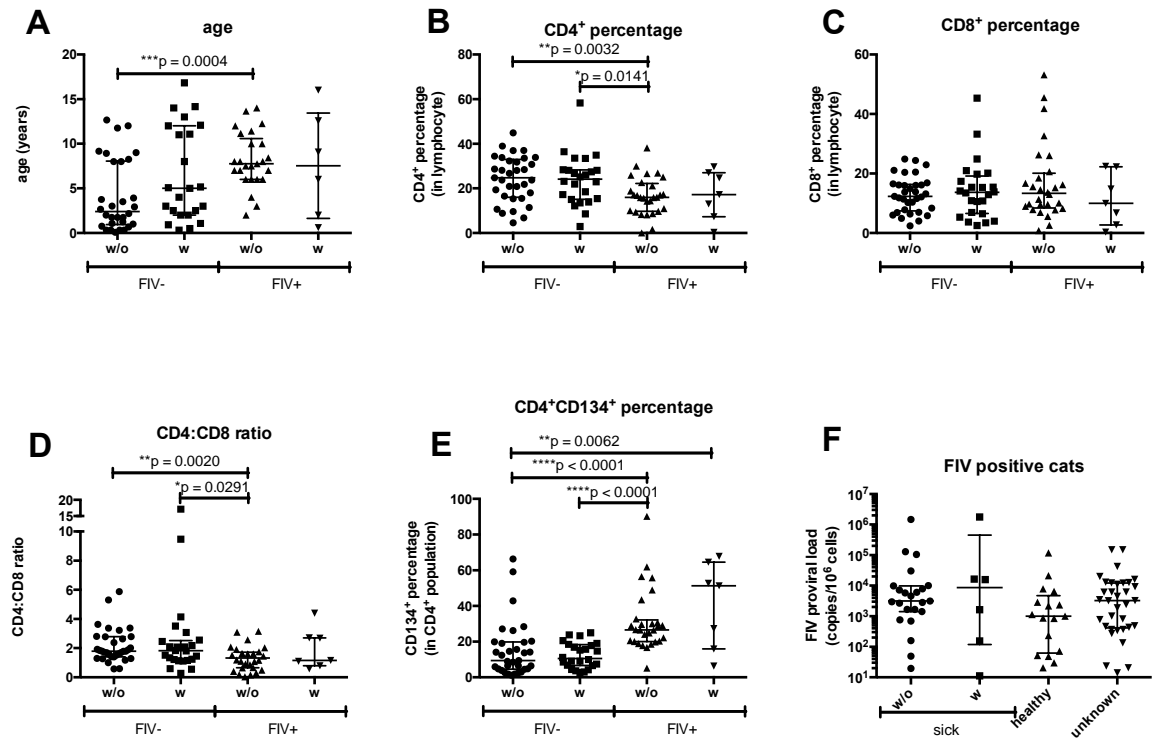


Figure 4-6 Comparisons of Age (A), percentage of CD4⁺ lymphocytes (B), percentage of CD8⁺ lymphocytes (C), CD4:CD8 ratio (D) and percentage of CD4⁺CD134⁺ lymphocytes (E) between groups according to their FIV serostatus and co-infections. w/o: without co-infections, w: with co-infections, Horizontal lines depict group median values with interquartile ranges. Comparison of FIV PVL (F) between sick cats with and without co-infections, healthy cats and cats of unknown clinical status. Statistical significance was determined using the Mann-Whitney test.

4.4.14 CD4⁺CD134⁺ T lymphocyte percentages decline following infection

The decrease in the percentages of CD4⁺CD134⁺ T lymphocytes (39.75% in healthy FIV infected cats vs. 26.68% in sick FIV infected cats) was consistent with findings observed in a cohort of specific pathogen free (SPF) cats, experimentally infected with an FIV clade A isolate (ongoing project, unpublished). The decline presumably reflects disease progression from the early asymptomatic phase towards the later immunodeficiency phase. As shown in Figure 4-7, the percentage of CD4⁺CD134⁺ T lymphocytes declined over a period of 44 weeks in these four cats experimentally infected with FIV (A831 - A834). It appears that the CD4⁺CD134⁺ T lymphocytes were partially replenished at four monthly intervals, suggesting an attempt at immune reconstitution in these cats. However, the percentages of CD4⁺CD134⁺ T lymphocytes were never restored to their original levels. Although the trend of declining CD4⁺CD134⁺ T lymphocyte numbers with time post infection was observed in all of these experimentally infected cats, without data from an age-matched uninfected control group, an age-related decline could not be discounted. Nevertheless, an age-related decline seems unlikely, as a significant positive correlation was observed between age and CD4⁺CD134⁺ T lymphocytes percentage in healthy FIV negative cats (Table 4-5).

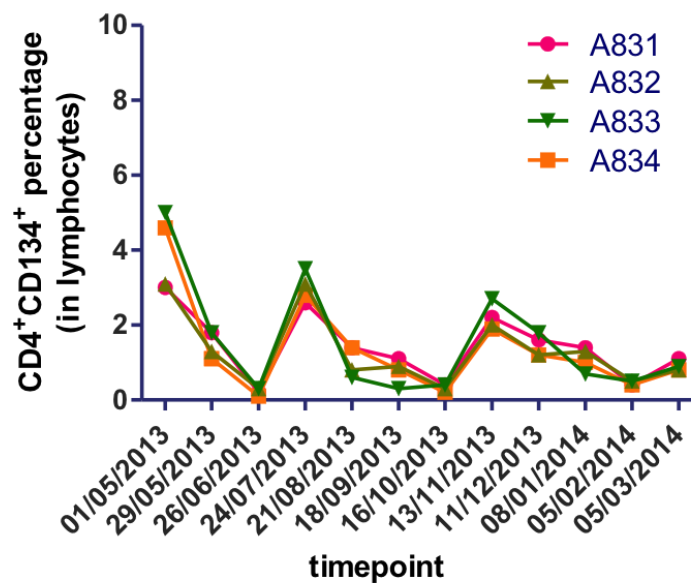


Figure 4-7 The declining trend in the percentage of CD4⁺CD134⁺ T lymphocytes was observed in a cohort of four FIV experimentally infected cats (A831 - 834) with time post infection.

4.4.15 Decreasing CD4⁺CD134⁺ T lymphocyte numbers might exert selective pressure on FIV population

Previous studies have demonstrated that different FIV strains interact with CD134 differently (Willett et al., 2006b). While some pathogenic primary strains such as GL8 and NCSU1 required a more complex interaction or showed a stronger binding affinity for CD134, isolates from cats in later stages of infection, such as B2452, were less dependent on CD134; the laboratory-adapted strain FIV PET was the most extreme, requiring only CXCR4 for infection (de Parseval et al., 2004b, de Parseval et al., 2005, Willett et al., 2006b). Moreover, it had been shown recently that this change in the way FIV interacts with its primary receptor CD134 altered as disease progressed. FIV variants recovered from the early phase of infection required both CRD1 and CRD2 of the CD134 molecule, whereas viruses in the later phase were CRD2-independent, requiring only CRD1 for infection (Willett et al., 2013, Beczkowski et al., 2014b). This change towards a less stringent requirement for CD134 might explain the broader spectrum of target cells observed later in infection (English et al., 1993, Dean et al., 1996). However, the driving force behind the tropism switch has yet to be unravelled.

Since the change from a complex to a more simple CD134 interaction of FIV variants occurred in parallel with the decline in CD4⁺CD134⁺ T lymphocytes over time, we speculated that target cell availability, i.e. CD4⁺CD134⁺ T lymphocyte numbers, might play a major role in the tropism switch, selecting for the fittest variant most capable of rapid replication. In order to test this hypothesis, a FIV-CD134 usage assay (Section 2.3.2) was conducted on HIV(FIV) pseudotypes bearing envelope glycoproteins (Env) obtained from both healthy (presumed to be in the early phase) and sick (presumed to be in the late phase) cats.

4.4.16 High proportion of incomplete *env* genes detected in the cohort

Full-length *env* genes were successfully amplified from 8 of 17 healthy and 12 of 29 sick FIV infected cats, respectively (Table 4-16). The number of clones obtained was relatively similar between two groups, despite sick cats harbouring higher FIV PVL than healthy cats (median of four vs. three clones per

cat, $p = 0.6291$). After screening no fewer than 2,000 colonies, at least 50 colonies for each sample, 141 *env* genes were obtained and submitted for sequencing. It was notable that the *env* genes from over half of the samples (11/20 cats) were incomplete, containing stop codons at the SU-TM junction (position 610, UK8) These incomplete sequences were included in a phylogenetic analysis but were excluded from CD134 usage and viral neutralisation assays, as these could not be used to prepare pseudotypes (Table 4-16).

Table 4-16 Number of *env* successfully cloned, used to prepare pseudotypes and tested for CD134 usage from 20 healthy and sick FIV positive cats

	I.D.	no of <i>env</i> cloned*	average within population diversity**	no of pseudotypes tested***
Healthy	346271	7	0.00612	2
	346302	15	0.00014	3
	346363	6	0.02459	0
	346540	1	n/c	0
	347178	9	0.00067	5
	347251	11	0.00131	1
	364791	5	0.00023	0
	368352	3	0.00000	1
Sick	346096	9	0.00433	0
	346223	5	0.01552	0
	346224	4	0.00391	0
	346301	5	0.00034	0
	346541	3	0.01152	0
	346660	2	0.00000	0
	346938	27	0.00765	3
	347076	18	0.00179	4
	347175	2	0.01035	0
	347202	7	0.02942	2
	365045	1	n/c	1
	367133	1	n/c	1

* The number indicated number of full *SU* or full-length *env* (*SU+TM*) sequences included in the phylogenetic analysis.

** Mean within population diversity was calculated using nucleotide sequences spanning the complete *SU* region (UK8 position 1- 1830) using Maximum Composite Likelihood model on Mega 5.1 (Tamura et al., 2011). Values shown represent the mean number of base substitutions per site within the population. n/c = incalculable

*** Only unique *env* gene clones were used to prepare pseudotypes and tested in each cat. Zero values indicate that the cloned *env* sequences were incomplete and thus could not be used to prepare pseudotypes.

4.4.17 Phylogenetic characterisation of FIV *env* genes

The average diversity of the entire population was 0.074 as calculated using maximum composite likelihood on Mega 5.1 software (Tamura and Nei, 1993, Tamura et al., 2011). This value was slightly lower than the diversity of FIV clade A isolates, reported previously as 0.091 (Samman et al., 2011). Different degrees of FIV population diversity within individual cats were observed, ranging from 0.0 to 0.02942 (Table 4-16). Although the *env* variants were less diverse in healthy cats compared to sick cats (median of 0.00067 (0.0 - 0.02459) vs. 0.00599 (0.0 - 0.02942), $p = 0.1674$), this difference was not statistically significant.

In order to determine the subtypes of the amplified FIV *env* variants, firstly a maximum likelihood (ML) tree was constructed using 141 deduced amino acid sequences comprising the full SU (UK8 position 1 - 610) obtained from 20 cats (Table 4-16), together with 20 reference sequences from clades A, B, C and D, which were available from Genbank (Figure 4-8). Phylogenetic analysis indicated that all of the *envs* belonged to FIV clade A as their sequences clustered together with the clade A reference sequences (Bootstrap value = 99%, Figure 4-8), consistent with previous findings that clade A was the major FIV subtype circulating in the British Isles (Samman et al., 2011).

On the SU tree, sequences from the same cats clustered together, with each forming a monophyletic branch. No evidence of separation of sequences from healthy and sick cats was observed; all sequences were intermingled with each other and with the reference sequences. Amongst the sequences from the same cat, a degree of polymorphism was evident, indicative of the existence of quasispecies within naturally FIV infected cats (Figure 4-8). Interestingly, more diverse intra-host *env* populations were observed in some cats. For example, clone 5 of cat 347202 (347202C5) was some distance from clone 4 amplified from the same cat (upper and lower red arrows respectively) (Figure 4-8). The SU gene from this cat was the most diverse, (average diversity 0.02942 (Table 4-16)). Similar divergence was also observed in cats 346938 and 346363. Although the average diversity of cat 346938 was relatively low at 0.00765, one highly diverse sequence, clone 43, clustered and formed a monophyletic branch with sequences from cat 347202 (top blue arrow and bottom red arrow), some

distance from the other sequences from the same cat (bottom blue arrow) (Table 4-16 and Figure 4-8). Cat 346363 showed the second highest average diversity at 0.02459 (Table 4-16). Clone 1 from this cat was more closely related to sequences from cat 346224 and was distinct from the other sequences amplified (bottom and top green arrow) (Figure 4-8).

It has been shown that the sequences from the region extending from variable loop 3 to variable loop 6 (V3-V6) of Env are the most polymorphic and these regions were used conventionally to define FIV subtypes (Kakinuma et al., 1995). Moreover, a fifth clade of FIV, clade E, was identified using sequences comprising the V3-V5 region of Env (Pecoraro et al., 1996). Since no full-length Env references sequences were available for clade E, a separate maximum likelihood tree was constructed using deduced amino acid sequences spanning the V3-V6 region (UK8 position 360 - 610) of Env from the same dataset. As shown in Figure 4-9, the V3-V6 ML tree confirmed that all FIV Env in this study belonged to clade A. Sequences from the same cats clustered together and formed monophyletic branches as observed in the SU tree (Figure 4-8 and Figure 4-9). Although their locations on the tree varied between each monophyletic branch, sequences 347202C5, 346938C43 and 346363C1 displayed similar relationships to those observed in the SU tree (Figure 4-8 and Figure 4-9).

Figure 4-10 shows a ML tree constructed from 76 full-length Env (deduced) amino acid sequences from five healthy and five sick FIV infected cats, together with 20 full-length reference sequences available from Genbank. This ML tree confirmed that all FIV Env belonged to clade A. Clones 347202C5 and 346938C43 appeared closely related and did not cluster with the other sequences, as observed in the SU and V3-V6 trees (Figure 4-8 to Figure 4-10).

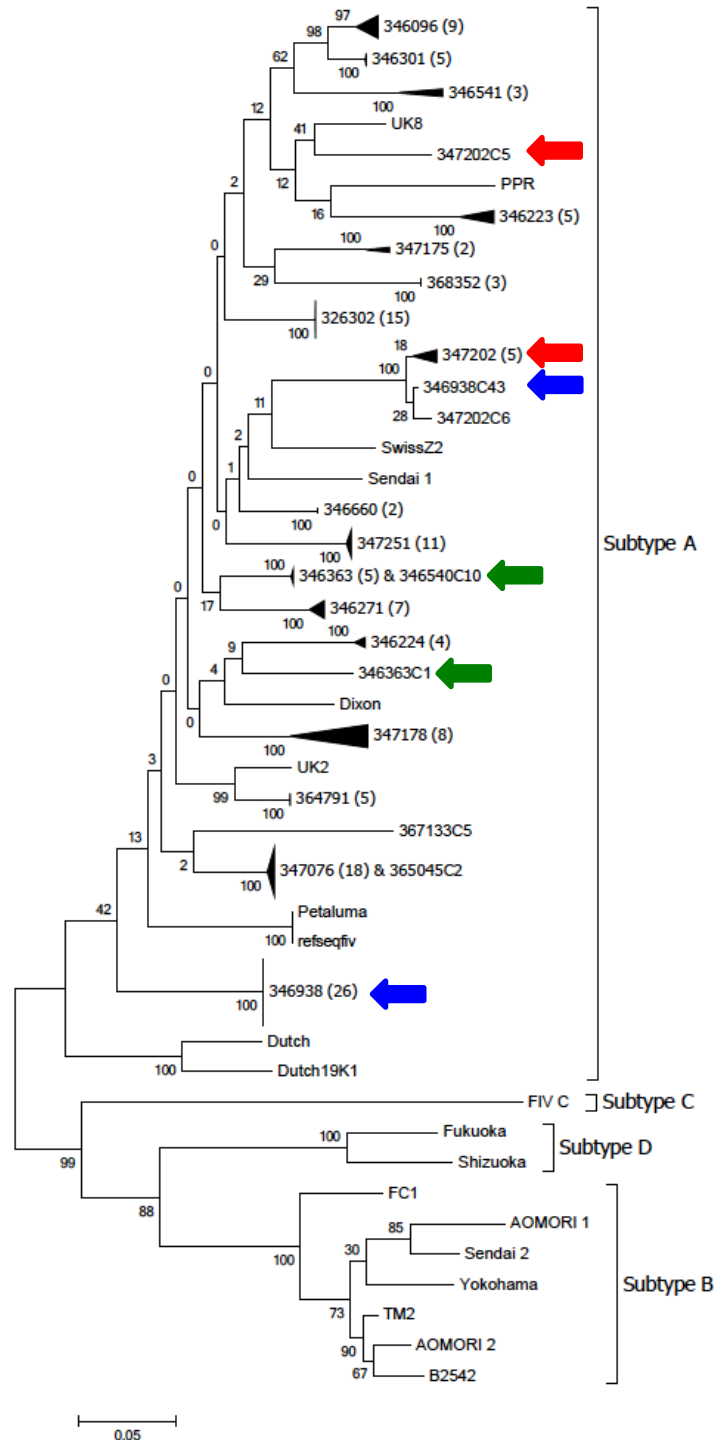


Figure 4-8 Unrooted maximum likelihood tree of 141 full SU amino acid (UK8 position 1 - 610) from eight healthy and 12 sick FIV infected cats together with 20 reference sequences (Genbank accession numbers in brackets); Clade A; Dixon (L00608.1), Dutch (X60725), Dutch 19K1 (M73964.1), Petaluma (M25381.1), PPR (M36968.1), refseqfiv (KKS) (NC_001482.1), Sendai1 (D37813.1), SwissZ2 (X57001.1), UK2 (X69494.1) and UK8 (X69496.1), Clade B; Aomori 1 (D37816), Aomori 2 (D37817.1), B2542 (USIL2989_7B), FC1 (AY621093), Sendai 2(D37814.1), TM2 (M59418.1) and Yokohama (D37812.1), Clade C; FIVC (AF474246.1) and Clade D; Fukuoka (D37815.1) and Shizuoka (D37811.1). Percentage bootstrap values (1000 replicates) were shown next to branches. Branch length scaled to the number of amino acid substitutions. Note that 347202C5 (top red arrow), 346938C43 (top blue arrow) and 346363C1 (bottom green arrow) were positioned apart from the monophyletic branches of all the others clones from the same cat, 347202 (bottom red arrow), 346938 (bottom blue arrow) and 346363 (top green arrow).

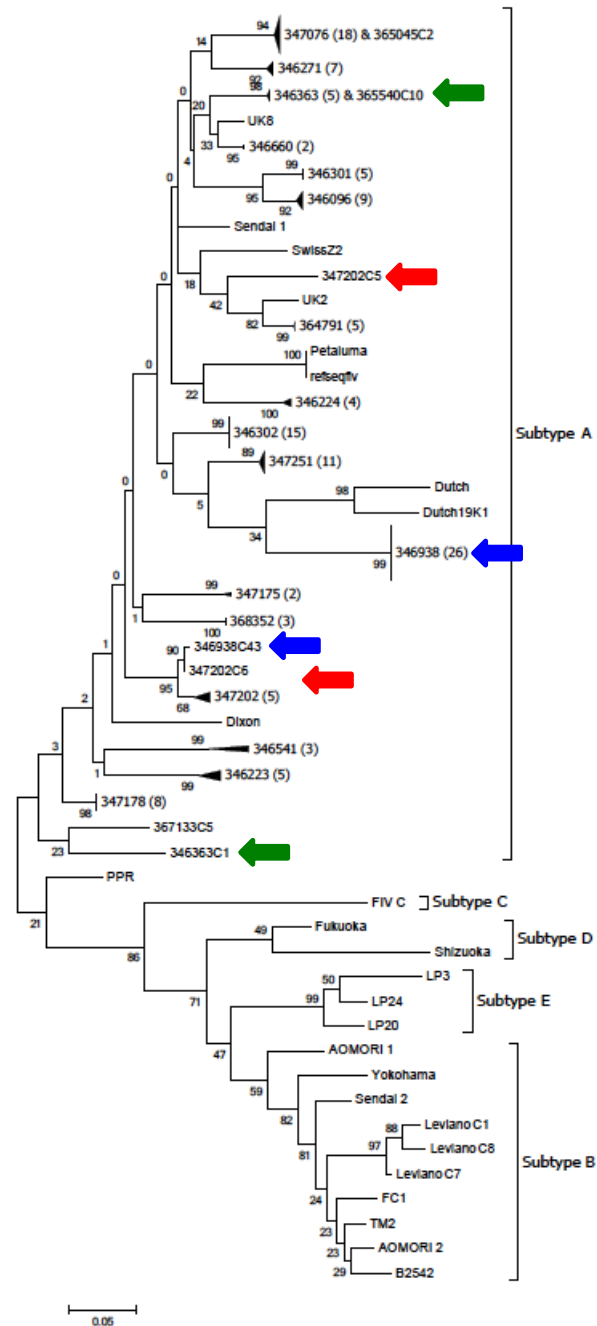


Figure 4-9 Unrooted maximum likelihood tree of 141 amino acid sequences spanning V3-V6 loop (UK8 position 360 - 610) from eight healthy and 12 sick FIV infected cats, together with 26 reference sequences (Genbank, accession numbers in brackets); Clade A; Dixon (L00608.1), Dutch (X60725), Dutch 19K1 (M73964.1), Petaluma (M25381.1), PPR (M36968.1), refseqfiv (KKS) (NC_001482.1), Sendai1 (D37813.1), SwizzZ2 (X57001.1), UK2 (X69494.1) and UK8 (X69496.1), Clade B; Aomori 1 (D37816), Aomori 2 (D37817.1), B2542 (USIL2989_7B), LevianoC1 (FJ374696.1), Leviano_C7 (FJ374697), Leviano_C8 (FJ374695), Sendai 2 (D37814.1), TM2 (M59418.1) and Yokohama (D37812.1), Clade C; FIVC (AF474246.1) and Clade D; Fukuoka (D37815.1) and Shizuoka (D37811.1) and Clade E; LP3 (D84496), LP20 (D84498) and LP24 (D84500). Percentage bootstrap values (1000 replicates) were shown next to branches. Branch length scaled to the number of amino acid substitutions. Note that 347202C5 (top red arrow), 346938C43 (bottom blue arrow) and 346363C1 (bottom green arrow) were positioned apart from the monophyletic branch of all other clones from the same cat, 347202 (bottom red arrow), 346938 (top blue arrow) and 346363 (top green arrow).

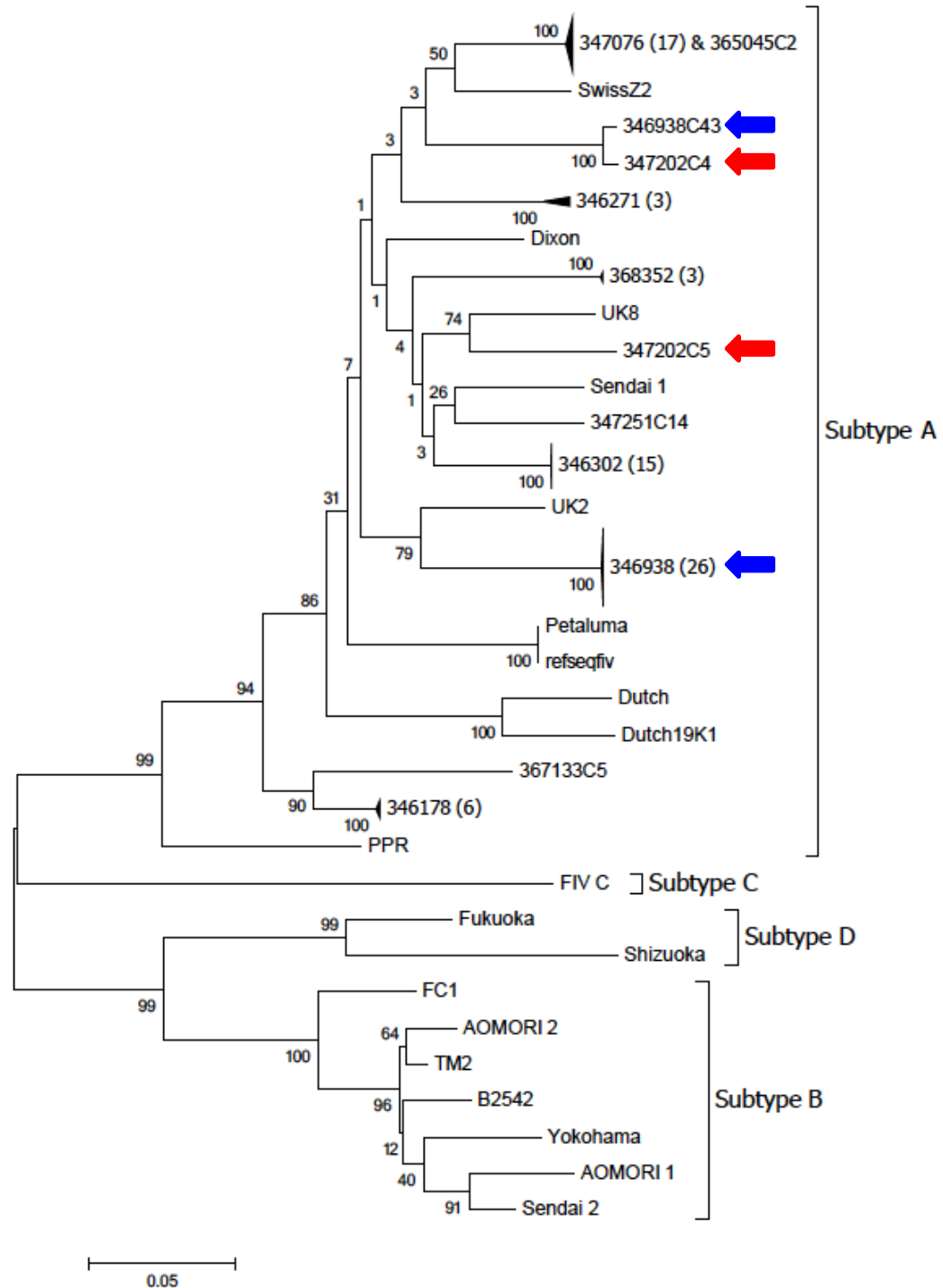


Figure 4-10 Unrooted maximum likelihood tree of 76 full-length Env amino acid sequences from five healthy and five sick FIV infected cats, together with 20 reference sequences (Genbank, accession numbers in brackets); Clade A; Dixon (L00608.1), Dutch (X60725), Dutch 19K1 (M73964.1), Petaluma (M25381.1), PPR (M36968.1), refseqfiv (KKS) (NC_001482.1), Sendai1 (D37813.1), SwizzZ2 (X57001.1), UK2 (X69494.1) and UK8 (X69496.1), Clade B; Aomori 1 (D37816), Aomori 2 (D37817.1), B2542 (USIL2989_7B), FC1 (AY621093), Sendai 2 (D37814.1), TM2 (M59418.1) and Yokohama (D37812.1), Clade C; FIVC (AF474246.1) and Clade D; Fukuoka (D37815.1) and Shizuoka (D37811.1). Percentage bootstrap values (1000 replicates) were shown next to branches. Branch length scaled to the number of amino acid substitutions. Note that 347202C4 (top red arrow) and 346938C43 (top blue arrow) clustered together and far away from 347202C5 (bottom red arrow) and the monophyletic branch of all the other clones from the same cat 346938 (bottom blue arrow).

4.4.18 CD134 usage and FIV clinical status

From the 76 full-length *env* gene sequences obtained, 24 sequences were unique (Table 4-16). These 24 unique *env* genes were used to construct HIV(FIV) pseudotypes which were then tested for CD134-usage. CRD2 dependence of each pseudotype was determined using the assay described in Section 2.3.2).

As shown in Table 4-18 and Figure 4-11, different degrees of CRD2 dependency were observed among 24 pseudotypes bearing Envs from healthy and sick cats. A mixed population of FIV Env variants with different CD134 usage was observed in cats for which more than one pseudotype was tested (Table 4-18), indicative of a quasispecies. We speculated that sick cats, having lower percentages of CD4⁺CD134⁺ T lymphocytes and tending to be older, might be expected to harbour more CRD2-independent FIV Env variants. Although two sick cats (346938 and 367133) gave rise to CRD2-independent Envs, compared to only one healthy cat (368352), similar numbers of FIV Env variants with CRD2-dependent, intermediate and CRD2-independent usage were observed between the two groups (healthy; 4:4:1, compared to sick; 5:2:2). It was notable that the percentage of CD4⁺CD134⁺ T lymphocytes of the cat with only CRD2-independent using Env (healthy cat 368352 and sick cat 367133) was the lowest in the group; cat 368352 displayed 16.78% CD4⁺CD134⁺ T lymphocytes compared to the healthy group median of 28.19% and cat 367133 displayed 5.10% CD4⁺CD134⁺ T lymphocytes compared to the sick group median of 29.05%) (Table 4-17 and Appendix 4-6). The presence of CRD2-independent Env variants in cat 368352 in the healthy group was striking, since this cat was only two years old at the time of sampling and so was likely in the early phase of infection. Cat 368352 had a higher PVL compared to the other healthy FIV-infected cats (6,504 compared to a group median of 1,010 copies/10⁶ cells) (Table 4-17). One possible explanation was that the transmitted population comprised both early and late variants. However, only three *env* genes were cloned from this cat and all were identical. In order to investigate this further, a larger population sample would be required.

Table 4-17 Demography, lymphocyte subpopulations and PVL of healthy and sick FIV positive cats from which functional pseudotypes were derived^a

	Healthy (n = 5)	Sick (n = 5)
Age	3Y (2Y - 6Y 10M)	6Y 9M (6Y - 10Y)
Gender (male:female)	4:1	5:0
CD4⁺ percentage	24.17 (13.02 - 26.77)	13.0 (1.62 - 25.92)
CD8⁺ percentage	15.56 (5.17 - 30.29)	16.20 (2.59 - 32.67)
CD4:CD8 ratio	1.43 (0.66 - 4.86)	0.58 (0.29 - 3.15)
CD4⁺CD134⁺ percentage	28.19 (16.78 - 67.37)	29.05 (5.10 - 51.25)
FIV proviral load (copies/10⁶ cells)	1,010 (20 - 7,903)	2,982 (1,629 - 7,204)

^a Values shown as group median values with range in brackets. Age: Y = years and M = months, CD4⁺ and CD8⁺ lymphocytes are shown as percentage of total lymphocytes, CD4⁺CD134⁺ lymphocytes are shown as percentage of CD4⁺ population, Statistical significance were determined using Mann-Whitney test and Fisher's exact test.

Table 4-18 CD134 usage and autologous neutralisation of HIV(FIV) pseudotypes bearing Env variants from healthy and sick FIV positive cats

	I.D.	<i>env</i> variants*	CD134 usage**	autologous neutralisation***
healthy	346271	C6	n.d.	n.a.
		C10	intermediate	n.a.
		C11	CRD2-dependent	n.a.
	346302	C2	CRD2-dependent	n.a.
		C18	intermediate	n.a.
		C21	intermediate	n.a.
	347178	C2, C13	n.d.	n.d.
C4		n.d.	n.d.	
C10		CRD2-dependent	no	
C11		CRD2-dependent	no	
C15		n.d.	n.d.	
347251	C14	intermediate	no	
368352	C20	CRD2-independent	yes	
sick	346938	C5	CRD2-dependent	n.a.
		C24	CRD2-independent	n.a.
		C43	CRD2-dependent	n.a.
	347076	C4	n.d.	n.d.
		C5	n.d.	n.d.
		C9	CRD2-dependent	no
		C31	CRD2-dependent	no
347202	C4	CRD2-dependent	no	
	C5	intermediate	no	
365045	C2	intermediate	no	
367133	C5	CRD2-independent	no	

*Clones representing unique *env* genes isolated from each individual cat.

**CD134 usage determined as ratio of ability to utilise feline CD134 (FFF) versus chimaeric feline x human CD134 (FFHH) (FFF:FFHH) for infection. Results shown were reproduced in 4 independent experiments (Appendix 4-11).

***n.a. = not analysed, due to inadequate plasma sample volume, n.a. = not determined, as luciferase activity of pseudotype was as low as vector control.

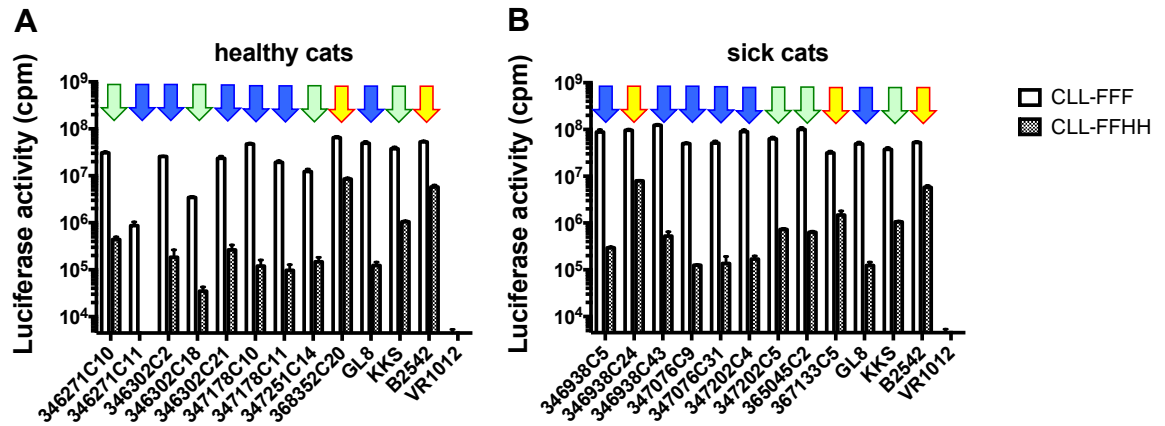


Figure 4-11 Representative result of CD134-usage assay for HIV(FIV) pseudotypes bearing Env variants derived from healthy (A) and sick (B) FIV infected cats. The infectivity of each pseudotype (indicated on the X-axis) in CLL-FFF (white bar) and CLL-FFHH (filled bar) is shown as mean luciferase activity (cpm, count per minute) with standard deviation (SD) of triplicate reads. CD134 usage was determined from the FFF:FFHH ratio, which was compared with the ratio for the prototypic GL8 for CRD2-dependent (blue arrow), KKS for intermediate (light green arrow) and B2542 for CRD-2-independent (yellow arrow) variants. The interpretations were made on the consensus readouts from 4 assay repeats (Appendix 4-11).

4.4.19 Autologous neutralisation and FIV clinical status

Previously, it has been shown for HIV-1 that tropism switching is associated with escape from immune selective pressures (McKnight and Clapham, 1995, McKnight et al., 1995). For FIV, it was also shown that a switch occurs between a complex, CRD2-dependent, CD134-FIV Env interaction to a simple, CRD2-independent interaction, associated with selective pressure from neutralising antibodies (Willett et al., 2008, Willett et al., 2010, Willett and Hosie, 2013). Since evasion from the immune response could influence FIV receptor usage, a virus neutralisation assay was performed using autologous plasma samples against the panel of HIV(FIV) pseudotypes bearing FIV Envs.

Unfortunately, due to limiting plasma sample volumes, neutralisation tests could be performed in only two healthy and four sick cats (Figure 4-12). Neutralising antibodies (NAb) were detected in only one of the healthy cats (368352, see Figure 4-12A). This finding was unexpected, since pseudotype 368352 showed CRD2-independent CD134 usage (Table 4-18 and Figure 4-11) and the emergence of CRD2-independent variants had been linked to evasion from NAb in the previous study (Willett et al., 2008, Willett et al., 2010). In spite of being the only cat with detectable NAb, the FIV PVL of this cat was relatively

high, compared to the other healthy FIV-infected cats (6,504 vs. a group median of 1,010 copies/ 10^6 cells) (Table 4-17). One possible explanation was that the *env* used for pseudotype production was derived from proviral sequence and so might not represent the population of Env variants circulating at the time of sampling. However, without circulating viral RNA-derived envelope sequence, we were unable to test this hypothesis.

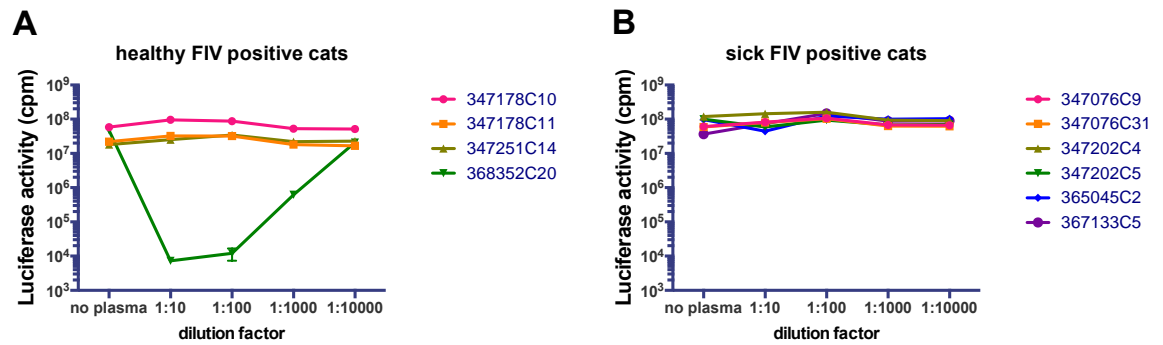


Figure 4-12 Autologous viral neutralisation assay of HIV(FIV) pseudotypes bearing Envs derived from healthy (A) and sick (B) FIV positive cats. X-axis indicated 10-fold serial dilutions of plasma ranging from 1:10 to 1:10,000. Y-axis showed log luciferase activity (counts per minute).

4.5 Discussion and Conclusion

In this chapter, the classical immunological parameters of FIV infection, i.e. levels of CD4⁺, CD8⁺ T lymphocytes and their ratios were investigated in a cohort of FIV⁺FeLV⁻ cats. We confirmed that decreased or inverted CD4:CD8 ratios were a hallmark of FIV infection, resulting from the combined effect of decreasing numbers of CD4⁺ T lymphocytes and expansion of the CD8⁺ T lymphocyte population (Figure 4-2C to Figure 4-2E) (Willett et al., 1993, Shimojima et al., 1998, Yamamoto et al., 2007, Hartmann, 2012, Sykes, 2013). The clinical signs observed in FIV infected cats in this study were consistent with those reported previously, in which gingivostomatitis and lethargy were the most common signs (Yamamoto et al., 2007, Hosie et al., 2011, Hartmann, 2012, Sykes, 2013). Similar to a previous study, no association was observed between the CD4:CD8 ratio and the health status of FIV infected cats (Beczowski et al., 2015a). Interestingly, similar CD4:CD8 ratios were observed between sick FIV negative cats and healthy FIV positive cats (Figure 4-4E). This finding suggested that low CD4:CD8 ratios are commonly seen in response to infections and not restricted to FIV infection.

The observation that senile cats usually displayed decreased CD4:CD8 ratios, together with the negative correlation between age and CD4:CD8 ratio in FIV negative cats, led to the speculation that the decreased ratio was associated with aging (Table 4-5) (Heaton et al., 2002, Day, 2010). In addition, a previous study of an Italian HIV negative cohort of patients reported a link between CD4:CD8 ratios less than one and immunosenescence, the natural aging of the immune system (Mascolini, 2014). However, the low CD4:CD8 ratio was unlikely to be age-related in this study, as the median ages of both sick FIV negative and healthy FIV positive cats were similar to those of the healthy FIV negative cats (Table 4-4). Since the percentages of CD4⁺ T lymphocytes were similar to those of healthy FIV negative cats, the decreased CD4:CD8 ratios observed in sick FIV negative and healthy FIV positive cats might have reflected their increased percentages of CD8⁺ T lymphocytes (Table 4-4).

CD8⁺ T lymphocytes proliferate in response to viral infection, therefore the low CD4:CD8 ratio observed in sick FIV negative cats might be related to other concurrent infections (Wherry and Ahmed, 2004). However, similar

CD4:CD8 ratios were observed between sick FIV negative cats, with or without detectable evidence of other infections (Table 4-15). The effect of FCV infection on the CD4:CD8 ratio has rarely been investigated and the few indirect observations reported in literature have been inconclusive. In one study, in which cats chronically infected with FIV were co-infected experimentally with FCV, FCV co-infection had no effect on the CD4:CD8 ratio (Reubel et al., 1994). In another study, proliferation of CD8⁺ T lymphocytes from FCV vaccinated cats was observed *in vitro* following re-stimulation with inactivated, but not infectious, FCV (Vermeulen et al., 2012). In this study, the FCV infected cats maintained high CD4:CD8 ratios (median 2.08, range 0.27 - 4.14), indicating that FCV infection had no effect on the CD4:CD8 ratio. In contrast, inversion of the CD4:CD8 ratio was reported in severe cases of human toxoplasmosis and also in cats experimentally infected with *Toxoplasma gondii* (Lin et al., 1992, Lappin et al., 1996, Darde et al., 1998). However, the median CD4:CD8 ratio was relatively high in sick FIV negative cats with *T.gondii* infection in this study (median 1.90, range 1.16 - 3.51). Therefore it was difficult to account for the low CD4:CD8 ratios observed in sick FIV negative cats (with or without evidence of co-infections), although it is possible that these cats were harbouring additional, unidentified infections since the panel of diagnostic tests conducted was not comprehensive.

Inflammatory oral disease, especially gingivitis and stomatitis, has been associated with FIV infection (Tenorio et al., 1991, Hosie et al., 2009, Hartmann, 2012, Sykes, 2013). Kornya and colleagues reported a significantly higher risk of FIV infection in cats with inflammatory oral diseases, with stomatitis being the highest risk (Kornya et al., 2014). In this study, however, such an association was not observed (Appendix 4-9); a higher percentage of cats with gingivitis tested FIV negative than FIV positive (20.17% (23/114) vs. 6.38% (6/94)). The lower number of FIV-infected cats presenting with gingivitis in this study might be related to variations in virulence amongst infecting strains of FIV (Hosie et al., 2000, Hosie et al., 2002, Stickney et al., 2013). In this study, all cats were infected with clade A isolates, confirming the results of a study conducted in UK in 2011 by Samman et al (Samman et al., 2011). The prevalence of gingivitis in sick FIV infected cats in this study (17.14% (6/35)) was similar to that observed previously (24% (6/25)) (Samman et al., 2011). Although several previous studies have suggested that isolates in FIV clades A and C were more virulent than clade

B isolates, the small number of experimental cohorts and differences in the definition of virulence made it difficult to make such comparisons (Kohmoto et al., 1998, Nishimura et al., 1998, Pedersen et al., 2001).

Overall, similar percentages of lymphocyte subpopulations were observed between sick FIV positive cats with and without co-infections (Table 4-15 and Figure 4-6). Since only seven cats were co-infected, this sample number was too small to detect statistically significant differences. Nonetheless, FIV infected cats with co-infections displayed higher percentages of CD4⁺CD134⁺ T lymphocytes as well as higher FIV PVL (Table 4-15). The increased FIV PVL and co-infections observed in these cats were likely attributable to the cats being in the final stage of infection, with depleted immune systems and the loss of ability to respond to opportunistic infections (Yamamoto et al., 2007, Hartmann, 2012, Sykes, 2013). However, it is possible that both groups of FIV-infected cats (with and without co-infections) were at similar stages of infection, since the median ages for both groups were similar (7Y 6M vs. 7Y 9M) (Table 4-15). A causal relationship could not be established because of the cross-sectional design of this study, but cell-mediated immune responses against co-infecting agents might have led to expansion of an antigen-specific memory T lymphocyte population (Song et al., 2008, Hua et al., 2012, Croft, 2014). Such newly activated populations would then be infected readily with FIV as they express high levels of the CD134 receptor molecule, as shown in Figure 4-6E (de Parseval et al., 2004a). Moreover, if this population had already been latently infected, immune activation in response to new co-infection(s) might also have led to increased viral replication (McDonnell et al., 2013). Both of these mechanisms would result in increased numbers of CD134⁺ target cells and activation of latently infected CD4⁺ T lymphocytes could also contribute to the elevated FIV PVL that was observed in FIV infected cats with co-infections (Figure 4-6F). To confirm this hypothesis, a larger, case-controlled, study would be required.

It is possible that FIV Env-CD134 engagement might trigger signal transduction, similar to the engagement of CD134L, the native ligand for CD134. However, there have been no reports of studies investigating this possibility. CD134L/CD134 engagement was shown to promote peripheral migration of T lymphocytes (Evans et al., 2001). These circulating antigen-specific T lymphocytes were functionally competent and long-lived, surviving for 196 days

after antigen-stimulation (Evans et al., 2001, Prell et al., 2003). This suggests that the elevated percentages of CD4⁺CD134⁺ T lymphocytes, which were observed only in FIV infected cats, might have arisen as a consequence of the FIV Env-CD134 interaction (Figure 4-2F, Figure 4-3F and Figure 4-4F). To confirm this relationship would require investigation of the CD134 signal transduction pathway using recombinant Envs of different FIV strains, ideally in the native trimeric conformation.

In this study a positive correlation was observed between CD4⁺CD134⁺ T lymphocytes and FIV PVL only in healthy FIV positive cats. As the healthy cats were likely to be in the early phase of infection, it appeared that some FIV variants replicated better and so outcompeted other variants in the quasispecies (Figure 4-5E). It was shown previously that the CRD2-dependent FIV GL8 isolate was insensitive to CD134L antagonism (Willett et al., 2009, Willett et al., 2010). This finding suggested that the Env from GL8, isolated from early infection, could utilise CD134 for infection, even when bound by CD134L. The ability to utilise both free and CD134L-bound CD134 receptor molecules for infection could provide this strain of FIV with more target cells for replication. Moreover, the highly activated immune status and longer lifespan of CD134L- bound CD4⁺CD134⁺ T lymphocytes might also confer more efficient viral replication (Hori, 2005, Soroosh et al., 2006, Song et al., 2008). Although there was no direct evidence of CD134 signalling affecting FIV replication, it was shown in an HIV-1 *in vitro* model that the CD134L/CD134 interaction, similar to TNF- α stimulation, enhanced virus production (Takahashi et al., 2001). Since the level of TNF- α was shown to be linked with the level of FIV core protein production, it would appear likely that CD134L ligation could also augment FIV production (Kraus et al., 1996). Hence, this mechanism might explain the higher replicative capacity of early, CRD2-dependent variants observed in the earlier phase of infection such as GL8, compared to the CRD2-independent variants that emerge later in infection (Willett et al., 2013, Willett and Hosie, 2013).

The positive correlation observed between CD4⁺CD134⁺ T lymphocytes and PVL might also reflect the classic pathogenesis of acquired immunodeficiency syndromes, with the initial T lymphocyte depletion stimulating the replenishment of lymphocytes from the memory pool (Grossman et al., 2006, Hua et al., 2012). Such migrating memory CD4⁺ T lymphocytes are of diverse

antigen specificity and continuously repopulate the lymphocyte population (Picker et al., 2004). However, it was shown, in SIV-infected macaques, that this process is incomplete; failure to repopulate the depleted lymphocytes coincided with the onset of immunodeficiency (Picker et al., 2004). Furthermore, these recently recruited, antigen-activated CD4⁺CD134⁺ T lymphocytes could in turn become fresh target cells (de Parseval et al., 2004a). Eventually this cycle would lead to the inability to replenish lost T lymphocytes, immune exhaustion, increasing PVL and the clinical signs of immunodeficiency, such as those observed in the sick FIV positive cats in this study.

In order to characterise the FIV variants of the cats of this study, 141 full-length *env* gene sequences were obtained from 20 of the cats naturally infected with FIV. Phylogenetic trees constructed from the deduced amino acid sequences of either the entire Env or spanning the V3-V6 loop, confirmed that FIV clade A is the predominant clade circulating in the UK, as reported in 2011 (Samman et al., 2011). The average inter-host diversity of *env* in this study was 7.4%; this was relatively similar to the diversity observed for FIV clade A isolates previously. In the USA, Sodora *et al* reported within subtype variation of 9.8% for clade A isolates (Sodora et al., 1994). In Western Europe, the average diversity of FIV clade A was 9.1% in the UK and 6.6% in the Benelux countries (Samman et al., 2011, Roukaerts et al., 2015). The average intra-host variation observed here (0.69%) was lower than had been reported in a previous study in the USA (3.7%, (Sodora et al., 1994)). This difference was unlikely related to the clinical status of the cats, since the CD4:CD8 ratios were similar in the two studies (median of 1.63 vs. 1.46 in this study). Moreover, no correlations were observed between the intra-host diversity and any of the parameters investigated in this study. However, the infecting strains differed; whereas the V3-V5 sequences of the isolates in the USA study were closely related to the FIV clade A Dixon strain, those in this study were divergent (Figure 4-10) (Sodora et al., 1994). Indeed, the similarly lower intra-host diversity observed in cats experimentally infected with FIV clade A GL8 (0.45%) also supported this speculation (Kraase et al., 2010).

In this study, we observed different CD134 usage of FIV variants, ranging from CRD2-dependent to CRD2-independent interactions. These different CRD2 requirements were detected at both population and within-host levels (Table 4-

18 and Figure 4-11). Similar findings were also reported in two cohorts of cats naturally infected with FIV isolates assigned to clade B or recombinant A/B isolates (Beczowski et al., 2014b). Together, these studies suggest that a broad spectrum of CD134 usage in FIV quasispecies is a common feature of natural FIV infection. However, the driving force behind this phenomenon remains to be elucidated. As shown in Chapter 3 and in some HIV studies, target cell availability could also exert selective pressure on the viral population (Klatt et al., 2008). Therefore, we speculated that the dominance of CRD2-dependent variants, detected more frequently in the early phase of infection, and the emergence of CRD2-independent variants in late infection were influenced by the dynamics of the CD4⁺CD134⁺ T lymphocyte population that gradually declined over the course of infection (Figure 4-7).

While sick cats, which were presumed to be in the later stage of infection since they were significantly older age than the healthy cats, harboured more CRD2-independent variants, the small sample size made it difficult to draw firm conclusions. However, the preliminary findings from two groups of five cats encouraged us to investigate the effect of target cell availability in natural infection. Since these FIV *env* genes were amplified from genomic DNA, they could represent either recently integrated provirus or an ancestral founder virus and so might not reflect the population of FIV variants circulating at the time of blood collection (Finzi et al., 1999, Lambotte et al., 2004). Moreover, since the percentages of CD4⁺CD134⁺ T lymphocytes in the five healthy and five sick cats studied were similar (28.19% (16.78% - 67.37%) vs. 29.05% (5.1% - 51.25%), Table 4-17), this might confound the speculated selective pressure of target cell availability and explain, at least in part, the similar proportion of early/intermediate/late viruses observed between the two groups of cats.

The presence of NAbs has been shown to be a major selective pressure leading to the emergence of late, CRD2-independent variants (Willett et al., 2008, Willett et al., 2010, Willett and Hosie, 2013). However, no association was observed between autologous neutralisation titres and the emergence of late variants in this study (Figure 4-12). The absence of correlation between CRD2-usage and NAbs has also been reported in naturally infected cats (Beczowski et al., 2014b). Therefore, although selective pressure can be exerted by NAbs and cell-mediated immune responses, further studies will be required to define the

link between FIV tropism switching and host immune responses (Beatty et al., 1996, Rambaut et al., 2004, Willett et al., 2010, Hosie et al., 2011, Willett et al., 2013).

The finding that *env* genes from the same cat could be positioned distantly on the phylogenetic tree (Figure 4-8 to Figure 4-10) was consistent with the data showing different CD134-usage (Table 4-18 and Figure 4-11) and suggested that FIV genotype could be a useful FIV prognostic tool; the late phenotype (CRD2-independence) was associated with clinical signs of immunodeficiency (Beczowski et al., 2014b, Beczowski et al., 2015a). It has been demonstrated clearly in HIV infection that mutations within the V3 region, which result in changes in the net charge of V3, play a critical role in HIV tropism switching from CCR5- to CXCR4-usage (Obermeier et al., 2012, Montagna et al., 2014). Indeed, several HIV tropism prediction algorithms have been developed, each with different validities and clinical relevance (Obermeier et al., 2012, Montagna et al., 2014, Gupta et al., 2015). Hence, we hypothesise that FIV receptor usage might also be governed by a change in charge at pH 7.0 of the FIV Env variable loops and, as our understanding about their relationship improves, a reliable FIV prognostic algorithm based on viral *env* sequences could be achieved. The development of such a tool would be one of many research opportunities arising from the findings of this study.

Chapter 5 Investigating the role of the target cell in the selection of FIV variants

5.1 Introduction

Natural FIV transmission usually occurs via biting and exposure to contagious blood (Yamamoto et al., 2007). This route, similar to the route of transmission among HIV intravenous drug users (IDU), results in a mixed population of viral variants, termed the “quasispecies”, being transmitted at the same time (Bar et al., 2010). However, it was observed in a large proportion of HIV cases that infection is usually established by a single variant (Keele et al., 2008). Host and viral factors, such as target cell availability and viral tropism, might play important roles in the selection that occurs before host immune responses are elicited. Studies described in previous chapters demonstrated that the number of $CD4^+CD134^+$ T lymphocytes also plays a role in tissue compartmentalisation (Chapter 3) and tropism switching (Chapter 4). In this chapter, an *in vitro* model was developed to test the hypothesis that the number of activated $CD4^+CD134^+$ T lymphocytes is a key determinant that preferentially selects for early variants of FIV.

5.2 Development of a red fluorescent protein (RFP) carrying lentiviral vector

Since the discovery of the first fluorescent protein “green fluorescent protein (GFP)” in 1992, several other fluorescent proteins (FPs) have been developed (Telford et al., 2012). However, their use is largely restricted to advanced platform confocal microscopy and/or flow cytometry with multiple excitation wavelengths. The flow cytometer in our institute, the Accuri C6, is a compact benchtop flow cytometer equipped with only four detectors and two standard lasers at 488 and 640 nm and so candidate FPs are limited. Yellow fluorescent protein (YFP) was available in our laboratory but was indistinguishable from GFP using this flow cytometer. An alternative was the red fluorescent protein (RFP) “DsRed” which could be detected in near-red channel (~580 nm), but its natural homotetrameric form greatly decreases its photostability, emission rate and brightness (Gross et al., 2000). Recently, a photostable monomeric RFP “TagRFP” was developed as a fluorescent tag for *in*

vivo cellular protein imaging (Shaner et al., 2008). Sharing the same emission wavelength as DsRed, TagRFP was a good candidate for a new FP-carrying pseudotype (Shaner et al., 2008). Therefore, a new lentiviral vector for the transduction of TagRFP was developed to facilitate this study.

5.2.1 Development of pCSRW vector

The *TagRFP* gene was double digested from the plasmid pLenti-C-EGFP-S-TagRFP (kindly provided by Dr. Sam Wilson, Medical Research Council-University of Glasgow Centre for Virus Research) using the restriction enzymes BamHI-HF[®] and NotI-HF[®] (New England Biolabs, UK) and then ligated into BamHI/NotI double digested pCSGW, a lentiviral vector capable of expressing EGFP under the spleen focus-forming virus (SFFV) promoter, using T4 DNA Ligase (Promega, UK). The ligated construct was then transformed into *Escherichia coli* MAX Efficiency[®] DH5 α [™] competent cells (Invitrogen, UK) and cultured for small scale DNA preparation (Section 2.1.11 - 2.1.12). To check the insert, plasmid DNA was digested with BglI (New England Biolabs, UK) and examined by gel electrophoresis (Figure 5-1A). Plasmid containing the correct insert was then scaled up for large scale DNA preparation (Section 2.1.14). This plasmid was named “pCSRW” (Figure 5-4A).

Plasmid pCSRW was used to prepare TagRFP-HIV(VSVG) pseudotypes by transient transfection together with pCMV-dR8.2 dvpr (Stewart et al., 2003) and pMD2.G (plasmid expressing the G protein of vesicular stomatitis virus (VSVG) into HEK 293T cells (Section 2.3.1). The plasmid pMD2.G was a gift from Didier Trono (Addgene plasmid # 12259). To test the TagRFP-pseudotype, CLL-fCD134 (Section 2.2.1.2) and MCC-fCD134 cells (Section 2.2.1.3) were used as targets. Cells were seeded at 2.5×10^5 cells per 500 μ l per well in 48 well plates, followed by the addition of 500 μ l of medium containing the TagRFP-pseudotype. The cells were spinoculated at 800 x g for 60 minutes at room temperature and the plates were incubated for 48 hours at 37°C, 5% CO₂. On day two, the plates were read on an Accuri C6 Flow cytometer (Beckton Dickinson bioscience bioscience). Empty pseudotypes bearing no viral envelopes (produced by co-transfection of empty VR1012 vector with pCMV-dR8.2 dvpr and pCSGW) were used as negative controls. The quantities of each pseudotype were determined according to the intensity of p24 CA protein staining following immunoblotting,

as the pseudotypes shared the same HIV Gag/Pol backbone (pCMV-dR8.2 dvpr) (Section 2.3.6) (Figure 5-6). The percentage of infected cells and mean fluorescence intensity (MFI) were analysed using CFlow Plus software version 1.0.227.4 (Beckton Dickinson bioscience, USA).

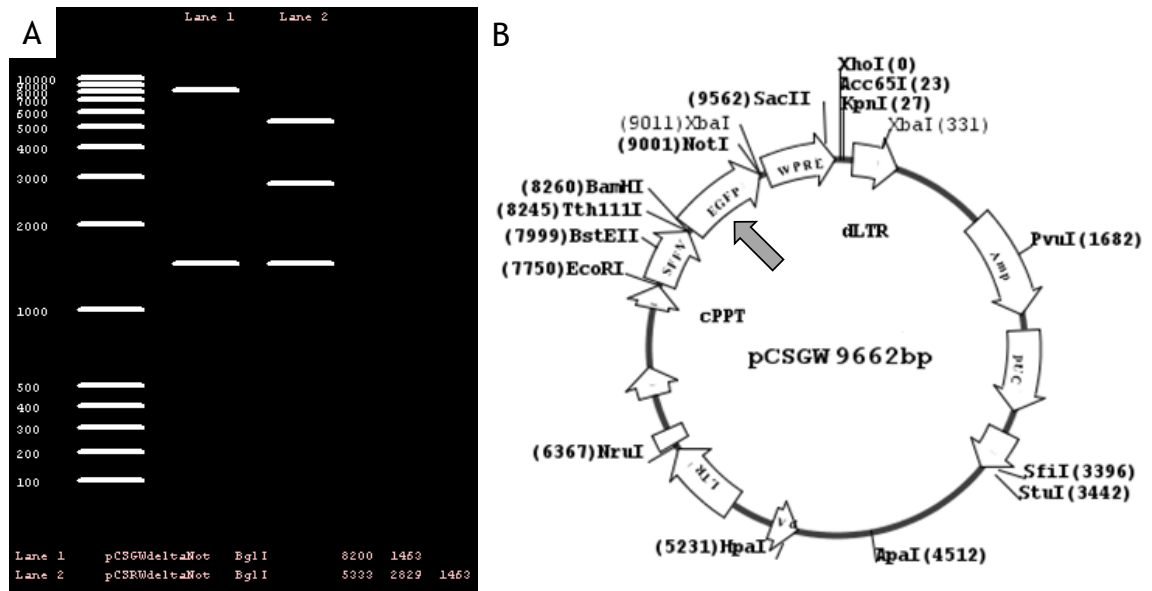


Figure 5-1 Illustration of pCSGW (lane 1) and pCSRW (lane 2), following digestion with BglI. The leftmost lane shows a virtual DNA ladder. pCSGW contains 2 BglI sites while pCSRW contains an additional site in the *TagRFP* gene, hence the appearance of two smaller bands at approximately 3,000 bp and 5,500 bp (A). The plasmid map of pCSGW (B), in which the *EGFP* gene (position 8260-9001, grey arrow) was replaced by *TagRFP* in pCSRW (Figure 5-4A)

5.2.2 Lower infectivity and mean fluorescence intensity of TagRFP-pseudotype

The GFP-HIV(VSVG) pseudotype infected both MCC-fCD134 and CLL-fCD134, although a higher percentage of CLL-fCD134 cells was infected compared to MCC-fCD134 cells (85.95% vs. 76.63% of GFP positive cells respectively) (Table 5-1). Similar results were obtained for the TagRFP-pseudotype; the percentage of TagRFP positive cells was approximately 30% higher in CLL-fCD134 compared to MCC-fCD134 cells (21.45% vs. 14.19% respectively) (Table 5-1). However, the MFI of GFP- and TagRFP-positive cells were approximately ten and three times higher respectively in MCC-fCD134 cells compared to CLL-fCD134 cells (Table 5-1). The higher intensity of both FPs in MCC-fCD134 was readily observed under the fluorescent microscope (Figure 5-2).

Table 5-1 Percentage and mean fluorescence intensity (MFI) of VSVG-GFP or VSVG-TagRFP infection of MCC-fCD134 and CLL-fCD134 cells

	GFP-HIV(VSVG) (pCSGW)		TagRFP-HIV(VSVG) (pCSRW)	
	percentage	MFI	percentage	MFI
MCC-fCD134	76.63%	3,150,000	14.19%	37,000
CLL-fCD134	85.95%	352,000	21.45%	11,600

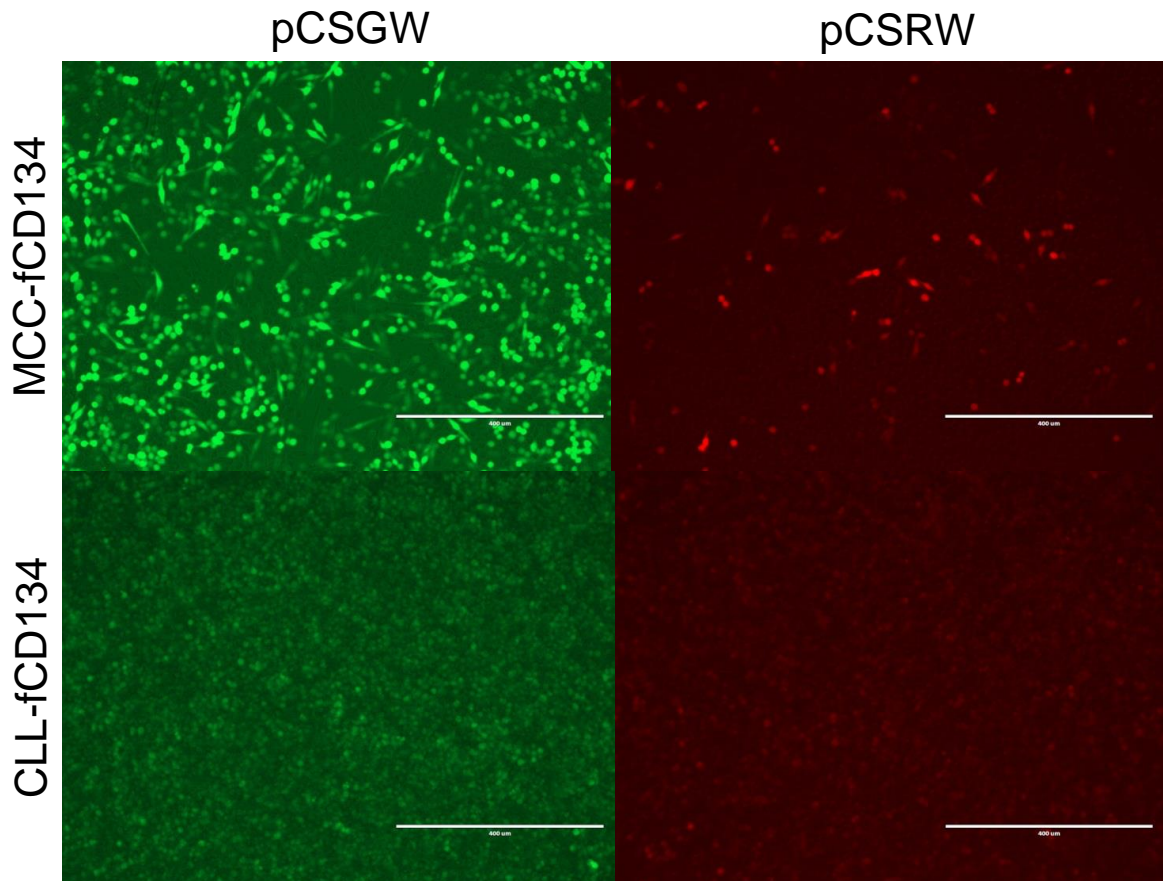


Figure 5-2 Representative images of MCC-fCD134 (top) and CLL-fCD134 (bottom) infected with HIV(VSVG)-GFP (pCSGW, left) or HIV(VSVG)-TagRFP (pCSRW, right) pseudotypes. 10x objective magnification on Evos *fl* microscope (AMG micro, USA)

5.2.3 Higher FP expression under the CMV promoter

Both GFP and TagRFP were expressed at lower intensities in CLL-fCD134 cells compared to MCC-fCD134 cells. This difference did not appear to be related to CD134 expression levels, since CD134 expression (detected by the anti-feline CD134 antibody A647) on both cell lines was approximately 98%. Moreover, pseudotypes bearing VSVG infected a broad range of mammalian cell types,

including CLL-fCD134 and MCC-fCD134 cells (Marsh and Helenius, 1989). Therefore, it appeared the SFFV promoter functioned better in MCC-fCD134 cells compared to CLL-fCD134 cells. To investigate this possibility, a new batch of GFP-HIV(VSVG) pseudotypes was prepared using pCCGW (kindly provided by Dr. Sam Wilson). Plasmid pCCGW has a similar genomic organisation to pCSGW, except GFP expression is under the control of the CMV promoter (Figure 5-4). The infectivity and MFI of the two new GFP-pseudotypes were then compared.

Under the CMV promoter, both the infectivity and GFP intensity were greater than had been observed under the SFFV promoter, although the increase in GFP intensity was more dramatic in CCL-fCD134 cells than MCC-fCD134 cells (Table 5-2 and Figure 5-3). In both cell lines, the percentage of infected cells increased by approximately 10%, with the infectivity in CLL-fCD134 reaching almost 100% (Table 5-2). The GFP intensity in CLL-fCD134 was 10 fold greater under the CMV promoter compared to the SFFV promoter (MFI of 4,300,000 vs. 352,000) (Table 5-2). These results indicated that the CMV promoter was more compatible with the target cells and therefore a new lentiviral vector expressing TagRFP under the control of the CMV promoter was developed, named “pCCRW”, using a similar protocol as described above for pCSRW (Section 5.2.1). Using these new vectors, GFP and TagRFP-HIV(FIV) pseudotypes were prepared in order to investigate the role of the target cell in the selection of FIV variants within a quasispecies.

Table 5-2 Percentage and mean fluorescence intensity (MFI) of VSVG pseudotypes carrying pCSGW or pCCGW in MCC-fCD134 and CLL-fCD134 cells

	VSVG-GFP (pCSGW)		VSVG-GFP (pCCGW)	
	percentage	MFI	percentage	MFI
MCC-fCD134	76.63%	3,150,000	89.32%	5,800,000
CLL-fCD134	85.95%	352,000	99.92%	4,300,000

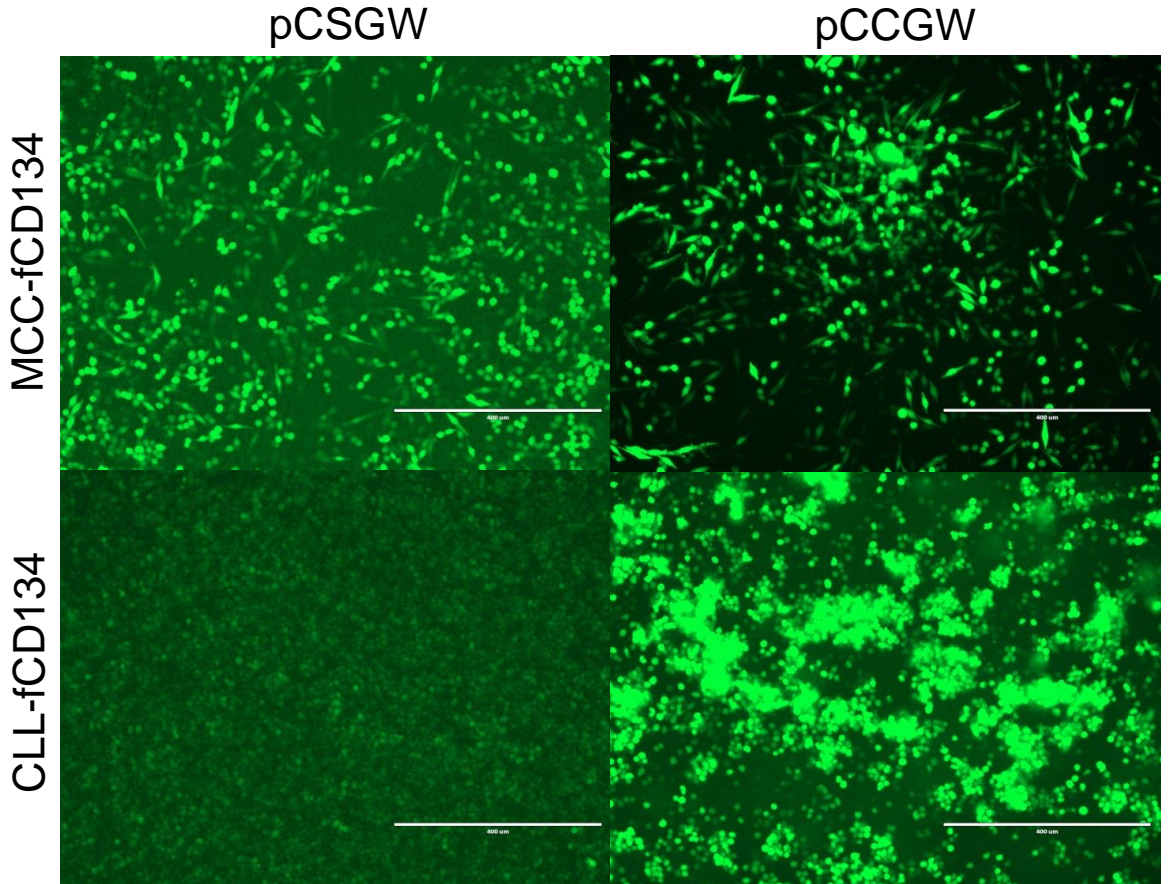


Figure 5-3 Representative images of MCC-fCD134 (top) and CLL-fCD134 (bottom) infected with VSVG pseudotypes carrying either pCSGW (left) or pCCGW (right). 10x objective magnification on Evos *fl* microscope (AMG micro, USA)

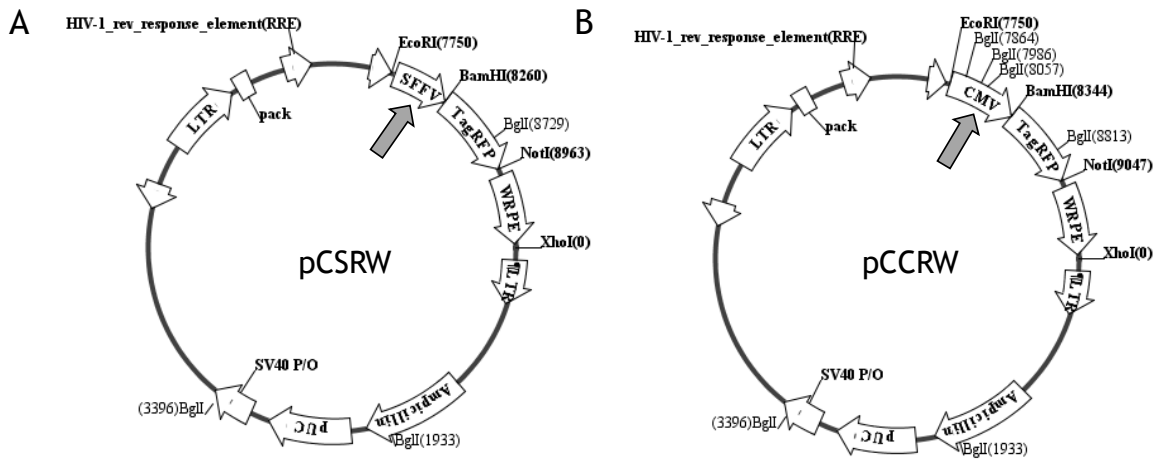


Figure 5-4 Plasmid maps of pCSRW (A) and pCCRW (B), SFFV and CMV promoters are indicated by grey arrows for pCSRW and PCCRW, respectively.

5.3 Investigating the competition between infecting V5 FIV variants in the transmitted quasispecies for cell entry

5.3.1 Development of competitive entry assay

The lower infectivity, as measured by the percentage of fluorescing cells and MFI, of the TagRFP-pseudotype was the result of a limitation of the Accuri C6 Flow cytometer. The optimal excitation wavelength for near-red FPs including TagRFP is ~550 nm (Shaner et al., 2008) and so under the blue laser at 440 nm, the excitation and detection of TagRFP was suboptimal, approximately 14-18%. Therefore, the proposal to directly compete two different HIV(FIV) pseudotypes, the first labelled with pCCGW (GFP) and the second with pCCRW (TagRFP), was not feasible. Therefore, to investigate the role of the target cell in FIV V5 variant selection after transmission, a competitive entry assay was developed. In this assay, the degree of competition was indirectly assessed by measuring the decrease in infectivity of a GFP-pseudotype (the principal) in the presence of a TagRFP-pseudotype (the competitor) (Figure 5-5). Although the suboptimal TagRFP excitation hindered its detection by flow cytometry, infection by TagRFP-pseudotypes could still be confirmed under the fluorescent microscope.

In this assay, a pairwise competition for target cell entry was assessed between GFP pseudotypes bearing Envs of each of the V5 variants; GL8, B14, B19, B28 and B30 (principal) and TagRFP-pseudotypes bearing GL8 Env (competitor) or empty vector control (mock) (Figure 5-5A). CLL cells, expressing either feline CD134 (FFF) or the human/feline chimaeric CD134 molecule containing the CRD2 region of human CD134 (FFHH), were used as target cells (Figure 5-5A and Section 2.2.1.2). This assay was designed to mimic the natural setting where the number of target cells varies, both between tissue compartments (see Chapter 3) and at different phases of infection (see Chapter 4). If the dominance of the CRD2-dependent GL8 Env, observed in CD4⁺CD134⁺ T lymphocyte-enriched compartments and during the earlier phase of infection, could be attributed to the higher entry fitness of the GL8 Env compared to the CRD2-independent V5 variants, then co-infection with GL8-TagRFP would significantly decrease GFP expression of the GFP-pseudotypes bearing the Envs of the V5 variants in CLL-FFF cells but not in cell lines expressing the chimaeric

CD134 (FFHH) molecule containing the CRD2 region of human CD134 (Figure 5-5B).

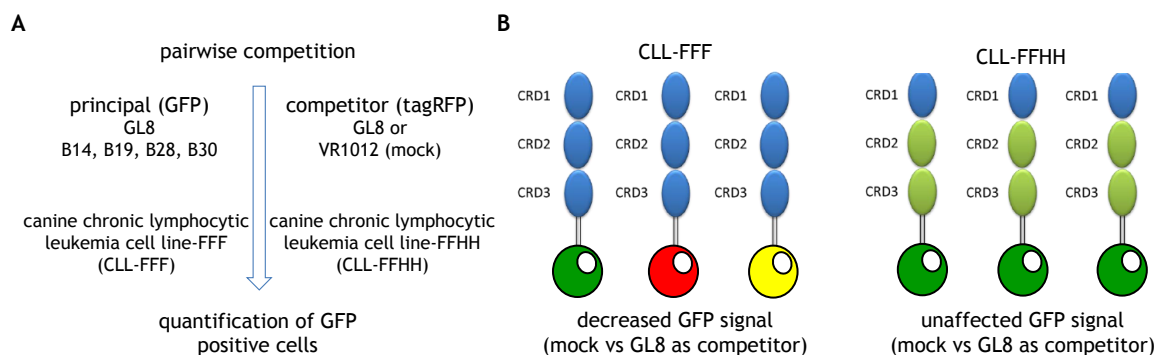


Figure 5-5 Outline of competitive entry assay (**A**); Each GFP-pseudotype (principal) bearing the Env of each of the V5 variants; GL8, B14, B19, B28 and B30 was competed with a TagRFP-pseudotype bearing GL8 Env (competitor) or no Env (mock empty VR1012 vector control). Pairwise competition was performed in two target cells; CLL-FFF (expressing feline CD134 to detect CRD2-dependent entry) and CLL-FFHH (expressing chimaeric human/feline CD134 to detect CRD2-independent entry). GFP positive cells were measured after 48 hours. Schematic representation of predicted outcomes (**B**); in CLL-FFF cells, it was predicted that GL8-TagRFP and V5-GFP pseudotypes would compete with each other for receptor binding, resulting in green (V5-GFP), red (GL8-TagRFP) and yellow (co-infected) cells (**left**). In contrast, in CLL-FFHH cells, the CRD2-dependent GL8-TagRFP pseudotypes would not compete with V5-GFP and, as a result, green cells (V5-GFP) would predominate (**right**).

Pseudotypes were prepared as described in Section 2.3.1. The quantity of each pseudotype was determined by HIV CA p24 immunoblotting (Section 2.3.6) (Figure 5-6) and concentrations were adjusted by diluting with R10 before the pairs of pseudotypes were mixed together, i.e. equal quantities of GL8-GFP were mixed with GL8-TagRFP or mock-TagRFP and similarly for the other V5 variants. One millilitre of each pseudotype pair was then added to each well of a 48 well plate (Corning, USA) containing 250 μ l of either CLL-FFF or CLL-FFHH cells at 1×10^5 cells/ml. Surface expression of CD134 and CXCR4 on each cell line was checked by flow cytometry to ensure a minimum of 99% of cells expressed the receptors (Section 2.3.7). Each pairwise competition was performed in triplicate. Each plate included six negative control wells, three inoculated with the empty VR1012-GFP and the remainder inoculated with VR1012-TagRFP pseudotypes. The plates were spinoculated at 800 x g for 60 minutes with no brake and then incubated for 48 hours at 37°C, 5% CO₂. On day two, the plates were agitated to disperse the cells, which were then examined using an Accuri C6 Flow cytometer (BD bioscience). GFP and tagRFP signals from the negative

control wells were used to set cutoff values for the positive population and for fluorescence spill-over compensation. Experiments were performed three times. Percentage infection rates were calculated using the equation below:

$$\text{percentage infection} = \frac{\text{GFP positive percentage with competitor}}{\text{GFP positive percentage with mock}} \times 100$$

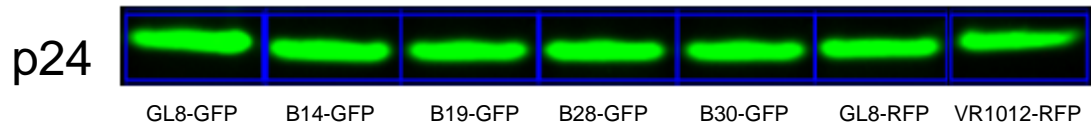


Figure 5-6 Representative HIV CA p24 immunoblot. Pseudotypes were blotted onto a nitrocellulose membrane and detected following incubation with 1:1000 mouse anti-HIV p24 antibody (183-H12-5C) followed by 1:1000 goat anti-mouse IgG DyLight™ 800. The fluorescence intensity was determined using the ODYSSEY™ system (LI-COR® Bioscience, Cambridge, UK) (Section 2.3.6).

5.3.2 GL8 outcompeted V5 variants in CLL-FFF but not CLL-FFHH cells

As shown in Figure 5-7A, in the presence of GL8-TagRFP, the percentage of cells infected with each V5 variant-GFP pseudotype decreased significantly. Moreover, the percentage of GFP positive cells decreased by 50% when GL8-GFP was competed with GL8-TagRFP (Figure 5-7A), confirming the reliability of the competitive entry assay. Examination of CLL-FFF cells by fluorescent microscopy revealed more red cells (GL8 infected cells) and yellow cells (co-infected cells) than green cells (B28 infected cells) (Figure 5-8 top panel). In contrast, co-infection with GL8-TagRFP did not compete with V5 variants-GFP in target cells expressing chimaeric CD134 (CLL-FFHH) (Figures 5-7B and 5-8 bottom panel).

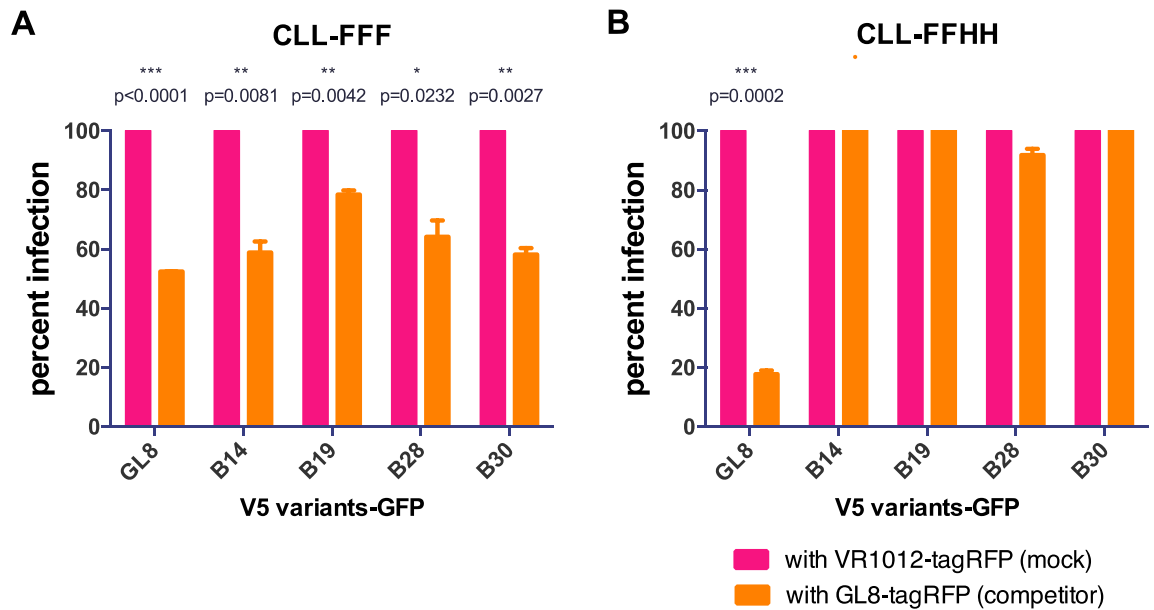


Figure 5-7 Representative result of competitive entry assay in CLL-FFF (A) and CLL-FFHH (B) cells. Each bar represents the average percentage of cells infected with the standard deviation. Statistical significance determined using paired T test.

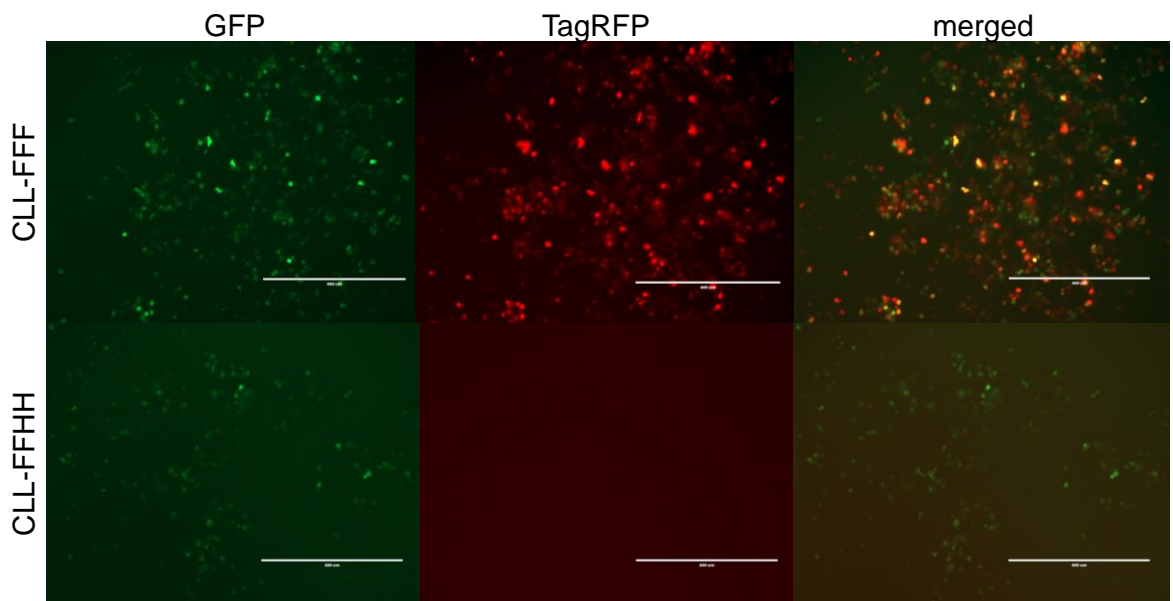


Figure 5-8 Representative images of CLL-FFF (top) and CLL-FFHH (bottom) cells, co-infected with GL8-TagRFP and B28-GFP pseudotypes and viewed under GFP (left), TagRFP (middle) and merged (right) channels. 10x objective magnification on Evos *fl* microscope (AMG micro, USA)

5.4 Investigating the role of CD8⁺ T lymphocytes as target cells

Inversion of the CD4:CD8 lymphocyte ratio is a key observation in both HIV and FIV infections (Yamamoto et al., 2007, Sykes, 2013). The inverted ratio results from both a decrease in CD4⁺ T lymphocytes as well as an increase in CD8⁺ T lymphocytes (Willett et al., 1993, Shimojima et al., 1998, Yamamoto et al., 2007, Hartmann, 2012, Sykes, 2013, Litster et al., 2014). Since the primary receptor for FIV infection, CD134, is expressed mainly on CD4⁺ T lymphocytes; inversion of the CD4:CD8 ratio might be another selective pressure on the FIV variants in the quasispecies during the course of infection (Willett et al., 2007, Willett and Hosie, 2013). As the number of CD4⁺CD134⁺ target cells declines, the increased number of CD8⁺ T lymphocytes (which may or may not express CD134) might select for FIV variants that are less dependent on CD134 for infection, such as the CRD2-independent V5 variants that emerged during the late stage of FIV infection (Kraase et al., 2010, Willett and Hosie, 2013). This hypothesis was supported by the observation that FIV targets cells other than CD4⁺CD134⁺ T lymphocytes, including CD8⁺ T lymphocytes, later in FIV infection (English et al., 1993, Dean et al., 1996, Willett and Hosie, 2008, Willett and Hosie, 2013).

The aim of this study was to investigate whether the appearance of CRD2-independent V5 variants in the late stage of FIV infection was associated with the ability to infect CD8⁺CD134^{+/-} T lymphocytes. To address this question, the susceptibility of CD8⁺CD134^{+/-} T lymphocytes to infection by GFP-pseudotypes bearing V5-variant Envs was examined.

5.4.1 *In vitro* expansion of T lymphocytes isolated from peripheral blood

Peripheral blood mononuclear cells (PBMC) were isolated from blood collected in EDTA from FIV seronegative cats by standard density-gradient centrifugation using Ficoll-Paque PLUS (Section 2.2.2). To optimise the *in vitro* expansion of T lymphocytes, three freshly isolated cultures of PBMC were each subcultured into four wells of a 12 well plate in R10 medium. Cells in each well were then treated with 10 µg/ml phytohaemagglutinin (PHA) (Sigma-Aldrich, Germany), 5 µg/ml of concanavalin A (ConA) (Sigma-Aldrich, Germany), 200 ng/ml mouse anti-feline CD3 monoclonal antibodies (in house) and 100 IU/ml recombinant feline IL-2 (in house), or R10 alone to serve as a negative control.

Cells were incubated at 37°C, 5% CO₂ for 7 days before the expanded PBMCs were stained with anti-feline CD8-phycoerythrin and anti-feline CD134-alexafluor 647 (AbD Serotec, UK) to determine their activation status, carboxyfluorescein succinimidyl ester (CFSE) (Invitrogen, USA) to assess proliferation capacity and 7-aminoactinomycin D (7-AAD) (Invitrogen, USA) to measure viability (Section 2.3.7) (Appendix 5-1 and 5-2). All analyses were performed using an Accuri C6 Flow cytometer with CFlow Plus software version 1.0.227.4 (Beckton Dickinson bioscience, USA).

All three stimulation protocols induced expansion of the PBMC cultures, to different degrees and with distinct characteristics. PBMC expansion following treatment with ConA and anti-feline CD3 was rapid; several small cellular clumps were observed at day four, increasing in size by day seven (Figure 5-9, bottom; middle-right and right). However, PHA stimulation resulted in the highest viability (95.54%), followed by anti-feline CD3 (85.55%) and Con A (74.59%) (Table 5-3 and Figure 5-10). The high viability of cells in the cultures stimulated with PHA might reflect its lower mitogenicity, since less cellular expansion was observed (3.67 fold) compared to ConA (7.75 fold) and anti-feline CD3 (4.44 fold), as shown in Table 5-3. Consequently, PHA appeared to be a good candidate for PBMC expansion, providing cells of high viability. However, PHA stimulation induced slower cellular proliferation and resulted in fewer cells, with final cell counts similar to those of the negative control. (Figure 5-9, middle-left). As insufficient cells were obtained following PHA-stimulation, these wells were excluded from further analyses.

Table 5-3 Effect of each mitogen on PBMC viability and proliferation at day seven*

mitogen**	% viability	proliferation index***
no stimulant	95.89% (95.50% - 97.50%)	1
phytohaemagglutinin	94.77% (94.50% - 97.34%)	3.67 (1.08 - 4.44)
concanavalin A	72.05% (65.90% - 85.84%)	7.75 (4.53 - 25.77)
anti-feline CD3	81.51% (80.64% - 94.51%)	4.44 (3.25 - 23.45)

*Data shown as median values (with range) for three cats. **All mitogens supplemented with 100 IU/ml recombinant feline IL-2. ***Proliferation index calculated as the cell number in mitogen-treated culture/no mitogen control.

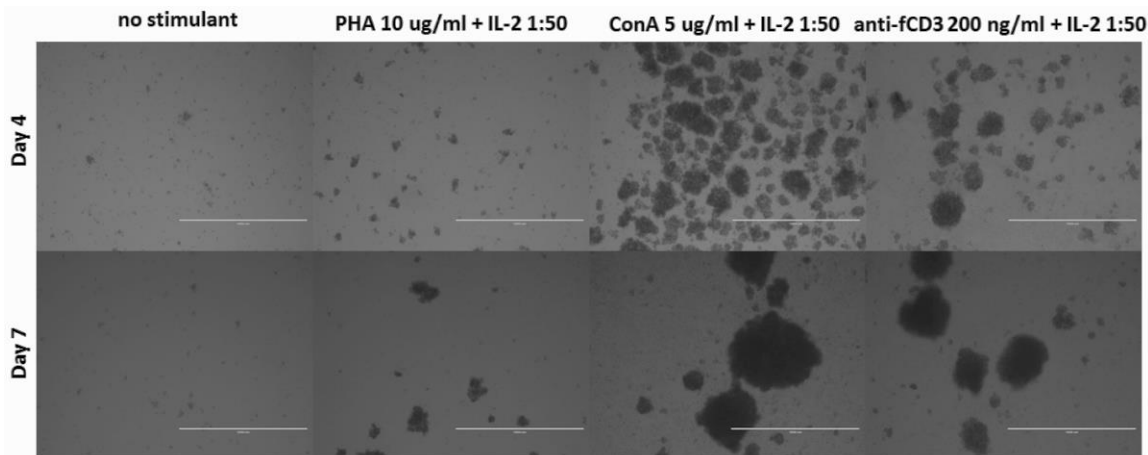


Figure 5-9 Representative images from inverted microscopy of PBMC at day 4 (top) and day 7 (bottom), following stimulation with; R10 alone (left), PHA with IL-2 (middle-left), ConA with IL-2 (middle-right) and anti-fCD3 antibody with IL-2 (right). 4x objective magnification on Evos *fl* microscope (AMG micro, USA).

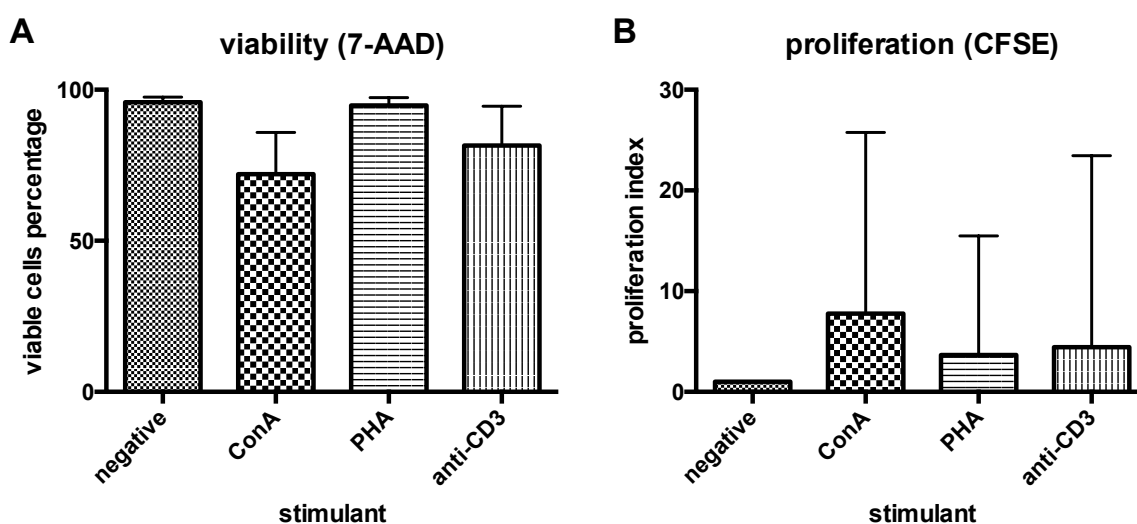


Figure 5-10 PBMC viability (A) and proliferation index (B) after stimulation with concanavalin A (ConA), phytohaemagglutinin (PHA) and anti-CD3 antibody (anti-CD3). All mitogens were supplemented with 100 IU/ml recombinant feline IL-2. Culture medium alone was used as a negative control. Proliferation index represents the ratio of cell number of culture with mitogen/no mitogen control. Each bar represents the median and range for three cats. Mann-Whitney test.

Both ConA and anti-feline CD3 antibody stimulation led to expansion of both CD4⁺ and CD8⁺ T lymphocyte subpopulations (Table 5-4 and Figure 5-11). However, there appeared to be a bias towards CD8⁺ T cell expansion following ConA stimulation, as reflected by a more marked inversion of the CD4:CD8 ratio in wells treated with ConA compared to anti-feline CD3 antibody (CD4:CD8 ratio

of 0.19 vs. 0.76) (Table 5-4 and Figure 5-11). A similar degree of T lymphocyte activation, reflected by CD134 expression, was observed between the two cultures. Although anti-CD3 stimulation yielded higher viability and a more balanced CD4:CD8 population, the absolute lymphocyte numbers were insufficient for further investigations. This limitation reflected the small leftover sample volumes received from the diagnostic lab, usually less than 1 ml of blood. Therefore, ConA stimulation was adopted for the expansion of PBMC for subsequent experiments, as it induced more rapid expansion and higher lymphocyte numbers compared to anti-CD3 treatment.

Table 5-4 Effect of concanavalin A and anti-feline CD3 antibody stimulation on lymphocyte subpopulations*

	Con A**	anti-feline CD3 antibody**
CD4 ⁺ percentage***	19.8 (16.30 - 40.40)	44.90 (19.60 - 47.70)
CD8 ⁺ percentage***	80.10 (59.60 - 83.70)	59.10 (52.30 - 80.30)
CD4:CD8 ratio	0.19 (0.17 - 0.25)	0.76 (0.24 - 0.91)
CD134 ⁺ percentage***	25.90 (11.90 - 39.90)	26.70 (8.10 - 34.30)

*Data shown as median values (with range) for three cats. **All mitogens were supplemented with 100 IU/ml recombinant feline IL-2. ***Percentage of CD4⁺, CD8⁺ and CD134⁺ subpopulations in total lymphocytes.

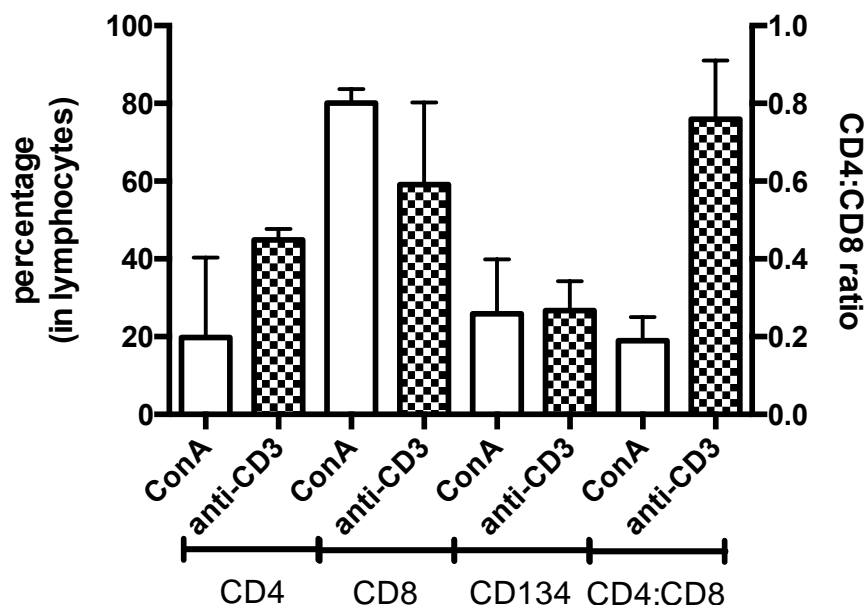


Figure 5-11 Composition of lymphocyte subpopulations following ConA and anti-CD3 stimulation of PBMC. Left axis indicates percentage of CD4⁺, CD8⁺ and CD134⁺ subpopulations in total lymphocytes. Right axis indicates CD4:CD8 ratio. Each bar represents median and range of three cats. Mann-Whitney test.

5.4.2 FIV infects CD4⁺CD134⁺ more efficiently than CD8⁺CD134^{+/-} T lymphocytes

Next, PBMC from a further three cats (331776, 331777 and 331787) were treated with Con A and IL-2 in order to investigate the susceptibility of lymphocyte subpopulations to FIV infection. Expanded PBMC were first stained for CD4, CD8, and CD134 to determine the proportion of each lymphocyte subpopulation (Table 5-5). In cats 331776 and 331787, both CD4⁺ and CD8⁺ T lymphocytes were expanded, but the former showed a higher proportion of CD4⁺ T lymphocytes whereas the latter was biased towards CD8⁺ T lymphocytes (Table 5-5). In cat 331777, the expanded cultures contained mainly CD8⁺ T lymphocytes (Table 5-5). It was noted that CD134 was expressed on both CD4⁺ and CD8⁺ T lymphocytes, but whereas CD134 was expressed in almost 100% of the CD4⁺ T lymphocytes, expression in CD8⁺ T lymphocytes ranged from 14.7% - 87.60% (Table 5-6). Nonetheless, cell surface expression of CD134, as determined by mean fluorescence intensity, was higher on CD4⁺ than CD8⁺ T lymphocytes (median values 53,809 vs. 16,951, Table 5-6)

Table 5-5 Lymphocyte subpopulations of PBMC cultures*

	%CD4	%CD4CD134	%CD8	%CD8CD134
331776	49.4	48.9	21	20.6
331777	0.7	0.7	92.9	14.2
331787	18.1	17.9	55.7	34.9

*values shown as percentage of total lymphocyte population

Table 5-6 Proportions of CD134⁺ subpopulations and mean fluorescence intensity (MFI) of CD134 expression in CD4⁺ and CD8⁺ T lymphocytes

	CD4⁺ T lymphocytes		CD8⁺ T lymphocytes	
	%CD134	MFI	%CD134	MFI
331776	99	53,809	87.6	16,951
331777	99	50,879	14.97	4,738
331787	97	54,834	60.9	19,362

In the culture from cat 331776 that contained a high proportion of CD4⁺ T lymphocytes (49.4% CD4 vs. 21% CD8, Table 5-5), the B28-GFP pseudotype preferentially infected CD8⁻ T lymphocytes (6.8% in CD8⁻ vs. 0.8% in CD8⁺) (Table 5-7 and Figure 5-12 top panel). Moreover, even in the culture derived from cat 331787 that contained more CD8⁺ than CD4⁺ T lymphocytes (18.1% CD4 vs. 55.7% CD8, Table 5-5), B28-GFP also infected more CD8⁻ T lymphocytes, although the difference was less marked (3.1% vs. 1.0%) (Table 5-7 and Figure 5-12 bottom panel). In contrast, in the culture from cat 331777 that contained few CD4⁺ T lymphocytes (0.7% CD4 vs. 92.9% CD8, Table 5-5), the B28-GFP pseudotype infected more CD8⁺CD134⁻ than CD8⁻ T lymphocytes (2.4% vs. 0.4%) (Table 5-7 and 5-12 middle panel). Although the B28-GFP pseudotype could infect the culture containing mostly CD8⁺ T lymphocytes (cat 311777, total GFP⁺ cells = 2.8%), its infectivity was greater in cultures containing higher proportions of CD8⁻ T lymphocytes (7.6% in cat 311776 and 4.2% in cat 311787).

Table 5-7 Percentage of GFP-positive cells in each lymphocyte subpopulation*

	331776	331777	331787
CD4 : CD8	49.4 : 21	0.7 : 92.9	18.1 : 55.7
CD8 ⁺	0.8	2.4	1.0
CD8 ⁻	6.8	0.4	3.1
CD134 ⁺	6.0	0.0	3.0
CD134 ⁻	1.6	2.8	1.2

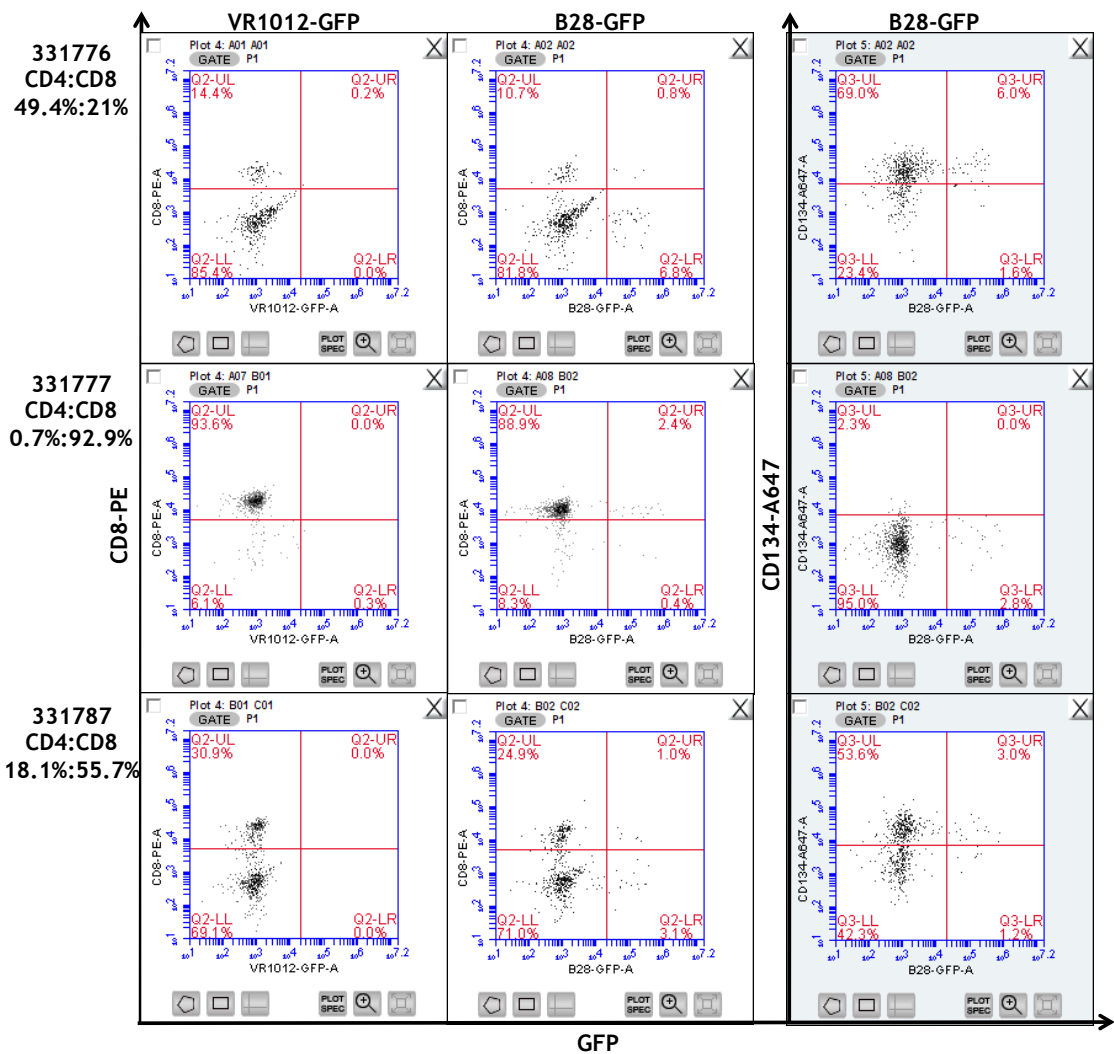


Figure 5-12 Representative contour plots of expanded lymphocyte cultures from three cats (331776, 331777 and 331787) that were infected with VR1012-GFP control (left column) and B28-GFP pseudotypes (middle and right column). **Top panel:** cat no.331776 (CD4:CD8, 49.4%:21%), **Middle panel:** cat no. 331777 (CD4:CD8, 0.7%:92.9%) and **Bottom panel:** cat no. 331787 (CD4:CD8, 18.1%:55.7%). The X-axes of each plot represent the log values for the fluorescence intensity of green fluorescent protein area (GFP-A) for VR1012-GFP and B28-GFP. The Y-axes in the left and middle columns represent log values for fluorescence intensity of phycoerythrin area (PE-A) for CD8-PE. The Y-axis in the right column show the log fluorescence intensity of Alexa fluor 647 area (A647-A) for CD134-A647.

The apparent selection of CD4⁺ T lymphocytes for FIV infection was likely associated with CD134 expression, as the majority of CD134⁺ T lymphocytes did not express CD8 (Figure 5-13). In addition, a trend was evident, demonstrating a positive correlation between the proportion of cells expressing CD134 and the percentage of cells infected (Figure 5-14).

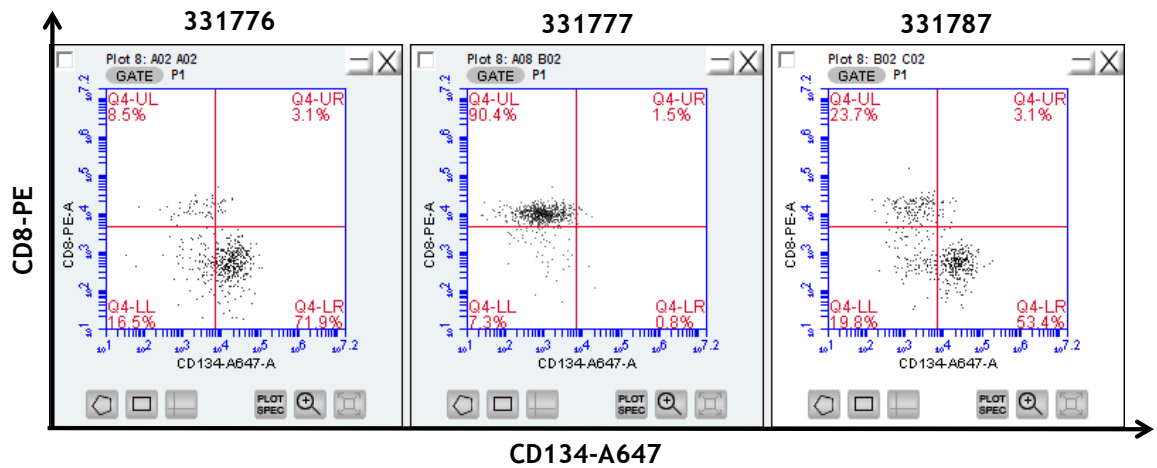


Figure 5-13 Representative contour plots of expanded lymphocyte cultures from three cats: 331776, 331777 and 331787. The X-axis shows the log fluorescence intensity of the Alexa fluor 647 area (A647-A)(for CD134-A647). The Y-axis shows the log fluorescence intensity of the phycoerythrin area (PE-A) for CD8-PE.

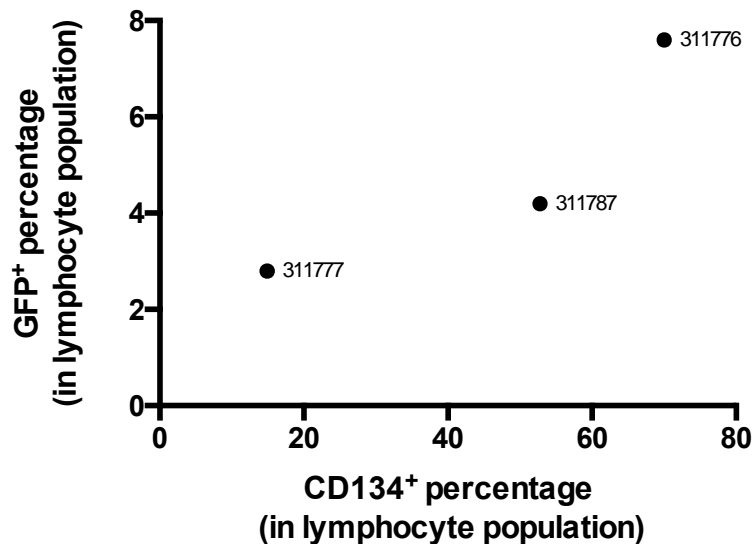


Figure 5-14 Relationship between the percentage of CD134⁺ T lymphocytes in culture and infectivity of GFP-FIV pseudotypes. The X-axis shows the percentage of CD134⁺ T lymphocytes and the Y-axis shows the percentage of infected cells (GFP⁺) in the total lymphocyte population.

5.5 Discussion and Conclusion

The studies described in this chapter indicate that target availability exerts selective pressure on FIV quasispecies diversity. Findings from the competitive entry assay confirmed that pseudotypes bearing the Env of the CRD2-dependent strain GL8 infect CD134⁺ target cells more efficiently than pseudotypes bearing Envs of CRD2-independent V5 variants of GL8.

The influences of the *env* gene on the efficiency of host cell entry have been shown previously for HIV (Ball et al., 2003, Rangel et al., 2003). However, some critical anti-retroviral drug (ARV) escape mutations in the *pol* gene also affected viral fitness (Rangel et al., 2003). Nevertheless, in the absence of these mutations in *pol* gene, the fitness of whole viruses and recombinant viruses expressing their Env on the HXB2 backbone were similar and in a statistically significant correlation, confirming the direct influence of Env in viral fitness (Rangel et al., 2003). In this chapter, by competing two pseudotypes bearing different Envs on the same backbone, the competitive entry assay permitted an investigation of the effect of Env polymorphisms on target cell entry.

Although cell culture systems cannot mimic fully the target cell population, or the selective pressures exerted *in vivo*, the competitive entry assay developed here provided the first evidence of the impact of target cell availability in FIV selection. In this assay, target cells were provided in excess, i.e. there were sufficient target cells for infection by both the principal and competitor pseudotypes. Therefore, the effects of Env polymorphisms were assessed solely in terms of entry fitness in this scenario. This was evident when pseudotypes bearing the same Env (GL8) were competed against each other. Since these pseudotypes expressed the same Env, their entry fitness was, theoretically, equivalent and indeed target cells were infected with GFP- and TagRFP-tagged pseudotypes at a ratio of 1:1 (Figure 5-7A, first column). The competitive entry assay also demonstrated the greater entry fitness of pseudotypes bearing the Env of the CRD2-dependent GL8 over its CRD2-independent variants for CD134⁺ target cells (CLL-FFF). Moreover, different entry fitness of pseudotypes bearing each V5 variant Env was also observed in which B19 was the fittest, followed by B28, B30 and B14 (Figure 5-7A).

The observed higher entry fitness of GL8 for CD134⁺ target cell (CLL-FFF) infection is likely related to a high affinity interaction occurring between the GL8 Env and CD134 (Willett et al., 2007, Willett et al., 2010, Willett and Hosie, 2013). It is possible that requirements for additional determinants on CRD2 might provide GL8 Env with a higher binding affinity for CD134 compared to the CRD2-independent V5 variant Envs (Willett et al., 2007). The higher entry fitness of the CRD2-dependent GL8 Env for CD134⁺ target cells is consistent with previous findings *in vivo*, where the GL8 molecular clone replicated more efficiently in experimentally infected cats throughout a 21 week study period, compared to four other molecular clones with Envs of the CRD2-independent V5 variants B14, B19, B28 and B30 in the same inoculum (Willett et al., 2013).

Moreover, the higher entry fitness of GL8 for CD134⁺ target cells is consistent with the dominance of CRD-2 dependent viruses such as GL8 and NCSU1 early after transmission (de Parseval et al., 2004b, de Parseval et al., 2005, Willett et al., 2006b). As CD4⁺CD134⁺ T lymphocytes are more abundant during the earlier phase of infection (Table 4-4 and Figure 4-4F), the higher entry fitness for CD134⁺ target cells would allow CRD2-dependent viruses to establish infection more efficiently than CRD2-independent viruses. However, the number of CD4⁺CD134⁺ T lymphocytes declines over the course of infection (Figure 4-7) and so the decreased proportion of CD134⁺ target cells likely exerts selective pressure on the virus population. This would result in those FIV variants that require only a minimal interaction with CD134, such as the CRD2-independent V5 variants described in this chapter, or field strains such as B2542, to predominate during the later stages of infection (Kraase et al., 2010, Willett and Hosie, 2013, Beczkowski et al., 2014b).

One factor that influences viral entry fitness is entry stoichiometry. For HIV and FIV, stoichiometry is determined by the number of host cell receptors and viral trimers required for membrane fusion (Kuhmann et al., 2000, Brandenburg et al., 2015a). It was shown that different HIV isolates require between one to seven trimers per virion for productive membrane fusion (Brandenburg et al., 2015a, Brandenburg et al., 2015b, Zarr and Siliciano, 2015). It was notable that, while most of the primary isolates tested here required only two to three trimers for cell entry, laboratory-adapted isolates such as NL4-3 and SF162 required many more (Brandenburg et al., 2015b).

Target cell entry by both HIV and FIV depends on the energy released following the conformational changes that occur in Env during sequential interactions with the primary cellular receptor and co-receptor (Elder et al., 2008, Klasse, 2012, Harrison, 2015). In order for viral-cellular membrane fusion to occur, a certain energy threshold must be overcome (Klasse, 2012, Harrison, 2015). Since Env has an open conformation in laboratory-adapted strains of HIV, the energetic state is low and therefore such strains require more trimers for infection (White et al., 2010, Munro et al., 2014, Brandenberg et al., 2015a, Munro and Mothes, 2015). It was reported that the Env of the CRD2-independent PPR strain adopted a similar open conformation (Hu et al., 2012). In addition, it is likely that the energy released following an interaction with determinants solely on CRD1 of the CD134 molecule is less than that released following an interaction involving both CRD1 and CRD2. Consequently, CRD2-independent variants would require more interacting molecules, both CD134 and Env trimers, compared to CRD2-dependent counterparts for successful membrane fusion. However, further studies focusing on FIV entry stoichiometry would be required to confirm this hypothesis.

As well as the differences in Env structure, which are linked to conformational change-associated energy release, polymorphisms that alter Env processing and the number of trimers incorporated into the virion would also affect entry stoichiometry. For HIV, it was reported that mutations in gp120 significantly decreased Env processing and resulted in increased numbers of uncleaved Env molecules (Blay et al., 2007). Although uncleaved Env could be incorporated into new virions, only cleaved Env was fusion competent (McCune et al., 1988, Herrera et al., 2005, Moore et al., 2006). Therefore viruses with a higher proportion of non-functional, uncleaved Env will have higher entry stoichiometry as more trimers will be required to increase the probability of there being sufficient functional molecules in the Env-receptor interaction. It was shown previously for HIV that V5 loop mutations altered Env processing and deletion of V5 led to virus assembly failure, which in turn hindered cell entry (Blay et al., 2007, Yuan et al., 2013). Therefore, it is possible that the lower entry fitness of the FIV V5 variants observed here, and their decreased infectivity *in vivo*, were related to the impact of their polymorphisms on Env processing (Willett et al., 2013). In addition to SU, polymorphisms within the HIV and FIV TM cytoplasmic tails have been shown to affect the intracellular

distribution of Env, which in turn affects Env incorporation into virions and viral replication capacity (Lambele et al., 2007, Affranchino and Gonzalez, 2014). Since the TM was identical in all of the V5 variants investigated here, however, it is more likely that V5 polymorphisms accounted for their lower replication fitness.

In human beings, CD134 is predominantly expressed on activated CD4⁺ T lymphocytes (de Parseval et al., 2004a, Shimojima et al., 2004, Croft, 2010). However, human CD134 is not restricted to CD4⁺ T lymphocytes but is also expressed on CD8⁺ T lymphocytes (Watts, 2005, Croft, 2010). Upon encountering a specific peptide-MHC complex, both CD4⁺ and CD8⁺ T lymphocytes upregulate CD134, although the kinetics differ, with prolonged CD134 expression on CD4⁺ T lymphocytes compared to transient expression on CD8⁺ T lymphocytes (Croft, 2010). CD134 signalling promotes the survival of both CD4⁺ and CD8⁺ T lymphocytes (Gramaglia et al., 1998, Bansal-Pakala et al., 2004). In contrast, feline CD134 expression was shown to be restricted to activated CD4⁺ T lymphocytes in the peripheral blood (Willett et al., 2007) and whether CD134 was expressed on feline CD8⁺ T lymphocytes remained debatable. Indeed, in one study, CD8⁺ T lymphocytes did not express CD134, even after mitogenic stimulation (de Parseval et al., 2004a). However, it is possible that this finding was related to the sensitivity and specificity of the detection method that used a recombinant dimeric fusion protein, comprising PPR Env fused to the Fc portion of immunoglobulin G (IgG) to detect CD134 (de Parseval et al., 2004a). Subsequently, Willett et al. used the anti-feline CD134 antibody 7D6 to examine CD134 expression *ex-vivo* and in mitogen-stimulated PBMC (Willett et al., 2007). In freshly isolated PBMC, CD134 was detected mainly on CD4⁺ T lymphocytes and was not detected on CD8⁺ T lymphocytes. However, when PBMC were stimulated with mitogen, either using ConA or PHA, CD8⁺ T lymphocytes were shown to express CD134 (Willett et al., 2007). Expression of CD134 on ConA-stimulated CD8⁺ T lymphocytes was also observed in this study, although the level of expression varied markedly. While CD134 expression had been only 1 to 2% in the previous study (Willett et al., 2007), expression levels between 14 to 34.9% were observed in this study. Therefore, it appears likely that feline CD8⁺ T lymphocytes might also express CD134 in response to potent stimulation.

In this chapter, we investigated the susceptibility of CD8⁺ T lymphocytes to FIV infection using ConA-stimulated PBMC and observed that CD8⁺ T lymphocytes were susceptible to FIV infection, although less susceptible than CD4⁺ T lymphocytes (Brown et al., 1991, English et al., 1993, Willett and Hosie, 2008). Intriguingly, in blood samples displaying a physiological range of CD4:CD8 ratio, a preference for infection of CD4⁺ T lymphocytes was observed (Figure 5-12). This is likely related to the level of CD134 expression, as the surface expression of CD134 was more than three times greater in CD4⁺ compared to CD8⁺ T lymphocytes (MFI of 53,809 vs. 16,951). This positive trend between CD134 expression and FIV infectivity had been observed previously in enriched splenic macrophages. LPS activation of macrophages led to a two-fold increase in CD134 expression, which in turn led to a two-fold increase in susceptibility to FIV infection (Willett et al., 2007). However, the preference for infection of CD4⁺ T lymphocytes might also be related to the higher proportion of CD134⁺ cells in the CD4⁺ T lymphocyte subpopulation. These findings not only confirm that FIV infects both CD4⁺ and CD8⁺ T lymphocytes, but also suggest a role for CD134 expression in the selection of FIV variants such as the CRD2-independent variants that emerged in the later stage of FIV infection (Brown et al., 1991).

Due to sample limitations, insufficient target cells were available to conduct a competitive entry assay to determine whether CD4⁺ and CD8⁺ T lymphocytes specifically select for CRD2-dependent or CRD2-independent strains of FIV. It was proposed that in cultures containing high numbers of CD134⁺ target cells (derived from cats 331776 and 331787), GL8 would infect CD4⁺ T lymphocytes more efficiently than the CRD2-independent V5 variants as a result of the stronger interaction between GL8 Env and CD134 that was observed in the competitive entry assay. In contrast, it was predicted that in the culture with fewer CD134⁺ target cells (derived from cat 331777), the PBMC comprising mainly CD8⁺ T lymphocytes, CRD2-independent strains such as B28 would predominate, as shown in Figure 5-12 in which all B28-infected cells tested negative for CD134.

These data, together with the results of the competitive entry assay support a role for CD134⁺ target cell availability in FIV pathogenesis. In the earlier phase of infection, CD134⁺ target cells, i.e. activated CD4⁺CD134⁺ T lymphocytes are abundant (as shown in Chapter 4). The higher entry fitness of

CRD2-dependent variants for CD134⁺ target cells would permit more rapid and efficient replication of such variants (Willett et al., 2013, Willett and Hosie, 2013), leading to a marked decline in CD4⁺ T lymphocyte numbers in the acute phase of infection (Yamamoto et al., 2007, Hartmann, 2012, Sykes, 2013). As disease progresses, the number of CD4⁺CD134⁺ T lymphocytes progressively declines and this eventually leads to the emergence of CRD2-independent variants, which are less dependent on CD134 for infection (Kraase et al., 2010, Beczkowski et al., 2014b). Therefore, the appearance of CRD2-independent variants is most likely the result of selective pressure from the declining numbers of CD4⁺CD134⁺ target cells, which occurs concurrently with the expansion of FIV tropism towards CD8⁺ T lymphocytes and B-lymphocytes in the later stage of infection (Brown et al., 1991, Beebe et al., 1994, Dean et al., 1996, Willett et al., 2007, Willett and Hosie, 2008, Kraase et al., 2010, Willett and Hosie, 2013, Beczkowski et al., 2014b).

One of the main difficulties encountered during this study was the limitation in fluorescent reporter proteins. Using GFP and TagRFP, competition between FIV variants could only be investigated in pairs. It would be necessary to develop an assay allowing simultaneous infection of target cells with multiple pseudotypes, each with different Envs and fluorescent proteins, to more closely mimic the diverse polymorphism of FIV quasispecies. With such tools, it would be possible to unravel the role of target cell-specific selection in FIV infection more extensively. Recently, new red fluorescent proteins (RFP) with compatible excitation wavelength have been developed, which could be used to improve the flow cytometric assay described here. Another candidate fluorescent protein is the short-red fluorescent protein large Stokes shift mOrange (LSSmOrange) (Shcherbakova et al., 2012, Pletnev et al., 2014) that, with its excitation and emission at 437 and 572 nm, respectively, could potentially solve the suboptimal excitation issue of TagRFP (Section 5.1). However, as LSSmOrange was developed for live cell imaging, its utility in flow cytometry-based techniques remains to be confirmed. Two other promising candidates are E2-Crimson and TagRFP657; both have a maximal excitation wavelength of 611 nm, which is compatible with a standard red laser (640 nm) and can also be detected by a far-red detector (Strack et al., 2009, Morozova et al., 2010, Piatkevich and Verkhusha, 2011). Using these new FPs should permit the optimal detection of a

second pseudotype and might lead to the testing of three pseudotypes simultaneously in the future.

Another direction for further investigations is an examination of the impact of CD134 surface expression on FIV selection. It appears likely that the susceptibility of cells to FIV infection depends on the level of CD134 expression. This speculation is based on the observation that the CRD2-independent variant B28 used in this study selectively infected CD4⁺ T lymphocytes with higher surface expression of CD134. Selective infection of target cells expressing higher levels of CD134 would promote FIV infection. As CD134 is only expressed on activated T lymphocytes, targeting infection to cells with the most active cellular machinery would ensure successful infection following viral transmission (Gramaglia et al., 1998, Walker et al., 1999, Croft, 2010). In addition, the increased longevity of CD134⁺ T lymphocytes permits sustained FIV production and expansion (Gramaglia et al., 1998, Watts, 2005, Croft, 2010). Furthermore, signalling via CD134 increases T lymphocyte migration, which in turn promotes FIV dissemination (Evans et al., 2001, Prell et al., 2003).

As a first step to addressing this issue, a novel CLL cell line with inducible CD134 expression was developed. This CLL cell line was transduced with pLKO-fCD134-IP plasmid, a lentiviral vector which expresses feline CD134 under the CMV promoter (Appendix 5-3). The plasmid was produced by replacing *TagRFP* (the original plasmid was pLKO-TagRFP-IP, kindly provided by Dr. Sam Wilson) with fCD134 from pDON-AI-fCD134 following double digestion with BmtI and EcoRI (Willett et al., 2006b). This plasmid constitutively expresses the tetracycline repressor (TetR) protein, which in turn binds to a tet operator sequence (*tetO*) located downstream of the CMV promoter and inhibits CD134 expression. Following the addition of tetracycline or doxycycline, TetR is released from *tetO*, turning on fCD134 expression (Wiederschain et al., 2009). However, the repression by TetR was incomplete, which resulted in basal CD134 expression of approximately 80% CLL-FFF cells (Appendix 5-4). This leakage prevented further use of this cell line.

Recently, there was a novel development in tetracycline inducible gene system technology. The pCMV-Tet3G expressed a gene of interest under the control of a TRE3G promoter (Clontech, Takara Bio Europe SAS, France). Unlike

pLKO-fCD134-IP, which relies on TetR control, this plasmid constitutively expresses Tet-on® 3G protein which is activated following the addition of doxycycline, then binds *tetO* and drives the TRE3G promoter (Kit manual). The manufacturer claims that activation of Tet-on, rather than repression, results in significantly lower basal expression levels and higher expression levels. Since efficient control of CD134 expression on the target cell surface will be necessary for the successful investigation of its role in FIV selection, further development of CLL-inducible CD134 cells could be pursued using this new pCMV-Tet3G plasmid. A conundrum remains: if the susceptibility of cells depends on CD134 expression, how do CRD2-independent variants infect CD8⁺ T lymphocytes more efficiently than CRD2-dependent variants, if CRD2-dependent variants display more efficient CD134-dependent entry? Surely the logical conclusion would be that CRD2-independent variants should only replicate in the absence of CD134 expressing cells?

Chapter 6 Final Conclusion

6.1 Introduction

The current study was designed to investigate the role of CD134⁺ target cell availability in the pathogenesis of FIV infection. By examining CD134⁺ target cells in tissues as well as the peripheral blood of experimental and naturally infected cats, this study demonstrated that the number of target cells is one of the players, commonly disregarded, in the multifactorial host-virus interaction. Results from Chapter 3 have shown that the number of permissive target cells in the tissues could exert selective pressure on the FIV variant population, promoting the expansion of the fittest variant and leading to the phenomenon of “tissue compartmentalisation”. Moreover, the level of CD4⁺CD134⁺ T lymphocytes at different stages of infection could also play a role in FIV tropism switching and the emergence of variants less dependent on CD134 for infection.

6.2 The role of CD134⁺ target cell availability in tissue compartmentalisation

In Chapter 3, the effects of sequence variation in the V5 region of Env were examined and were shown to affect the utilisation of CD134 for infection, thereby leading to FIV tissue compartmentalisation. Moreover, a correlation was observed between the number of CD134⁺ target cells and the pattern of tissue-specific selection, at least in the bone marrow and thymus. Although the elucidation of the direct mechanisms leading to the compartmentalisation of FIV variants was limited by the nature of the available tissue samples and the approaches adopted, we proposed that the numbers and types of target cells in tissues could exert a selective pressure on FIV variants migrating through the tissues together with anatomical barriers. A proposed model for the role of resident CD134⁺ target cell availability in FIV tissue compartmentalisation is depicted in Figure 6-1.

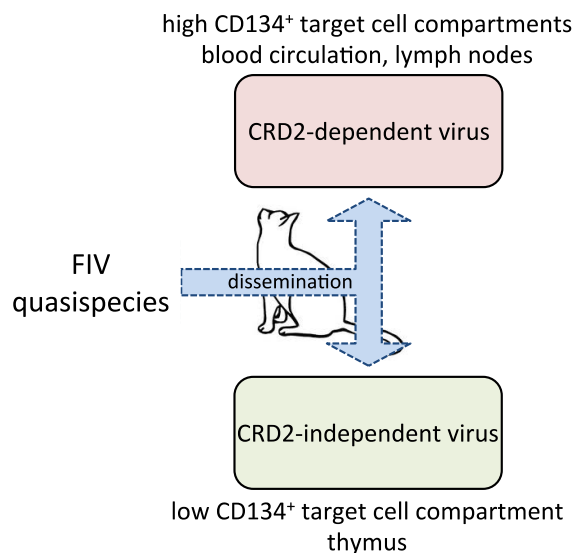


Figure 6-1 Proposed model for the role of resident CD134⁺ target cell availability in FIV tissue compartmentalisation

Following transmission to a new host, before the appearance of FIV-specific immune responses, FIV quasispecies disseminate throughout the body. Compartmentalisation of individual FIV variants within the quasispecies depends on the type and number of target cells inside the tissues. Tissue compartments with high levels of CD4⁺CD134⁺ T lymphocytes, such as draining lymph nodes, would support the more rapid and efficient replication of CRD2-dependent variants, reflecting the higher entry fitness of CRD2-dependent variants for CD134⁺ target cells. In contrast, tissues with fewer CD4⁺CD134⁺ T lymphocytes, such as the thymus, might select for CRD2-independent variants that are less dependent on CD134 for infection.

6.3 The dominance of CRD2-dependent virus in the early phase

It was suggested that differences in pathogenicity between R5 and X4 variants of HIV might explain the early dominance of R5 viruses after transmission (Rodrigo, 1997). Since X4 viruses induce syncytium formation while R5 viruses do not, R5-infected cells would survive longer than cells infected with X4 variants, such that R5 virus replication would be more sustainable. However, this hypothesis might not extend to FIV infection as both CRD2-dependent and independent strains can induce syncytium formation (Shimojima et al., 2004, Dietrich et al., 2011b), because both require CXCR4 for infection and syncytium formation by FIV is dependent on CXCR4-binding (Willett et al., 1997, Willett et

al., 1998). Moreover, it was reported that the cell culture-adapted strain PET_{F14}, which can infect target cells independently of CD134, was less virulent than the CRD2-dependent strain GL8 (Hosie et al., 2002). Thus, the early dominance of CRD2-dependent viruses is more likely attributable to other characteristics that provide some fitness advantage, rather than differences in pathogenicity.

It has been shown in HIV-infection that specific immune responses play an important role in HIV tropism switching (McKnight and Clapham, 1995, McKnight et al., 1995). By analogy to HIV, differences in immune-evasion properties between CRD2-dependent and -independent FIV variants could contribute to their dominance *in vivo*. Data from previous studies suggest that CRD2-independent variants might be more susceptible to specific antibody neutralisation as the Env of CRD2-independent variants adopts a more “open” conformation, exposing neutralisation epitopes (Hu et al., 2012), as well as lacking some potential N-linked glycosylation sites (Willett et al., 2008). The finding that mutations in key amino acid residues on the V3 and V5 loops of the Env of the FIV strain PET_{F14} *in vivo*, which resulted in the loss of CD134-independent infectivity, restored the virulence of PET_{F14} to that of the CRD2-dependent GL8 strain, provides further evidence that CRD2-independent virus strains are more susceptible to neutralisation (Hosie et al., 2002). Therefore, it is most likely that the early dominance of CRD2-dependent variants is associated with the Env of such variants being highly “shielded” from NAb.

6.4 Emergence of CRD2-independent virus variants

CRD2-independent viruses were reported in several experimental studies, following the inoculation of cats with a molecularly cloned strain of FIV (Hosie et al., 2002, Kraase et al., 2010). These studies strongly argued that CRD2-independent viruses emerged as a result of *de novo* evolution of CRD2-dependent variants. The late appearance of CRD2-independent variants is consistent with this argument. In HIV infection, the switching from R5 to X4 tropism was reported to be a sequential process, requiring a step-by-step fixation of multiple mutations in the population before the switch was complete (Pastore et al., 2004, Salemi et al., 2007). Moreover, the FIV *env* gene has been reported to be genetically stable, with relatively low divergence over time (Ikeda et al., 2004, Motokawa et al., 2005, Beczkowski, 2013). Thus, the

emergence of CRD2-independent variants in the later stage of infection might merely be related to the slow evolutionary rate of FIV, which requires a longer time to accumulate sufficient mutations for the switch to CRD2-independence. However, the question is why? If CRD2-independence decreases FIV entry fitness and renders the virus more susceptible to neutralisation, what might be the evolutionary advantage for virus that is less dependent on CD134 for infection?

6.5 The role of target cell availability in the emergence of CRD2-independent virus variants

In this thesis, it was discovered that the number of CD4⁺CD134⁺ T lymphocytes was dynamic at different stages of FIV infection. The very high levels of CD4⁺CD134⁺ T lymphocytes observed in the early phase gradually declined over the course of infection (Chapter 4). Also, CRD2-independent variants of FIV had lower entry fitness for CD134⁺ target cells than their CRD2-dependent counterparts but were able to infect CD8⁺CD134^{+/-} T lymphocytes (Chapter 5). Thus, by becoming less dependent on CD134 for infection, CRD2-independent variants are capable of infecting a broader spectrum of target cells, sustaining the virus population in the later stage of infection, when activated CD4⁺CD134⁺ T lymphocytes are limiting. Considering these findings, we propose that the emergence of CRD2-independent variants of FIV is influenced by CD4⁺CD134⁺ T lymphocyte availability. Figure 6-2 illustrates the model proposed here for the clinical course of FIV infection.

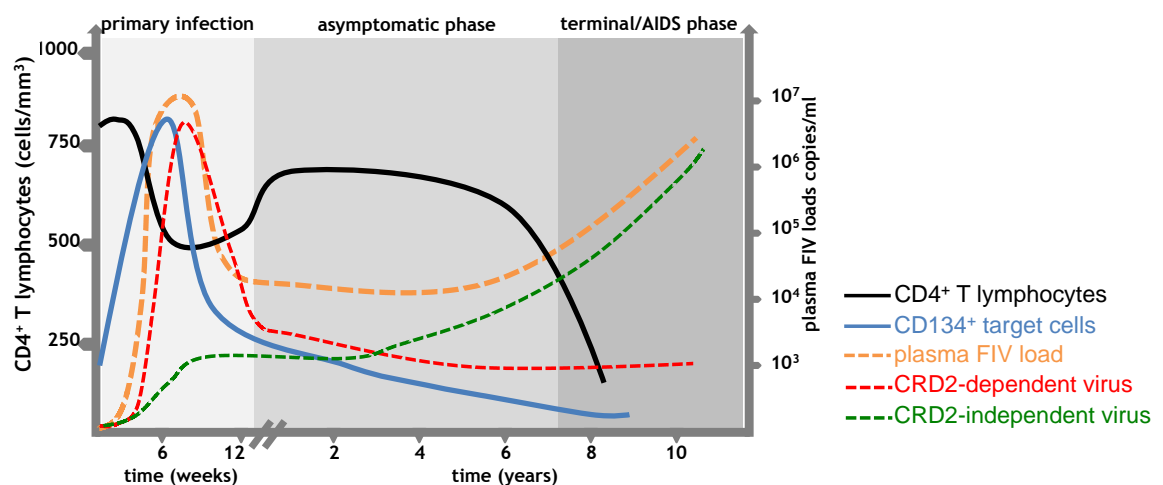


Figure 6-2 Proposed model for the role of CD134⁺ target cells in the emergence of CRD2-independent variants of FIV

In the proposed model, the switch that has been observed between CRD2-dependent FIV isolates with high CD134 affinity (such as GL8 and CPG41), which dominate in early infection and CRD2-independent isolates requiring a less stringent interaction (such as PPR), which arise during the later stages of infection, is related to the size of the CD134⁺ target cell population. During the primary infection phase, generalized immune activation results in increased numbers of CD134-expressing CD4⁺ T lymphocytes (blue solid line). These high numbers of activated CD134⁺ target cells favour the expansion of “early”, CRD2-dependent variants (dotted red line) with a high affinity for CD134. As disease progresses, the numbers of CD4⁺CD134⁺ T lymphocytes decrease irreversibly, as a result of exhaustion and dysregulation of the immune system. This depletion of the CD134⁺ target cell population leads to the expansion of “late”, CRD2-independent variants (dotted green line), which outgrow the CRD2-dependent variants.

6.6 CRD2-independent virus variants hiding place?

The proposed model, illustrated in Figure 6-2 above, is based on the assumption that a mixed population of CRD2-dependent and -independent viruses is transmitted in the quasispecies. The natural route of FIV transmission via biting and exposure to infected blood is consistent with this assumption (Hosie et al., 2009, Sykes, 2013). However, if both CRD2-dependent and -independent variants were indeed transmitted together, where do CRD2-independent viruses reside during the early phase of infection?

According to the data presented in Chapter 3, we speculate that CRD2-independent variants reside in tissue compartments such as thymus, in a latent stage. This speculation has its basis in a model proposed for HIV suggesting that HIV latency is generated during thymopoiesis (Brooks et al., 2001). The transcription machinery of immature thymocytes, which are highly active during the early stages of thymopoiesis, becomes quiescent after maturation. In the thymus, high CXCR4 expression and the lack of CD134 expression on thymocytes would provide CRD2-independent variants with a selective advantage over CRD2-dependent variants (Kitchen and Zack, 1997, Zaitseva et al., 1998, Willett et al., 2007). Therefore, if CD134⁻CXCR4⁺ immature thymocytes were infected with CRD2-independent variants during their development, they would become

latently infected naïve T lymphocytes awaiting activation after migrating out of the thymus into the periphery. This hypothesis is supported by HIV studies that suggested a role for the thymus in the emergence of X4 viruses. In HIV infected patients, there is a unidirectional flow of X4 viruses from the thymus to the lymph nodes that is consistent with the migratory route of CD4⁺ recent thymic emigrants (Salemi et al., 2007). In addition, in a group of maraviroc (CCR5 antagonist)-treated patients, X4 viruses emerged from a pretreatment reservoir (Westby et al., 2006). However, the tissue in which these X4 viruses resided was not identified in the study.

6.7 Concluding remarks

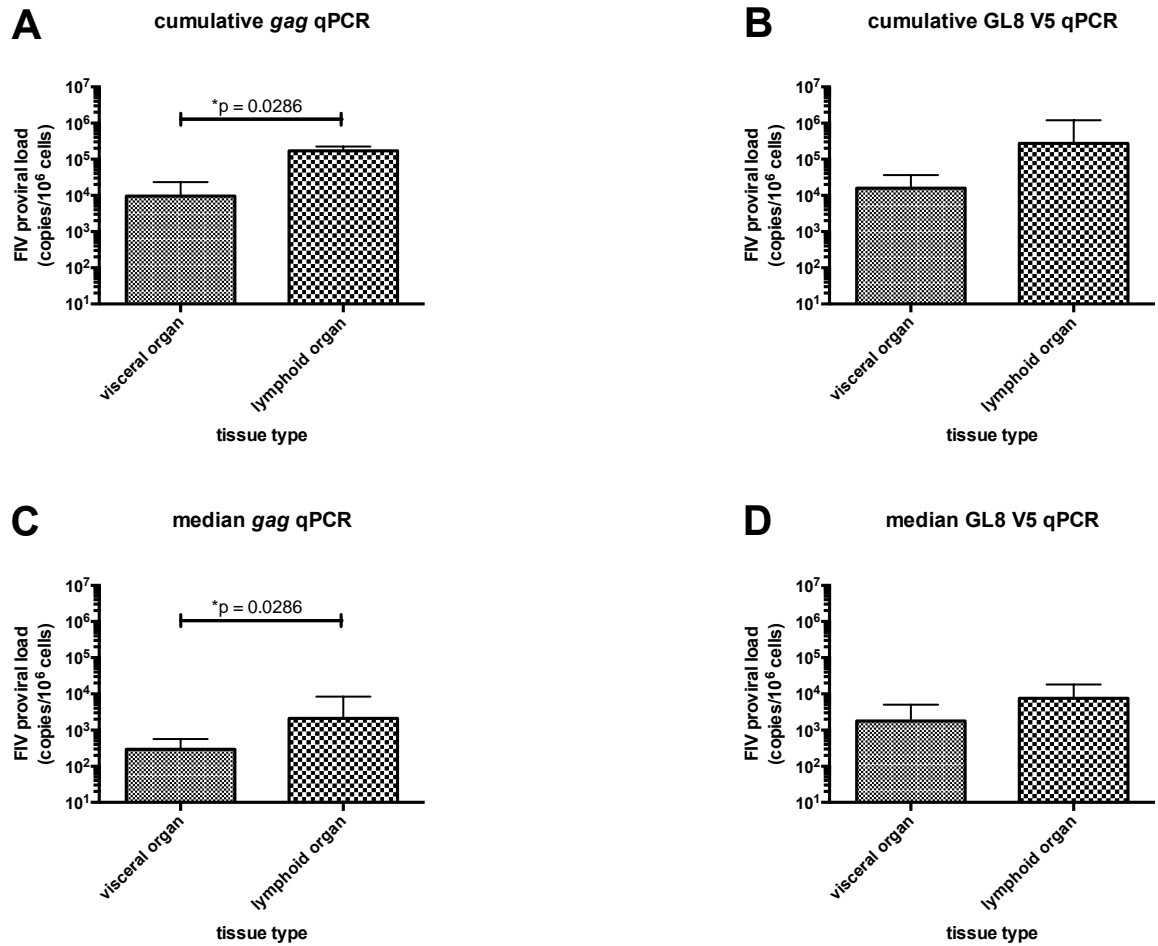
In summary, this current study demonstrates the importance of target cell availability in the pathogenesis of FIV infection. Target cell types and numbers in tissues, as well as their dynamics were observed to play important roles in the selection and expansion of FIV quasispecies in both experimentally and naturally infected cats. Nevertheless, it is likely that the model proposed here is not restricted to FIV infection but most likely applies to any viral infection in which a heterogeneous population is transmitted simultaneously, such as HIV or HCV. Improved understanding of the pathogenesis of infection will inform the future development of vaccine strategies that will be effective in preventing transmission of virulent circulating viral variants.

Appendices

Appendix 3-1 Characteristics of V5 variants in terms of CD134 usage, sensitivity to neutralising antibodies and FIV-CD134 antagonists*

	GL8	B19	B30	B14	B28
CRD2-dependent ^a	yes	no	no	no	no
Nabs ^b	+	-	-	-	-
α -CD134 ^c	-	+/-	+/-	+	+
sFc-CD134 ^d	+	+	+	-	-
sFc-CD134L ^e	-	-	-	+	+

*adapted from (Willett et al., 2010), B14, B19, B28 and B30 were FIV variants with different V5 loop sequences (V5 variants), which emerged at 322 weeks post infection with FIV clade A strain GL8 (UK8, accession no: X69496.1) in cat A613 (Kraase et al., 2010). Env of these V5 variants were observed with different characteristics including CD134-usage^a, sensitivity to neutralizing antibodies^b and different FIV-CD134 antagonists^{c-e}. ^aCD134 CRD2-dependency as determined by FFF/FFHH ratio (section 2.3.2); yes = CRD2-dependent, no = CRD2-independent (Willett et al., 2010). Sensitivity to neutralising antibodies and FIV-CD134 antagonists; + = sensitive, +/- = intermediate and - = resistant, ^bsensitivity to neutralizing antibodies (NABs), pseudotypes was incubated autologous plasma of cat A613 collected post-mortem (Willett et al., 2010). ^csensitivity to anti-feline CD134 antibody, clone 7D6 (α -CD134) (Willett et al., 2007), target cells were incubated with antibodies 30 minutes before infection, ^dsensitivity to soluble-Fc tagged-CD134 (sFc-CD134) (Willett et al., 2009), pseudotypes were cultured with sFc-CD134 30 minutes before infection and ^esensitivity to soluble-Fc tagged-CD134 ligand (sFc-CD134L) (Willett et al., 2009), target cells were incubated with sFc-CD134L30 minutes before infection. Different sensitivity to FIV-CD134 antagonists possibly reflects CD134-binding affinity. It is very likely that interactions between CD134 and Env of B14 and B28 variants (dark blue highlighted) are weaker than that of B19, B30 (blue highlighted) and GL8 as they were sensitive to α -CD134 and sFc-CD134L antagonisms. Sensitivity of B19 and B30 to the antagonists are very similar to GL8, although they are intermediately sensitive to α -CD134 antagonism.



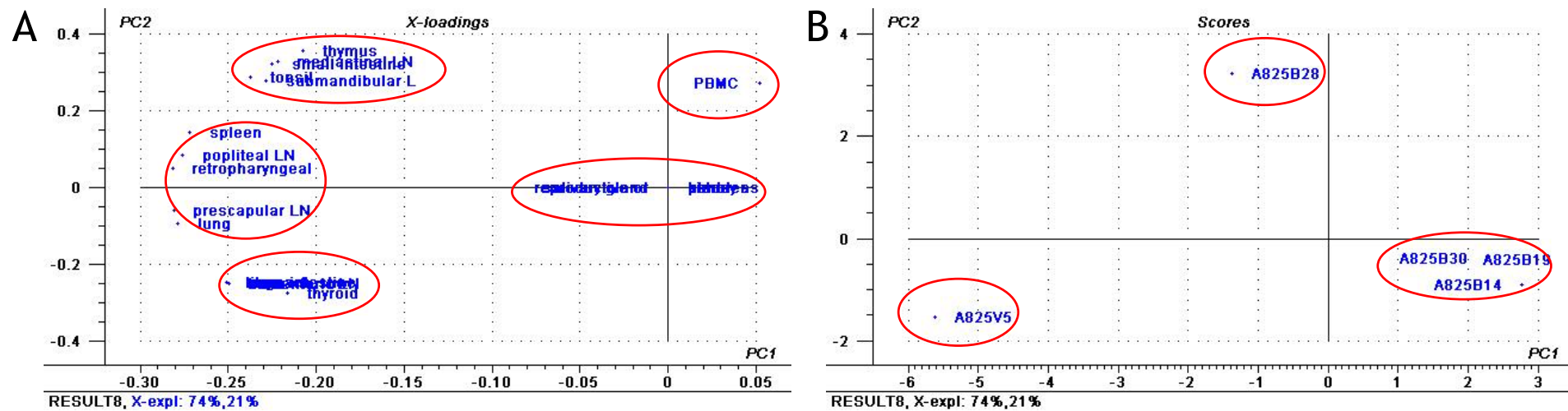
Appendix 3-2 Comparisons of FIV PVL (copies/10⁶ cells) between visceral (11) and lymphoid organs (10) as determined by *gag* (A, C) and GL8 V5 (B, D) quantitative PCR (qPCR). A and B showed median cumulative quantity of each tissue type with range for four cats. C and D showed median of median quantities for each tissue type with range for four cats. Y-axis begins at the lower limit of detection (≤ 10 copies/10⁶). Mann-Whitney test.

Appendix 3-3 Two-way ANOVA results of FIV PVL as determined by each set of primer and probe^{a,b}

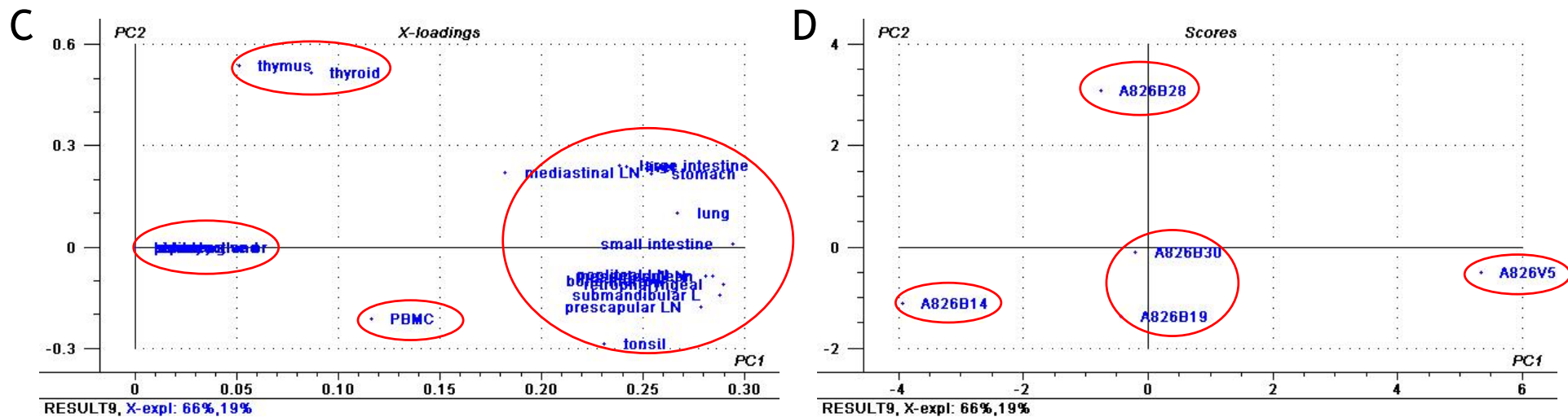
	Interaction	Compartments	Variants
B14, B19, B28, B30	31.07 ($p < 0.0001^{****}$)	10.04 ($p = 0.0186^*$)	2.56 ($p = 0.0494^*$)
<i>gag</i>, GL8 V5	12.86 ($p = 0.3114$)	29.27 ($p = 0.0019^{**}$)	1.776 ($p = 0.1121$)

^aTwo-way ANOVA with Tukey's multiple comparisons, average quantity of each variant of the four cats was analysed as column factor while individual compartment as row factor.

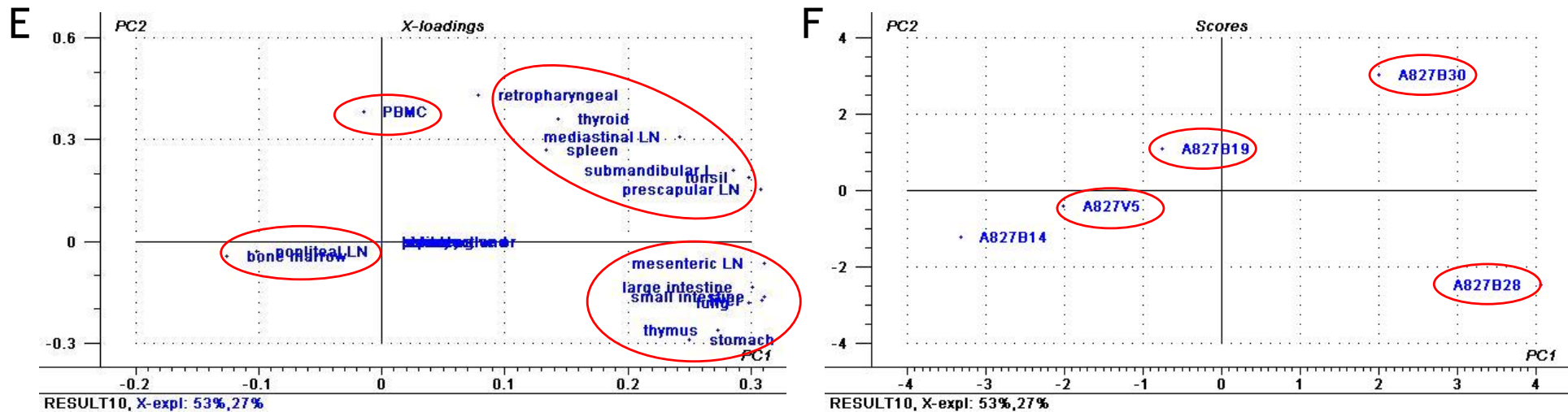
^bTable shows percentage of total variance, p value is shown in bracket.



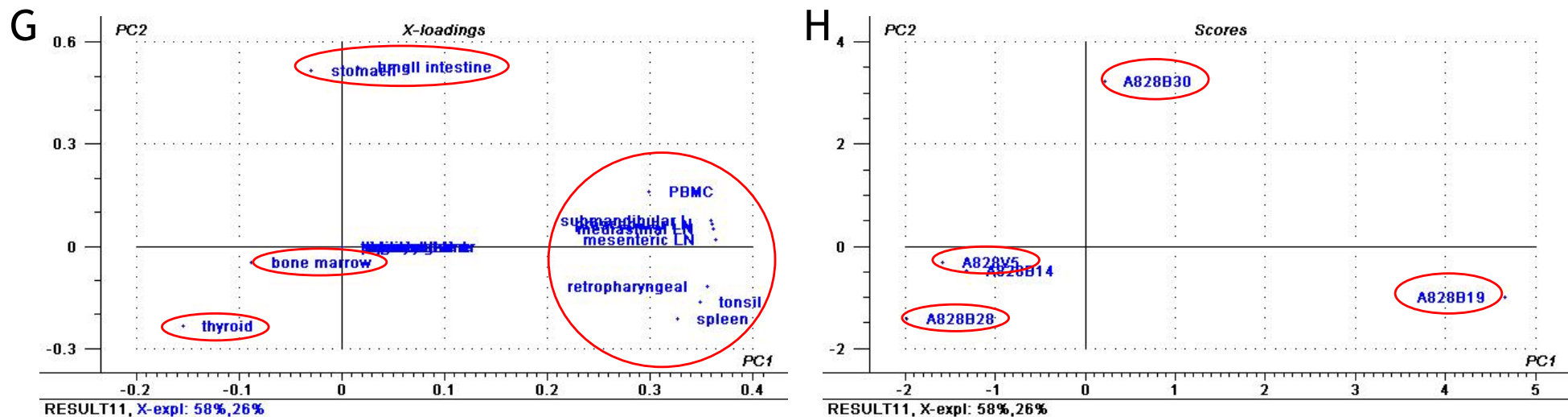
PCA loading (A) and score (B) plots of Cat A825. X-axis and Y-axis shows PC1 and PC2, which accounted for 74% and 21% of the variables, respectively. Together, these two PC explain 95% of all the variables. In the bi-plot (PC1 + PC2), tissue compartments were grouped together into five clusters (marked by red circle) according to the PVL of each of the five V5 variants determined. On PC1 (X-axis), most of tissue compartments (three clusters on the left hand side, Figure A), including both lymphoid and visceral organs were grouped together by the PVL of GL8 V5 (Figure B). The rest of the compartments were grouped together by PVL of the other four V5 variants (B14, B19, B28 and B30). There was evidence of separation between GL8 V5 and its V5 variants, in which B14, B19 and B30 are more close to each other compared to B28, on PC1 (X-axis). On PC2 (Y-axis), the grouping of submandibular LN, tonsil, mediastinal LN, thymus, small intestine and PBMC was driven by their B28 PVL. The grouping of the remainder was driven by the PVL of GL8 V5 and its three V5 variants, B14, B19 and B30. Again, B28 appeared separate from the other V5 variants investigated in this study, which strongly suggested that the selective pressure for B28 is different than for the other V5 variants. When both PC were analysed together, GL8 V5 PVL appeared to be the main driver of visceral organs while most of the lymphoid organs were grouped together by the combination of both B28 and GL8 V5 PVL in this cat. The rest of the tissues were influenced by the PVL of B14, B19 and B30.



PCA loading (C) and score (D) plots of Cat A826. X-axis and Y-axis shows PC1 and PC2, which accounted for 66% and 19% of the variables, respectively. Together, these two PC explain 85% of all the variables. In these two PCs (PC1 + PC2), tissue compartments grouped together into four clusters according to the PVL of each of the five V5 variants determined. In this cat, B14 appeared to be the least influential driver of the relationship, which in line with its low quantity, since it was only detected in the liver (Figure 3-7 and Appendix 3-5B). GL8 V5 PVL appears to be the main driver for most of the tissues on PC1 (X-axis) with additional influence from B14, B19 and B30 PVL on PC2 (Y-axis). Interestingly, B28 PVL appears to be the main driver for the cluster of thyroid and thymus, separating them from the rest of the tissue compartments on both PC1 and PC2.



PCA loading (E) and score (F) plots of Cat A827. X-axis and Y-axis shows PC1 and PC2, which accounted for 53% and 27% of the variables, respectively. Together, these two PC explain 80% of all the variables. In this cat, most of the tissues were grouped together (two major clusters on the right side of Figure E) by the PVL of both B28 and B30 (F), while bone marrow, popliteal LN, liver and PBMC were driven by GL8 V5 and B19 on PC1 (X-axis). Similar to A826, B14 showed the least influence as its PVL was very low and detectable only in PBMC (Figure 3-7 and Appendix 3-5C). On PC2 (Y-axis), tissue compartments were separated into three groups in which, similar to PC1, bone marrow, popliteal LN and liver were driven by GL8 V5 PVL (in the middle), a second group composed mainly of lymphoid organs, driven by B30 and partially by B19 (above zero on Y-axis) and a third group composed mainly of visceral organs including thymus were driven by B28 (below zero on Y-axis).



PCA loading (G) and score (H) plots of Cat A828. X-axis and Y-axis shows PC1 and PC2, which accounted for 58% and 26% of the variables, respectively. Together, these two PC explain 84% of all the variables. On both PC1 and PC2, most of the tissues were grouped together under the influence of B19 PVL. Stomach and intestine were driven by B30 PVL and were grouped together at the top of the plot whereas bone marrow and the remaining tissues were driven by GL8 V5 PVL. The dominance of B28 in the thyroid explains its separation from the rest of the tissues at the far left corner of the plot. Unlike the other three cats in which GL8 V5 and B28 appeared to be on the opposite direction of the plot, they were positioned close to each other. This might be related to the undetectable PVL in the thymus of this cat by any qPCR, since the influence of B28 PVL on the position of thymus was the only consistent pattern observed in the other three cats (Appendix 3-5)

Appendix 3-6 FIV PVL in thymus and bone marrow^a

	GL8 V5	B14^{b,c}	B19	B28^c	B30
bone marrow	108,883 (14,967 - 218,000)	-	9,675 (2,090 - 13,800)	-	1,606 (632 - 5,553)
thymus	71,200 (5,727 - 865,333)	-	27,300 (5,900 - 37,150)	217,000 (167,333 - 1,397,646)	30,667 (19,967 - 61,700)

^amedian (copies/10⁶ cells with range in brackets) was calculated from PVL of four cats.

^bB14 and B28 were undetectable in bone marrow of all cats.

^cB14 was only detectable in thymus of A825.

Appendix 3-7 Level of CD134 and CXCR4 mRNA in nine tissues of four cats*

	CD134 mRNA (range)	CXCR4 mRNA (range)
A825	1,190 (584 - 2,823)	3,306 (1,177 - 37,846)
A826	2,494 (946 - 4,892)	13,787 (1,314 - 56,609)
A827	1,715 (307 - 3,067)	3,544 (1,764 - 35,009)
A828	1,897 (575 - 4,144)	6,838 (1,892 - 49,295)

*median of nine tissues; thyroid gland, spleen, submandibular lymph node, retropharyngeal lymph node, prescapular lymph node, mesenteric lymph nodes, popliteal lymph node, bone marrow and thymus gland.

Appendix 3-8 Level of CD134 and CXCR4 mRNA in nine tissue compartments*

	CD134 mRNA (range)	CXCR4 mRNA (range)
thyroid	1,187 (946 - 1,697)	4,827 (2,515 - 7,219)
spleen	1,149 (575 - 2,669)	2,730 (1,773 - 5,167)
submandibular LN	950 (747 - 2,851)	7,366 (1,764 - 16,528)
retropharyngeal LN	1,774 (307 - 3,130)	11,845 (3,306 - 30,553)
prescapular LN	2,505 (2,162 - 3,674)	32,224 (7,912 - 45,662)
mesenteric LN	3,484 (1,714 - 4,892)	36,428 (24,402 - 56,609)
popliteal LN	2,306 (1,037 - 3,067)	2,096 (1,177 - 3,293)
bone marrow	1,619 (1,031 - 2,618)	2,285 (1,514 - 3,153)
thymus	2,268 (1,190 - 2,534)	17,281 (6,817 - 49,295)

*median of four cats; A825 - A828, plasmid copies number

Appendix 3-9 CD134 mRNA:CXCR4 mRNA ratio of each tissue*

	A825	A826	A827	A828	median
thyroid	0.47	0.34	0.24	0.18	0.29
spleen	0.33	0.52	0.51	0.27	0.42
SMLN	0.09	0.17	0.42	0.42	0.30
RPLN	0.50	0.16	0.09	0.06	0.12
PSLN	0.27	0.07	0.09	0.08	0.08
MSLN	0.07	0.09	0.05	0.17	0.08
PLN	2.21	0.79	0.93	0.70	0.86
BM	0.68	0.74	0.83	0.68	0.71
thymus	0.17	0.18	0.10	0.05	0.14
median	0.33	0.18	0.24	0.18	0.25**

*mRNA quantifications were performed in triplicate, ratios calculated from the mean of triplicates

**median of all tissues of four cats

Appendix 3-10 Comparisons of the level of CD134 and CXCR4 mRNA in three tissue compartments of the FIV negative and positive cats*

	CD134 mRNA (range)		CXCR4 (range)	
	FIV negative	FIV positive	FIV negative	FIV positive
bone marrow	98 (68 - 368)	388 (286 - 582)	114 (86 - 441)	343 (164 - 486)
spleen	37 (16 - 58)	248 (172 - 492)	13 (2 - 22)	145 (46 - 331)
thymus	363 (94 - 645)	334 (181 - 602)	2,238 (32 - 3,145)	1,049 (434 - 3,101)

*median of three cats; FIV negative A810 - A812, FIV positive A825 - A827, plasmid copies number

Appendix 4-1 Type and number of tests requested between groups

Test requested*	FIV negative	FIV positive	
		detectable PVL	undetectable PVL
Feline gingivitis profile (FHV & FCV isolation, FeLV Ag, FIV Ab)	27	4	2
Feline neurological profile (FeLV Ag, FIV & FCoV Ab, <i>Toxoplasma gondii</i> Ab)	4	1	
Feline pyrexia profile (FeLV Ag, FIV & FCoV Ab, haematology, ALP, ALT)	2	1	
Feline uveitis (FeLV Ag, FIV & FCoV Ab, <i>Toxoplasma gondii</i> Ab)	4	2	1
FeRV profile (FeLV Ag + FIV IF)	52	15	1
FeRV profile + FPV profile (FPV PCR & Ab)		1	
FeRV + FCoV (FCoV Ab)	3		1
FeRV + FIP (FCoV Ab, α 1-AGP, haematology/cytology)	2		
FeLV Ag (ELISA)	14		
FIV + FCoV + FCV (FeLV Ag,	2		
FCoV + <i>Chlamydia felis</i> PCR	1		
FHV + <i>Chlamydia felis</i> PCR	1		
<i>Chlamydia felis</i> PCR	1		
FIV Western Blot			1
FIV Ab (Immunofluorescence)	1	56	8
total	114	80	14

* Ag = antigens, Ab = antibodies, α 1-AGP = alpha-1-acid glycoprotein, FCV = feline calicivirus, FCoV = feline coronavirus, FeLV = feline leukaemia virus, FeRV = Feline Retrovirus, FIV = feline immunodeficiency virus, FHV = feline herpesvirus, FPV = feline parvovirus

Appendix 4-2 Type and number of tests requested between groups

Test requested*	FIV negative		FIV positive	
	Healthy**	sick	Healthy	sick
Feline gingivitis profile (FHV & FCV isolation, FeLV Ag, FIV Ab)	1	26		4
Feline neurological profile (FeLV Ag, FIV & FCoV Ab, <i>Toxoplasma gondii</i> Ab)		2		1
Feline pyrexia profile (FeLV Ag, FIV & FCoV Ab, haematology, ALP, ALT)		5		1
Feline uveitis (FeLV Ag, FIV & FCoV Ab, <i>Toxoplasma gondii</i> Ab)	1	3		2
FeRV profile (FeLV Ag + FIV IF)	14	8	6	6
FeRV profile + FPV profile (FPV PCR & Ab)				1
FeRV + FCoV (FCoV Ab)	2	6		
FeRV + FIP (FCoV Ab, α 1-AGP, haematology/cytology)		4		
FeLV Ag (ELISA)	1			
FIV + FCoV + FCV (FeLV Ag, FCoV + <i>Chlamydia felis</i> PCR)		2		
<i>Chlamydia felis</i> PCR	1	1		
FIV Ab (Immunofluorescence)			11	14
total	21	57	17	29

* Ag = antigens, Ab = antibodies, α 1-AGP = alpha-1-acid glycoprotein, FCV = feline calicivirus, FCoV = feline coronavirus, FeLV = feline leukaemia virus, FeRV = Feline Retrovirus, FIV = feline immunodeficiency virus, FHV = feline herpesvirus, FPV = feline parvovirus, ** one unknown

Appendix 4-3 Clinical History of FIV negative cats

I.D.	Age*	Sex	neuter	Breed**	sick/healthy	single/multi
364289	1Y 9M	female	neuter	DSH	healthy	unk
364296	1Y 9M	male	neuter	ragamuffin	unk	unk
364530	<1Y	female	unk	DSH	healthy	unk
364610	unk	female	unk	DSH	healthy	unk
364613	1Y 9M	female	unk	maine coon	healthy	unk
364614	1Y 11M	female	unk	maine coon	healthy	unk
364648	8Y 3M	female	neuter	DSH	sick	unk
364853	1Y	female	unk	unk	healthy	unk
364865	11Y 6M	male	neuter	DSH	unk	multi
364966	5M	male	neuter	DSH	unk	unk
365010	2Y 10M	male	unk	DSH	unk	unk
365013	12Y 8 M	female	neuter	persian	sick	unk
365043	12Y	female	neuter	DSH	sick	unk
365093	2Y 8M	female	neuter	DLH	sick	unk
365084	unknown	unk	unk	DSH	healthy	unk
365117	>1Y	female	neuter	DMH	sick	unk
365136	3Y 9M	female	neuter	DSH	sick	unk
366828	1Y 9M	female	neuter	DSH	sick	unk
366831	6W	female	unk	DSH	unk	unk
366832	unknown	female	unk	DSH	unk	unk
366836	6W	male	unk	DSH	unk	unk
366837	unknown	male	unk	DLH	unk	unk
366838	6W	male	unk	DSH	unk	unk
366864	6M	female	unk	bengal	healthy	unk
366865	1Y 3M	female	neuter	DSH	sick	unk
366866	7Y	female	neuter	DLH	healthy	unk
366884	unknown	female	unk	DSH	unk	unk
366889	1M	female	unk	british blue cross	sick	unk
366892	13Y	female	unk	burmese	sick	unk
366893	unknown	female	unk	DSH	unk	unk
366933	8M	male	neuter	BSH	sick	unk
366935	2M	female	unk	BSH	healthy	unk
366936	10Y	male	unk	DLH	unk	unk
366941	11Y 1M	male	unk	DSH	sick	unk
366953	12M	male	unk	DSH	sick	unk
366955	15M	female	unk	DSH	healthy	unk
366961	4Y 2W	female	unk	DSH	healthy	unk

I.D.	Age*	Sex	neuter	Breed**	sick/healthy	single/multi
366975	3Y	male	unk	DSH	unk	multi
366976	unk	unk	unk	DSH	unk	multi
366981	2Y 6M	female	neuter	DSH	sick	unk
366985	3Y	male	neuter	ragdoll	sick	unk
367015	1Y1M	female	neuter	DSH	sick	unk
367055	1Y 2M	male	neuter	DSH	healthy	multi
367064	14Y	male	unk	DSH	sick	unk
367069	3Y 6M	female	unk	DSH	sick	unk
367082	9M	female	neuter	DSH	sick	unk
367123	3Y	male	neuter	DSH	unk	unk
367124	17Y	male	neuter	DSH	unk	unk
367179	unknown	female	unk	DSH	unk	unk
367182	3Y	male	neuter	DSH	sick	multi
367231	16Y 10M	male	neuter	DSH	sick	unk
367237	11Y 9M	female	unk	DLH	sick	multi
367288	11Y	male	neuter	DSH	sick	unk
367289	unknown	female	unk	DSH	unk	unk
367290	5Y 2M	female	unk	tortoise shell	sick	unk
367291	3Y 11M	female	neuter	ragdoll	sick	single
367320	unk	male	neuter	DSH	sick	unk
367328	8Y	female	unk	DSH	sick	unk
367344	>1Y	male	entire	DSH	unk	unk
367345	1Y	female	unk	bsh	sick	unk
367353	7Y	female	neuter	DSH	unk	unk
367393	4Y	female	neuter	DSH	sick	unk
367404	11M	female	neuter	cornish rex	sick	multi
367420	2Y 2M	male	unk	DSH	sick	unk
367421	1Y 9M	female	neuter	DSH	sick	unk
367422	1Y 9M	female	neuter	DSH	sick	multi
367424	5Y 1M	male	neuter	DSH	sick	unk
367425	5Y 10M	female	neuter	unk	healthy	unk
367428	4M	male	entire	burmese	sick	multi
367443	2Y 6M	female	neuter	DSH	sick	unk
367448	8Y 11M	male	neuter	siamese	sick	unk
367468	unk	female	unk	DSH	sick	unk
367477	6M	male	entire	DSH	sick	unk
367479	4Y	male	neuter	DSH	sick	unk
372359	11Y 10M	male	neuter	DSH	unk	unk
372269	11Y 8M	male	neuter	bengal	healthy	unk
367523	2Y 11M	female	neuter	DSH	sick	unk

I.D.	Age*	Sex	neuter	Breed**	sick/healthy	single/multi
367535	1Y 1M	female	neuter	DSH	sick	multi
367551	unk	female	entire	DSH	unk	unk
367564	2Y	male	neuter	DSH	sick	unk
367565	2Y	female	neuter	DSH	sick	unk
367566	12Y 1M	male	neuter	DLH	sick	unk
372506	unk	unk	unk	DLH	unk	unk
367578	4M	male	entire	DSH	sick	unk
367580	4M	male	entire	DSH	sick	unk
367581	8Y	female	neuter	siamese	sick	unk
367582	4M	female	entire	DSH	sick	unk
367594	unk	unk	unk	unk	sick	unk
367595	5Y	female	neuter	DSH	sick	unk
367597	14Y 2M	female	neuter	DSH	sick	unk
367607	11M	male	entire	DSH	healthy	multi
367626	3Y	male	neuter	DSH	sick	unk
367644	15Y	female	neuter	persian	unk	unk
367645	4Y 3M	famale	neuter	DSH	healthy	unk
367646	7Y 1M	male	unk	DLH	healthy	unk
367652	6M	female	neuter	DSH	unk	unk
367654	unk	male	neuter	DLH	healthy	unk
367655	4Y	female	unk	DLH	unk	unk
367661	11M	male	unk	DSH	unk	unk
367662	9Y 2M	male	neuter	DSH	sick	unk
367663	11W	female	unk	DSH	unk	unk
367664	11M	male	entire	DSH	unk	unk
367665	9Y	female	neuter	DSH	sick	unk
367684	6Y 2M	male	neuter	british blue	unk	unk
367699	1Y 6M	male	unk	DSH	unk	unk
372770	3Y 6M	female	neuter	DSH	unk	unk
367704	10Y	male	neuter	DSH	unk	unk
367708	8Y	male	neuter	DSH	sick	unk
367743	2Y 6M	female	unk	DSH	healthy	unk
367744	7Y	female	unk	DSH	healthy	unk
367747	2Y	female	neuter	bengal cross	sick	unk
367748	3Y	female	unk	DLH	unk	unk
367749	5Y	male	unk	DSH	unk	unk
367728	4Y	female	unk	DSH	unk	unk

*Age: Y = year, M= month and W = week, unk = unknown

**BSH = british short hair, DSH = domestic short hair, DMH, domestic medium hair and DLH = domestic long hair, All the cross and DSH, DMH and DLH were treated as being mixed breed.

Appendix 4-4 Lymphocyte subpopulations of FIV negative cats

I.D.	%CD4*	%CD8*	CD4:CD8	%CD4CD134**
364289	28.95	13.61	2.13	6.25
364296	18.58	8.50	2.19	10.35
364530	28.68	8.95	3.20	20.84
364610	27.12	5.92	4.58	9.48
364613	17.61	5.58	3.16	12.64
364614	22.02	6.26	3.52	10.02
364648	23.76	4.04	5.88	19.89
364853	29.05	8.05	3.61	23.09
364865	40.60	21.52	1.89	13.31
364966	10.87	7.61	1.43	16.52
365010	17.56	25.88	0.68	15.00
365013	15.52	13.16	1.18	26.20
365043	8.84	6.86	1.29	42.87
365093	36.99	22.92	1.61	28.36
365084	19.46	7.36	2.64	71.31
365117	20.93	11.40	1.84	66.27
365136	10.61	8.38	1.27	59.09
366828	6.75	2.40	2.81	3.87
366831	9.44	2.13	4.43	10.92
366832	6.06	2.73	2.22	10.86
366836	0.51	0.48	1.06	15.62
366837	5.12	1.48	3.46	20.00
366838	0.93	0.32	2.91	8.49
366864	39.58	8.78	4.51	7.97
366865	20.86	12.33	1.69	2.58
366866	30.78	15.29	2.01	1.40
366884	26.85	9.34	2.87	8.68
366889	31.79	21.08	1.51	8.47
366892	33.56	15.36	2.18	23.81
366893	47.31	8.02	5.90	3.04
366933	26.78	14.94	1.79	1.82
366935	30.14	4.66	6.47	14.78
366936	5.91	7.70	0.77	13.75
366941	15.00	24.87	0.60	19.02
366953	22.99	19.79	1.16	6.58
366955	22.77	6.58	3.46	8.10
366961	46.01	11.38	4.04	8.39
366975	26.63	19.89	1.34	5.44

I.D.	%CD4*	%CD8*	CD4:CD8	%CD4CD134**
366976	22.17	11.65	1.90	9.60
366981	26.71	12.88	2.07	4.18
366985	13.52	6.48	2.09	6.77
367015	27.43	10.77	2.55	9.96
367055	42.30	9.44	4.48	2.69
367064	33.44	10.89	3.07	20.54
367069	16.58	4.90	3.38	6.47
367082	37.05	6.98	5.31	2.25
367123	3.66	9.84	0.37	7.37
367124	24.28	12.55	1.93	8.77
367179	28.83	10.84	2.66	4.02
367182	4.58	7.84	0.58	19.65
367231	34.93	3.69	9.47	17.78
367237	28.69	16.12	1.78	8.95
367288	8.54	6.90	1.24	14.68
367289	47.35	11.56	4.10	11.28
367290	18.50	33.22	0.56	2.74
367291	28.43	20.35	1.40	2.96
367320	33.57	10.39	3.23	1.15
367328	2.88	2.52	1.14	7.34
367344	33.89	10.67	3.18	6.46
367345	30.74	16.05	1.92	1.75
367353	28.42	11.09	2.56	4.09
367393	12.15	45.35	0.27	24.96
367404	28.11	20.97	1.34	9.01
367420	18.00	13.83	1.30	6.47
367421	32.32	20.46	1.58	4.68
367422	21.82	6.01	3.63	4.45
367424	15.46	13.84	1.12	23.29
367425	17.11	11.70	1.46	8.08
367428	58.30	3.40	17.15	4.36
367443	28.09	13.49	2.08	2.93
367448	23.74	13.79	1.72	27.09
367468	11.42	6.38	1.79	5.89
367477	13.87	3.95	3.51	3.60
367479	24.77	24.86	1.00	9.41
372359	12.91	4.95	2.61	16.12
372269	17.26	3.69	4.68	8.12
367523	38.96	11.57	3.37	13.68
367535	33.88	16.87	2.01	4.80
367551	20.64	21.56	0.96	7.27

I.D.	%CD4*	%CD8*	CD4:CD8	%CD4CD134**
367564	26.04	10.57	2.46	16.87
367565	36.41	20.15	1.81	15.18
367566	17.23	14.10	1.22	15.71
372506	15.29	4.84	3.16	25.79
367578	33.83	12.12	2.79	14.04
367580	15.37	5.85	2.63	15.61
367581	34.42	24.36	1.41	6.36
367582	28.05	11.80	2.38	19.03
367594	21.99	5.31	4.14	9.06
367595	28.39	15.45	1.84	8.53
367597	25.19	17.39	1.45	18.44
367607	23.04	12.59	1.83	11.75
367626	23.19	15.33	1.51	11.11
367644	22.19	21.11	1.05	29.80
367645	11.76	4.60	2.56	23.35
367646	15.95	15.77	1.01	32.27
367652	22.22	13.64	1.63	22.98
367654	26.12	16.45	1.59	22.58
367655	16.44	11.93	1.38	26.67
367661	40.82	28.29	1.44	15.25
367662	28.13	16.52	1.70	20.18
367663	11.58	1.82	6.36	10.85
367664	41.17	10.92	3.77	14.88
367665	19.35	10.22	1.89	14.52
367684	17.28	6.75	2.56	23.31
367699	32.45	10.06	3.23	22.43
372770	24.25	18.43	1.32	38.02
367704	18.77	18.01	1.04	30.75
367708	9.66	15.97	0.60	14.13
367743	31.06	18.45	1.68	7.81
367744	25.70	21.83	1.18	32.05
367747	44.87	16.12	2.78	12.40
367748	34.10	11.33	3.01	9.39
367749	28.42	33.70	0.84	24.47
367728	21.86	25.73	0.85	32.86

*%CD4 and %CD8 showed their percentage in lymphocyte population

**%CD4CD134 showed its percentage in CD4⁺ population

Appendix 4-5 Clinical History of FIV positive cats

I.D.	Age*	Sex	neuter	Breed**	sick/healthy	single/multi
345921	4Y	male	neuter	DSH	unk	unk
345998	unk	male	entire	DSH	unk	unk
346096	12Y 7M	male	neuter	DSH	sick	multi
346171	3Y 10M	male	neuter	DSH	unk	unk
346173	unk	female	unk	DSH	unk	unk
346223	8Y	male	neuter	DSH	sick	single
346224	7Y	female	unk	unk	sick	unk
346225	2Y	male	unk	DSH	healthy	unk
346271	6Y 10M	male	unk	DSH	healthy	multi
346346	2Y 1M	male	neuter	DSH	unk	unk
346267	6Y	male	neuter	DSH	sick	unk
346301	9Y 1M	male	unk	DSH	sick	unk
346303	2Y 10M	male	entire	DSH	unk	unk
346363	>1Y	male	unk	DSH	healthy	unk
346302	>1Y	female	unk	DSH	healthy	unk
346466	>1Y	male	unk	DSH	healthy	unk
346537	unk	male	unk	DSH	healthy	multi
346512	14Y	male	entire	DSH	sick	unk
346540	>1Y	male	unk	DSH	healthy	unk
346541	8Y 5M	male	unk	DSH	sick	unk
346660	2Y	male	unk	DSH	sick	unk
346661	>1Y	male	neuter	DSH	healthy	unk
346681	>1Y	male	unk	DSH	healthy	unk
346795	>1Y	male	entire	unk	unk	unk
346805	>1Y	male	neuter	persian cross	sick	unk
346913	7Y	male	unk	DSH	sick	multi
346938	6Y	male	neuter	DSH	sick	multi
346940	3Y	male	neuter	DSH	healthy	unk
346970	5Y	male	entire	DSH	unk	unk
346998	10Y	male	neuter	DSH	sick	unk
347076	>1Y	male	unk	DSH	sick	unk
347024	>1Y	male	unk	DSH	healthy	unk
347075	2Y 9M	female	neuter	DSH	unk	multi
347138	12Y	male	unk	DSH	sick	multi
347175	11Y 2M	female	neuter	DSH	sick	multi
347178	>1Y	male	unk	DSH	healthy	unk
347202	6Y	male	neuter	DSH	sick	unk

I.D.	Age*	Sex	neuter	Breed**	sick/healthy	single/multi
347251	3Y	male	neuter	DSH	healthy	multi
364247	5Y	male	entire	DLH	unk	unk
364298	11Y 5M	male	entire	DSH	sick	single
364324	6Y	male	entire	DSH	unk	unk
364455	6Y	male	unk	DSH	sick	unk
364456	3Y	male	unk	DSH	unk	unk
364459	unk	male	neuter	DSH	unk	unk
364483	1Y 6M	male	neuter	unk	unk	unk
364457	unk	female	unk	DSH	sick	single
364480	2Y	male	neuter	DSH	unk	unk
364506	8Y	male	neuter	DSH	sick	multi
364611	unk	male	unk	DSH	unk	multi
364726	>1Y	male	unk	unk	unk	unk
364735	3Y	male	neuter	DLH	unk	unk
364791	2Y	male	neuter	DSH	healthy	unk
366922	2Y	male	neuter	DSH	unk	unk
364944	4Y	male	neuter	DSH	unk	unk
364983	2Y	male	entire	DSH	unk	unk
365045	10Y	male	unk	DSH	sick	multi
365078	unk	male	unk	DSH	healthy	unk
365085	7Y	male	unk	DSH	sick	unk
365092	>1Y	male	entire	DSH	unk	unk
365194	unk	male	entire	DSH	unk	unk
365292	3Y	male	entire	DSH	sick	unk
365294	4Y 6M	male	entire	DSH	unk	unk
365363	2Y	female	neuter	DSH	sick	unk
365434	>1Y	male	unk	DSH	unk	unk
366973	8Y 6M	male	neuter	Maine Coon	unk	unk
367097	unk	male	unk	DSH	unk	unk
367133	7Y 6M	male	neuter	DSH	sick	unk
367206	>1Y	male	unk	DSH	unk	unk
367396	3Y 6M	male	neuter	DSH	unk	unk
367418	2Y 5M	male	entire	DSH	healthy	unk
367423	3Y	female	entire	DSH	unk	unk
367516	5Y	male	unk	DSH	unk	unk
367517	7M	female	unk	DSH	sick	unk
367647	unk	male	neuter	DSH	unk	unk
368231	12Y 3M	male	unk	DSH	sick	single/multi
368352	2Y	male	neuter	DSH	healthy	unk
368353	>1Y	male	unk	DSH	unk	unk
368406	9Y	male	neuter	DSH	unk	unk

I.D.	Age*	Sex	neuter	Breed**	sick/healthy	single/multi
368407	7Y 5M	male	neuter	DLH	sick	unk
368508	8Y	male	entire	DSH	sick	unk

*Age: Y = year, M= month and W = week, unk = unknown

** DSH = domestic short hair and DLH = domestic long hair, All the cross and DSH and DLH were treated as being mixed breed.

Appendix 4-6 Lymphocyte subpopulations of FIV positive cats

I.D.	%CD4*	%CD8*	CD4:CD8	%CD4CD134**	FIV proviral load***
345921	6.75	1.45	4.66	15.24	779
345998	23.20	20.94	1.11	19.76	21
346096	17.20	14.83	1.16	52.73	156
346171	19.61	25.29	0.78	40.02	368
346173	12.94	26.25	0.49	27.85	13,038
346223	8.32	53.16	0.16	19.81	105,446
346224	17.01	26.27	0.65	20.55	9,827
346225	30.11	22.55	1.34	96.96	21,212
346271	26.77	7.85	3.41	20.43	72
346346	7.38	8.08	0.91	22.75	3,257
346267	17.12	8.96	1.91	18.89	4,583
346301	29.70	6.75	4.40	6.30	11
346303	33.25	7.55	4.40	11.82	488
346363	24.60	14.19	1.73	43.18	851
346302	25.15	5.17	4.86	67.37	7,903
346466	21.58	16.07	1.34	47.83	872
346537	13.73	11.45	1.20	39.75	30
346512	25.11	15.57	1.61	18.56	1,418
346540	25.54	17.46	1.46	22.67	52
346541	22.61	14.57	1.55	61.84	129,829
346660	0.27	0.34	0.79	27.27	1,758,848
346661	21.02	11.97	1.76	38.78	2,362
346681	29.49	5.48	5.38	24.06	49
346795	32.28	24.32	1.33	28.82	1,902
346805	24.71	22.43	1.10	67.83	15,762
346913	16.83	41.84	0.40	56.44	49
346938	8.16	2.59	3.15	29.63	2,983
346940	37.50	5.24	7.16	83.75	2,871
346970	25.86	11.54	2.24	51.75	14
346998	14.29	12.96	1.10	48.92	20
347076	25.92	16.20	1.60	24.91	3,143

I.D.	%CD4*	%CD8*	CD4:CD8	%CD4CD134**	FIV proviral load***
347024	8.70	18.27	0.48	45.63	2,168
347075	16.17	24.16	0.67	40.90	464
347138	9.40	7.89	1.19	43.49	159
347175	15.87	9.65	1.64	30.08	10,102
347178	24.17	30.29	0.80	39.95	20
347202	13.00	22.28	0.58	51.25	1,629
347251	13.02	19.61	0.66	28.19	1,010
364247	13.87	2.19	6.33	12.37	24
364298	14.42	9.58	1.51	17.82	7,936
364324	30.57	13.99	2.19	26.30	12,251
364455	17.31	26.00	0.67	55.80	5,760
364456	3.94	1.33	2.96	12.50	2,408
364459	42.94	13.92	3.08	31.94	6,178
364483	21.04	18.07	1.16	46.65	3,505
364457	0.03	0.80	0.04	20.00	1,467,822
364480	28.97	21.79	1.33	47.55	150,280
364506	10.94	10.05	1.09	26.48	6,077
364611	21.79	11.91	1.83	10.41	4,512
364726	14.86	25.81	0.58	20.92	369
364735	4.92	15.18	0.32	28.35	16,167
364791	27.22	9.19	2.96	22.84	1,145
366922	22.78	20.97	1.09	35.65	9,242
364944	17.09	20.21	0.85	38.17	11,133
364983	17.21	24.68	0.70	33.20	42,246
365045	15.92	32.67	0.49	29.05	7,204
365078	4.21	6.98	0.60	50.51	117,882
365085	8.72	45.53	0.19	26.68	1,671
365092	6.12	23.83	0.26	27.74	12,425
365194	13.68	30.87	0.44	11.83	342
365292	18.86	20.62	0.91	28.74	692
365294	13.65	15.34	0.89	25.27	12,693
365363	26.60	15.23	1.75	22.16	767
365434	28.73	20.18	1.42	20.52	134
366973	25.50	6.67	3.82	14.71	6,174
367097	26.59	20.41	1.30	9.48	6,142
367133	1.62	5.57	0.29	5.10	1,669
367206	22.20	23.62	0.94	16.81	432
367396	30.22	12.57	2.40	22.62	3,221
367418	36.93	21.46	1.72	7.75	233
367423	18.27	16.01	1.14	10.08	1,021
367516	21.35	14.97	1.43	5.56	815

I.D.	%CD4*	%CD8*	CD4:CD8	%CD4CD134**	FIV proviral load***
367517	7.32	2.72	2.69	15.90	16,521
367647	20.52	22.62	0.91	29.22	20,028
368231	15.64	7.76	2.02	26.47	2,840
368352	22.20	15.56	1.43	16.78	6,504
368353	23.81	11.85	2.01	25.68	274
368406	6.41	5.48	1.17	68.22	150,972
368407	9.70	11.34	0.86	32.68	2,690
368508	26.89	16.70	1.61	16.74	30,2401

*%CD4 and %CD8 showed their percentage in lymphocyte population

**%CD4CD134 showed its percentage in CD4⁺ population

***FIV Proviral load was reported as copies/10⁶ cells.

Appendix 4-7 Clinical Histories of FIV positive with FIV PVL below limit of detection

I.D.	Age*	Sex	Neuter	Breed**	sick/healthy	Single/Multi
346098	5Y 6M	male	unk	DSH	healthy	unk
364351	13Y 8M	male	neuter	DSH	sick	unk
364423	1Y 6M	male	neuter	DSH	unk	unk
364462	6Y	male	neuter	DSH	sick	unk
364484	1Y	female	unk	unk	unk	unk
365042	2Y 7M	male	neuter	DSH	healthy	single
365119	6Y 4M	male	neuter	DSH	unk	unk
367007	unk	unk	unk	unk	unk	unk
368206	4y	male	unk	DLH	sick	unk
368324	>1Y	male	unk	DSH	unk	unk
368351	>1Y	male	neuter	DSH	sick	multicat
368362	7Y 9M	male	unk	DSH	sick	unk
368366	>1Y	male	unk	DSH	unk	unk
377855	16Y	male	neuter	DLH	sick	unk

*Age: Y = year, M= month and W = week, unk = unknown

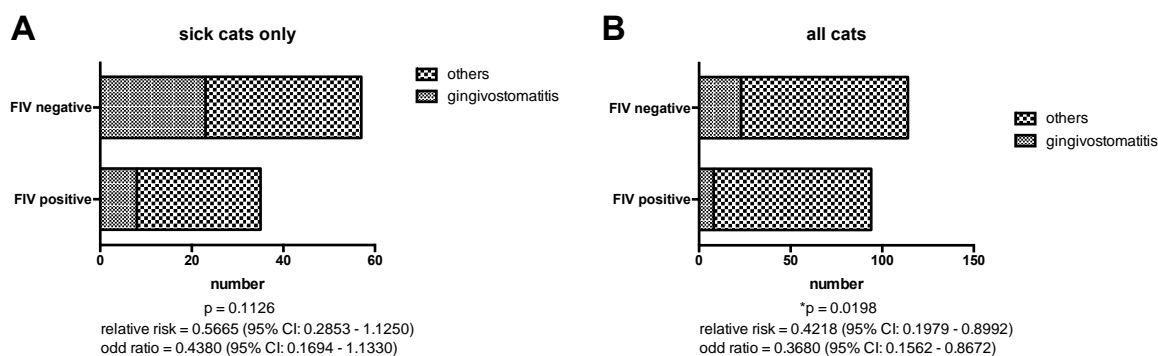
** DSH = domestic short hair and DLH = domestic long hair, All the cross and DSH and DLH were treated as being mixed breed.

Appendix 4-8 Lymphocyte subpopulations of FIV positive with PVL below limit of detection (10 copies/10⁶ cells)

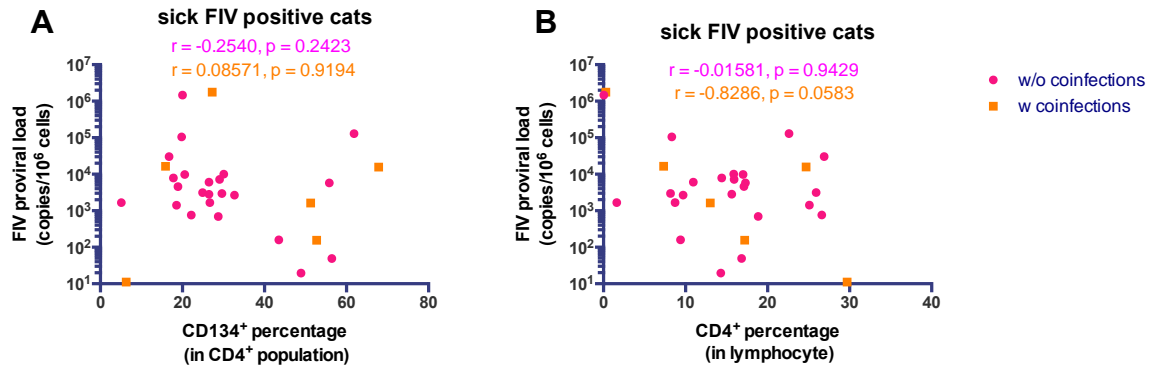
I.D.	%CD4*	%CD8*	CD4:CD8	%CD4CD134**
346098	34.68%	15.11%	2.30	93.17%
364351	10.03%	6.94%	1.45	24.05%
364423	13.39%	3.71%	3.61	13.28%
364462	29.99%	9.72%	3.09	20.33%
364484	23.88%	24.96%	0.96	38.10%
365042	14.93%	15.49%	0.96	42.02%
365119	7.03%	4.32%	1.63	36.78%
367007	15.26%	10.49%	1.45	16.48%
368206	21.16%	8.22%	2.57	90.20%
368324	17.96%	18.55%	0.97	39.44%
368351	38.16%	18.45%	2.07	30.61%
368362	16.03%	13.66%	1.17	28.78%
368366	13.36%	13.30%	1.00	20.01%
377855	27.00%	9.98%	2.71	64.54%

*%CD4 and %CD8 shown as percentage of total lymphocyte population

**%CD4CD134 shown as percentage of CD4⁺ population



Appendix 4-9 Effect of FIV serostatus and clinical manifestation of gingivostomatitis in sick cats (A) and all cats (B), Fischer's exact test and presented as relative risk and odd ratio. 95% CI: 95% confidential interval



Appendix 4-10 Correlation between percentage of CD4⁺CD134⁺ T lymphocytes (A) and CD4⁺ T lymphocytes (B) and FIV PVL in sick FIV positive cats with (orange squares) and without (pink circles) co-infections. X-axis shows percentage of cells and Y-axis shows FIV PVL (copies/10⁶ cells), Spearman r test

Appendix 4-11 CD134-usage (phenotype) of pseudotypes bearing Envs from healthy and sick FIV positive cats*

		15/10/15	23/11/15	25/11/15	29/11/15	Phenotype
healthy	346271C10	88.18	111.51	70.11	79.61	intermediate
	346271C11	n.a.	363.90	291.02	134.31	early
	346302C2	34.76	273.60	139.12	212.43	early
	346302C18	19.11	299.14	98.59	88.56	intermediate
	346302C21	36.16	250.26	89.40	175.55	intermediate
	347178C10	27.78	309.07	396.48	367.00	early
	347178C11	n.a.	301.15	198.67	319.47	early
	347251C14	11.43	192.22	83.65	92.36	intermediate
	368352C20	86.41	535.14	7.60	7.00	late
sick	346938C5	434.58	343.56	298.07	266.78	early
	346938C24	62.98	272.52	12.12	11.92	late
	346938C43	n.a.	351.25	233.90	244.06	early
	347076C9	137.47	840.62	399.08	392.84	early
	347076C31	88.40	416.90	372.85	417.23	early
	347202C4	568.21	1064.96	529.52	820.43	early
	347202C5	18.33	117.68	86.30	89.93	intermediate
	365045C2	88.54	208.22	157.50	185.29	intermediate
	367133C5	6.77	19.91	21.20	28.53	late
control	GL8	195.49	1730.62	395.13	646.26	early
	KKS	25.64	63.66	35.70	40.14	intermediate
	B2542	4.69	10.55	9.05	8.60	late
	VR1012	0.97	2.89	4.50	3.50	negative

*The values shown are the FFF/FFHH ratios for each HIV(FIV) pseudotype (row). The assay was repeated 4 times on 4 different dates (columns). The ratio of each pseudotype was compared with the ratio of three prototypic control pseudotypes; GL8 for early, KKS for intermediate and B2542 for late variants. Early variants are highlighted in blue, intermediate variants are highlighted in green and late variants are highlighted in yellow. The interpretations were made on the consensus readouts of the 4 repeats. n.a. = not analysed. Note: only very low ratios were designated as late variants.

Appendix 4-13 Sample submission form for the diagnosis of feline infectious disease



Veterinary Diagnostic Services, School of Veterinary Medicine,
College of Medical, Veterinary and Life Sciences, University of Glasgow,
Bearsden Road, Glasgow G61 1QH, United Kingdom
Tel: +44 (0) 141 330 5777 Fax: +44 (0) 141 330 5748
email: vet-sch-vds@glasgow.ac.uk Website: www.glasgow.ac.uk/vds
University of Glasgow, charity number SC004401

Feline Infectious Disease

VETERINARY SURGEON'S NAME & ADDRESS

VDS vet ref no:
Submitting vet name:
Vet practice name & address
Postcode:
Tel: Fax:
Results email:

Sick Healthy Indoor cat Free-roaming

Samples sent (Please tick box)

Hep EDTA Blood Serum Plasma Ascites Pleural Effusion Faeces Urine
SWABS: VTM Charcoal Dry SWAB SITE: Conjunctival Oropharynx Nasal

Brief clinical history

Please enclose printed clinical notes if appropriate

Please include drugs at time of sampling

Tests required (please tick box)

To qualify for profile discounts, samples must be sent together

- Feline infectious peritonitis (FIP) profile
For FIP diagnosis in sick cats
(FCoV antibodies, haematology/cytology, A:G ratio, α 1-AGP)
Dry FIP: 2 x 1ml heparin blood, 1ml EDTA blood
Wet FIP: 1ml heparin blood & 2 samples of 1-2ml effusion in plain & EDTA tubes. Please send effusion if possible
- Feline coronavirus (FCoV) antibodies (immunofluorescence, IF)
1ml heparin blood or serum
- Feline coronavirus (FCoV) antibodies and α 1-AGP
1ml heparin blood or serum
- FCoV RT-PCR (real-time PCR)
For FCoV shedding: 5g faeces (NO cat litter)
For wet FIP confirmation: 1ml effusion in EDTA or plain tube
- Feline leukaemia virus (FeLV) antigen (p27 ELISA)
To detect FeLV antigen: screening test only
1ml heparin blood AND 1ml EDTA blood
- Feline leukaemia virus (FeLV) virus isolation
To detect FeLV viraemia (& confirm in-clinic test positive)
1ml heparin blood AND 1ml EDTA blood
- *New* Feline leukaemia virus (FeLV) qPCR
To detect FeLV proviral DNA (& confirm in-clinic test positive)
1ml heparin blood AND 1ml EDTA blood
- Feline immunodeficiency virus (FIV) antibodies (IF)
1ml heparin blood or serum
- Feline retrovirus profile (FeLV antigen, FIV antibodies)
1ml heparin blood AND 1ml EDTA blood
- FeLV, FIV and FCoV (FeLV antigen, FIV and FCoV antibodies)
1ml heparin blood AND 1ml EDTA blood

RESPIRATORY DISEASE *Free on request

- Virus isolation (Feline calicivirus, Feline herpesvirus)
Oropharyngeal swab in our virus transport medium (VTM)*
- Feline herpesvirus (real-time PCR)
Oropharyngeal or conjunctival swab in VTM* or dry
Do not send samples containing fluorescein
- Chlamydomphila felis (PCR)
Conjunctival swab in VTM* or dry
- Bordetella bronchiseptica (culture & sensitivity)
Nasal swab in bacterial transport medium* or tracheal wash. All bacteria isolated will be reported.

Lab use only

Date received

F / E

ANIMAL DETAILS NB: please use separate forms for each cat

Owner name:
Animal name:
Breed:
Sex:
Age/DOB:
Previous ref:

Date sampled: Please send VTM:

Pre-mating Single cat Multi-cat house

<input type="checkbox"/> Feline conjunctivitis profile (FHV PCR, Chlamydomphila felis PCR, Mycoplasma felis culture & PCR)	Conjunctival swab (dry OR VTM*) AND conjunctival swab in bacterial transport medium*
<input type="checkbox"/> Gingivitis profile (Virus isolation, FeLV, FIV)	Oropharyngeal swab in VTM*, 1ml heparin blood AND 1ml EDTA blood
<input type="checkbox"/> Diarrhoea profile (Bacteriology, parasitology NOT Cryptosporidium)	> 10g faeces
<input type="checkbox"/> Diarrhoea profile PLUS (Bacteriology, parasitology INC. Cryptosporidium, FCoV PCR & T. foetus PCR)	> 15g faeces- NO cat litter
<input type="checkbox"/> Pyrexia cat profile (FeLV, FIV, FCoV, FIA, haematology, ALP, ALT)	2 x 1ml heparin blood, 2 x 1ml EDTA blood and 2 air-dried smears
<input type="checkbox"/> Old thin cat profile (FIV, T4, urea, creatinine, ALP, ALT)	2 x 1ml heparin blood or serum
<input type="checkbox"/> Uveitis profile (FeLV, FIV, FCoV, Toxoplasma)	1ml heparin blood, 1ml serum and 1ml EDTA blood
<input type="checkbox"/> Feline parvovirus (FPV, feline panleucopaenia) profile FPV DNA (PCR) and FPV antibody titre (HAI)	Faeces (NO cat litter) or gut contents and 1ml heparin blood or serum
<input type="checkbox"/> Feline neutralising antibodies immune status (neutralising titre)	1ml heparin blood or serum
<input type="checkbox"/> Feline parvovirus antibodies (HAI)	1ml heparin blood or serum
<input type="checkbox"/> Feline parvovirus DNA (PCR)	Faeces or gut contents- NO cat litter
<input type="checkbox"/> Feline pox (Cowpox virus)	Lesion material or crust in a sterile container or VTM*
<input type="checkbox"/> Feline blood groups	1ml EDTA blood
<input type="checkbox"/> Feline calicivirus plaque typing (To distinguish vaccine FCV from field FCV)	Oropharyngeal swab in VTM* plus vial of vaccine batch

BACTERIOLOGY AND MYCOLOGY PLACE SWABS FOR BACTERIOLOGY IN BACTERIAL TRANSPORT MEDIUM*

<input type="checkbox"/> Full culture and sensitivity	
<input type="checkbox"/> Aerobic culture and sensitivity (urine, ears)	
<input type="checkbox"/> Enrichment culture (blood, joint fluid)	
<input type="checkbox"/> Fungal culture including Dermatophytes	Plucked hair sample or toothbrush
<input type="checkbox"/> Mycoplasma felis culture and real-time PCR	Swab in bacterial transport medium* and BAL samples in plain sterile tube

PARASITOLOGY

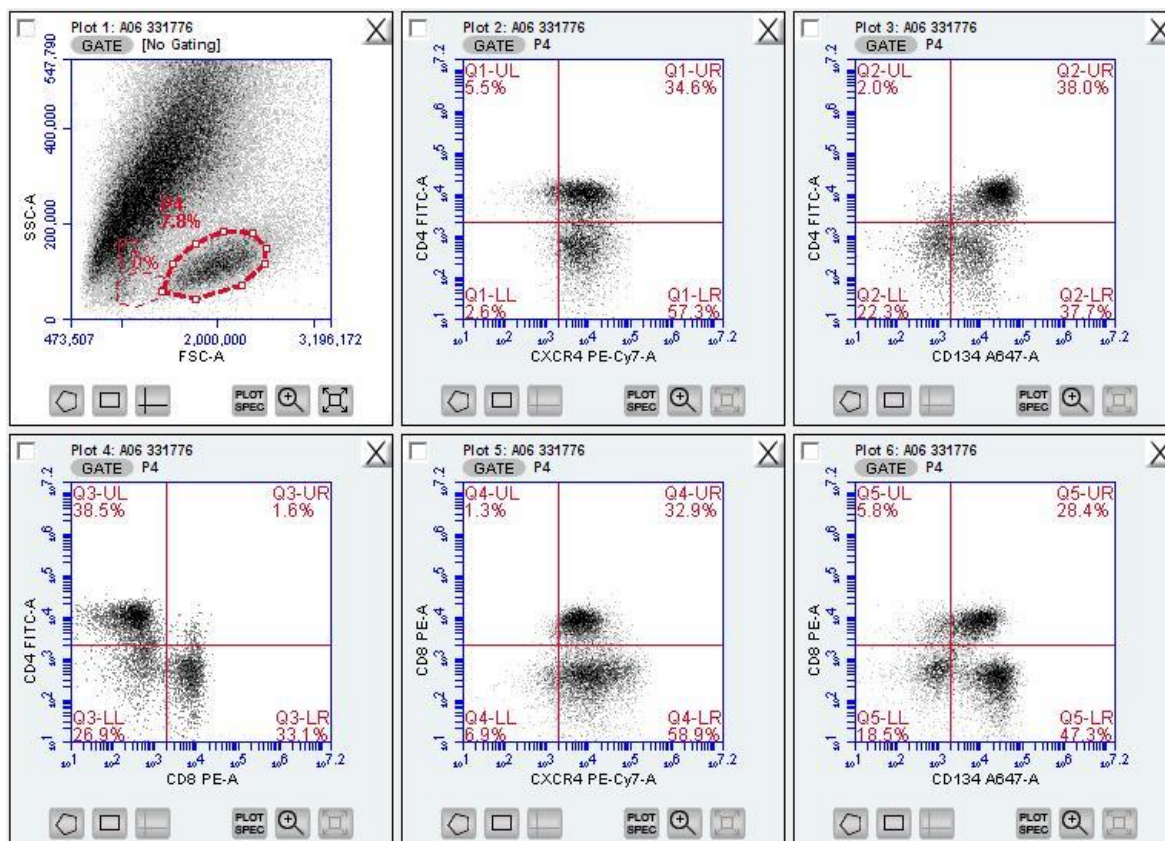
<input type="checkbox"/> Toxoplasma gondii antibodies (latex agglutination test)	1ml <u>SERUM ONLY</u> (not plasma)
<input type="checkbox"/> Protozoa screen (Giardia, Isopora etc)	Faecal sample (at least 5g)
<input type="checkbox"/> Cryptosporidium spp (ZN staining)	Faecal sample (at least 5g)
<input type="checkbox"/> Aelurostrongylus abstrusus (modified Baermann technique)	BAL preferred/sputum/faeces (>10g)
<input type="checkbox"/> Nematode and cestode egg screen (McMaster technique)	Faecal sample (at least 10g)
<input type="checkbox"/> Ectoparasite screen	Skin scrape on a slide (no sellotape or KOH)

Any other testing (please specify):

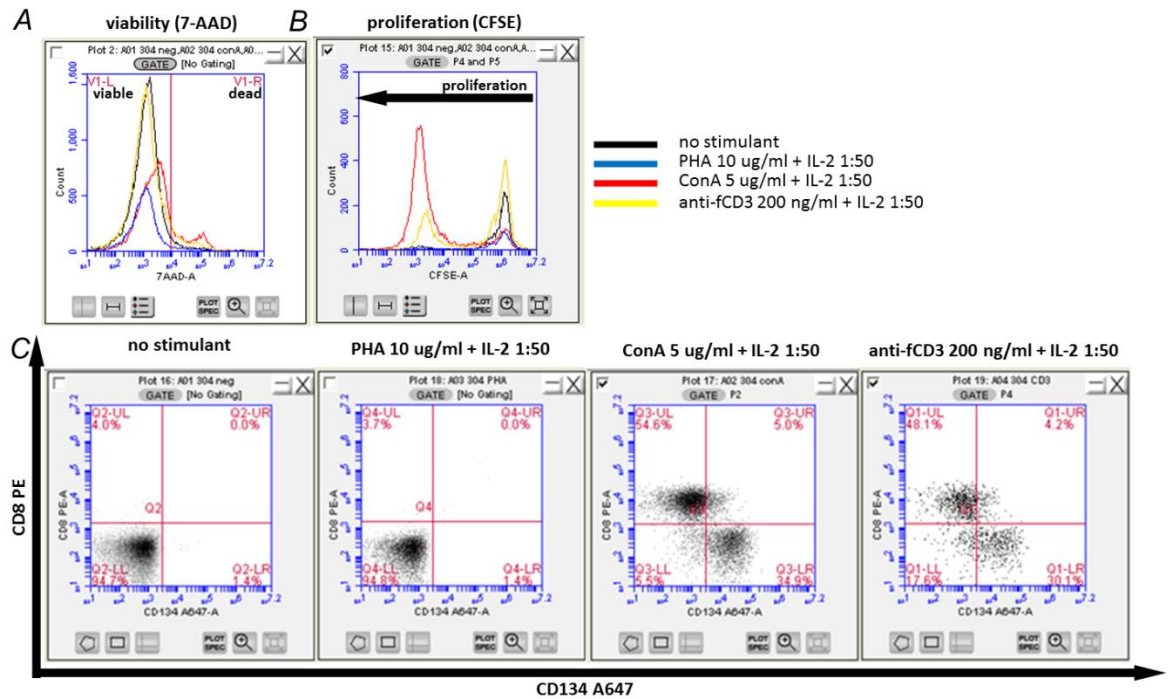
For more information or to download submission forms please visit our website at www.glasgow.ac.uk/vds

Residual samples may be used for approved research, test development or teaching.

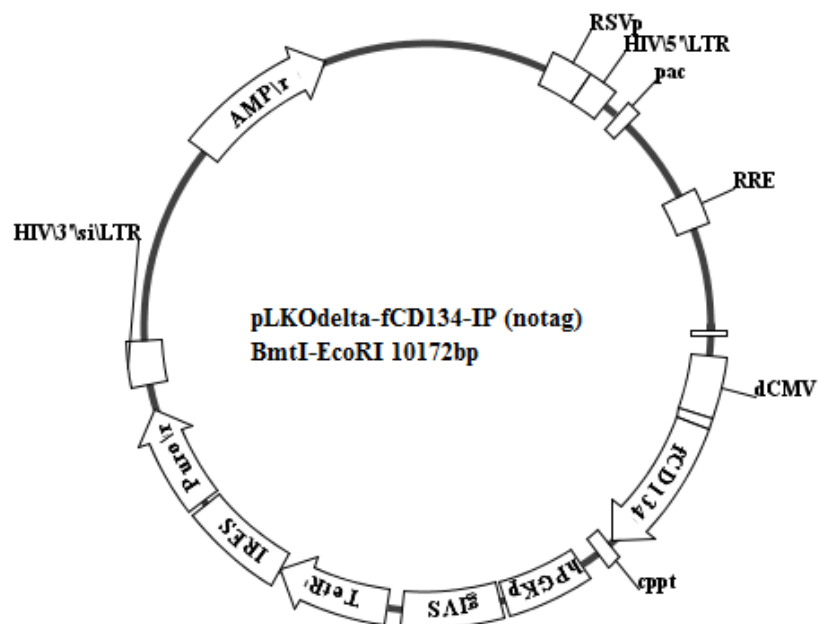
If the client indicates that they would prefer that residual samples are not used in this way, please check this box



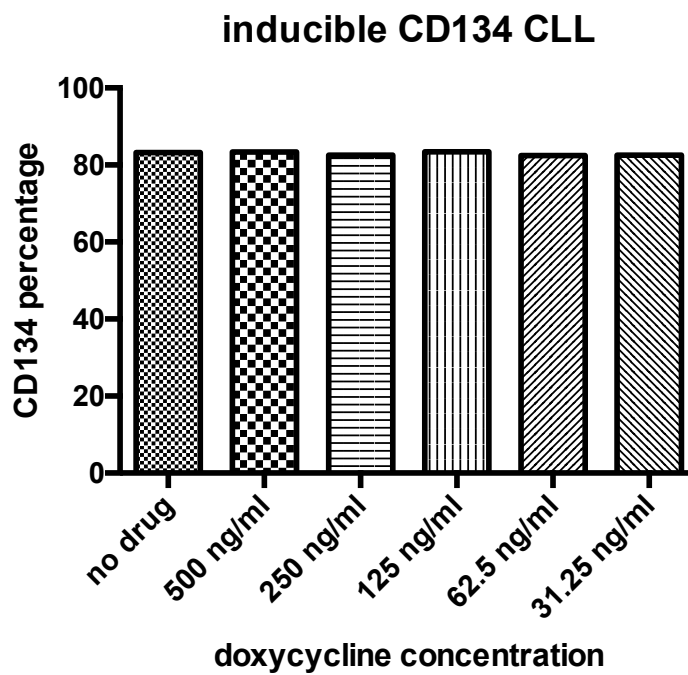
Appendix 5-1 Representative gating strategy and contour plots to identify lymphocyte subpopulations of mitogen-stimulated PBMC. Lymphocytes (P4) were identified by size (forward scatter area, FSC-A, X-axis) and granularity (size scatter area, SSC-A, y-axis) (**top left**). Single CD4 and CD8 positive T lymphocytes was identified by plotting CD4-FITC against CD8-PE (**bottom left**). Level of CXCR4 and CD134 expression on CD4⁺ (**top**) and CD8⁺ (**bottom**) T lymphocytes was determined by plotting either CD4-FITC or CD8-PE against CXCR4 (**middle**) and CD134 (**right**), respectively.



Appendix 5-2 Representative plots for the determination of viability (A), proliferation (B) and lymphocyte subpopulations (C) of PBMC cultures expanded from cat 310304, 7 days after isolation. Cell viability was determined by 7-aminoactinomycin D (7-AAD) staining, with 7-AAD positivity denoting dead cells (A). Cell proliferation was determined by carboxyfluorescein succinimidyl ester (CFSE) staining, in which CFSE positive cells were non-proliferative (B). PBMC with no stimulant was used to set the cut-off (black line). Each individual stimulant was defined using a different colour; PHA with IL-2 (blue), ConA with IL-2 (red) and anti-feline CD3 with IL-2 (yellow) (A, B).



Appendix 5-3 Map of Plasmid pLKO-fCD134-IP



Appendix 5-4 CD134 expression (as a percentage) of the inducible CD134 CLL cell line at different concentrations of doxycycline.

List of References

2013. *Consolidated Guidelines on the Use of Antiretroviral Drugs for Treating and Preventing HIV Infection: Recommendations for a Public Health Approach*. Geneva.
- ADDIE, D. D., DENNIS, J. M., TOTH, S., CALLANAN, J. J., REID, S. & JARRETT, O. 2000. Long-term impact on a closed household of pet cats of natural infection with feline coronavirus, feline leukaemia virus and feline immunodeficiency virus. *Vet Rec*, 146, 419-24.
- AFFRANCHINO, J. L. & GONZALEZ, S. A. 2010. In vitro assembly of the feline immunodeficiency virus Gag polyprotein. *Virus Res*, 150, 153-7.
- AFFRANCHINO, J. L. & GONZALEZ, S. A. 2014. Understanding the process of envelope glycoprotein incorporation into virions in simian and feline immunodeficiency viruses. *Viruses*, 6, 264-83.
- ALBRIGHT, A. V., SHIEH, J. T., ITOH, T., LEE, B., PLEASURE, D., O'CONNOR, M. J., DOMS, R. W. & GONZALEZ-SCARANO, F. 1999. Microglia express CCR5, CXCR4, and CCR3, but of these, CCR5 is the principal coreceptor for human immunodeficiency virus type 1 dementia isolates. *J Virol*, 73, 205-13.
- ALEXAKI, A., LIU, Y. & WIGDAHL, B. 2008. Cellular reservoirs of HIV-1 and their role in viral persistence. *Curr HIV Res*, 6, 388-400.
- BACH, J. M., HURTREL, M., CHAKRABARTI, L., GANIERE, J. P., MONTAGNIER, L. & HURTREL, B. 1994. Early stages of feline immunodeficiency virus infection in lymph nodes and spleen. *AIDS Res Hum Retroviruses*, 10, 1731-8.
- BACHMANN, M. H., MATHIASON-DUBARD, C., LEARN, G. H., RODRIGO, A. G., SODORA, D. L., MAZZETTI, P., HOOVER, E. A. & MULLINS, J. I. 1997. Genetic diversity of feline immunodeficiency virus: dual infection, recombination, and distinct evolutionary rates among envelope sequence clades. *J Virol*, 71, 4241-53.
- BAI, B., SONG, W., JI, Y., LIU, X., TIAN, L., WANG, C., CHEN, D., ZHANG, X. & ZHANG, M. 2009. Microglia and microglia-like cell differentiated from DC inhibit CD4 T cell proliferation. *PLoS One*, 4, e7869.
- BAJARIA, S. H., WEBB, G., CLOYD, M. & KIRSCHNER, D. 2002. Dynamics of naive and memory CD4⁺ T lymphocytes in HIV-1 disease progression. *J Acquir Immune Defic Syndr*, 30, 41-58.
- BALL, S. C., ABRAHA, A., COLLINS, K. R., MAROZSAN, A. J., BAIRD, H., QUINONES-MATEU, M. E., PENN-NICHOLSON, A., MURRAY, M., RICHARD, N., LOBRITZ, M., ZIMMERMAN, P. A., KAWAMURA, T., BLAUVELT, A. & ARTS, E. J. 2003. Comparing the ex vivo fitness of CCR5-tropic human immunodeficiency virus type 1 isolates of subtypes B and C. *J Virol*, 77, 1021-38.
- BANSAL-PAKALA, P., HALTEMAN, B. S., CHENG, M. H. & CROFT, M. 2004. Costimulation of CD8 T cell responses by OX40. *J Immunol*, 172, 4821-5.
- BAR, K. J., LI, H., CHAMBERLAND, A., TREMBLAY, C., ROUTY, J. P., GRAYSON, T., SUN, C., WANG, S., LEARN, G. H., MORGAN, C. J., SCHUMACHER, J. E., HAYNES, B. F., KEELE, B. F., HAHN, B. H. & SHAW, G. M. 2010. Wide variation in the multiplicity of HIV-1 infection among injection drug users. *J Virol*, 84, 6241-7.
- BEATTY, J. 2014. Viral causes of feline lymphoma: retroviruses and beyond. *Vet J*, 201, 174-80.
- BEATTY, J. A., WILLETT, B. J., GAULT, E. A. & JARRETT, O. 1996. A longitudinal study of feline immunodeficiency virus-specific cytotoxic T lymphocytes in

- experimentally infected cats, using antigen-specific induction. *J Virol*, 70, 6199-206.
- BECZKOWSKI, P. M. 2013. *Virus evolution in the progression of natural feline immunodeficiency virus infection*. Doctor of Philosophy, University of Glasgow.
- BECZKOWSKI, P. M., HUGHES, J., BIEK, R., LITSTER, A., WILLETT, B. J. & HOSIE, M. J. 2014a. Feline immunodeficiency virus (FIV) env recombinants are common in natural infections. *Retrovirology*, 11, 80.
- BECZKOWSKI, P. M., LITSTER, A., LIN, T. L., MELLOR, D. J., WILLETT, B. J. & HOSIE, M. J. 2015a. Contrasting clinical outcomes in two cohorts of cats naturally infected with feline immunodeficiency virus (FIV). *Vet Microbiol*, 176, 50-60.
- BECZKOWSKI, P. M., LOGAN, N., MCMONAGLE, E., LITSTER, A., WILLETT, B. J. & HOSIE, M. J. 2015b. An investigation of the breadth of neutralizing antibody response in cats naturally infected with feline immunodeficiency virus. *J Gen Virol*, 96, 671-80.
- BECZKOWSKI, P. M., TECHAKRIENGKRAI, N., LOGAN, N., MCMONAGLE, E., LITSTER, A., WILLETT, B. J. & HOSIE, M. J. 2014b. Emergence of CD134 cysteine-rich domain 2 (CRD2)-independent strains of feline immunodeficiency virus (FIV) is associated with disease progression in naturally infected cats. *Retrovirology*, 11, 95.
- BEEBE, A. M., DUA, N., FAITH, T. G., MOORE, P. F., PEDERSEN, N. C. & DANDEKAR, S. 1994. Primary stage of feline immunodeficiency virus infection: viral dissemination and cellular targets. *J Virol*, 68, 3080-91.
- BENDINELLI, M., PISTELLO, M., LOMBARDI, S., POLI, A., GARZELLI, C., MATTEUCCI, D., CECCHERINI-NELLI, L., MALVALDI, G. & TOZZINI, F. 1995. Feline immunodeficiency virus: an interesting model for AIDS studies and an important cat pathogen. *Clin Microbiol Rev*, 8, 87-112.
- BERGER, E. A., DOMS, R. W., FENYO, E. M., KORBER, B. T., LITTMAN, D. R., MOORE, J. P., SATTENTAU, Q. J., SCHUITEMAKER, H., SODROSKI, J. & WEISS, R. A. 1998. A new classification for HIV-1. *Nature*, 391, 240.
- BERGER, E. A., MURPHY, P. M. & FARBER, J. M. 1999. Chemokine receptors as HIV-1 coreceptors: roles in viral entry, tropism, and disease. *Annu Rev Immunol*, 17, 657-700.
- BIENZLE, D. 2014. FIV in cats--a useful model of HIV in people? *Vet Immunol Immunopathol*, 159, 171-9.
- BLAY, W. M., KASPRZYK, T., MISHER, L., RICHARDSON, B. A. & HAIGWOOD, N. L. 2007. Mutations in envelope gp120 can impact proteolytic processing of the gp160 precursor and thereby affect neutralization sensitivity of human immunodeficiency virus type 1 pseudoviruses. *J Virol*, 81, 13037-49.
- BLEUL, C. C., WU, L., HOXIE, J. A., SPRINGER, T. A. & MACKAY, C. R. 1997. The HIV coreceptors CXCR4 and CCR5 are differentially expressed and regulated on human T lymphocytes. *Proc Natl Acad Sci U S A*, 94, 1925-30.
- BLOM, B. & SPITS, H. 2006. Development of human lymphoid cells. *Annu Rev Immunol*, 24, 287-320.
- BODMER, J. L., SCHNEIDER, P. & TSCHOPP, J. 2002. The molecular architecture of the TNF superfamily. *Trends Biochem Sci*, 27, 19-26.
- BOETTLER, T., MOECKEL, F., CHENG, Y., HEEG, M., SALEK-ARDAKANI, S., CROTTY, S., CROFT, M. & VON HERRATH, M. G. 2012. OX40 facilitates control of a persistent virus infection. *PLoS Pathog*, 8, e1002913.
- BRANDENBERG, O. F., MAGNUS, C., REGOES, R. R. & TRKOLA, A. 2015a. The HIV-1 Entry Process: A Stoichiometric View. *Trends Microbiol*, 23, 763-74.

- BRANDENBERG, O. F., MAGNUS, C., RUSERT, P., REGOES, R. R. & TRKOLA, A. 2015b. Different infectivity of HIV-1 strains is linked to number of envelope trimers required for entry. *PLoS Pathog*, 11, e1004595.
- BRITES-ALVES, C., NETTO, E. M. & BRITES, C. 2015. Coinfection by Hepatitis C Is Strongly Associated with Abnormal CD4/CD8 Ratio in HIV Patients under Stable ART in Salvador, Brazil. *J Immunol Res*, 2015, 174215.
- BROOKS, D. G., KITCHEN, S. G., KITCHEN, C. M., SCRIPTURE-ADAMS, D. D. & ZACK, J. A. 2001. Generation of HIV latency during thymopoiesis. *Nat Med*, 7, 459-64.
- BROWN, W. C., BISSEY, L., LOGAN, K. S., PEDERSEN, N. C., ELDER, J. H. & COLLISSON, E. W. 1991. Feline immunodeficiency virus infects both CD4+ and CD8+ T lymphocytes. *J Virol*, 65, 3359-64.
- BRUNNER, D. & PEDERSEN, N. C. 1989. Infection of peritoneal macrophages in vitro and in vivo with feline immunodeficiency virus. *J Virol*, 63, 5483-8.
- BURKHARD, M. J. & DEAN, G. A. 2003. Transmission and immunopathogenesis of FIV in cats as a model for HIV. *Curr HIV Res*, 1, 15-29.
- CALLANAN, J. J., THOMPSON, H., TOTH, S. R., O'NEIL, B., LAWRENCE, C. E., WILLETT, B. & JARRETT, O. 1992. Clinical and pathological findings in feline immunodeficiency virus experimental infection. *Vet Immunol Immunopathol*, 35, 3-13.
- CAMPBELL, D. J., RAWLINGS, J. M., KOELSCH, S., WALLACE, J., STRAIN, J. J. & HANNIGAN, B. M. 2004. Age-related differences in parameters of feline immune status. *Vet Immunol Immunopathol*, 100, 73-80.
- CANESTRI, A., LESCURE, F. X., JAUREGUIBERRY, S., MOULIGNIER, A., AMIEL, C., MARCELIN, A. G., PEYTAVIN, G., TUBIANA, R., PIALOUX, G. & KATLAMA, C. 2010. Discordance between cerebral spinal fluid and plasma HIV replication in patients with neurological symptoms who are receiving suppressive antiretroviral therapy. *Clin Infect Dis*, 50, 773-8.
- CAVANAGH, L. L., BONASIO, R., MAZO, I. B., HALIN, C., CHENG, G., VAN DER VELDEN, A. W., CARIAPPA, A., CHASE, C., RUSSELL, P., STARNBACH, M. N., KONI, P. A., PILLAI, S., WENINGER, W. & VON ANDRIAN, U. H. 2005. Activation of bone marrow-resident memory T cells by circulating, antigen-bearing dendritic cells. *Nat Immunol*, 6, 1029-37.
- CHENEY, C. M., ROJKO, J. L., KOCIBA, G. J., WELLMAN, M. L., DI BARTOLA, S. P., REZANKA, L. J., FORMAN, L. & MATHES, L. E. 1990. A feline large granular lymphoma and its derived cell line. *In Vitro Cell Dev Biol*, 26, 455-63.
- CHHETRI, B. K., BERKE, O., PEARL, D. L. & BIENZLE, D. 2015. Comparison of risk factors for seropositivity to feline immunodeficiency virus and feline leukemia virus among cats: a case-case study. *BMC Vet Res*, 11, 30.
- CHOI, C. & BENVENISTE, E. N. 2004. Fas ligand/Fas system in the brain: regulator of immune and apoptotic responses. *Brain Res Brain Res Rev*, 44, 65-81.
- COCHRANE, A. W., CHEN, C. H. & ROSEN, C. A. 1990. Specific interaction of the human immunodeficiency virus Rev protein with a structured region in the env mRNA. *Proc Natl Acad Sci U S A*, 87, 1198-202.
- CONNOR, R. I., CHEN, B. K., CHOE, S. & LANDAU, N. R. 1995. Vpr is required for efficient replication of human immunodeficiency virus type-1 in mononuclear phagocytes. *Virology*, 206, 935-44.
- COURCHAMP, F. & PONTIER, D. 1994. Feline immunodeficiency virus: an epidemiological review. *C R Acad Sci III*, 317, 1123-34.
- CRIVELLATO, E., VACCA, A. & RIBATTI, D. 2004. Setting the stage: an anatomist's view of the immune system. *Trends Immunol*, 25, 210-7.

- CROFT, M. 2010. Control of immunity by the TNFR-related molecule OX40 (CD134). *Annu Rev Immunol*, 28, 57-78.
- CROFT, M. 2014. The TNF family in T cell differentiation and function--unanswered questions and future directions. *Semin Immunol*, 26, 183-90.
- DARDE, M. L., VILLENA, I., PINON, J. M. & BEGUINOT, I. 1998. Severe toxoplasmosis caused by a *Toxoplasma gondii* strain with a new isoenzyme type acquired in French Guyana. *J Clin Microbiol*, 36, 324.
- DAY, M. J. 2010. Ageing, immunosenescence and inflammaging in the dog and cat. *J Comp Pathol*, 142 Suppl 1, S60-9.
- DE PARSEVAL, A., CHATTERJI, U., MORRIS, G., SUN, P., OLSON, A. J. & ELDER, J. H. 2005. Structural mapping of CD134 residues critical for interaction with feline immunodeficiency virus. *Nat Struct Mol Biol*, 12, 60-6.
- DE PARSEVAL, A., CHATTERJI, U., SUN, P. & ELDER, J. H. 2004a. Feline immunodeficiency virus targets activated CD4+ T cells by using CD134 as a binding receptor. *Proc Natl Acad Sci U S A*, 101, 13044-9.
- DE PARSEVAL, A. & ELDER, J. H. 1999. Demonstration that orf2 encodes the feline immunodeficiency virus transactivating (Tat) protein and characterization of a unique gene product with partial rev activity. *J Virol*, 73, 608-17.
- DE PARSEVAL, A., GRANT, C. K., SASTRY, K. J. & ELDER, J. H. 2006. Sequential CD134-CXCR4 interactions in feline immunodeficiency virus (FIV): soluble CD134 activates FIV Env for CXCR4-dependent entry and reveals a cryptic neutralization epitope. *J Virol*, 80, 3088-91.
- DE PARSEVAL, A., NGO, S., SUN, P. & ELDER, J. H. 2004b. Factors that increase the effective concentration of CXCR4 dictate feline immunodeficiency virus tropism and kinetics of replication. *J Virol*, 78, 9132-43.
- DE SOUSA ABREU, R., PENALVA, L. O., MARCOTTE, E. M. & VOGEL, C. 2009. Global signatures of protein and mRNA expression levels. *Mol Biosyst*, 5, 1512-26.
- DEAN, G. A., REUBEL, G. H., MOORE, P. F. & PEDERSEN, N. C. 1996. Proviral burden and infection kinetics of feline immunodeficiency virus in lymphocyte subsets of blood and lymph node. *J Virol*, 70, 5165-9.
- DI ROSA, F. & PABST, R. 2005. The bone marrow: a nest for migratory memory T cells. *Trends Immunol*, 26, 360-6.
- DIEHL, L. J., MATHIASON-DUBARD, C. K., O'NEIL, L. L. & HOOVER, E. A. 1996. Plasma viral RNA load predicts disease progression in accelerated feline immunodeficiency virus infection. *J Virol*, 70, 2503-7.
- DIEHL, L. J., MATHIASON-DUBARD, C. K., O'NEIL, L. L., OBERT, L. A. & HOOVER, E. A. 1995. Induction of accelerated feline immunodeficiency virus disease by acute-phase virus passage. *J Virol*, 69, 6149-57.
- DIETRICH, I. 2012. *Feline Restriction Factors to Lentiviral Replication*. Doctor of Philosophy, University of Glasgow.
- DIETRICH, I., HOSIE, M. J. & WILLETT, B. J. 2011a. The role of BST2/tetherin in feline retrovirus infection. *Vet Immunol Immunopathol*, 143, 255-64.
- DIETRICH, I., MCEWAN, W. A., HOSIE, M. J. & WILLETT, B. J. 2011b. Restriction of the felid lentiviruses by a synthetic feline TRIM5-CypA fusion. *Vet Immunol Immunopathol*, 143, 235-42.
- DOUEK, D. C., ROEDERER, M. & KOUP, R. A. 2009. Emerging concepts in the immunopathogenesis of AIDS. *Annu Rev Med*, 60, 471-84.
- DOW, S. W., DREITZ, M. J. & HOOVER, E. A. 1992. Feline immunodeficiency virus neurotropism: evidence that astrocytes and microglia are the primary target cells. *Vet Immunol Immunopathol*, 35, 23-35.
- DOW, S. W., POSS, M. L. & HOOVER, E. A. 1990. Feline immunodeficiency virus: a neurotropic lentivirus. *J Acquir Immune Defic Syndr*, 3, 658-68.

- DUARTE, A. & TAVARES, L. 2006. Phylogenetic analysis of Portuguese Feline Immunodeficiency Virus sequences reveals high genetic diversity. *Vet Microbiol*, 114, 25-33.
- DUBEY, C., CROFT, M. & SWAIN, S. L. 1995. Costimulatory requirements of naive CD4⁺ T cells. ICAM-1 or B7-1 can costimulate naive CD4 T cell activation but both are required for optimum response. *J Immunol*, 155, 45-57.
- EGBERINK, H. F. & HORZINEK, M. C. 1992. Feline AIDS: symptoms and treatment. *Tijdschr Diergeneeskd*, 117 Suppl 1, 26S.
- EGBERINK, H. F., KELDERMANS, C. E., KOOLEN, M. J. & HORZINEK, M. C. 1992. Humoral immune response to feline immunodeficiency virus in cats with experimentally induced and naturally acquired infections. *Am J Vet Res*, 53, 1133-8.
- ELDER, J. H., LERNER, D. L., HASSELKUS-LIGHT, C. S., FONTENOT, D. J., HUNTER, E., LUCIW, P. A., MONTELARO, R. C. & PHILLIPS, T. R. 1992. Distinct subsets of retroviruses encode dUTPase. *J Virol*, 66, 1791-4.
- ELDER, J. H. & PHILLIPS, T. R. 1995. The genomic organization of feline immunodeficiency virus. In: WILLETT, B. J. & JARRETT, O. (eds.) *Feline immunology and immunodeficiency*. Oxford, Great Britain: Oxford University Press.
- ELDER, J. H., SUNDSTROM, M., DE ROZIERES, S., DE PARSEVAL, A., GRANT, C. K. & LIN, Y. C. 2008. Molecular mechanisms of FIV infection. *Vet Immunol Immunopathol*, 123, 3-13.
- ENGLISH, R. V., JOHNSON, C. M., GEBHARD, D. H. & TOMPKINS, M. B. 1993. In vivo lymphocyte tropism of feline immunodeficiency virus. *J Virol*, 67, 5175-86.
- ENGLISH, R. V., NELSON, P., JOHNSON, C. M., NASISSE, M., TOMPKINS, W. A. & TOMPKINS, M. B. 1994. Development of clinical disease in cats experimentally infected with feline immunodeficiency virus. *J Infect Dis*, 170, 543-52.
- EVANS, D. E., PRELL, R. A., THALHOFER, C. J., HURWITZ, A. A. & WEINBERG, A. D. 2001. Engagement of OX40 enhances antigen-specific CD4(+) T cell mobilization/memory development and humoral immunity: comparison of alphaOX-40 with alphaCTLA-4. *J Immunol*, 167, 6804-11.
- FAUCI, A. S. 1993. Multifactorial nature of human immunodeficiency virus disease: implications for therapy. *Science*, 262, 1011-8.
- FENG, Y., BRODER, C. C., KENNEDY, P. E. & BERGER, E. A. 1996. HIV-1 entry cofactor: functional cDNA cloning of a seven-transmembrane, G protein-coupled receptor. *Science*, 272, 872-7.
- FINZI, D., BLANKSON, J., SILICIANO, J. D., MARGOLICK, J. B., CHADWICK, K., PIERSON, T., SMITH, K., LISZIEWICZ, J., LORI, F., FLEXNER, C., QUINN, T. C., CHAISSON, R. E., ROSENBERG, E., WALKER, B., GANGE, S., GALLANT, J. & SILICIANO, R. F. 1999. Latent infection of CD4⁺ T cells provides a mechanism for lifelong persistence of HIV-1, even in patients on effective combination therapy. *Nat Med*, 5, 512-7.
- FLETCHER, N. F., MEEKER, R. B., HUDSON, L. C. & CALLANAN, J. J. 2011. The neuropathogenesis of feline immunodeficiency virus infection: barriers to overcome. *Vet J*, 188, 260-9.
- FLINT, S. J., RACANIELLO, V. R., RALL, G. F., SKALKA, A. M. & ENQUIST, L. W. 2015. *Principles of virology*, Washington, DC, ASM Press.
- FLYNN, J. N., BEATTY, J. A., CANNON, C. A., STEPHENS, E. B., HOSIE, M. J., NEIL, J. C. & JARRETT, O. 1995a. Involvement of gag- and env-specific cytotoxic T lymphocytes in protective immunity to feline immunodeficiency virus. *AIDS Res Hum Retroviruses*, 11, 1107-13.

- FLYNN, J. N., CANNON, C. A., REID, G., RIGBY, M. A., NEIL, J. C. & JARRETT, O. 1995b. Induction of feline immunodeficiency virus-specific cell-mediated and humoral immune responses following immunization with a multiple antigenic peptide from the envelope V3 domain. *Immunology*, 85, 171-5.
- FLYNN, J. N., DUNHAM, S., MUELLER, A., CANNON, C. & JARRETT, O. 2002. Involvement of cytolytic and non-cytolytic T cells in the control of feline immunodeficiency virus infection. *Vet Immunol Immunopathol*, 85, 159-70.
- FOURATI, S., LAMBERT-NICLOT, S., SOULIE, C., WIRDEN, M., MALET, I., VALANTIN, M. A., TUBIANA, R., SIMON, A., KATLAMA, C., CARCELAIN, G., CALVEZ, V. & MARCELIN, A. G. 2014. Differential impact of APOBEC3-driven mutagenesis on HIV evolution in diverse anatomical compartments. *AIDS*, 28, 487-91.
- GARDNER, M. B. 1991. Simian and feline immunodeficiency viruses: animal lentivirus models for evaluation of AIDS vaccines and antiviral agents. *Antiviral Res*, 15, 267-86.
- GEMENIANO, M. C., SAWAI, E. T., LEUTENEGGER, C. M. & SPARGER, E. E. 2003. Feline immunodeficiency virus ORF-Ais required for virus particle formation and virus infectivity. *J Virol*, 77, 8819-30.
- GEMENIANO, M. C., SAWAI, E. T. & SPARGER, E. E. 2004. Feline immunodeficiency virus Orf-A localizes to the nucleus and induces cell cycle arrest. *Virology*, 325, 167-74.
- GERARD, C. & ROLLINS, B. J. 2001. Chemokines and disease. *Nat Immunol*, 2, 108-15.
- GESKUS, R. B., PRINS, M., HUBERT, J. B., MIEDEMA, F., BERKHOUT, B., ROUZIOUX, C., DELFRAISSY, J. F. & MEYER, L. 2007. The HIV RNA setpoint theory revisited. *Retrovirology*, 4, 65.
- GOTO, Y., NISHIMURA, Y., BABA, K., MIZUNO, T., ENDO, Y., MASUDA, K., OHNO, K. & TSUJIMOTO, H. 2002. Association of plasma viral RNA load with prognosis in cats naturally infected with feline immunodeficiency virus. *J Virol*, 76, 10079-83.
- GOULDER, P. J. & WATKINS, D. I. 2004. HIV and SIV CTL escape: implications for vaccine design. *Nat Rev Immunol*, 4, 630-40.
- GRAHAM, F. L., SMILEY, J., RUSSELL, W. C. & NAIRN, R. 1977. Characteristics of a human cell line transformed by DNA from human adenovirus type 5. *J Gen Virol*, 36, 59-74.
- GRAMAGLIA, I., JEMBER, A., PIPPIG, S. D., WEINBERG, A. D., KILLEEN, N. & CROFT, M. 2000. The OX40 costimulatory receptor determines the development of CD4 memory by regulating primary clonal expansion. *J Immunol*, 165, 3043-50.
- GRAMAGLIA, I., WEINBERG, A. D., LEMON, M. & CROFT, M. 1998. Ox-40 ligand: a potent costimulatory molecule for sustaining primary CD4 T cell responses. *J Immunol*, 161, 6510-7.
- GROSS, L. A., BAIRD, G. S., HOFFMAN, R. C., BALDRIDGE, K. K. & TSIEN, R. Y. 2000. The structure of the chromophore within DsRed, a red fluorescent protein from coral. *Proc Natl Acad Sci U S A*, 97, 11990-5.
- GROSSMAN, Z., MEIER-SCHELLERSHEIM, M., PAUL, W. E. & PICKER, L. J. 2006. Pathogenesis of HIV infection: what the virus spares is as important as what it destroys. *Nat Med*, 12, 289-95.
- GUPTA, S., NEOGI, U., SRINIVASA, H. & SHET, A. 2015. Performance of genotypic tools for prediction of tropism in HIV-1 subtype C V3 loop sequences. *Intervirology*, 58, 1-5.

- HAASE, A. T. 1999. Population biology of HIV-1 infection: viral and CD4⁺ T cell demographics and dynamics in lymphatic tissues. *Annu Rev Immunol*, 17, 625-56.
- HALL, T. A. 1999. Bioedit: a user-friendly biological sequence alignment editor and analysis program for Window 95/98/NT. *Nucl. Acids. Symp. Ser*, 41, 95-98.
- HARDING, F. A., MCARTHUR, J. G., GROSS, J. A., RAULET, D. H. & ALLISON, J. P. 1992. CD28-mediated signalling co-stimulates murine T cells and prevents induction of anergy in T-cell clones. *Nature*, 356, 607-9.
- HARRISON, S. C. 2015. Viral membrane fusion. *Virology*, 479-480, 498-507.
- HARRISON, T. M., MAZET, J. K., HOLEKAMP, K. E., DUBOVI, E., ENGH, A. L., NELSON, K., VAN HORN, R. C. & MUNSON, L. 2004. Antibodies to canine and feline viruses in spotted hyenas (*Crocuta crocuta*) in the Masai Mara National Reserve. *J Wildl Dis*, 40, 1-10.
- HARTIKKA, J., SAWDEY, M., CORNEFERT-JENSEN, F., MARGALITH, M., BARNHART, K., NOLASCO, M., VAHLSING, H. L., MEEK, J., MARQUET, M., HOBART, P., NORMAN, J. & MANTHORPE, M. 1996. An improved plasmid DNA expression vector for direct injection into skeletal muscle. *Hum Gene Ther*, 7, 1205-17.
- HARTMANN, K. 1998. Feline immunodeficiency virus infection: an overview. *Vet J*, 155, 123-37.
- HARTMANN, K. 2012. Clinical aspects of feline retroviruses: a review. *Viruses*, 4, 2684-710.
- HAYWARD, J. J. & RODRIGO, A. G. 2008. Recombination in feline immunodeficiency virus from feral and companion domestic cats. *Virol J*, 5, 76.
- HAYWARD, J. J. & RODRIGO, A. G. 2010a. The distribution of feline immunodeficiency virus in tissue compartments of feral domestic cats. *Arch Virol*, 155, 411-6.
- HAYWARD, J. J. & RODRIGO, A. G. 2010b. Molecular epidemiology of feline immunodeficiency virus in the domestic cat (*Felis catus*). *Vet Immunol Immunopathol*, 134, 68-74.
- HAYWARD, J. J., TAYLOR, J. & RODRIGO, A. G. 2007. Phylogenetic analysis of feline immunodeficiency virus in feral and companion domestic cats of New Zealand. *J Virol*, 81, 2999-3004.
- HE, J., CHOE, S., WALKER, R., DI MARZIO, P., MORGAN, D. O. & LANDAU, N. R. 1995. Human immunodeficiency virus type 1 viral protein R (Vpr) arrests cells in the G2 phase of the cell cycle by inhibiting p34cdc2 activity. *J Virol*, 69, 6705-11.
- HE, J. & LANDAU, N. R. 1995. Use of a novel human immunodeficiency virus type 1 reporter virus expressing human placental alkaline phosphatase to detect an alternative viral receptor. *J Virol*, 69, 4587-92.
- HEATON, P. R., BLOUNT, D. G., DEVLIN, P., KOELSCH, S., MANN, S. J., SMITH, B. H., STEVENSON, J. & HARPER, E. J. 2002. Assessing age-related changes in peripheral blood leukocyte phenotypes in Labrador retriever dogs using flow cytometry. *J Nutr*, 132, 1655S-7S.
- HEL, Z., MCGHEE, J. R. & MESTECKY, J. 2006. HIV infection: first battle decides the war. *Trends Immunol*, 27, 274-81.
- HERRERA, C., KLASSE, P. J., MICHAEL, E., KAKE, S., BARNES, K., KIBLER, C. W., CAMPBELL-GARDENER, L., SI, Z., SODROSKI, J., MOORE, J. P. & BEDDOWS, S. 2005. The impact of envelope glycoprotein cleavage on the antigenicity, infectivity, and neutralization sensitivity of Env-pseudotyped human immunodeficiency virus type 1 particles. *Virology*, 338, 154-72.

- HONG, Y., FINK, E., HU, Q. Y., KIOSSES, W. B. & ELDER, J. H. 2010. OrfA downregulates feline immunodeficiency virus primary receptor CD134 on the host cell surface and is important in viral infection. *J Virol*, 84, 7225-32.
- HORI, T. 2005. Roles of OX40 in the pathogenesis and the control of disease. *International journal of hematology*, 83, 6.
- HOSIE, M. J., ADDIE, D., BELAK, S., BOUCRAUT-BARALON, C., EGBERINK, H., FRYMUS, T., GRUFFYDD-JONES, T., HARTMANN, K., LLORET, A., LUTZ, H., MARSILIO, F., PENNISI, M. G., RADFORD, A. D., THIRY, E., TRUYEN, U. & HORZINEK, M. C. 2009. Feline immunodeficiency. ABCD guidelines on prevention and management. *J Feline Med Surg*, 11, 575-84.
- HOSIE, M. J., BROERE, N., HESSELGESSER, J., TURNER, J. D., HOXIE, J. A., NEIL, J. C. & WILLETT, B. J. 1998. Modulation of feline immunodeficiency virus infection by stromal cell-derived factor. *J Virol*, 72, 2097-104.
- HOSIE, M. J., DUNSFORD, T., KLEIN, D., WILLETT, B. J., CANNON, C., OSBORNE, R., MACDONALD, J., SPIBEY, N., MACKAY, N., JARRETT, O. & NEIL, J. C. 2000. Vaccination with inactivated virus but not viral DNA reduces virus load following challenge with a heterologous and virulent isolate of feline immunodeficiency virus. *J Virol*, 74, 9403-11.
- HOSIE, M. J. & JARRETT, O. 1990. Serological responses of cats to feline immunodeficiency virus. *AIDS*, 4, 215-20.
- HOSIE, M. J., PAJEK, D., SAMMAN, A. & WILLETT, B. J. 2011. Feline immunodeficiency virus (FIV) neutralization: a review. *Viruses*, 3, 1870-90.
- HOSIE, M. J., ROBERTSON, C. & JARRETT, O. 1989. Prevalence of feline leukaemia virus and antibodies to feline immunodeficiency virus in cats in the United Kingdom. *Vet Rec*, 125, 293-7.
- HOSIE, M. J., WILLETT, B. J., KLEIN, D., DUNSFORD, T. H., CANNON, C., SHIMOJIMA, M., NEIL, J. C. & JARRETT, O. 2002. Evolution of replication efficiency following infection with a molecularly cloned feline immunodeficiency virus of low virulence. *J Virol*, 76, 6062-72.
- HU, Q. Y., FINK, E. & ELDER, J. H. 2012. Mapping of Receptor Binding Interactions with the FIV surface Glycoprotein (SU); Implications Regarding Immune surveillance and cellular Targets of Infection. *Retrovirology (Auckl)*, 2012, 1-11.
- HU, Q. Y., FINK, E., HONG, Y., WANG, C., GRANT, C. K. & ELDER, J. H. 2010. Fine definition of the CXCR4-binding region on the V3 loop of feline immunodeficiency virus surface glycoprotein. *PLoS One*, 5, e10689.
- HUA, W., JIAO, Y., ZHANG, H., ZHANG, T., CHEN, D., ZHANG, Y., CHEN, X. & WU, H. 2012. Central memory CD4 cells are an early indicator of immune reconstitution in HIV/AIDS patients with anti-retroviral treatment. *Immunol Invest*, 41, 1-14.
- HURTREL, B., CHAKRABARTI, L., HURTREL, M., BACH, J. M., GANIERE, J. P. & MONTAGNIER, L. 1994. Early events in lymph nodes during infection with SIV and FIV. *Res Virol*, 145, 221-7.
- IKEDA, Y., MIYAZAWA, T., NISHIMURA, Y., NAKAMURA, K., TOHYA, Y. & MIKAMI, T. 2004. High genetic stability of TM1 and TM2 strains of subtype B feline immunodeficiency virus in long-term infection. *J Vet Med Sci*, 66, 287-9.
- ISHII, T., NISHIHARA, M., MA, F., EBIHARA, Y., TSUJI, K., ASANO, S., NAKAHATA, T. & MAEKAWA, T. 1999. Expression of stromal cell-derived factor-1/pre-B cell growth-stimulating factor receptor, CXC chemokine receptor 4, on CD34+ human bone marrow cells is a phenotypic alteration for committed lymphoid progenitors. *J Immunol*, 163, 3612-20.

- JORDAN, H. L., HOWARD, J., BARR, M. C., KENNEDY-STOSKOPF, S., LEVY, J. K. & TOMPKINS, W. A. 1998a. Feline immunodeficiency virus is shed in semen from experimentally and naturally infected cats. *AIDS Res Hum Retroviruses*, 14, 1087-92.
- JORDAN, H. L., HOWARD, J. G., BUCCI, J. G., BUTTERWORTH, J. L., ENGLISH, R., KENNEDY-STOSKOPF, S., TOMPKINS, M. B. & TOMPKINS, W. A. 1998b. Horizontal transmission of feline immunodeficiency virus with semen from seropositive cats. *J Reprod Immunol*, 41, 341-57.
- KAKINUMA, S., MOTOKAWA, K., HOHDATSU, T., YAMAMOTO, J. K., KOYAMA, H. & HASHIMOTO, H. 1995. Nucleotide sequence of feline immunodeficiency virus: classification of Japanese isolates into two subtypes which are distinct from non-Japanese subtypes. *J Virol*, 69, 3639-46.
- KANG, Y., MORESSI, C. J., SCHEETZ, T. E., XIE, L., TRAN, D. T., CASAVANT, T. L., AK, P., BENHAM, C. J., DAVIDSON, B. L. & MCCRAY, P. B., JR. 2006. Integration site choice of a feline immunodeficiency virus vector. *J Virol*, 80, 8820-3.
- KARRIS, M. A. & SMITH, D. M. 2011. Tissue-specific HIV-1 infection: why it matters. *Future Virol*, 6, 869-882.
- KEAWCHAROEN, J., WATTANADORN, S., PUSOONTHRONTHUM, R. & ORAVEERAKUL, K. Phylogenetic analysis of a feline immunodeficiency virus isolated from a Thai cat. the Annual Conference of the Faculty of Veterinary Science, Chulalongkorn University, 2006 Bangkok, Thailand.
- KEELE, B. F., GIORGI, E. E., SALAZAR-GONZALEZ, J. F., DECKER, J. M., PHAM, K. T., SALAZAR, M. G., SUN, C., GRAYSON, T., WANG, S., LI, H., WEI, X., JIANG, C., KIRCHHERR, J. L., GAO, F., ANDERSON, J. A., PING, L. H., SWANSTROM, R., TOMARAS, G. D., BLATTNER, W. A., GOEPFERT, P. A., KILBY, J. M., SAAG, M. S., DELWART, E. L., BUSCH, M. P., COHEN, M. S., MONTEFIORI, D. C., HAYNES, B. F., GASCHEN, B., ATHREYA, G. S., LEE, H. Y., WOOD, N., SEOIGHE, C., PERELSON, A. S., BHATTACHARYA, T., KORBER, B. T., HAHN, B. H. & SHAW, G. M. 2008. Identification and characterization of transmitted and early founder virus envelopes in primary HIV-1 infection. *Proc Natl Acad Sci U S A*, 105, 7552-7.
- KEMAL, K. S., FOLEY, B., BURGER, H., ANASTOS, K., MINKOFF, H., KITCHEN, C., PHILPOTT, S. M., GAO, W., ROBISON, E., HOLMAN, S., DEHNER, C., BECK, S., MEYER, W. A., 3RD, LANDAY, A., KOVACS, A., BREMER, J. & WEISER, B. 2003. HIV-1 in genital tract and plasma of women: compartmentalization of viral sequences, coreceptor usage, and glycosylation. *Proc Natl Acad Sci U S A*, 100, 12972-7.
- KENYON, J. C. & LEVER, A. M. 2011. The molecular biology of feline immunodeficiency virus (FIV). *Viruses*, 3, 2192-213.
- KITCHEN, S. G. & ZACK, J. A. 1997. CXCR4 expression during lymphopoiesis: implications for human immunodeficiency virus type 1 infection of the thymus. *J Virol*, 71, 6928-34.
- KLASSE, P. J. 2012. The molecular basis of HIV entry. *Cell Microbiol*, 14, 1183-92.
- KLATT, N. R., VILLINGER, F., BOSTIK, P., GORDON, S. N., PEREIRA, L., ENGRAM, J. C., MAYNE, A., DUNHAM, R. M., LAWSON, B., RATCLIFFE, S. J., SODORA, D. L., ELSE, J., REIMANN, K., STAPRANS, S. I., HAASE, A. T., ESTES, J. D., SILVESTRI, G. & ANSARI, A. A. 2008. Availability of activated CD4+ T cells dictates the level of viremia in naturally SIV-infected sooty mangabeys. *J Clin Invest*, 118, 2039-49.
- KLEIN, D., JANDA, P., STEINBORN, R., MULLER, M., SALMONS, B. & GUNZBURG, W. H. 1999. Proviral load determination of different feline immunodeficiency virus isolates using real-time polymerase chain

- reaction: influence of mismatches on quantification. *Electrophoresis*, 20, 291-9.
- KOHMOTO, M., UETSUKA, K., IKEDA, Y., INOSHIMA, Y., SHIMOJIMA, M., SATO, E., INADA, G., TOYOSAKI, T., MIYAZAWA, T., DOI, K. & MIKAMI, T. 1998. Eight-year observation and comparative study of specific pathogen-free cats experimentally infected with feline immunodeficiency virus (FIV) subtypes A and B: terminal acquired immunodeficiency syndrome in a cat infected with FIV petaluma strain. *J Vet Med Sci*, 60, 315-21.
- KOLENDA-ROBERTS, H. M., KUHN, L. A., JENNINGS, R. N., MERGIA, A., GENGOZIAN, N. & JOHNSON, C. M. 2007. Immunopathogenesis of feline immunodeficiency virus infection in the fetal and neonatal cat. *Front Biosci*, 12, 3668-82.
- KORNYA, M. R., LITTLE, S. E., SCHERK, M. A., SEARS, W. C. & BIENZLE, D. 2014. Association between oral health status and retrovirus test results in cats. *J Am Vet Med Assoc*, 245, 916-22.
- KRAASE, M., SLOAN, R., KLEIN, D., LOGAN, N., MCMONAGLE, L., BIEK, R., WILLETT, B. J. & HOSIE, M. J. 2010. Feline immunodeficiency virus env gene evolution in experimentally infected cats. *Vet Immunol Immunopathol*, 134, 96-106.
- KRAUS, L. A., BRADLEY, W. G., ENGELMAN, R. W., BROWN, K. M., GOOD, R. A. & DAY, N. K. 1996. Relationship between tumor necrosis factor alpha and feline immunodeficiency virus expressions. *J Virol*, 70, 566-9.
- KUHMANN, S. E., PLATT, E. J., KOZAK, S. L. & KABAT, D. 2000. Cooperation of multiple CCR5 coreceptors is required for infections by human immunodeficiency virus type 1. *J Virol*, 74, 7005-15.
- LAGANA, D. M., LEE, J. S., LEWIS, J. S., BEVINS, S. N., CARVER, S., SWEANOR, L. L., MCBRIDE, R., MCBRIDE, C., CROOKS, K. R. & VANDEWOUDE, S. 2013. Characterization of regionally associated feline immunodeficiency virus (FIV) in bobcats (*Lynx rufus*). *J Wildl Dis*, 49, 718-22.
- LAMBELE, M., LABROSSE, B., ROCH, E., MOREAU, A., VERRIER, B., BARIN, F., ROINGEARD, P., MAMMANO, F. & BRAND, D. 2007. Impact of natural polymorphism within the gp41 cytoplasmic tail of human immunodeficiency virus type 1 on the intracellular distribution of envelope glycoproteins and viral assembly. *J Virol*, 81, 125-40.
- LAMBOTTE, O., CHAIX, M. L., GUBLER, B., NASREDDINE, N., WALLON, C., GOUJARD, C., ROUZIQUX, C., TAOUFIK, Y. & DELFRAISSY, J. F. 2004. The lymphocyte HIV reservoir in patients on long-term HAART is a memory of virus evolution. *AIDS*, 18, 1147-58.
- LAPPIN, M. R., GEORGE, J. W., PEDERSEN, N. C., BARLOUGH, J. E., MURPHY, C. J. & MORSE, L. S. 1996. Primary and secondary *Toxoplasma gondii* infection in normal and feline immunodeficiency virus-infected cats. *J Parasitol*, 82, 733-42.
- LEE, B., SHARRON, M., MONTANER, L. J., WEISSMAN, D. & DOMS, R. W. 1999. Quantification of CD4, CCR5, and CXCR4 levels on lymphocyte subsets, dendritic cells, and differentially conditioned monocyte-derived macrophages. *Proc Natl Acad Sci U S A*, 96, 5215-20.
- LERNER, D. L., WAGAMAN, P. C., PHILLIPS, T. R., PROSPERO-GARCIA, O., HENRIKSEN, S. J., FOX, H. S., BLOOM, F. E. & ELDER, J. H. 1995. Increased mutation frequency of feline immunodeficiency virus lacking functional deoxyuridine-triphosphatase. *Proc Natl Acad Sci U S A*, 92, 7480-4.
- LEUTENEGGER, C. M., KLEIN, D., HOFMANN-LEHMANN, R., MISLIN, C., HUMMEL, U., BONI, J., BORETTI, F., GUENZBURG, W. H. & LUTZ, H. 1999. Rapid feline immunodeficiency virus provirus quantitation by polymerase chain

- reaction using the TaqMan fluorogenic real-time detection system. *J Virol Methods*, 78, 105-16.
- LEVY, J. K., SCOTT, H. M., LACHTARA, J. L. & CRAWFORD, P. C. 2006. Seroprevalence of feline leukemia virus and feline immunodeficiency virus infection among cats in North America and risk factors for seropositivity. *J Am Vet Med Assoc*, 228, 371-6.
- LIMA, M., ALMEIDA, J., DOS ANJOS TEIXEIRA, M., ALGUERO MD MDEL, C., SANTOS, A. H., BALANZATEGUI, A., QUEIROS, M. L., BARCENA, P., IZARRA, A., FONSECA, S., BUENO, C., JUSTICA, B., GONZALEZ, M., SAN MIGUEL, J. F. & ORFAO, A. 2003. TCRalpha⁺/CD4⁺ large granular lymphocytosis: a new clonal T-cell lymphoproliferative disorder. *Am J Pathol*, 163, 763-71.
- LIN, D. S., BOWMAN, D. D. & JACOBSON, R. H. 1992. Immunological changes in cats with concurrent *Toxoplasma gondii* and feline immunodeficiency virus infections. *J Clin Microbiol*, 30, 17-24.
- LITSTER, A., LIN, J. M., NICHOLS, J. & WENG, H. Y. 2014. Diagnostic utility of CD4⁺:CD8⁺ low% T-lymphocyte ratio to differentiate feline immunodeficiency virus (FIV)-infected from FIV-vaccinated cats. *Vet Microbiol*, 170, 197-205.
- LIU, P., HUDSON, L. C., TOMPKINS, M. B., VAHLENKAMP, T. W. & MEEKER, R. B. 2006. Compartmentalization and evolution of feline immunodeficiency virus between the central nervous system and periphery following intracerebroventricular or systemic inoculation. *J Neurovirol*, 12, 307-21.
- LUTTGE, B. G. & FREED, E. O. 2010. FIV Gag: virus assembly and host-cell interactions. *Vet Immunol Immunopathol*, 134, 3-13.
- MAHALANABIS, M., JAYARAMAN, P., MIURA, T., PEREYRA, F., CHESTER, E. M., RICHARDSON, B., WALKER, B. & HAIGWOOD, N. L. 2009. Continuous viral escape and selection by autologous neutralizing antibodies in drug-naive human immunodeficiency virus controllers. *J Virol*, 83, 662-72.
- MAIER, T., GUELL, M. & SERRANO, L. 2009. Correlation of mRNA and protein in complex biological samples. *FEBS Lett*, 583, 3966-73.
- MALIM, M. H. & EMERMAN, M. 2008. HIV-1 accessory proteins--ensuring viral survival in a hostile environment. *Cell Host Microbe*, 3, 388-98.
- MALLET, S., FOSSUM, S. & BARCLAY, A. N. 1990. Characterization of the MRC OX40 antigen of activated CD4 positive T lymphocytes--a molecule related to nerve growth factor receptor. *EMBO J*, 9, 1063-8.
- MANSKY, L. M., PREVERAL, S., SELIG, L., BENAROUS, R. & BENICHO, S. 2000. The interaction of vpr with uracil DNA glycosylase modulates the human immunodeficiency virus type 1 In vivo mutation rate. *J Virol*, 74, 7039-47.
- MARCHETTI, G., TINCATI, C. & SILVESTRI, G. 2013. Microbial translocation in the pathogenesis of HIV infection and AIDS. *Clin Microbiol Rev*, 26, 2-18.
- MARGOLIS, L. & SHATTOCK, R. 2006. Selective transmission of CCR5-utilizing HIV-1: the 'gatekeeper' problem resolved? *Nat Rev Microbiol*, 4, 312-7.
- MARSH, M. & HELENIUS, A. 1989. Virus entry into animal cells. *Adv Virus Res*, 36, 107-51.
- MASCOLINI, M. 2014. Low CD4/CD8 ratio predicts non-AIDS illness in large Italian cohort. *Conference on Retroviruses and Opportunistic Infections*. Boston, MA, USA.
- MASSA, P. T. 1993. Specific suppression of major histocompatibility complex class I and class II genes in astrocytes by brain-enriched gangliosides. *J Exp Med*, 178, 1357-63.
- MASSA, P. T., OZATO, K. & MCFARLIN, D. E. 1993. Cell type-specific regulation of major histocompatibility complex (MHC) class I gene expression in astrocytes, oligodendrocytes, and neurons. *Glia*, 8, 201-7.

- MATTAPALLIL, J. J., DOUEK, D. C., HILL, B., NISHIMURA, Y., MARTIN, M. & ROEDERER, M. 2005. Massive infection and loss of memory CD4⁺ T cells in multiple tissues during acute SIV infection. *Nature*, 434, 1093-7.
- MAZO, I. B., HONCZARENKO, M., LEUNG, H., CAVANAGH, L. L., BONASIO, R., WENINGER, W., ENGELKE, K., XIA, L., MCEVER, R. P., KONI, P. A., SILBERSTEIN, L. E. & VON ANDRIAN, U. H. 2005. Bone marrow is a major reservoir and site of recruitment for central memory CD8⁺ T cells. *Immunity*, 22, 259-70.
- MCCUNE, J. M., RABIN, L. B., FEINBERG, M. B., LIEBERMAN, M., KOSEK, J. C., REYES, G. R. & WEISSMAN, I. L. 1988. Endoproteolytic cleavage of gp160 is required for the activation of human immunodeficiency virus. *Cell*, 53, 55-67.
- MCDONNELL, S. J., SPARGER, E. E. & MURPHY, B. G. 2013. Feline immunodeficiency virus latency. *Retrovirology*, 10, 69.
- MCEWAN, W. A., MCMONAGLE, E. L., LOGAN, N., SERRA, R. C., KAT, P., VANDEWOUDE, S., HOSIE, M. J. & WILLETT, B. J. 2008. Genetically divergent strains of feline immunodeficiency virus from the domestic cat (*Felis catus*) and the African lion (*Panthera leo*) share usage of CD134 and CXCR4 as entry receptors. *J Virol*, 82, 10953-8.
- MCKNIGHT, A. & CLAPHAM, P. R. 1995. Immune escape and tropism of HIV. *Trends Microbiol*, 3, 356-61.
- MCKNIGHT, A., WEISS, R. A., SHOTTON, C., TAKEUCHI, Y., HOSHINO, H. & CLAPHAM, P. R. 1995. Change in tropism upon immune escape by human immunodeficiency virus. *J Virol*, 69, 3167-70.
- MEBIUS, R. E. & KRAAL, G. 2005. Structure and function of the spleen. *Nat Rev Immunol*, 5, 606-16.
- MEHANDRU, S., POLES, M. A., TENNER-RACZ, K., HOROWITZ, A., HURLEY, A., HOGAN, C., BODEN, D., RACZ, P. & MARKOWITZ, M. 2004. Primary HIV-1 infection is associated with preferential depletion of CD4⁺ T lymphocytes from effector sites in the gastrointestinal tract. *J Exp Med*, 200, 761-70.
- MELLORS, J. W., RINALDO, C. R., JR., GUPTA, P., WHITE, R. M., TODD, J. A. & KINGSLEY, L. A. 1996. Prognosis in HIV-1 infection predicted by the quantity of virus in plasma. *Science*, 272, 1167-70.
- MILLER, M. M., THOMPSON, E. M., SUTER, S. E. & FOGLE, J. E. 2013. CD8⁺ clonality is associated with prolonged acute plasma viremia and altered mRNA cytokine profiles during the course of feline immunodeficiency virus infection. *Vet Immunol Immunopathol*, 152, 200-8.
- MIYAZAWA, T., FUKASAWA, M., HASEGAWA, A., MAKI, N., IKUTA, K., TAKAHASHI, E., HAYAMI, M. & MIKAMI, T. 1991. Molecular cloning of a novel isolate of feline immunodeficiency virus biologically and genetically different from the original U.S. isolate. *J Virol*, 65, 1572-7.
- MIYAZAWA, T., FURUYA, T., ITAGAKI, S., TOHYA, Y., TAKAHASHI, E. & MIKAMI, T. 1989. Establishment of a feline T-lymphoblastoid cell line highly sensitive for replication of feline immunodeficiency virus. *Arch Virol*, 108, 131-5.
- MIYAZAWA, T., TOMONAGA, K., KAWAGUCHI, Y. & MIKAMI, T. 1994. The genome of feline immunodeficiency virus. *Arch Virol*, 134, 221-34.
- MOENCH, T. R. 2014. Cell-associated transmission of HIV type 1 and other lentiviruses in small-animal models. *J Infect Dis*, 210 Suppl 3, S654-9.
- MONTAGNA, C., DE CRIGNIS, E., BON, I., RE, M. C., MEZZAROMA, I., TURRIZIANI, O., GRAZIOSI, C. & ANTONELLI, G. 2014. V3 net charge: additional tool in HIV-1 tropism prediction. *AIDS Res Hum Retroviruses*, 30, 1203-12.
- MOOG, C., FLEURY, H. J., PELLEGRIN, I., KIRN, A. & AUBERTIN, A. M. 1997. Autologous and heterologous neutralizing antibody responses following

- initial seroconversion in human immunodeficiency virus type 1-infected individuals. *J Virol*, 71, 3734-41.
- MOORE, P. L., CROOKS, E. T., PORTER, L., ZHU, P., CAYANAN, C. S., GRISE, H., CORCORAN, P., ZWICK, M. B., FRANTI, M., MORRIS, L., ROUX, K. H., BURTON, D. R. & BINLEY, J. M. 2006. Nature of nonfunctional envelope proteins on the surface of human immunodeficiency virus type 1. *J Virol*, 80, 2515-28.
- MOROZOVA, K. S., PIATKEVICH, K. D., GOULD, T. J., ZHANG, J., BEWERSDORF, J. & VERKHUSHA, V. V. 2010. Far-red fluorescent protein excitable with red lasers for flow cytometry and superresolution STED nanoscopy. *Biophys J*, 99, L13-5.
- MOTOKAWA, K., HOHDATSU, T., IMORI, A., ARAI, S. & KOYAMA, H. 2005. Mutations in feline immunodeficiency (FIV) virus envelope gene V3-V5 regions in FIV-infected cats. *Vet Microbiol*, 106, 33-40.
- MUNRO, J. B., GORMAN, J., MA, X., ZHOU, Z., ARTHOS, J., BURTON, D. R., KOFF, W. C., COURTER, J. R., SMITH, A. B., 3RD, KWONG, P. D., BLANCHARD, S. C. & MOTHESE, W. 2014. Conformational dynamics of single HIV-1 envelope trimers on the surface of native virions. *Science*, 346, 759-63.
- MUNRO, J. B. & MOTHESE, W. 2015. Structure and Dynamics of the Native HIV-1 Env Trimer. *J Virol*, 89, 5752-5.
- MURPHY, K. & JANEWAY, C. A. 2012. *Janeway's immunobiology*, New York, N.Y. ; London, Garland Science.
- NAKAMURA, K., SUZUKI, Y., IKEO, K., IKEDA, Y., SATO, E., NGUYEN, N. T., GOJOBORI, T., MIKAMI, T. & MIYAZAWA, T. 2003. Phylogenetic analysis of Vietnamese isolates of feline immunodeficiency virus: genetic diversity of subtype C. *Arch Virol*, 148, 783-91.
- NICKLE, D. C., JENSEN, M. A., SHRINER, D., BRODIE, S. J., FRENKEL, L. M., MITTLER, J. E. & MULLINS, J. I. 2003a. Evolutionary indicators of human immunodeficiency virus type 1 reservoirs and compartments. *J Virol*, 77, 5540-6.
- NICKLE, D. C., SHRINER, D., MITTLER, J. E., FRENKEL, L. M. & MULLINS, J. I. 2003b. Importance and detection of virus reservoirs and compartments of HIV infection. *Curr Opin Microbiol*, 6, 410-6.
- NISHIMURA, Y., BROWN, C. R., MATTAPALLIL, J. J., IGARASHI, T., BUCKLER-WHITE, A., LAFONT, B. A., HIRSCH, V. M., ROEDERER, M. & MARTIN, M. A. 2005. Resting naive CD4+ T cells are massively infected and eliminated by X4-tropic simian-human immunodeficiency viruses in macaques. *Proc Natl Acad Sci U S A*, 102, 8000-5.
- NISHIMURA, Y., GOTO, Y., PANG, H., ENDO, Y., MIZUNO, T., MOMOI, Y., WATARI, T., TSUJIMOTO, H. & HASEGAWA, A. 1998. Genetic heterogeneity of env gene of feline immunodeficiency virus obtained from multiple districts in Japan. *Virus Res*, 57, 101-12.
- NOLTE, M. A., HAMANN, A., KRAAL, G. & MEBIUS, R. E. 2002. The strict regulation of lymphocyte migration to splenic white pulp does not involve common homing receptors. *Immunology*, 106, 299-307.
- O'NEIL, L. L., BURKHARD, M. J., DIEHL, L. J. & HOOVER, E. A. 1995. Vertical transmission of feline immunodeficiency virus. *AIDS Res Hum Retroviruses*, 11, 171-82.
- OBERMEIER, M., SYMONS, J. & WENSING, A. M. 2012. HIV population genotypic tropism testing and its clinical significance. *Curr Opin HIV AIDS*, 7, 470-7.
- OLSEN, H. S., COCHRANE, A. W., DILLON, P. J., NALIN, C. M. & ROSEN, C. A. 1990a. Interaction of the human immunodeficiency virus type 1 Rev protein with a structured region in env mRNA is dependent on multimer

- formation mediated through a basic stretch of amino acids. *Genes Dev*, 4, 1357-64.
- OLSEN, H. S., NELBOCK, P., COCHRANE, A. W. & ROSEN, C. A. 1990b. Secondary structure is the major determinant for interaction of HIV rev protein with RNA. *Science*, 247, 845-8.
- OVERBAUGH, J. & BANGHAM, C. R. 2001. Selection forces and constraints on retroviral sequence variation. *Science*, 292, 1106-9.
- OVERBAUGH, J. & MORRIS, L. 2012. The Antibody Response against HIV-1. *Cold Spring Harb Perspect Med*, 2, a007039.
- PABST, R. 1988. The spleen in lymphocyte migration. *Immunol Today*, 9, 43-5.
- PABST, R. 2007. Plasticity and heterogeneity of lymphoid organs. What are the criteria to call a lymphoid organ primary, secondary or tertiary? *Immunol Lett*, 112, 1-8.
- PAILLOT, R., RICHARD, S., BLOAS, F., PIRAS, F., POULET, H., BRUNET, S., ANDREONI, C. & JUILLARD, V. 2005. Toward a detailed characterization of feline immunodeficiency virus-specific T cell immune responses and mediated immune disorders. *Vet Immunol Immunopathol*, 106, 1-14.
- PANCINO, G., FOSSATI, I., CHAPPEY, C., CASTELOT, S., HURTREL, B., MORAILLON, A., KLATZMANN, D. & SONIGO, P. 1993. Structure and variations of feline immunodeficiency virus envelope glycoproteins. *Virology*, 192, 659-62.
- PASTORE, C., RAMOS, A. & MOSIER, D. E. 2004. Intrinsic obstacles to human immunodeficiency virus type 1 coreceptor switching. *J Virol*, 78, 7565-74.
- PATERSON, D. J., JEFFERIES, W. A., GREEN, J. R., BRANDON, M. R., CORTHESEY, P., PUKLAVEC, M. & WILLIAMS, A. F. 1987. Antigens of activated rat T lymphocytes including a molecule of 50,000 Mr detected only on CD4 positive T blasts. *Mol Immunol*, 24, 1281-90.
- PEAR, W. S., NOLAN, G. P., SCOTT, M. L. & BALTIMORE, D. 1993. Production of high-titer helper-free retroviruses by transient transfection. *Proc Natl Acad Sci U S A*, 90, 8392-6.
- PECORARO, M. R., TOMONAGA, K., MIYAZAWA, T., KAWAGUCHI, Y., SUGITA, S., TOHYA, Y., KAI, C., ETCHEVERRIGARAY, M. E. & MIKAMI, T. 1996. Genetic diversity of Argentine isolates of feline immunodeficiency virus. *J Gen Virol*, 77 (Pt 9), 2031-5.
- PEDERSEN, N. C., HO, E. W., BROWN, M. L. & YAMAMOTO, J. K. 1987. Isolation of a T-lymphotropic virus from domestic cats with an immunodeficiency-like syndrome. *Science*, 235, 790-3.
- PEDERSEN, N. C., LEUTENEGGER, C. M., WOO, J. & HIGGINS, J. 2001. Virulence differences between two field isolates of feline immunodeficiency virus (FIV-APetaluma and FIV-CPGammar) in young adult specific pathogen free cats. *Vet Immunol Immunopathol*, 79, 53-67.
- PEJCHAL, R. & WILSON, I. A. 2010. Structure-based vaccine design in HIV: blind men and the elephant? *Curr Pharm Des*, 16, 3744-53.
- PETERS, P. J., DUENAS-DECAMP, M. J., SULLIVAN, W. M. & CLAPHAM, P. R. 2007. Variation of macrophage tropism among HIV-1 R5 envelopes in brain and other tissues. *J Neuroimmune Pharmacol*, 2, 32-41.
- PHILLIPS, T. R., LAMONT, C., KONINGS, D. A., SHACKLETT, B. L., HAMSON, C. A., LUCIW, P. A. & ELDER, J. H. 1992. Identification of the Rev transactivation and Rev-responsive elements of feline immunodeficiency virus. *J Virol*, 66, 5464-71.
- PHILLIPS, T. R., TALBOTT, R. L., LAMONT, C., MUIR, S., LOVELACE, K. & ELDER, J. H. 1990. Comparison of two host cell range variants of feline immunodeficiency virus. *J Virol*, 64, 4605-13.

- PIATKEVICH, K. D. & VERKHUSHA, V. V. 2011. Guide to red fluorescent proteins and biosensors for flow cytometry. *Methods Cell Biol*, 102, 431-61.
- PICKER, L. J., HAGEN, S. I., LUM, R., REED-INDERBITZIN, E. F., DALY, L. M., SYLWESTER, A. W., WALKER, J. M., SIESS, D. C., PIATAK, M., JR., WANG, C., ALLISON, D. B., MAINO, V. C., LIFSON, J. D., KODAMA, T. & AXTHELM, M. K. 2004. Insufficient production and tissue delivery of CD4⁺ memory T cells in rapidly progressive simian immunodeficiency virus infection. *J Exp Med*, 200, 1299-314.
- PLETNEV, S., SHCHERBAKOVA, D. M., SUBACH, O. M., PLETNEVA, N. V., MALASHKEVICH, V. N., ALMO, S. C., DAUTER, Z. & VERKHUSHA, V. V. 2014. Orange fluorescent proteins: structural studies of LSSmOrange, PSmOrange and PSmOrange2. *PLoS One*, 9, e99136.
- POTSCHKA, H. 2010. Targeting the brain--surmounting or bypassing the blood-brain barrier. *Handb Exp Pharmacol*, 411-31.
- PRELL, R. A., EVANS, D. E., THALHOFER, C., SHI, T., FUNATAKE, C. & WEINBERG, A. D. 2003. OX40-mediated memory T cell generation is TNF receptor-associated factor 2 dependent. *J Immunol*, 171, 5997-6005.
- RAMBAUT, A., POSADA, D., CRANDALL, K. A. & HOLMES, E. C. 2004. The causes and consequences of HIV evolution. *Nat Rev Genet*, 5, 52-61.
- RANGEL, H. R., WEBER, J., CHAKRABORTY, B., GUTIERREZ, A., MAROTTA, M. L., MIRZA, M., KISER, P., MARTINEZ, M. A., ESTE, J. A. & QUINONES-MATEU, M. E. 2003. Role of the human immunodeficiency virus type 1 envelope gene in viral fitness. *J Virol*, 77, 9069-73.
- REGGETI, F., ACKERLEY, C. & BIENZLE, D. 2008. CD134 and CXCR4 expression corresponds to feline immunodeficiency virus infection of lymphocytes, macrophages and dendritic cells. *J Gen Virol*, 89, 277-87.
- REGGETI, F. & BIENZLE, D. 2004. Feline immunodeficiency virus subtypes A, B and C and intersubtype recombinants in Ontario, Canada. *J Gen Virol*, 85, 1843-52.
- REUBEL, G. H., GEORGE, J. W., HIGGINS, J. & PEDERSEN, N. C. 1994. Effect of chronic feline immunodeficiency virus infection on experimental feline calicivirus-induced disease. *Vet Microbiol*, 39, 335-51.
- RICHARDSON, J., PANCINO, G., MERAT, R., LESTE-LASSERRE, T., MORAILLON, A., SCHNEIDER-MERGENER, J., ALIZON, M., SONIGO, P. & HEVEKER, N. 1999. Shared usage of the chemokine receptor CXCR4 by primary and laboratory-adapted strains of feline immunodeficiency virus. *J Virol*, 73, 3661-71.
- RICHMAN, D. D., WRIN, T., LITTLE, S. J. & PETROPOULOS, C. J. 2003. Rapid evolution of the neutralizing antibody response to HIV type 1 infection. *Proc Natl Acad Sci U S A*, 100, 4144-9.
- RIMMELZWAAN, G. F., SIEBELINK, K. H., BROOS, H., DROST, G. A., WEIJER, K., VAN HERWIJNEN, R. & OSTERHAUS, A. D. 1994. gag- and env-specific serum antibodies in cats after natural and experimental infection with feline immunodeficiency virus. *Vet Microbiol*, 39, 153-65.
- ROCHE, S., EL GARCH, H., BRUNET, S., POULET, H., IWAZ, J., ECOCHARD, R. & VANHEMS, P. 2013. Diversity of trends of viremia and T-cell markers in experimental acute feline immunodeficiency virus infection. *PLoS One*, 8, e56135.
- RODRIGO, A. G. 1997. Dynamics of syncytium-inducing and non-syncytium-inducing type 1 human immunodeficiency viruses during primary infection. *AIDS Res Hum Retroviruses*, 13, 1447-51.
- ROELKE, M. E., PECON-SLATTERY, J., TAYLOR, S., CITINO, S., BROWN, E., PACKER, C., VANDEWOUDE, S. & O'BRIEN, S. J. 2006. T-lymphocyte

- profiles in FIV-infected wild lions and pumas reveal CD4 depletion. *J Wildl Dis*, 42, 234-48.
- ROGERS, P. R., SONG, J., GRAMAGLIA, I., KILLEEN, N. & CROFT, M. 2001. OX40 promotes Bcl-xL and Bcl-2 expression and is essential for long-term survival of CD4 T cells. *Immunity*, 15, 445-55.
- ROUKAERTS, I. D., THEUNS, S., TAFFIN, E. R., DAMINET, S. & NAUWYNCK, H. J. 2015. Phylogenetic analysis of feline immunodeficiency virus strains from naturally infected cats in Belgium and The Netherlands. *Virus Res*, 196, 30-6.
- RYAN, G., KLEIN, D., KNAPP, E., HOSIE, M. J., GRIMES, T., MABRUK, M. J., JARRETT, O. & CALLANAN, J. J. 2003. Dynamics of viral and proviral loads of feline immunodeficiency virus within the feline central nervous system during the acute phase following intravenous infection. *J Virol*, 77, 7477-85.
- SADLER, R., BATEMAN, E. A., HEATH, V., PATEL, S. Y., SCHWINGSHACKL, P. P., CULLINANE, A. C., AYERS, L. & FERRY, B. L. 2014. Establishment of a healthy human range for the whole blood "OX40" assay for the detection of antigen-specific CD4⁺ T cells by flow cytometry. *Cytometry B Clin Cytom*, 86, 350-61.
- SALEMI, M., BURKHARDT, B. R., GRAY, R. R., GHAFFARI, G., SLEASMAN, J. W. & GOODENOW, M. M. 2007. Phylodynamics of HIV-1 in lymphoid and non-lymphoid tissues reveals a central role for the thymus in emergence of CXCR4-using quasispecies. *PLoS One*, 2, e950.
- SAMMAN, A., LOGAN, N., MCMONAGLE, E. L., ISHIDA, T., MOCHIZUKI, M., WILLETT, B. J. & HOSIE, M. J. 2010. Neutralization of feline immunodeficiency virus by antibodies targeting the V5 loop of Env. *J Gen Virol*, 91, 242-9.
- SAMMAN, A., MCMONAGLE, E. L., LOGAN, N., WILLETT, B. J., BIEK, R. & HOSIE, M. J. 2011. Phylogenetic characterisation of naturally occurring feline immunodeficiency virus in the United Kingdom. *Vet Microbiol*, 150, 239-47.
- SANDLER, N. G. & DOUEK, D. C. 2012. Microbial translocation in HIV infection: causes, consequences and treatment opportunities. *Nat Rev Microbiol*, 10, 655-66.
- SANKALE, J. L., DE LA TOUR, R. S., MARLINK, R. G., SCHEIB, R., MBOUP, S., ESSEX, M. E. & KANKI, P. J. 1996. Distinct quasi-species in the blood and the brain of an HIV-2-infected individual. *Virology*, 226, 418-23.
- SCHULZ, T. F., JAMESON, B. A., LOPALCO, L., SICCARDI, A. G., WEISS, R. A. & MOORE, J. P. 1992. Conserved structural features in the interaction between retroviral surface and transmembrane glycoproteins? *AIDS Res Hum Retroviruses*, 8, 1571-80.
- SCHWARTZ, E. J., NEUMANN, A. U., TEIXEIRA, A. V., BRUGGEMAN, L. A., RAPPAPORT, J., PERELSON, A. S. & KLOTMAN, P. E. 2002. Effect of target cell availability on HIV-1 production in vitro. *AIDS*, 16, 341-5.
- SCOTT, V. L., BURGESS, S. C., SHACK, L. A., LOCKETT, N. N. & COATS, K. S. 2008. Expression of CD134 and CXCR4 mRNA in term placentas from FIV-infected and control cats. *Vet Immunol Immunopathol*, 123, 90-6.
- SHACKLETT, B. L. & LUCIW, P. A. 1994. Analysis of the vif gene of feline immunodeficiency virus. *Virology*, 204, 860-7.
- SHANER, N. C., LIN, M. Z., MCKEOWN, M. R., STEINBACH, P. A., HAZELWOOD, K. L., DAVIDSON, M. W. & TSIEN, R. Y. 2008. Improving the photostability of bright monomeric orange and red fluorescent proteins. *Nat Methods*, 5, 545-51.

- SHANKARAPPA, R., MARGOLICK, J. B., GANGE, S. J., RODRIGO, A. G., UPCHURCH, D., FARZADEGAN, H., GUPTA, P., RINALDO, C. R., LEARN, G. H., HE, X., HUANG, X. L. & MULLINS, J. I. 1999. Consistent viral evolutionary changes associated with the progression of human immunodeficiency virus type 1 infection. *J Virol*, 73, 10489-502.
- SHAPSHAK, P., SEGAL, D. M., CRANDALL, K. A., FUJIMURA, R. K., ZHANG, B. T., XIN, K. Q., OKUDA, K., PETITO, C. K., EISDORFER, C. & GOODKIN, K. 1999. Independent evolution of HIV type 1 in different brain regions. *AIDS Res Hum Retroviruses*, 15, 811-20.
- SHCHERBAKOVA, D. M., HINK, M. A., JOOSEN, L., GADELLA, T. W. & VERKHUSHA, V. V. 2012. An orange fluorescent protein with a large Stokes shift for single-excitation multicolor FCCS and FRET imaging. *J Am Chem Soc*, 134, 7913-23.
- SHEEHY, A. M., GADDIS, N. C. & MALIM, M. H. 2003. The antiretroviral enzyme APOBEC3G is degraded by the proteasome in response to HIV-1 Vif. *Nat Med*, 9, 1404-7.
- SHIMOJIMA, M., MIYAZAWA, T., IKEDA, Y., MCMONAGLE, E. L., HAINING, H., AKASHI, H., TAKEUCHI, Y., HOSIE, M. J. & WILLETT, B. J. 2004. Use of CD134 as a primary receptor by the feline immunodeficiency virus. *Science*, 303, 1192-5.
- SHIMOJIMA, M., MIYAZAWA, T., KOHMOTO, M., IKEDA, Y., NISHIMURA, Y., MAEDA, K., TOHYA, Y. & MIKAMI, T. 1998. Expansion of CD8alpha+beta-cells in cats infected with feline immunodeficiency virus. *J Gen Virol*, 79 (Pt 1), 91-4.
- SHIPKOVA, M. & WIELAND, E. 2012. Surface markers of lymphocyte activation and markers of cell proliferation. *Clin Chim Acta*, 413, 1338-49.
- SIEBELINK, K. H., KARLAS, J. A., RIMMELZWAAN, G. F., OSTERHAUS, A. D. & BOSCH, M. L. 1995. A determinant of feline immunodeficiency virus involved in Crandell feline kidney cell tropism. *Vet Immunol Immunopathol*, 46, 61-9.
- SILVOTTI, L., KRAMER, L., CORRADI, A., BUSANI, L., TEDESCHI, F., BRANDI, G., BENDINELLI, M. & PIEDIMONTE, G. 1997. Modulation of host cell activation during feline immunodeficiency virus (FIV) infection. *J Comp Pathol*, 116, 263-71.
- SINGH, A., BESSON, G., MOBASHER, A. & COLLMAN, R. G. 1999. Patterns of chemokine receptor fusion cofactor utilization by human immunodeficiency virus type 1 variants from the lungs and blood. *J Virol*, 73, 6680-90.
- SLATKIN, M. & MADDISON, W. P. 1990. Detecting isolation by distance using phylogenies of genes. *Genetics*, 126, 249-60.
- SODORA, D. L., COURCELLE, J., BROJATSCH, J., BERSON, A., WANG, Y. C., DOW, S. W., HOOVER, E. A. & MULLINS, J. I. 1995. Analysis of a feline immunodeficiency virus provirus reveals patterns of gene sequence conservation distinct from human immunodeficiency virus type 1. *AIDS Res Hum Retroviruses*, 11, 531-3.
- SODORA, D. L., SHPAER, E. G., KITCHELL, B. E., DOW, S. W., HOOVER, E. A. & MULLINS, J. I. 1994. Identification of three feline immunodeficiency virus (FIV) env gene subtypes and comparison of the FIV and human immunodeficiency virus type 1 evolutionary patterns. *J Virol*, 68, 2230-8.
- SONG, J., SO, T. & CROFT, M. 2008. Activation of NF-kappaB1 by OX40 contributes to antigen-driven T cell expansion and survival. *J Immunol*, 180, 7240-8.

- SONG, W., COLLISSON, E. W., BILLINGSLEY, P. M. & BROWN, W. C. 1992. Induction of feline immunodeficiency virus-specific cytolytic T-cell responses from experimentally infected cats. *J Virol*, 66, 5409-17.
- SOROOSH, P., INE, S., SUGAMURA, K. & ISHII, N. 2006. OX40-OX40 ligand interaction through T cell-T cell contact contributes to CD4 T cell longevity. *J Immunol*, 176, 5975-87.
- SOULIE, C., CALVEZ, V. & MARCELIN, A. G. 2012. Coreceptor usage in different reservoirs. *Curr Opin HIV AIDS*, 7, 450-5.
- STEPHENS, E. B., MONCK, E., REPPAS, K. & BUTFILOSKI, E. J. 1991. Processing of the glycoprotein of feline immunodeficiency virus: effect of inhibitors of glycosylation. *J Virol*, 65, 1114-23.
- STEWART, S. A., DYKXHOORN, D. M., PALLISER, D., MIZUNO, H., YU, E. Y., AN, D. S., SABATINI, D. M., CHEN, I. S., HAHN, W. C., SHARP, P. A., WEINBERG, R. A. & NOVINA, C. D. 2003. Lentivirus-delivered stable gene silencing by RNAi in primary cells. *RNA*, 9, 493-501.
- STICKNEY, A. L., DUNOWSKA, M. & CAVE, N. J. 2013. Sequence variation of the feline immunodeficiency virus genome and its clinical relevance. *Vet Rec*, 172, 607-14.
- STRACK, R. L., HEIN, B., BHATTACHARYYA, D., HELL, S. W., KEENAN, R. J. & GLICK, B. S. 2009. A rapidly maturing far-red derivative of DsRed-Express2 for whole-cell labeling. *Biochemistry*, 48, 8279-81.
- STREBEL, K. 2013. HIV accessory proteins versus host restriction factors. *Curr Opin Virol*, 3, 692-9.
- SUNDSTROM, M., WHITE, R. L., DE PARSEVAL, A., SASTRY, K. J., MORRIS, G., GRANT, C. K. & ELDER, J. H. 2008. Mapping of the CXCR4 binding site within variable region 3 of the feline immunodeficiency virus surface glycoprotein. *J Virol*, 82, 9134-42.
- SWANSTROM, R. & COFFIN, J. 2012. HIV-1 pathogenesis: the virus. *Cold Spring Harb Perspect Med*, 2, a007443.
- SYKES, J. E. 2013. Feline Immunodeficiency Virus Infection. In: SYKES, J. E. (ed.) *Canine and Feline Infectious Diseases*. St. Louis, Missouri: Saunders.
- TAKAHASHI, Y., TANAKA, Y., YAMASHITA, A., KOYANAGI, Y., NAKAMURA, M. & YAMAMOTO, N. 2001. OX40 stimulation by gp34/OX40 ligand enhances productive human immunodeficiency virus type 1 infection. *J Virol*, 75, 6748-57.
- TALBOTT, R. L., SPARGER, E. E., LOVELACE, K. M., FITCH, W. M., PEDERSEN, N. C., LUCIW, P. A. & ELDER, J. H. 1989. Nucleotide sequence and genomic organization of feline immunodeficiency virus. *Proc Natl Acad Sci U S A*, 86, 5743-7.
- TAMURA, K. & NEI, M. 1993. Estimation of the number of nucleotide substitutions in the control region of mitochondrial DNA in humans and chimpanzees. *Mol Biol Evol*, 10, 512-26.
- TAMURA, K., PETERSON, D., PETERSON, N., STECHER, G., NEI, M. & KUMAR, S. 2011. MEGA5: molecular evolutionary genetics analysis using maximum likelihood, evolutionary distance, and maximum parsimony methods. *Mol Biol Evol*, 28, 2731-9.
- TANIWAKI, S. A., FIGUEIREDO, A. S. & ARAUJO, J. P., JR. 2013. Virus-host interaction in feline immunodeficiency virus (FIV) infection. *Comp Immunol Microbiol Infect Dis*, 36, 549-57.
- TANSIRI, Y., ROWLAND-JONES, S. L., ANANWORANICH, J. & HANSASUTA, P. 2015. Clinical outcome of HIV viraemic controllers and noncontrollers with normal CD4 counts is exclusively determined by antigen-specific CD8+ T-cell-mediated HIV suppression. *PLoS One*, 10, e0118871.

- TECHAKRIENGRKAI, N., TANSIRI, Y. & HANSASUTA, P. 2013. Poor HIV control in HLA-B*27 and B*57/58 noncontrollers is associated with limited number of polyfunctional Gag p24-specific CD8⁺ T cells. *AIDS*, 27, 17-27.
- TELENTI, A. & JOHNSON, W. E. 2012. Host genes important to HIV replication and evolution. *Cold Spring Harb Perspect Med*, 2, a007203.
- TELFORD, W. G., HAWLEY, T., SUBACH, F., VERKHUSHA, V. & HAWLEY, R. G. 2012. Flow cytometry of fluorescent proteins. *Methods*, 57, 318-30.
- TENORIO, A. P., FRANTI, C. E., MADEWELL, B. R. & PEDERSEN, N. C. 1991. Chronic oral infections of cats and their relationship to persistent oral carriage of feline calici-, immunodeficiency, or leukemia viruses. *Vet Immunol Immunopathol*, 29, 1-14.
- TOMARAS, G. D. & HAYNES, B. F. 2009. HIV-1-specific antibody responses during acute and chronic HIV-1 infection. *Curr Opin HIV AIDS*, 4, 373-9.
- TOMPKINS, M. B., BULL, M. E., DOW, J. L., BALL, J. M., COLLISSON, E. W., WINSLOW, B. J., PHADKE, A. P., VAHLENKAMP, T. W. & TOMPKINS, W. A. 2002. Feline immunodeficiency virus infection is characterized by B7+CTLA4⁺ T cell apoptosis. *J Infect Dis*, 185, 1077-93.
- TOMPKINS, M. B. & TOMPKINS, W. A. 2008. Lentivirus-induced immune dysregulation. *Vet Immunol Immunopathol*, 123, 45-55.
- TROYER, J. L., VANDEWOUDE, S., PECON-SLATTERY, J., MCINTOSH, C., FRANKLIN, S., ANTUNES, A., JOHNSON, W. & O'BRIEN, S. J. 2008. FIV cross-species transmission: an evolutionary prospective. *Vet Immunol Immunopathol*, 123, 159-66.
- TROYER, R. M., THOMPSON, J., ELDER, J. H. & VANDEWOUDE, S. 2013. Accessory genes confer a high replication rate to virulent feline immunodeficiency virus. *J Virol*, 87, 7940-51.
- VALCOUR, V., SITHINAMSUWAN, P., LETENDRE, S. & ANCES, B. 2011. Pathogenesis of HIV in the central nervous system. *Curr HIV/AIDS Rep*, 8, 54-61.
- VERMEULEN, B. L., GLEICH, S. E., DEDEURWAERDER, A., OLYSLAEGERS, D. A., DESMARETS, L. M., DEWERCHIN, H. L. & NAUWYNCK, H. J. 2012. In vitro assessment of the feline cell-mediated immune response against feline panleukopeniavirus, calicivirus and felid herpesvirus 1 using 5-bromo-2'-deoxyuridine labeling. *Vet Immunol Immunopathol*, 146, 177-84.
- VERSCHOOR, E. J., BOVEN, L. A., BLAAK, H., VAN VLIET, A. L., HORZINEK, M. C. & DE RONDE, A. 1995. A single mutation within the V3 envelope neutralization domain of feline immunodeficiency virus determines its tropism for CRFK cells. *J Virol*, 69, 4752-7.
- VERSCHOOR, E. J., HULSKOTTE, E. G., EDERVEEN, J., KOOLEN, M. J., HORZINEK, M. C. & ROTTIER, P. J. 1993. Post-translational processing of the feline immunodeficiency virus envelope precursor protein. *Virology*, 193, 433-8.
- VOGEL, C. & MARCOTTE, E. M. 2012. Insights into the regulation of protein abundance from proteomic and transcriptomic analyses. *Nat Rev Genet*, 13, 227-32.
- WAGAMAN, P. C., HASSELKUS-LIGHT, C. S., HENSON, M., LERNER, D. L., PHILLIPS, T. R. & ELDER, J. H. 1993. Molecular cloning and characterization of deoxyuridine triphosphatase from feline immunodeficiency virus (FIV). *Virology*, 196, 451-7.
- WALKER, L. S., GULBRANSON-JUDGE, A., FLYNN, S., BROCKER, T., RAYKUNDALIA, C., GOODALL, M., FORSTER, R., LIPP, M. & LANE, P. 1999. Compromised OX40 function in CD28-deficient mice is linked with failure to develop CXC chemokine receptor 5-positive CD4 cells and germinal centers. *J Exp Med*, 190, 1115-22.

- WATERS, A. K., DE PARSEVAL, A. P., LERNER, D. L., NEIL, J. C., THOMPSON, F. J. & ELDER, J. H. 1996. Influence of ORF2 on host cell tropism of feline immunodeficiency virus. *Virology*, 215, 10-6.
- WATTS, T. H. 2005. TNF/TNFR family members in costimulation of T cell responses. *Annu Rev Immunol*, 23, 23-68.
- WEAVER, E. A., COLLISSON, E. W., SLATER, M. & ZHU, G. 2004. Phylogenetic analyses of Texas isolates indicate an evolving subtype of the clade B feline immunodeficiency viruses. *J Virol*, 78, 2158-63.
- WEINBERG, A. D., EVANS, D. E., THALHOFER, C., SHI, T. & PRELL, R. A. 2004. The generation of T cell memory: a review describing the molecular and cellular events following OX40 (CD134) engagement. *J Leukoc Biol*, 75, 962-72.
- WEINBERG, A. D., VELLA, A. T. & CROFT, M. 1998. OX-40: life beyond the effector T cell stage. *Semin Immunol*, 10, 471-80.
- WEISS, R. A. 1993. How does HIV cause AIDS? *Science*, 260, 1273-9.
- WESTBY, M., LEWIS, M., WHITCOMB, J., YOULE, M., POZNIAK, A. L., JAMES, I. T., JENKINS, T. M., PERROS, M. & VAN DER RYST, E. 2006. Emergence of CXCR4-using human immunodeficiency virus type 1 (HIV-1) variants in a minority of HIV-1-infected patients following treatment with the CCR5 antagonist maraviroc is from a pretreatment CXCR4-using virus reservoir. *J Virol*, 80, 4909-20.
- WHERRY, E. J. & AHMED, R. 2004. Memory CD8 T-cell differentiation during viral infection. *J Virol*, 78, 5535-45.
- WHITE, T. A., BARTESAGHI, A., BORGNIA, M. J., MEYERSON, J. R., DE LA CRUZ, M. J., BESS, J. W., NANDWANI, R., HOXIE, J. A., LIFSON, J. D., MILNE, J. L. & SUBRAMANIAM, S. 2010. Molecular architectures of trimeric SIV and HIV-1 envelope glycoproteins on intact viruses: strain-dependent variation in quaternary structure. *PLoS Pathog*, 6, e1001249.
- WIEDERSCHAIN, D., WEE, S., CHEN, L., LOO, A., YANG, G., HUANG, A., CHEN, Y., CAPONIGRO, G., YAO, Y. M., LENGAUER, C., SELLERS, W. R. & BENSON, J. D. 2009. Single-vector inducible lentiviral RNAi system for oncology target validation. *Cell Cycle*, 8, 498-504.
- WILLETT, B. J., ADEMA, K., HEVEKER, N., BRELOT, A., PICARD, L., ALIZON, M., TURNER, J. D., HOXIE, J. A., PEIPER, S., NEIL, J. C. & HOSIE, M. J. 1998. The second extracellular loop of CXCR4 determines its function as a receptor for feline immunodeficiency virus. *J Virol*, 72, 6475-81.
- WILLETT, B. J., CANNON, C. A. & HOSIE, M. J. 2002. Upregulation of surface feline CXCR4 expression following ectopic expression of CCR5: implications for studies of the cell tropism of feline immunodeficiency virus. *J Virol*, 76, 9242-52.
- WILLETT, B. J. & HOSIE, M. J. 2008. Chemokine receptors and co-stimulatory molecules: unravelling feline immunodeficiency virus infection. *Vet Immunol Immunopathol*, 123, 56-64.
- WILLETT, B. J. & HOSIE, M. J. 2013. The virus-receptor interaction in the replication of feline immunodeficiency virus (FIV). *Curr Opin Virol*, 3, 670-5.
- WILLETT, B. J., HOSIE, M. J., CALLANAN, J. J., NEIL, J. C. & JARRETT, O. 1993. Infection with feline immunodeficiency virus is followed by the rapid expansion of a CD8⁺ lymphocyte subset. *Immunology*, 78, 1-6.
- WILLETT, B. J., HOSIE, M. J., NEIL, J. C., TURNER, J. D. & HOXIE, J. A. 1997. Common mechanism of infection by lentiviruses. *Nature*, 385, 587.
- WILLETT, B. J. & JARRETT, O. 1995. *Feline immunology and immunodeficiency*, Oxford, Oxford University Press.

- WILLETT, B. J., KRAASE, M., LOGAN, N., MCMONAGLE, E., VARELA, M. & HOSIE, M. J. 2013. Selective expansion of viral variants following experimental transmission of a reconstituted feline immunodeficiency virus quasispecies. *PLoS One*, 8, e54871.
- WILLETT, B. J., KRAASE, M., LOGAN, N., MCMONAGLE, E. L., SAMMAN, A. & HOSIE, M. J. 2010. Modulation of the virus-receptor interaction by mutations in the V5 loop of feline immunodeficiency virus (FIV) following in vivo escape from neutralising antibody. *Retrovirology*, 7, 38.
- WILLETT, B. J., MCMONAGLE, E. L., BONCI, F., PISTELLO, M. & HOSIE, M. J. 2006a. Mapping the domains of CD134 as a functional receptor for feline immunodeficiency virus. *J Virol*, 80, 7744-7.
- WILLETT, B. J., MCMONAGLE, E. L., LOGAN, N., SAMMAN, A. & HOSIE, M. J. 2008. A single site for N-linked glycosylation in the envelope glycoprotein of feline immunodeficiency virus modulates the virus-receptor interaction. *Retrovirology*, 5, 77.
- WILLETT, B. J., MCMONAGLE, E. L., LOGAN, N., SCHNEIDER, P. & HOSIE, M. J. 2009. Enforced covalent trimerisation of soluble feline CD134 (OX40)-ligand generates a functional antagonist of feline immunodeficiency virus. *Mol Immunol*, 46, 1020-30.
- WILLETT, B. J., MCMONAGLE, E. L., LOGAN, N., SPILLER, O. B., SCHNEIDER, P. & HOSIE, M. J. 2007. Probing the interaction between feline immunodeficiency virus and CD134 by using the novel monoclonal antibody 7D6 and the CD134 (Ox40) ligand. *J Virol*, 81, 9665-79.
- WILLETT, B. J., MCMONAGLE, E. L., RIDHA, S. & HOSIE, M. J. 2006b. Differential utilization of CD134 as a functional receptor by diverse strains of feline immunodeficiency virus. *J Virol*, 80, 3386-94.
- WONG, J. K., IGNACIO, C. C., TORRIANI, F., HAVLIR, D., FITCH, N. J. & RICHMAN, D. D. 1997. In vivo compartmentalization of human immunodeficiency virus: evidence from the examination of pol sequences from autopsy tissues. *J Virol*, 71, 2059-71.
- WYNN, H. E., BRUNDAGE, R. C. & FLETCHER, C. V. 2002. Clinical implications of CNS penetration of antiretroviral drugs. *CNS Drugs*, 16, 595-609.
- YAMAMOTO, J. K., HANSEN, H., HO, E. W., MORISHITA, T. Y., OKUDA, T., SAWA, T. R., NAKAMURA, R. M. & PEDERSEN, N. C. 1989. Epidemiologic and clinical aspects of feline immunodeficiency virus infection in cats from the continental United States and Canada and possible mode of transmission. *J Am Vet Med Assoc*, 194, 213-20.
- YAMAMOTO, J. K., PU, R., SATO, E. & HOHDATSU, T. 2007. Feline immunodeficiency virus pathogenesis and development of a dual-subtype feline-immunodeficiency-virus vaccine. *AIDS*, 21, 547-63.
- YAMAMOTO, J. K., SANOU, M. P., ABBOTT, J. R. & COLEMAN, J. K. 2010. Feline immunodeficiency virus model for designing HIV/AIDS vaccines. *Curr HIV Res*, 8, 14-25.
- YAMAMOTO, J. K., SPARGER, E., HO, E. W., ANDERSEN, P. R., O'CONNOR, T. P., MANDELL, C. P., LOWENSTINE, L., MUNN, R. & PEDERSEN, N. C. 1988. Pathogenesis of experimentally induced feline immunodeficiency virus infection in cats. *Am J Vet Res*, 49, 1246-58.
- YANG, J. S., ENGLISH, R. V., RITCHEY, J. W., DAVIDSON, M. G., WASMOEN, T., LEVY, J. K., GEBHARD, D. H., TOMPKINS, M. B. & TOMPKINS, W. A. 1996. Molecularly cloned feline immunodeficiency virus NCSU1 JSY3 induces immunodeficiency in specific-pathogen-free cats. *J Virol*, 70, 3011-7.
- YUAN, T., LI, J. & ZHANG, M. Y. 2013. HIV-1 envelope glycoprotein variable loops are indispensable for envelope structural integrity and virus entry. *PLoS One*, 8, e69789.

- YUKL, S. A., GIANELLA, S., SINCLAIR, E., EPLING, L., LI, Q., DUAN, L., CHOI, A. L., GIRLING, V., HO, T., LI, P., FUJIMOTO, K., LAMPIRIS, H., HARE, C. B., PANDORI, M., HAASE, A. T., GUNTARD, H. F., FISCHER, M., SHERGILL, A. K., MCQUAID, K., HAVLIR, D. V. & WONG, J. K. 2010. Differences in HIV burden and immune activation within the gut of HIV-positive patients receiving suppressive antiretroviral therapy. *J Infect Dis*, 202, 1553-61.
- YUKL, S. A., SHERGILL, A. K., HO, T., KILLIAN, M., GIRLING, V., EPLING, L., LI, P., WONG, L. K., CROUCH, P., DEEKS, S. G., HAVLIR, D. V., MCQUAID, K., SINCLAIR, E. & WONG, J. K. 2013. The distribution of HIV DNA and RNA in cell subsets differs in gut and blood of HIV-positive patients on ART: implications for viral persistence. *J Infect Dis*, 208, 1212-20.
- ZAITSEVA, M. B., LEE, S., RABIN, R. L., TIFFANY, H. L., FARBER, J. M., PEDEN, K. W., MURPHY, P. M. & GOLDING, H. 1998. CXCR4 and CCR5 on human thymocytes: biological function and role in HIV-1 infection. *J Immunol*, 161, 3103-13.
- ZARATE, S., POND, S. L., SHAPSHAK, P. & FROST, S. D. 2007. Comparative study of methods for detecting sequence compartmentalization in human immunodeficiency virus type 1. *J Virol*, 81, 6643-51.
- ZARR, M. & SILICIANO, R. 2015. Stoichiometric parameters of HIV-1 entry. *Virology*, 474, 1-9.
- ZAUNDERS, J. J., MUNIER, M. L., SEDDIKI, N., PETT, S., IP, S., BAILEY, M., XU, Y., BROWN, K., DYER, W. B., KIM, M., DE ROSE, R., KENT, S. J., JIANG, L., BREIT, S. N., EMERY, S., CUNNINGHAM, A. L., COOPER, D. A. & KELLEHER, A. D. 2009. High levels of human antigen-specific CD4+ T cells in peripheral blood revealed by stimulated coexpression of CD25 and CD134 (OX40). *J Immunol*, 183, 2827-36.
- ZHANG, L., ROWE, L., HE, T., CHUNG, C., YU, J., YU, W., TALAL, A., MARKOWITZ, M. & HO, D. D. 2002. Compartmentalization of surface envelope glycoprotein of human immunodeficiency virus type 1 during acute and chronic infection. *J Virol*, 76, 9465-73.
- ZHANG, L. Q., MACKENZIE, P., CLELAND, A., HOLMES, E. C., BROWN, A. J. & SIMMONDS, P. 1993. Selection for specific sequences in the external envelope protein of human immunodeficiency virus type 1 upon primary infection. *J Virol*, 67, 3345-56.
- ZIELONKA, J. & MUNK, C. 2011. Cellular restriction factors of feline immunodeficiency virus. *Viruses*, 3, 1986-2005.